

**A novel targeting probe for fluorescent guided surgery in  
colorectal cancer resections**

Helen Mary Andrew

Student ID: 201037374

Submitted in accordance with the requirements for the degree of Doctor of Medicine

The University of Leeds

Leeds Institute of Medical Research at St. James's

School of Medicine

Faculty of Medicine and Health

December 2020

## Intellectual Property and Publication Statements

The candidate confirms that the work submitted is her own, except where work which has formed part of jointly-authored publications has been included. The contribution of the candidate and the other authors to this work has been explicitly indicated below. The candidate confirms that appropriate credit has been given within the thesis where reference has been made to the work of others.

The work in Chapter 3 of the thesis has appeared in publication as follows:

**Andrew H**, Gossedge G, Croft J, Corrigan N, Brown JM, West N, Quirke P, Tolan D, Cahill R, Jayne DG. Next Generation intraoperative Lymph node staging for Stratified colon cancer surgery (GLiSten): a multicentre, multinational feasibility study of fluorescence in predicting lymph node positive disease.

**Efficacy Mech Eval** 2016;3(6)

*My involvement:* clinical trial recruitment, analysis, manuscript

*Involvement of others:* conception, trial design, clinical trial recruitment, supervision, guidance, manuscript correction

This copy has been supplied on the understanding that it is copyright material and that no quotation from the thesis may be published without proper acknowledgement.

© 2020 The University of Leeds and Helen Mary Andrew.

The right of Helen Mary Andrew to be identified as Author of this work has been asserted by her in accordance with the Copyright, Designs and Patents Act 1988.

## Acknowledgements

I would like to express my gratitude to all of my supervisors, especially Professor David Jayne, who have shown true patience in the face of eternal procrastination and empty promises. Without your support, advice and encouragement this thesis would never have seen the light of day. I would also like to thank all the research laboratory staff and students for their expertise, teaching and for making the lab a friendly and approachable environment. I truly enjoyed my time in research which I had not anticipated. Particular thanks must go to Sarah Perry for her wisdom and eternal optimism as well as Ibrahim Khot for his unwavering support, the sheer comedy value of his research presentations and Monday bow ties.

It goes without saying that I would never have been able to complete my research without the care and love of my family and friends. To my parents, your endless support has meant the world to me and enabled me to accomplish all of my achievements so far. I would not be where I am today without you. To my brother, this thesis literally would not have been written without the loan of your computer. I realise that this loan has been somewhat longer than anticipated so thank you for your patience and understanding. To Kevin, my husband, who has been unfailingly positive throughout the unsuccessful experiments, IT disasters and general complaining; I could not have done this without you. You always had such faith that I would complete this thesis and I am very glad that your faith can, at long last, be rewarded.

Finally, I would like to thank my daughter, Elizabeth, for being the best and most brilliant of all babies because you are the real reason why I have been able to finish writing this manuscript and complete this postgraduate degree.

## Abstract

### Background

Tailoring the extent of colorectal cancer surgical resection on an individual basis would improve patient outcomes, but to achieve this goal, staging of the disease, particularly lymph node status, must be improved. Sentinel lymph node mapping has been effective in other tumour types but is ineffective in colorectal cancer. Near infra-red fluorophores are of interest in fluorescent guided surgery, but lack the ability to target the specific tissue of interest. The aim of this research is to develop a targeted near infra-red based probe to identify tumour and lymph node metastases.

### Methods

Immunofluorescence was used to determine appropriate target and control recognition molecules in addition to appropriate target and control cell lines. Semiconducting organic polymer CN-PPV nanoparticles were produced utilising a self-assembly method and characterised over time. The selected target and control recognition molecules were conjugated to non-functionalised (NPs) and maleimide functionalised (MNPs) semiconducting organic polymer CN-PPV nanoparticles and cell binding, as well as cell toxicity, were evaluated *in vitro*.

### Results

Both the target anti-CEA recognition molecules bound specifically to the target cell lines and not to controls. Characterisation of the NPs and MNPs displayed physical stability over time as well as demonstrating negligible adverse cytotoxic effects. Conjugation of both target and control antibody recognition molecules to the MNP led to non-specific binding of the conjugate to control cell lines. The target affimer recognition molecule NP conjugates

demonstrated increased binding to target cell lines (42%,  $p < 0.0001$ ) and little non-specific binding to control cell lines (14%,  $p = 0.3348$ ).

## **Conclusions**

Fluorescent guided surgery is a promising route for intraoperative stratification of colorectal cancer resections if an accurate probe were to be developed. I have shown that the semiconducting organic polymer nanoparticle used in this research possesses the attributes required of a clinical probe for fluorescent guided surgery. However, it requires modification with an appropriate recognition molecule to accurately target colorectal cancer tissue. The affimer NP conjugate is a more promising candidate for this role than its antibody MNP counterpart.

## Table of Contents

<b>Intellectual Property and Publication Statements .....</b>	<b>ii</b>
<b>Acknowledgements .....</b>	<b>iii</b>
<b>Abstract.....</b>	<b>iv</b>
<b>Table of Contents.....</b>	<b>vi</b>
<b>List of Figures .....</b>	<b>xiii</b>
<b>List of Tables .....</b>	<b>xvii</b>
<b>List of Equations .....</b>	<b>xviii</b>
<b>List of Abbreviations .....</b>	<b>xix</b>
<b>1 Introduction .....</b>	<b>2</b>
1.1 Colorectal cancer .....	2
1.1.1 Background information .....	2
1.1.2 Complete mesocolic resection and D3 evidence .....	6
1.2 Staging of colorectal cancer .....	9
1.2.1 Current practice and importance of lymph node staging .....	9
1.2.2 Limitations of current staging strategies.....	11
1.2.3 Area of clinical need.....	12
1.3 Strategies to improve staging of lymph node involvement.....	13
1.3.1 Sentinel lymph node biopsy and mapping.....	13
1.3.1.1 Sentinel lymph node mapping in colorectal cancers.....	17
1.3.2 One Step Nucleic Acid Amplification .....	24
1.3.3 Fluorescence-guided surgery in colorectal resections.....	25
1.3.3.1 Fluorescence .....	25
1.3.3.2 Indocyanine Green .....	30
1.3.3.3 5-aminolevulinic acid .....	34
1.4 Nanomedicine .....	37
1.4.1 Targeting of tumour.....	40
1.4.1.1 Passive targeting .....	40
1.4.1.2 Active targeting .....	46
1.4.2 Recognition molecules.....	48
1.4.2.1 Antibodies .....	49
1.4.2.1.1 Studies using monoclonal antibodies as recognition molecules	

1.4.2.2	Affimers .....	55
1.4.3	Nanoparticles .....	60
1.4.3.1	Opsonization and the Mononuclear phagocyte system .	61
1.4.3.2	PEGylation .....	62
1.4.3.3	Fluorescent nanoparticles .....	64
1.4.3.3.1	Semiconducting polymer nanoparticles.....	67
1.5	Summary .....	72
1.6	Aims and Objectives .....	74
<b>2</b>	<b>Materials and Methods .....</b>	<b>76</b>
2.1	Next Generation intraoperative Lymph node staging for Stratified colon cancer surgery.....	76
2.1.1	Trial protocol.....	76
2.1.2	Patient samples.....	82
2.1.2.1	Snap freezing specimens .....	82
2.1.2.2	Cryoscrolling and cryosectioning snap frozen specimens .....	82
2.1.2.3	H&E staining of sectioned tissue specimens .....	83
2.1.2.4	Extraction of RNA from snap frozen specimens .....	83
2.1.2.4.1	RNA separation using PureLink™ RNA Mini Kit – Protocol 184	
2.1.2.4.2	RNA separation using PureLink™ RNA Mini Kit – Protocol 284	
2.1.2.4.3	RNA extraction using PureLink™ RNA Mini Kit.....	85
2.1.2.4.4	RNA extraction using RNeasy Mini Kit – Protocol 3.....	85
2.1.2.4.5	Analysing the quality of extracted RNA .....	86
2.1.2.5	Gene expression analysis .....	87
2.2	Recognition molecules.....	87
2.2.1	Immunofluorescence.....	87
2.2.1.1	Cell lines.....	87
2.2.1.2	Passaging cell lines .....	88
2.2.1.3	Fixing cells .....	88
2.2.1.4	Immunofluorescence protocol .....	88
2.2.2	Antibodies.....	89
2.2.2.1	Reduction of antibody .....	89
2.2.2.2	Gel electrophoresis.....	90

2.2.2.3	Dot blotting.....	91
2.2.2.4	Western blotting.....	92
2.2.2.5	Oxidation of antibody.....	92
2.2.2.6	Biotinylation of antibody.....	93
2.2.3	Biotinylation of affimer.....	94
2.3	Nanoparticle.....	95
2.3.1	Fabrication of nanoparticles.....	95
2.3.2	Characterisation of nanoparticles.....	97
2.3.2.1	Characterisation of nanoparticle sizes.....	97
2.3.2.2	Characterisation of the nanoparticle absorption and emission profiles.....	98
2.3.2.2.1	Determining optimum dilution for testing absorption and emission profiles	98
2.3.3	Testing the effect of centrifugation on nanoparticle characterisation.....	98
2.3.3.1	Testing effects of repeated centrifugation on nanoparticle characterisation.....	99
2.3.4	Cell viability after exposure to bare maleimide functionalised nanoparticle.....	99
2.3.4.1	Cell counting for seeding 96-well plates.....	99
2.3.4.2	MTT Assay.....	100
2.3.5	Testing for non-specific binding of nanoparticle to cell lines.....	100
2.4	Conjugation.....	101
2.4.1	Conjugating anti-CEA antibody to heterobifunctional crosslinker.....	101
2.4.1.1	Testing antibody – dye labelled crosslinker conjugate against cell lines using 0.5% skimmed milk as the blocking agent.....	102
2.4.1.2	Testing antibody – dye labelled crosslinker conjugate against cell lines using 0.1% bovine serum albumin as blocking the agent.....	102
2.4.1.3	Testing components of antibody – dye labelled crosslinker conjugate.....	103
2.4.2	Conjugation of antibody recognition molecule to maleimide functionalised nanoparticle.....	103
2.4.2.1	Conjugating heterobifunctional crosslinker to maleimide functionalised nanoparticle.....	104
2.4.2.2	Testing anti-CEA antibody – nanoparticle conjugate against LoVo cell line.....	105

2.4.2.3	Testing target (anti-CEA) and control (anti-CD31) antibody – nanoparticle conjugates against target and control cell lines.....	106
2.4.3	Optimising the protocol for conjugating antibodies to maleimide functionalised nanoparticle .....	108
2.4.3.1	Optimisation step 1: Comparing different extraction techniques to remove excess antibody from antibody-nanoparticle conjugates.....	108
2.4.3.1.1	Extraction of excess antibody by dialysis .....	108
2.4.3.1.2	Extraction of excess antibody by magnetism .....	109
2.4.3.2	Optimisation step 2: Galactose-mediated blocking of unoccupied hydrazide groups on crosslinker .....	110
2.4.3.3	Optimisation step 3: Assessing the effect of conjugation time between oxidised antibody and PDPH-MNP conjugate.....	111
2.4.3.4	Optimisation step 4: Investigating the effect of increasing the amount of Target (anti-CEA) antibodies incubated with PDPH-MNP in conjugation reactions .....	111
2.4.3.5	Optimisation step 5: Investigating optimum dilution of maleimide functionalised nanoparticle in conjugation reaction.....	112
2.4.3.6	Optimisation step 6: The influence of wash cycles following the incubation of cells with conjugates.....	112
2.4.3.7	Optimisation step 7: Investigating the different parameters of incubation .....	113
2.4.4	Testing target and control antibody – nanoparticle conjugates against target and control cell lines using streptavidin functionalised nanoparticle .....	113
2.4.5	Conjugation of anti-CEA affimer to maleimide functionalised nanoparticle.....	114
2.4.5.1	Preparing anti-CEA affimers.....	114
2.4.5.2	Testing variants of anti-CEA affimer-maleimide functionalised nanoparticle conjugates.....	115
2.4.5.3	Comparing different incubation settings for affimer-conjugated nanoparticle.....	116
2.4.5.4	Testing target and control affimer – nanoparticle conjugates against target and control cell lines .....	117
2.5	Statistical analysis.....	118
<b>3</b>	<b>Next Generation of Laparoscopic intraoperative Lymph node staging for Stratified colon cancer surgery (GLiSten) clinical trial .....</b>	<b>120</b>
3.1	Introduction.....	120

3.2	Results .....	122
3.2.1	GLiSten study results.....	122
3.2.2	Primary objective: Diagnostic accuracy of intraoperative 5-ALA fluorescence .....	123
3.2.2.1	Cohort 1 .....	123
3.2.2.2	Cohort 2 .....	126
3.2.3	Secondary objectives: Preoperative CT imaging .....	128
3.2.4	Secondary objectives: Histopathology.....	130
3.2.5	Complications relating to surgery and 5-ALA administration .....	131
3.2.6	Gene expression analysis.....	133
3.2.6.1	Comparison of RNA extraction techniques .....	135
3.2.6.2	Gene expression analysis report.....	136
3.3	Discussion .....	139
<b>4</b>	<b>Cancer targeting agents.....</b>	<b>146</b>
4.1	Introduction.....	146
4.2	Results .....	147
4.2.1	Antibody testing on fixed cells .....	147
4.2.1.1	Testing target and control antibodies on fixed cells.....	147
4.2.1.2	Testing oxidised antibodies on fixed cells .....	148
4.2.1.3	Testing biotinylated antibodies on fixed cells.....	149
4.2.2	Gel electrophoresis of reduced antibody .....	150
4.2.3	Testing for presence of glycoprotein on antibody .....	153
4.2.3.1	Western blotting.....	154
4.2.4	Testing biotinylated affimers .....	155
4.3	Discussion .....	156
<b>5</b>	<b>Nanoparticles .....</b>	<b>165</b>
5.1	Introduction.....	165
5.2	Results .....	167
5.2.1	Nanoparticle characterisation .....	167
5.2.1.1	Characterisation of nanoparticle sizes .....	167
5.2.1.2	Absorption and emission spectra .....	170
5.2.1.2.1	Optimum dilution of nanoparticles .....	170
5.2.1.2.2	Absorption and emission spectra for non-functionalised nanoparticles.....	172

5.2.1.2.3	Absorption and emission spectra for maleimide functionalised nanoparticles	173
5.2.1.2.4	Absorption and emission spectra for short PEG nanoparticles	174
5.2.1.3	Testing the effects of conjugation processes on nanoparticle characterisation	176
5.2.2	Investigating cell viability after exposure to bare maleimide functionalised nanoparticles	179
5.2.3	Non-specific binding of nanoparticles	181
5.3	Discussion	185
<b>6</b>	<b>Conjugation and binding assays</b>	<b>193</b>
6.1	Introduction	193
6.2	Results	195
6.2.1	Conjugation of target (anti-CEA) antibody to heterobifunctional crosslinker	195
6.2.2	Conjugation of antibody to maleimide functionalised nanoparticle using heterobifunctional crosslinker	199
6.2.2.1	Conjugating heterobifunctional crosslinker to maleimide functionalised nanoparticles	199
6.2.2.2	Testing anti-CEA antibody – nanoparticle conjugate against LoVo cell line	200
6.2.2.3	Testing target and control antibody – nanoparticle conjugates against target and control cell lines	203
6.2.3	Optimisation of antibody-nanoparticle conjugation	208
6.2.3.1	Optimisation step 1: Comparing different extraction techniques to remove excess antibody from antibody-nanoparticle conjugates	208
6.2.3.2	Optimisation step 2: Galactose-mediated blocking of unoccupied hydrazide groups on crosslinker	210
6.2.3.3	Optimisation step 3: Assessing the effect of conjugation time between oxidised antibody and PDPH-MNP conjugate	212
6.2.3.4	Optimisation step 4: Investigating the effect of increasing the amount of Target (anti-CEA) antibodies incubated with PDPH-MNP in conjugation reactions	213
6.2.3.5	Optimisation step 5: Investigating optimum dilution of maleimide functionalised nanoparticle in conjugation reaction	215

6.2.3.6	Optimisation step 6: The influence of wash cycles following the incubation of cells with conjugates .....	217
6.2.3.7	Optimisation step 7: Investigating the different parameters of incubation .....	219
6.2.4	Testing target and control antibody – nanoparticle conjugates against target and control cell lines using streptavidin functionalised nanoparticle .....	221
6.2.5	Conjugation of anti-CEA affimer to maleimide functionalised nanoparticle .....	223
6.2.5.1	Testing target and control affimers on fixed cells.....	223
6.2.5.2	Testing variants of anti-CEA affimer maleimide functionalised nanoparticle conjugates.....	224
6.2.5.3	Comparing different incubation settings for affimer-conjugated nanoparticle .....	226
6.2.5.4	Testing target and control affimer–nanoparticle conjugates against target and control cell lines .....	228
6.3	Discussion .....	231
<b>7</b>	<b>Research summary, conclusion, limitations and future work.....</b>	<b>248</b>
7.1	Summary and conclusions.....	248
7.2	Limitations of study .....	250
7.3	Future work .....	251
<b>8</b>	<b>References .....</b>	<b>255</b>

## List of Figures

Figure 1.1. Diagram depicting different levels of lymph node stations within colonic mesentery. ....	5
Figure 1.2. Illustration depicting sentinel lymph node mapping technique in breast cancer surgery. ....	14
Figure 1.3. Axillary sentinel lymph node identified during lymphatic mapping in a breast cancer patient. ....	15
Figure 1.4. Energy level diagram for fluorescence (Jablonski Diagram). ....	27
Figure 1.5. Excitation and emission spectra of Indocyanine Green in water. .	28
Figure 1.6. ICG fluorescence during laparoscopic right hemicolectomy showing the position of regional lymph nodes within the mesentery. ....	31
Figure 1.7. 5-ALA fluorescence of colonic tumour and lymph node metastases within mesentery. ....	36
Figure 1.8. Diagram illustrating Passive drug targeting. ....	41
Figure 1.9. Representative diagram of the tumour micro-environment and passive targeting of a nanomedicine system using the EPR effect. ....	44
Figure 1.10. Diagram illustrating Active drug targeting. ....	47
Figure 1.11. A schematic representation of the structure of an IgG monoclonal antibody. ....	50
Figure 1.12. Examples of different antibody fragments formed from an IgG monoclonal antibody. ....	51
Figure 1.13. Diagram depicting the process of Systematic Evolution of Ligands by Exponential Enrichment (SELEX). ....	57
Figure 1.14. Proposed structure of self-assembled fluorescent CN-PPV dye-doped PLGA-PEG semiconducting polymer NP. ....	71
Figure 2.1. GLiSten trial flow diagram. ....	80
Figure 2.2. Image showing separation of magnetic maleimide functionalised NP from solution using DynaMag™-2 Magnet magnetic separator. ....	109
Figure 3.1. Comparison of the quality of RNA extraction from GLiSten trial specimens. ....	135
Figure 3.2. Heatmap showing the strength of association between technical and clinical factors within the study samples. ....	137
Figure 3.3. KEGG Enrichment Analysis of A) upregulated and B) downregulated enriched KEGG pathways. ....	138
Figure 4.1. Binding of target and control antibodies on target and control cell lines using immunofluorescence on fixed cells. ....	148
Figure 4.2. Binding of oxidised target and control antibodies on target and control cell lines using immunofluorescence on fixed cells. ....	149

<b>Figure 4.3. Binding of biotinylated anti-CEA and anti-CD31 antibodies on target and control cell lines using immunofluorescence on fixed cells.</b>	<b>150</b>
<b>Figure 4.4. Developed gel electrophoresis membrane depicting weights of antibody fragments following reduction with different reduction agents.</b>	<b>151</b>
<b>Figure 4.5. Dot blot highlighting the biotinylation of oxidised anti-CEA antibody and non-oxidised anti-CEA antibody control.</b>	<b>153</b>
<b>Figure 4.6. Western Blot showing biotinylation of oxidised and non-oxidised anti-CEA antibody.</b>	<b>155</b>
<b>Figure 4.7. Binding of biotinylated anti-CEA affimer on target and control cell lines compared to BSA control using immunofluorescence on fixed cells.</b>	<b>156</b>
<b>Figure 5.1. Fluorescent imaging of NIR fluorescent CN-PPV dye-doped PLGA-PEG semiconducting polymer NP.</b>	<b>166</b>
<b>Figure 5.2. Mean hydrodynamic diameters of CN-PPV/PLGA-PEG NPs over time.</b>	<b>168</b>
<b>Figure 5.3. Mean hydrodynamic diameters of long and short PEG polymer chain functionalised CN-PPV/PLGA-PEG NPs.</b>	<b>169</b>
<b>Figure 5.4. Mean polydispersity index of CN-PPV/PLGA-PEG NPs over time.</b>	<b>170</b>
<b>Figure 5.5. Absorption profiles of serial dilutions of non-functionalised CN-PPV/PLGA-PEG NPs.</b>	<b>172</b>
<b>Figure 5.6. Absorption and emission profiles of non-functionalised CN-PPV/PLGA-PEG NPs at optimum dilution over time.</b>	<b>173</b>
<b>Figure 5.7. Absorption and emission profiles for maleimide functionalised CN-PPV/PLGA-PEG NPs.</b>	<b>174</b>
<b>Figure 5.8. Absorption and emission profiles for non-functionalised and maleimide functionalised short PEG CN-PPV/PLGA-PEG NPs.</b>	<b>175</b>
<b>Figure 5.9. Effects of centrifugation on NPs.</b>	<b>177</b>
<b>Figure 5.10. Effects of repeated centrifugation on hydrodynamic diameters and fluorescent emission on bare maleimide functionalised NPs.</b>	<b>178</b>
<b>Figure 5.11. Cell viability in cell lines after being exposed to varying concentrations of bare NPs containing the maleimide terminal group.</b>	<b>180</b>
<b>Figure 5.12. Fluorescence in cell lines after incubation of bare non-functionalised (0% MNP) and maleimide functionalised NPs with varying concentrations of maleimide PLGA-PEG (25% MNP to 100% MNP).</b>	<b>182</b>
<b>Figure 5.13. Fluorescence in cell lines after incubation with varying concentrations of cysteine-blocked bare non-functionalised (0% MNP) and maleimide functionalised NPs with varying concentrations of maleimide PLGA-PEG (25% MNP to 100% MNP).</b>	<b>184</b>
<b>Figure 6.1. Chemical structure of heterobifunctional 3-(2-Pyridyldithio)propionyl hydrazide (PDPH) crosslinker</b>	<b>195</b>

<b>Figure 6.2. Binding of target antibody and target antibody - dye labelled PDPH heterobifunctional crosslinker on target and control cell lines using immunofluorescence on fixed cells.....</b>	<b>196</b>
<b>Figure 6.3. Binding of target antibody and target antibody - dye labelled PDPH crosslinker on target and control cell lines using BSA blocking protocol on fixed cells.....</b>	<b>197</b>
<b>Figure 6.4. Binding of different components of DyLight dye labelled anti-CEA antibody – PDPH heterobifunctional crosslinker conjugate on target and control cell lines using immunofluorescence on fixed cells.....</b>	<b>198</b>
<b>Figure 6.5. Assessment of optimal incubation time for conjugation of maleimide functionalised NP (MNP) to heterobifunctional crosslinker.....</b>	<b>200</b>
<b>Figure 6.6. Assessment of binding of bare NPs and antibody-NP conjugate (AbMNP) to LoVo cells. ....</b>	<b>202</b>
<b>Figure 6.7. Binding of target antibody-NP conjugate (Anti-CEA AbMNP) on target cell line using immunofluorescence on fixed cells.....</b>	<b>203</b>
<b>Figure 6.8. Binding of target and control antibody-NP conjugates (AbMNP) against target and control cell lines. ....</b>	<b>205</b>
<b>Figure 6.9. Binding of target and control antibody-NP conjugates on target and control cell lines using immunofluorescence on fixed cells. ....</b>	<b>207</b>
<b>Figure 6.10. Assessment of binding of target antibody-NP conjugate to LoVo cells using different extraction methods to remove excess oxidised target antibody. ....</b>	<b>209</b>
<b>Figure 6.11. Assessment of binding of target antibody-NP conjugate (AbMNP) against target and control cells using oxidised galactose to block unoccupied hydrazide functional groups on heterobifunctional crosslinker. ....</b>	<b>211</b>
<b>Figure 6.12. Comparing binding of target antibody-NP conjugates where the antibody and PDPH-MNP have incubated for different time periods against target and control cell lines.....</b>	<b>213</b>
<b>Figure 6.13. Comparison of the binding of target antibody-NP conjugates (AbMNP) with different ratios of antibody to PDPH – maleimide functionalised NP conjugates and different post conjugation processes against target and control cell lines.....</b>	<b>215</b>
<b>Figure 6.14. Comparison of the binding of target antibody-NP conjugates (AbMNP) with different dilutions of maleimide functionalised NP used in the conjugation reaction against target and control cell lines. ....</b>	<b>217</b>
<b>Figure 6.15. Comparison of the binding of target antibody-NP conjugates (AbMNP) having undergone different numbers of wash cycles against target and control cell lines.....</b>	<b>218</b>
<b>Figure 6.16. Comparison of the binding of unblocked and blocked target antibody-NP conjugates (AbMNP) under different incubation conditions.....</b>	<b>220</b>

<b>Figure 6.17. Binding of target and control antibody-streptavidin functionalised NP conjugates (AbSNP) against target and control cell lines. ....</b>	<b>222</b>
<b>Figure 6.18. Binding of target and control affimers on target and control cell lines using immunofluorescence.....</b>	<b>224</b>
<b>Figure 6.19. Comparison of binding of control and various target affimer-NP conjugates (AffMNP) against target and control cell lines. ....</b>	<b>226</b>
<b>Figure 6.20. Assessing optimum conditions for binding of affimer-conjugated NP (AffMNP) against the target (LoVo) cell line.....</b>	<b>228</b>
<b>Figure 6.21. Binding of target and control affimer-conjugated NPs (AffMNP) against target and control cell lines. ....</b>	<b>230</b>
<b>Figure 6.22. Binding of target and control affimer-NP conjugates (AffMNP) on target and control cell lines using immunofluorescence on fixed cells. ....</b>	<b>231</b>

## List of Tables

<b>Table 1.1. TNM Classification of Malignant Tumours staging system (8<sup>th</sup> edition) .....</b>	<b>10</b>
<b>Table 1.2. Ideal characteristics of a molecular probe.....</b>	<b>48</b>
<b>Table 2.1. Inclusion and exclusion criteria .....</b>	<b>77</b>
<b>Table 3.1. Patient Demographics .....</b>	<b>122</b>
<b>Table 3.2. Fluorescence results in Cohort 1 .....</b>	<b>123</b>
<b>Table 3.3. Comparison of fluorescence and histopathology LN results in Cohort 1.....</b>	<b>124</b>
<b>Table 3.4. Fluorescence results in Cohort 2.....</b>	<b>126</b>
<b>Table 3.5. Comparison of fluorescence and histopathology results in Cohort 2.....</b>	<b>127</b>
<b>Table 3.6. Preoperative CT prediction of LN stage compared with histopathology .....</b>	<b>128</b>
<b>Table 3.7. Preoperative CT prediction of EMVI compared with histopathology .....</b>	<b>129</b>
<b>Table 3.8. Preoperative CT prediction of T stage compared with histopathology .....</b>	<b>130</b>
<b>Table 3.9. Comparison of resection procedures between cohorts.....</b>	<b>131</b>
<b>Table 3.10. Major risks associated with major laparoscopic colorectal surgery .....</b>	<b>131</b>
<b>Table 3.11. Patient demographics of selected samples for gene microarray</b>	<b>134</b>
<b>Table 4.1. Densitometry analysis of the resulting anti-CEA antibody fragments following reduction with TCEP, 2-ME and 2-MEA .....</b>	<b>152</b>
<b>Table 6.1. Summary of nanoparticle conjugation protocol optimisation steps .....</b>	<b>239</b>

## List of Equations

<b>Equation 3.1. Determining 5-ALA mediated fluorescence sensitivity and specificity.....</b>	<b>124</b>
<b>Equation 3.2. Determining preoperative CT imaging sensitivity and specificity for LN staging.....</b>	<b>128</b>
<b>Equation 3.3. Determining preoperative CT imaging sensitivity and specificity for detecting EMVI .....</b>	<b>129</b>

## List of Abbreviations

Ab-SCNP	Antibody – semiconducting nanoparticle conjugate
BM	Basement membrane
$\beta$ -ME	$\beta$ -mercaptoethanol
BMI	Body mass index
BSA	Bovine Serum Albumin
CEA	Carcinoembryonic antigen
CI	Confidence Interval
CK19	Cytokeratin-19
CMR	Complete mesocolic resection
CNPPV	Poly(2,5-di(hexyloxy)cyanoterephthalyidene)
CO <sub>2</sub>	Carbon dioxide
CT	Computed tomography
DAPI	4',6-diamidino-2-phenylindole
DMEC	Data Monitoring and Ethics Committee
DMSO	Dimethyl sulfoxide
DTT	Dithiothreitol
ECL	Enhanced chemiluminescent
ECM	Extracellular matrix
EDTA	Ethylenediaminetetraacetic acid

EGFR	Epithelial growth factor receptor
EPR	Enhanced permeability and retention
FCS	Foetal calf serum
FIT	Faecal immunochemical test
FOBT	Faecal occult blood test
FR $\alpha$	Folate receptor- $\alpha$
FDA	Food and Drug Administration
FITC	Fluorescein isothiocyanate
HER2-	Human epidermal growth factor receptor 2 negative
HER+	Human epidermal growth factor receptor 2 positive
ICG	Indocyanine green
IgG	Immunoglobulin G
IHC	Immunohistochemistry
KDa	Kilodalton
LN	Lymph node
mg	Milligram
ml	Millilitre
mM	Micromolar
Mn	Number average molecular weight
MNP	Nanoparticle containing PEG terminated with maleimide group (maleimide functionalised nanoparticle)
MPBH	4-(4-N-maleimidophenyl)butyric acid hydrazide

MRI	Magnetic Resonance Imaging
MTT	3-(4,5-dimethylthiazol-2-yl)-2,5-diphenyltetrazolium bromide
M <sub>2</sub> C <sub>2</sub> H	4-(N-maleimidomethyl)cyclohexane-1-carboxyl-hydrazide
NBCSP	National Bowel Cancer Screening Programme
NICE	National Institute for Health and Care Excellence
NIR	Near infra-red
NOTES	Natural orifice transluminal endoscopic surgery
NP	Nanoparticle
OCT	Optimal cutting temperature compound
OSNA	One Step Nucleic Acid Amplification
PBS	Phosphate buffered saline
PBST	Phosphate buffered saline containing Tween
PCA	Principal component analysis
PDD	Photodynamic diagnosis
PDPH	3-(2-pyridyldithio)propionyl hydrazide
PDT	Photodynamic therapy
PEG	Poly(ethylene glycol)
PLGA	Poly(lactic-co-glycolic acid)
PLGA-PEG	Poly(ethylene glycol) methyl ether-block-poly(lactide-co-glycolide)
QD	Quantum dot
RIN	RNA integrity number
RLPL	Extended retroperitoneal and lateral pelvic lymphadenectomy

scFv	Single chain Fv antibody fragment
SDS	Sodium dodecyl sulfate
SLN	Sentinel lymph node
SLNB	Sentinel lymph node biopsy
SLNM	Sentinel lymph node mapping
SPION	Super paramagnetic iron oxide nanoparticle
TAG-72	Tumour-associated glycoprotein-72
TCEP	Tris(2-carboxyethyl)phosphine
THF	Tetrahydrofuran
TME	Total mesorectal excision
TSC	Trial Steering Committee
UK	United Kingdom
USA	United States of America
$\mu\text{g}$	Microgram
$\mu\text{l}$	Microliter
VEGF	Vascular endothelial growth factor
WMS	0.5% skimmed milk solution (working milk solution)
2-ME	2-mercaptoethanol
2-MEA	2-mercaptoethylamine-HCl
5-ALA	5-aminolevulinic acid

# **Chapter One**

## **Introduction**

# 1 Introduction

## 1.1 Colorectal cancer

### 1.1.1 Background information

Colorectal cancer is the fourth most common cancer in the UK accounting for 12% of all new cancer diagnoses with 41,800 new patients presenting in 2015(1). It is the second most common cause of cancer deaths and in 2016 accounted for approximately 10% of all cancer-related mortalities. However, over the last 40 years, long-term survival rates have improved(1). Recently, the Office for National Statistics published data regarding cancer survival which highlighted that the age-standardised 5-year net survival for colon cancer is 59% and around 62% for cancers of the rectum(2). Survival is stage-dependent with higher rates of being observed in earlier stages of disease(1–3). However, more than 50% of patients are diagnosed at a late stage, with a quarter of patients presenting with metastatic disease.

Typically, patients are diagnosed either through referrals from general practitioners with concerning symptoms, such as a change in bowel habit or rectal bleeding (less than 10% of 2 week wait referrals are positively diagnosed(4)). Alternatively, patients can also be diagnosed through the National Bowel Cancer Screening Programme. Identified patients will undergo diagnostic tests, such as colonoscopy or Computed tomography (CT)-based examinations, with biopsies taken of suspicious lesions(5). Following histological confirmation of malignancy, patients undergo staging investigations to establish whether the tumour is resectable and to determine the presence of any metastases. Magnetic Resonance Imaging (MRI) imaging of the pelvis is performed in patients with rectal tumours in addition to CT imaging of the thorax, chest and abdomen

for all colorectal tumours(6). In addition to determining which patients can be put forward for surgery, staging also allows for the identification of those patients who may benefit from neo-adjuvant therapies, such as chemoradiotherapy(3,6). Surgery with curative intent, plus or minus other therapies, is the only management option whereby a cure is possible(7). All decisions regarding a patient's care in the UK originate from discussions at the local multi-disciplinary meeting(6,8). Input is received from different specialties to ensure that the patient receives the best individualised care.

Surgery for colorectal cancer entails segmental resection of the bowel with en-bloc resection of the regional lymph nodes. Unless indicated by preoperative imaging or by intraoperative findings, the highest level of lymph nodes, the D3 nodes in the para-aortic area, are not routinely removed for surgeries performed in the UK (Figure 1.1). Rather, it is more common for only the D1 and D2 lymph nodes to be removed during routine segmental colectomy(9).

The resected specimen is examined by histopathologists to accurately stage the depth of penetration of the tumour through the bowel wall (T-stage) and the presence of lymph node metastases (N-stage), which is important for predicting the patient's prognosis. Involvement of the lymph nodes is an important prognostic factor, with lymph node positive disease correlating with poor prognosis(10–13). If the cancer has progressed beyond the bowel wall, infiltrated the lymph nodes, or spread to distant organs, then the chances of cure with surgery alone are greatly diminished.

The lymphatic system is one route by which malignant tumour cells can spread throughout the human body(14). The lymphatic vessels follow the vascular supply to the different segments of the colon. The lymphatic drainage of the colon is believed to follow an orderly procession from the tumour into the epicolic lymph nodes, D1, then

sequentially up the lymphatic chain to the level of the para-aortic nodes, D3 (Figure 1.1). However, there are instances where lymph node metastasis can “skip” levels or drain to lymph nodes outside the conventional resection area, known as aberrant drainage, and these phenomena are noted in other solid tumours(15). Another definition of lymph node skip metastasis is metastases found within non-sentinel lymph nodes despite the sentinel lymph node being negative for disease. It is of vital importance to examine the lymph nodes within the resected specimen as the presence of nodal disease substantially alters the patient’s prognosis and therapeutic options(9). Around 25-40% of patients are found to have lymph node positive disease(10,16).

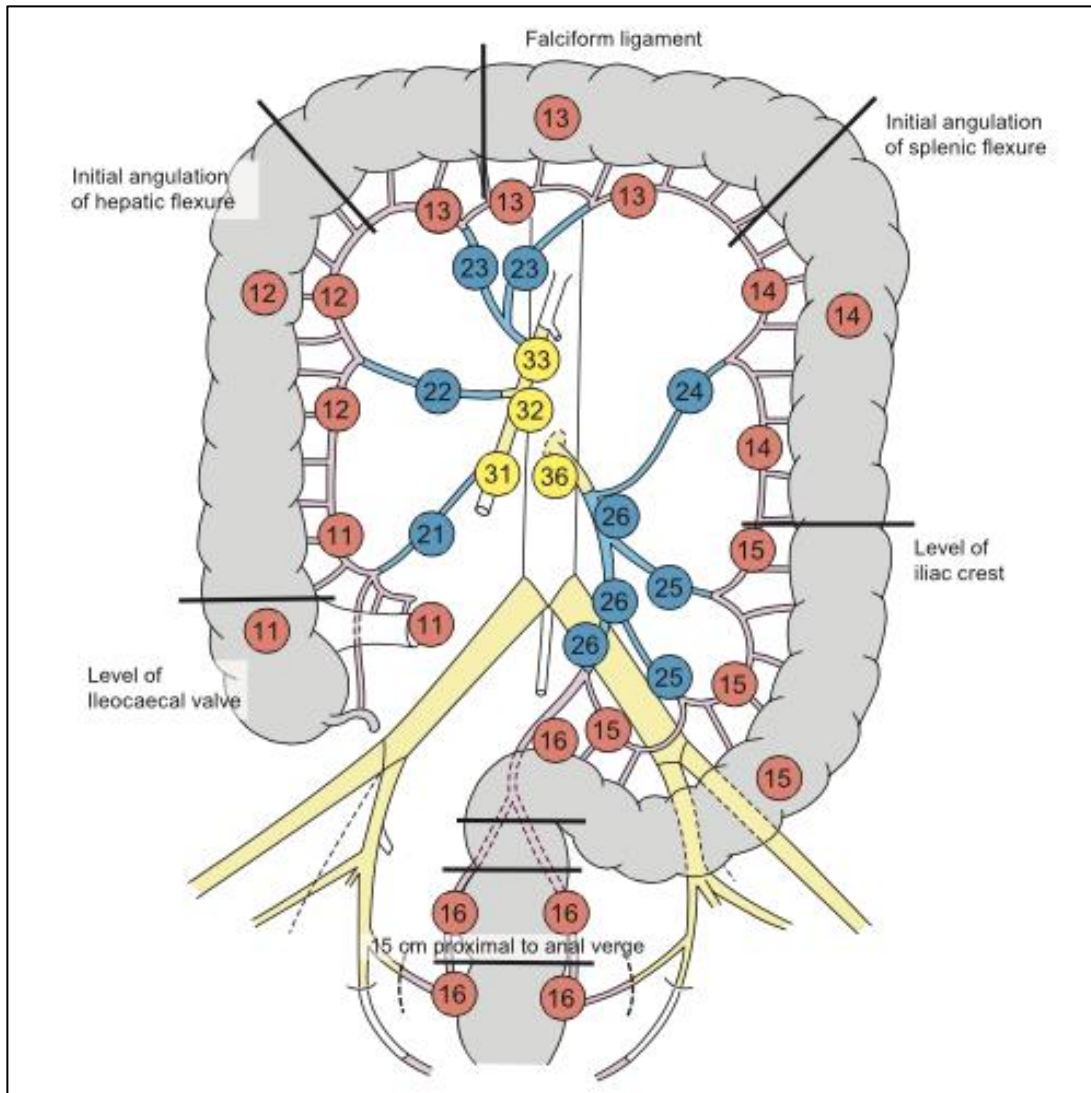


**Figure 1.1. Diagram depicting different levels of lymph node stations within colonic mesentery.** Taken from Andrew *et al.*(9). D1 lymph nodes = red, D2 nodes = blue, and D3 nodes = yellow. Coding for the lymph node stations; the first number of the code indicates the position of the lymph node and correlates with its colour (epicolic and paracolic D1 lymph nodes are denoted as 1X, intermediate D2 lymph nodes are denoted as 2X and the D3 lymph nodes are denoted as 3X) and the second number indicates the position of the lymph node along the main arterial trunk (X1 nodes follow the ileo-colic artery, X2 follow the right colic artery, X3 follow the middle colic artery, X4 follow the left colic artery, X5 follow the sigmoid artery and X6 follow the superior rectal artery). For example, lymph node station 21 represents intermediate D2 nodes located along the ileo-colic artery.

Currently, there is no reliable method to confirm the presence of lymph node metastases prior to histopathological examination of the resected colorectal specimen. This presents a clinical dilemma; if the patient has undergone a D2 lymphadenectomy and positive lymph nodes are found upon histological examination, then there is potential for residual

disease to persist within the higher level (D3) nodes. Conversely, if there is no disease present in the lymph nodes then the patient has had a more extensive resection than required.

### **1.1.2 Complete mesocolic resection and D3 evidence**

The basis of CMR is the resection of the tumour and its draining lymphatics and vascular supply within a complete mesocolic envelope of mesenteric fascia and visceral peritoneum, similar to the now familiar total mesorectal excision (TME) dissection for rectal tumours(17,18). There is evidence suggesting lower rates of local recurrence and improved 5-year disease-free survival with complete mesocolic resection (CMR) of the tumour with central vascular ligation or extended D3 lymphadenectomy(19–23).

Hohenberger *et al.*(19) introduced the technique of CMR and central vascular ligation into their surgical unit and were able to demonstrate with prospective data a 7% increase in 5-year survival and a 2.9% reduction in local recurrence rates compared with conventional resection. Bertelson *et al.*(24) performed a retrospective study comparing the disease-free survival in 1031 patients with conventional resections for their colonic tumours versus 364 patients who underwent CMR. They showed an increase in 4-year disease-free survival of 10.2%, 14% and 6% in stage I, II and III disease respectively. CMR was shown to be a significant independent predicative factor for improved disease-free survival on multivariable Cox regression.

Advocates for CMR or extended D3 lymphadenectomies highlight the oncological advantages in the technique in addition to a higher yield of excised LNs which studies have shown correlate to an increased survival rate(17,19). Chang *et al.*(25) performed a systematic review to determine whether the number of LNs examined following resections of colon cancer impact the patients oncological outcomes. Of the 17 studies included in the review, 16 demonstrated improved survival outcomes in patients with

stage II colon cancer with an increased number of evaluated LNs although they acknowledge that a minimum or threshold number of LNs could not be determined. Their review also showed that of six studies that looked specifically at stage III disease four studies were able to demonstrate improved survival outcomes with increased examined LNs. Studies have also suggested an additional survival benefit with increasing numbers of negative LNs within the resected specimen(17). West *et al.*(23) demonstrated a 15% increase in 5-year survival in patients with stage III disease who had a complete mesocolic resection of their tumour with no disruption of the mesocolic envelope.

Saha *et al.*(26) conducted an investigation into the lymphatic mapping of 500 consecutive patients with colorectal cancer and found the incidence of skip metastases to be 11% for colon cancer and 7% for rectal tumours. This means that even if all the examined lymph nodes within the resected specimen are negative for metastatic disease there may be D3 nodes or nodes outside of the traditional resection territories which are node positive. Supporters of CMR or extended D3 lymphadenectomy propose that skip metastases should be included in within the specimen addressing this issue(17,18).

Criticisms of CMR and extended D3 lymphadenectomy include the lack of robust evidence of benefit as there have been no randomised controlled trials comparing the technique to standard conventional resection, doubts about the validity of the survival advantages and concerns regarding the exposure of patients to additional risks and functional problems(17,20). The study by Hohenberger *et al.*(19) showed increased disease-survival rate with reduced local recurrence when comparing CMR with extended D3 lymphadenectomy to conventional surgical resection in a large series of patients within a single unit. However, this study fails to take into account the introduction of adjuvant chemotherapy, which occurred around the same time as the change in surgical technique, and represents a significant confounding factor in these reported results(17).

It has also been suggested that the survival benefits seen in CMR and extended D3 lymphadenectomy actually represents upstaging of tumours from stages I-II to III-IV with the increased likelihood of discovering occult LN metastases.

There are concerns that an extended D3 lymphadenectomy might expose patients to increased intraoperative risks(27,28). CMR guidelines advise en-bloc resection of the LNs at the origin of the supplying vessel to the tumour but this exposes patients to the risk of nerve damage as well as vascular injury(18). Nerve injuries can lead to severe diarrhoea, sexual dysfunction and urological disorders. Killeen *et al.*(29) conducted a systematic review evaluating CMR with an extended D3 lymphadenectomy against patient survival statistics, local recurrence rates, and morbidity and mortality. Most of the studies were retrospective in nature, and there were no randomised control trials to provide more robust data. The review concluded that there were limitations within the included studies, such that CMR with extended D3 lymphadenectomy could not be recommended as standard practice, although the report did acknowledge that complications, morbidity and mortality rates of CMR with extended D3 lymphadenectomy were comparable to standard resections.

It should also be noted that, as the vast majority of patients undergoing colorectal cancer surgery do not have lymph node disease, performing an extended lymphadenectomy in every individual would be over-treating ~70% of patients with node negative disease and potentially expose them to unnecessary risk with an unclear evidence base of survival benefit for doing so. In addition, LN metastases outside the conventional field of resection can be missed even with extended lymphadenectomy(18), under-treating a small proportion of patients. The parallel progression model of LN metastases theorizes that nodal involvement reflects the underlying biological behaviour of the tumour(30), indicating that these tumours are more aggressive and have disseminated cancer cells

early in their life span. If this model is correct it would suggest that the poor survival outcomes of patients with nodal disease is related to the tumour biology and therefore the extent of lymphadenectomy would not greatly impact the patient outcomes.

Improvement in the ability to accurately stage the disease and locate metastatic disease prior to resection of the specimen would enable clinicians the opportunity to determine whether more extensive dissection of the LNs does in fact confer a survival advantage to patients and to strategize and counsel patients appropriately.

## **1.2 Staging of colorectal cancer**

### **1.2.1 Current practice and importance of lymph node staging**

The staging system most commonly used is the TNM system classified by the American Joint Committee on Cancer (AJCC) and is based on the extent of the tumour growth (T), presence of disease within the regional lymph nodes (N), and spread to distant sites (M) (Table 1.1). Standard practice in the UK, as recommended by The National Institute for Health and Care Excellence (NICE), is for patients with colorectal cancer to have a contrast-enhanced CT scan of the chest, abdomen and pelvis to provisionally stage the disease(5). CT scanning indicates how far the tumour has penetrated through the bowel wall, potential involvement of regional lymph nodes, and the presence of distant metastatic disease(31), which are all prognostic factors. Patients with rectal cancer also undergo MRI to assess the resection margin, which determines whether surgery can completely remove the cancer or whether "down-staging" neo-adjuvant therapy is required.

<b>Table 1.1.TNM Classification of Malignant Tumours staging system (8<sup>th</sup> edition)(32)</b>		
<b>Tumour</b>		
T0		No evidence of primary tumour
Tis		Carcinoma in situ
T1		Tumour confined to submucosa
T2		Tumour grown into (but not through) muscularis propria
T3		Tumour grown into (but not through) serosa
T4	a	Tumour penetrated through serosa and peritoneal surface
	b	Perforation of bowel
Tx		Main tumour cannot be assessed due to lack of information
<b>Nodes</b>		
N0		No regional lymph nodes contain tumour cells
N1	a	Tumour cells present in 1 regional lymph nodes
	b	Tumour cells present in 2-3 regional lymph nodes
	c	Tumour deposits present locally but regional lymph nodes do not contain tumour cells
N2	a	Tumour cells present in 4-6 regional lymph nodes
	b	Tumour cells present in $\geq 7$ regional lymph nodes
Nx		Regional lymph nodes cannot be assessed due to lack of information
<b>Metastases</b>		
M0		No metastasis to distant organs
M1	a	Metastasis confined to one organ

	b	Metastasis in $\geq 1$ organ
	c	Metastasis to the peritoneum +/- other organ involvement
Mx		Metastasis cannot be assessed due to lack of information

Staging of colorectal cancer is important because it determines whether the cancer is curable with surgery alone, or whether adjuvant chemo/radiotherapy is required. Staging also enables identification of patients with resectable distant metastatic disease, for instance within the liver. Patients who undergo resection of liver metastases have a 40% 5-year survival rate compared with 0% survival at 5 years in untreated patients or patients with unresectable liver metastases(31).

### 1.2.2 Limitations of current staging strategies

CT and MRI are both limited in the accuracy of predicting nodal status in patients with colorectal cancer. Radiological criteria for possible lymph node metastases include irregular lymph node walls, calcification and nodes over 1cm in size. However, these criteria can be misleading, for example normal sized lymph nodes can contain metastases whereas enlarged lymph nodes can simply be reactive(31). For staging purposes, therefore, the value of radiological imaging is mainly to predict the depth of penetration of the tumour through the bowel wall and the presence of distant metastatic disease.

A prospective study investigating CT scanning to identify lymph node metastases showed a diagnostic accuracy of 58% (95%CI: 48, 68), sensitivity of 64% (95%CI: 48, 77) and specificity of 53% (95%CI: 39, 67)(33). A meta-analysis of 19 studies with a total of 907 patients indicated sensitivity and specificity for CT-detected malignant lymph nodes of 70% (95%CI: 59, 80) and 78% (95%CI: 66, 86)(34) respectively.

Positive emission tomography (PET) also has a role in assessing patients with primary and recurrent colorectal cancers. It has long been demonstrated that malignant tissues have an increased rate of glycolysis due to the increased presence of glucose transporters on the plasma membranes of cancer cells, such as GLUT-1, in addition to the increased expression of glycolysis rate-limiting enzymes, such as hexokinase(35). This phenomenon is exploited during FDG-PET imaging where the majority of malignant cells show an increased uptake of the glucose analogue, fluoro-2-deoxyglucose (FDG)(35). A prospective study of 104 patients comparing the pre-operative staging of colorectal cancer between conventional CT imaging and fluorine-18 fluorodeoxyglucose PET (FDG-PET) showed that the results for determining the nodal status between the two imaging modalities were similar(31). The accuracy for CT and FDG-PET were found to be 60% and 56% respectively. The sensitivity for detecting nodal disease was 25% and 21% respectively for CT and FDG-PET. The authors concluded that although 2-3mm sized lymph nodes could be seen on these imaging techniques the reliable detection of metastatic nodes remains impossible using radiological imaging alone.

### **1.2.3 Area of clinical need**

In order for the radicality of surgery to be tailored to the fitness of the patient and the biology of the primary cancer it is necessary to accurately identify, either preoperatively or during intraoperative assessment, the nodal status of the patient prior to surgical resection. Without an accurate knowledge of lymph node status, introducing a routine policy of radical resection with extended lymphadenectomy could have a detrimental effect on the outcome for elderly patients(9). The incidence of lymph node metastases in early cancer is low and therefore radical resection with extended lymphadenopathy would again be exposing patients to increased surgical risks with no survival benefit(9,27). Current radiological staging is not sensitive enough to accurately detect lymph node metastases pre-operatively(33,34,36). Therefore, there is a need for a

clinical modality to accurately predict nodal status in patients, prior to a decision regarding the extent of lymphatic resection.

## **1.3 Strategies to improve staging of lymph node involvement**

### **1.3.1 Sentinel lymph node biopsy and mapping**

Sentinel lymph node biopsy (SLNB) and mapping was first described in 1992 by Morton *et al.* investigating patients with melanoma(37) and is a technique that has been developed to aid lymph node identification during surgery. The sentinel lymph node (SLN) is defined as the first regional lymph node that receives lymphatic drainage from the primary tumour and is considered to be the first potential site for lymphatic metastasis. Sentinel node mapping is based on the concept that the status of the sentinel lymph node reflects the status of the remaining regional lymph nodes(38). Therefore, if the sentinel lymph node does not contain any metastases it is assumed that the remaining lymph nodes are also free of metastatic activity(39).

Sentinel lymph node mapping (SLNM) involves a peritumoural injection (Figure 1.2) of a colorimetric dye, such as methylene blue. It is given prior to resection and ligation of the supplying vasculature and it spreads through the draining lymphatic system, allowing the draining nodes (Figure 1.3) to be identified (13,37). A radioisotope tracer is frequently added to the colorimetric dye in an effort to improve detection rates and diagnostic accuracy(40).

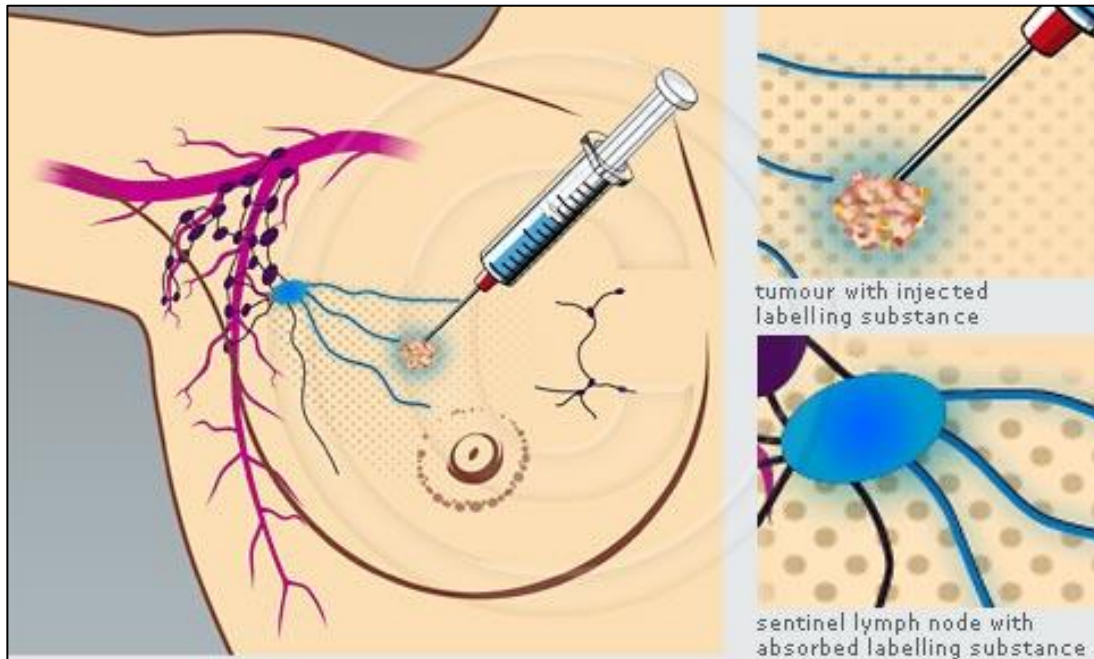


**Figure 1.2. Illustration depicting sentinel lymph node mapping technique in breast cancer surgery.** Taken from [www.medicallook.com](http://www.medicallook.com)(41). The labelling agent is injected into the breast tumour where it disperses into the lymphatic system enabling the surgeon to identify the initial lymph nodes within the axilla receiving the lymphatic drainage from the malignant tissue.

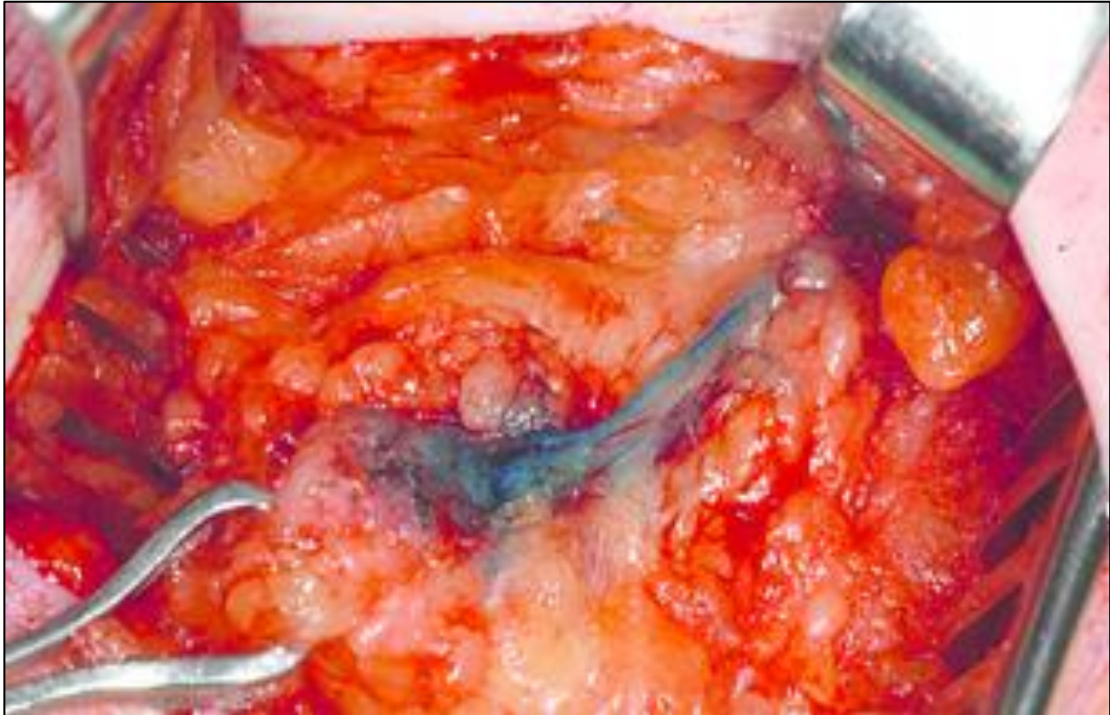


**Figure 1.3. Axillary sentinel lymph node identified during lymphatic mapping in a breast cancer patient.** Taken from ClinicalGate(42). Intraoperative photograph demonstrating lymphatic vessels draining into an axillary sentinel lymph node during a sentinel lymph node biopsy for breast cancer staging. The lymphatic vessels and lymph nodes are easily identifiable due to the presence of the colorimetric dye, methylene blue.

SLNB has become routine practice for certain cancers, such as breast cancer (43,44). It has reduced the morbidity associated with axillary lymph node clearance to determine lymph node status. SLNB has been shown to be accurate at predicting the nodal status in breast cancer and melanoma patients (45). This has stimulated a number of studies investigating whether SLNB can be used in other cancers. Some early studies of SLNB in colorectal cancer have suggested improved staging, increased lymph node yield(26,46) and evidence of aberrant lymphatic drainage outside the planned resection area(45). Saha *et al.*(47) used blue dye sentinel lymph node mapping in 192 patients with colon cancer and found that aberrant lymphatic drainage was present in 22%. These patients subsequently underwent extended mesenteric dissection and interestingly there was a higher incidence of nodal disease within this sub-cohort compared to those patients without aberrant drainage (62% vs 43%).

Sentinel lymph node mapping techniques have also been attempted with oesophago-gastric tumours, with the intention of avoiding unnecessary lymphadenectomy and permitting the use of minimally invasive techniques whilst maintaining adequate oncological resection. Matsuda *et al.*(39) used a dual tracer technique in 15 patients with junctional oesophago-gastric tumours and managed to detect a mean of 5.5 SLNs per patient with a 100% identification rate. 56% of SLNs were detected with radioactivity alone, 20% with only methylene blue dye and the remaining 24% were both blue and radioactive. Sensitivity was 100%, however, only two patients in the cohort of 15 had nodal disease and therefore these results may not be truly representative due to the low numbers. An additional limitation to this study is that only patients with cT1 N0 M0 tumours of a diameter < 4cm were included, which have a low incidence of nodal disease (2-18%)(48). Ishizaki *et al.*(49) investigated 101 patients with T1/2 gastric cancer to determine if SLNM with blue dye alone could accurately stage the nodal status and consequently be used to prevent unnecessary gastrectomy with D2 lymphadenectomy in node-negative patients. They found an identification rate of 100%, with a sensitivity of 85.7% and 3 false-negatives (3%). The main concern regarding this study is that although it has a large number of patients, changes were made to histopathological examination of the LNs, with extensive examination of all SLNs and non-SLNs in the last 32 patients, accounting for a third of the cohort. This increased the sensitivity and reduced the false-negative rate, but it is unfeasible to implement such extensive examination of all lymph nodes in standard practice. A similar, smaller study of 29 patients was conducted by Cozzaglio *et al.*(48) in T1/2 gastric cancer patients, using blue dye SLNM performed by a single operator. The detection rate was 96.6% although the authors excluded the single patient where a SLN was not identified from further analysis. The sensitivity was 75% with a false-negative rate of 18%. Collectively, the main conclusions from these studies is that conventional SLNM is technically feasible in oesophago-gastric cancer patients but is lacking in the ability to accurately stage the nodal status of the patient and therefore cannot be recommended.

### **1.3.1.1 Sentinel lymph node mapping in colorectal cancers**

Difficulties in utilising SLNM techniques in colorectal cancer could be attributable in part to the higher complexity and non-linear distribution of the lymphatic pathways in the colon, as compared to the breast(50). In addition to the anatomical challenge in colorectal cancer, the current gold standard is a full lymphadenectomy as described earlier and sentinel node studies have not yet demonstrated sufficient accuracy at identifying nodal status to influence surgical strategy. Neoadjuvant chemotherapy(26) or radiotherapy(13) can cause sclerosis of the lymphatic pathways, resulting in a distorted lymphatic anatomy. Other technical errors include incorrect injection of dye, insufficient experience with the technique, resecting the specimen before or immediately after dye injection thereby disrupting the lymphatic basin, and the administration of an insufficient volume of dye(13,51). There is also the potential issue of tumour deposits within the lymphatic channels causing obstruction and thereby affecting the results of SLNM(52). It has been suggested that the lower identification rates in obese patients is attributable to the lipophilic nature of the colorimetric dye(13,45,51). Sentinel lymph node mapping has disadvantages including the limited tissue penetration of the colorimetric dyes, making identification of deeper lymph nodes difficult. The use of dyes for SLNM has also been associated with causing potential allergic reactions(53). Laparoscopic lymphatic mapping has posed problems with the correct identification of the peritumour injection site, particularly when the tumours are small(50), as well as intra-abdominal spillage of the dye(52). Radioisotopes carry the disadvantage of potential harm from ionising radiation, as well as posing difficulties in handling radioactive substances in the operating theatre (40). Colorimetric dyes carry the potential risk of adverse reactions, which include a mild urticarial reaction, discoloured urine, interference with pulse oximetry, and severe anaphylaxis(44).

Bembenek *et al.*(45) performed a controlled multi-centre prospective trial, enrolling 315 patients with colon carcinoma. The primary aim of the study was to establish whether SLNB using colorimetric dye alone in these patients could accurately predict the nodal status of the specimen. Nineteen university hospital centres were recruited for the study. The study design was strong with a sizable cohort of patients, however, peritumoural injection of the dye was performed following mobilisation of the colon which may have influenced the results. If the SLN was clear of disease on routine sectioning more invasive histopathological techniques (Haematoxylin & Eosin staining and immunohistochemistry) were performed. 85% of patients in the study had at least one sentinel lymph node detected although this was significantly affected by the experience of the centre. A ROC-curve analysis demonstrated a learning curve with a cut-off of 22 patients. The SLN detection rate in centres with less than 22 patients was 76.4% compared to 91% in centres with more than 22 patients.

Within the Bembenek *et al.*(45) study, 31% of the cohort had positive nodal disease. The sensitivity of SLNB in this cohort was 54%, with a false-negative rate of 46%, which the authors acknowledged clearly does not support using SLNB in colon cancer to stage nodal disease. Further subset analysis indicated that there was an effect on the sensitivity of SLNB related to the patient's body mass index (BMI). A ROC-curve analysis showed that the sensitivity of SLNB increased to 80% where the BMI was less than or equal to 24. The sensitivity was 42% in patients with a BMI greater than 24. Sixteen patients out of 315 met the criteria of having a BMI  $\leq$  24 and had their SLNB and resection performed in a centre with more than 22 patients enrolled in the study. Analysis of these 16 patients results showed a sensitivity of 88%, which is still too low to recommend implementing this strategy into current practice. Although numbers are low, it would be interesting if the study was repeated to see what the detection rates, sensitivity and false-negative rates would be if these parameters were part of the trial inclusion criteria.

Another area of interest in SLNM in colon cancer is whether it could identify aberrant lymphatic drainage thereby altering the resection margins. Bembenek *et al.*(45) found aberrant drainage in only five patients (1.6% of the cohort), with no evidence of metastatic disease in the aberrant nodes and concluded that blue dye SLNB could not be relied upon to identify the resection margins of the tumour specimen. The study also assessed whether SLNB could be used to upstage patients by identifying micrometastases and isolated tumour cells within the SLN. There was an overall upstaging rate of 21.3% in node negative patients which increased to 24.2% in the clinically important Stage II patients. However, the prognostic significance of micrometastases and isolated tumour cells is unclear, and there is no current evidence to alter patient's post-operative management on the basis of these histopathological findings.

Bianchi *et al.*(50) agree that in today's climate with changing demographics and minimally invasive techniques, such as natural orifice transluminal endoscopic surgery (NOTES), there should be an emphasis on avoiding unnecessary extended lymphadenectomy. The authors propose that sentinel lymph node mapping could be an effective solution. They published results from a cohort of 75 patients over five years with early disease colon cancer and demonstrated a false-negative rate of 22.2%.

Furthermore, in ~10% of patients, *ex vivo* lymphatic mapping was necessary to identify at least a single sentinel lymph node. A smaller cohort of eight patients who received a radiocolloid tracer, instead of the colorimetric dye, showed an impressive negative predictive value of 100% with no false-negatives or side-effects from the tracer. This shows promise, but it is difficult to judge these results with such a small cohort of patients and there is a lack of data investigating the combination of colorimetric dye and radiocolloid tracer in colon cancer.

Park *et al.*(52) compared *in vivo* versus *ex vivo* SLNM techniques to determine whether either techniques could improve nodal staging by focused intensive histopathological examination of the SLN. The study was conducted in a cohort of 69 consecutive patients with colorectal cancer. The authors described that *ex vivo* SLNM could be as accurate as *in vivo* SLNM but without the disadvantages inherent in performing blue dye mapping intraoperatively. In both techniques, the specimen was mobilised prior to blue dye injection. This raises the concern that the results could have been affected by disruption of the lymphatic pathways. Overall, with the combination of the two techniques, the overall SLN detection rate was 85.5% with 89.8% accuracy, 81.2% sensitivity, and 18.8% false-negative rate.

The detection rates of SLN were 81.1% and 90.6% for the *in vivo* and *ex vivo* techniques, respectively. With regard to accuracy (93.1% vs. 86.6%), sensitivity (86.7% vs. 76.5%) and false-negative rates (13.3% vs. 23.5%), the *ex vivo* technique outperformed the *in vivo* technique, although no significant difference was found between the results. Neither technique has performed adequately to recommend a change to clinical practice. Although *ex vivo* SLNM had similar results to *in vivo* SLNM, the authors have not addressed the issue of missing any aberrant lymphatic drainage with the *ex vivo* technique. They also fail to justify *ex vivo* SLNM with respect to disrupting the lymphatic pathways by resecting the specimen and ligating the supplying vasculature.

The overall disease recurrence rate in patients with early stage node-negative disease is 20-30% and this is thought to be due to inadequate lymphadenectomy, histopathological understaging of the specimen or a combination of the two. Chan *et al.*(44) hypothesised that SLNM could reduce the recurrence rate by accurately identifying patients with positive nodal disease and enabling focused histopathological examination of the SLN.

They conducted a prospective trial of blue dye SLNM in 31 patients undergoing surgery for colorectal cancer and demonstrated a detection rate of 80.7%. The detection rate for colonic tumours was 94.7% (19 patients) compared with 58.3% for rectal tumours. The false-negative rate was 21.4% with a sensitivity of 78.6% and an accuracy of 88%. The sensitivity of SLNM in colonic versus rectal tumours was 75% and 83.3% respectively. The discrepancy between the colonic and rectal tumour results was attributed by the authors to the time delay between peritumoural submucosal injection of the dye via a proctoscope and visual inspection of the specimen for SLNs, which is a plausible explanation. The results from this study (with the exception of the detection rate in the colonic tumours alone) are in concordance with other studies. However, there are several concerns regarding the methodology. In addition to the tumour being mobilised prior to blue dye injection, the median number of LNs harvested from the patients was 6 with a mean of 7.48. This is below the recommended minimum of 12 harvested LNs(54) and therefore raises questions either about the surgical technique or the histopathological examination.

Albayrak *et al.*(13) had a SLNM detection rate of 94.7% in a cohort of 38 colon cancer patients with a sensitivity of 100% and a false-negative rate of 0% using blue dye. The authors suggested that their high detection and accuracy rates could be related to the fact that the procedure was carried out by an experienced single operator in patients with Stage I-III disease. However, the numbers are low, especially compared with studies such as Bembenek *et al.*(42), and are not representative of other larger studies.

In Japan, patients with T3/4 low rectal tumours undergo radical extended retroperitoneal and lateral pelvic lymphadenectomy (RLPL) as part of their standard surgical resection. However, this technique is not part of Western practice mainly due to the increased morbidity, the low incidence of nodal metastases within this distribution of lymph nodes,

and the belief that disease present in these nodes may represent incurable, systemic disease(55). Japanese surgeons, therefore, have a similar dilemma faced by breast surgeons prior to SLNB, where they were unnecessarily exposing node negative patients to the increased morbidity of axillary clearance. Quadros *et al.*(55) used a combination of blue dye and radiocolloid tracer to investigate SLNB in 97 patients undergoing resection of invasive rectal adenocarcinoma by a single surgeon. Although this is a worthwhile endeavour, which at first glance has favourable results with an accuracy of 100%, sensitivity of 100% and a 0% false-negative rate, there are a number of serious issues with the study. Firstly, the TME was performed prior to lymphatic mapping, which potentially disrupts the lymphatic pathways, and secondly the authors analysed the accuracy, sensitivity and false-negative rates in patients where identification of SLNs was achieved; this only occurred in 37.1% of the cohort which is a low identification rate. In addition, only blue radioactive SLNs underwent intensive histopathological analysis due to budget constraints and therefore the false-negative data could potentially be inaccurate.

Van der Zaag *et al.* performed a meta-analysis(56) of 57 studies comprising a total of 3934 patients investigating sentinel lymph node mapping in colorectal cancer. The majority of studies were conducted using an *in vivo* technique. However, there were a number of studies using the *ex vivo* technique and eight studies used a combination of the two. Identification of the SLNB was either by colorimetric dye alone or with a radiocolloid tracer; 11 studies used a dual approach. Although the meta-analysis showed an overall detection rate of 92%, there was an overall false-negative rate of 30% and a diagnostic accuracy of 69%. It should be noted that only 10 out of 57 studies had a cohort larger than 100 patients. Mulsow *et al.* (57) conducted an earlier similar systematic review of SLNM methods including both blue dye and radiocolloid tracer alone and with a combination of both as well as *in vivo* and *ex vivo* techniques. Their results demonstrated low and variable detection rates of 58-98%, with sensitivity rates

varying between 40% and 100%. They also reported a high false-negative rate of up to 60%. Therefore, sentinel lymph node mapping as a staging procedure in colorectal cancer resections is not routinely practiced.

Typically, histopathologists examine a single section level in each lymph node for metastases on standard analysis of a resected specimen. Metastatic foci of tumour cells can be unevenly distributed throughout the node and therefore missed using this technique, ultimately understaging the patient(13). This is termed tissue allocation bias and can be reduced by intensive histopathological analysis, in combination with immunohistochemistry (IHC). However, this is time consuming and expensive, rendering it impossible to employ for every node harvested from each patient. Retter *et al.*(51) suggested that sentinel lymph node mapping could be employed to better identify patients who should have more intensive examination of their lymph nodes. A prospective study in 31 patients undergoing laparoscopic resection of colon cancer using blue dye only was undertaken and showed a sentinel lymph node detection rate of 90%. It was noted that sentinel lymph node mapping was not achievable in the patients with morbid obesity (two patients), and it was felt this could be related to the lipophilic nature of the patent blue dye. Twelve patients had stage III disease and it was found on a subset analysis of these patients that there was a high false-negative SLNB rate of 66%. This suggests that perhaps SLNB should only be considered in patients with early stage disease, especially given that SLNB is recommended only for small to medium sized tumours in patients with melanoma or breast cancer(58). The published data from this study has not included the number of patients with positive nodal disease, which precludes confirmation of the statistical analysis. However, the rate of upstaging from stage II to stage III disease by employing intensive histopathological techniques in patients with sentinel lymph nodes containing metastatic disease was 5%. Although there were low numbers in the study, the authors felt that given the poor results and an accuracy of 14%, SLNB could not be supported in predicting the nodal status of patients

with colon cancer. One factor not considered within this study is that sentinel node mapping was performed post mobilisation of the colon which may have disrupted the lymphatic pathways producing poor results.

The above studies have also shown that blue dye sentinel lymph node mapping is safe and does not caused additional harm to patients(51).

In summary, SLNM in colorectal cancer patients has not been able to achieve the high SLN identification and sensitivity rates, as well as the low false-negative rates, achieved with SLNM in melanoma and breast cancer patients. This means that with the current techniques available, SLNM with blue dye +/- radiocolloid tracer, cannot be recommended for intraoperative lymph node staging for colorectal adenocarcinoma.

### **1.3.2 One Step Nucleic Acid Amplification**

NICE has recently recommended the use of One Step Nucleic Acid Amplification (OSNA) *in vitro* diagnostic molecular assay system in the post-operative staging of colorectal cancer(59). This system detects the level of a biomarker, cytokeratin-19 (CK19), which correlates with the number of metastatic cells present in the examined tissue and was originally developed as a tool to reduce the burden of pathologists examining SLNs for breast cancer patients(60). Although this technique was developed for use in breast cancer, several other studies have explored using OSNA in other tumours such as gastric, lung, thyroid and colorectal cancer. Three studies(61–63) investigating the use of OSNA in patients with colorectal cancer, with a combined total of 253 patients and 2,232 lymph nodes, showed a sensitivity of 92.5-94.5%, a specificity of 96.5-97.6% and an upstaging of node negative to node positive disease in up to 25% of patients. A more recent study conducted in Japan included 284 patients and examined

1925 lymph nodes using the OSNA system. Yamamoto *et al.*(64) showed a concordance rate of 95.7% between one slice of H&E staining and OSNA with a sensitivity of 86.2% and specificity of 96.5% for the latter technique.

OSNA allows the entire lymph node to be assessed thereby reducing the effect of tissue allocation bias and has been shown to be more accurate than standard histopathological assessment. However, it is unclear whether the increased detection of malignant lymph nodes is due to OSNA detecting micrometastases, which are of uncertain clinical significance(65), and one study suggested that intensive histopathological assessment with IHC had comparable results. Currently, OSNA is only recommended for assessment of lymph nodes obtained from the pathology specimen. However, there is scope to investigate its ability to assess sentinel lymph nodes taken at the time of surgery in order to facilitate intraoperative decision-making.

### **1.3.3 Fluorescence-guided surgery in colorectal resections**

#### **1.3.3.1 Fluorescence**

A potential solution to intra-operative lymph node staging involves fluorescence-guided surgery with the intention of allowing identification of the tumour and the presence of lymph node metastases. Several photoactive drugs have been investigated for this purpose, including indocyanine green (ICG) and 5-aminolevulinic acid (5-ALA).

Fluorescence refers to the emission of light from a photoactive molecule (fluorophore) after it has absorbed electromagnetic radiation from an external source and ceases as soon as the exciting radiation is withdrawn. This phenomenon can be exploited clinically with fluorescence imaging, whereby a fluorophore is exposed to the excitation radiation and a light detecting instrument is used to detect and image the emitted light.

The emission of light from a molecule is termed luminescence; luminescence is further characterised into fluorescence and phosphorescence depending on whether the luminescence is due to excitation of an electron in the singlet or triplet state respectively. Fluorescence occurs when a fluorophore (a fluorescent chemical compound that can re-emit light upon excitation) is exposed to a wavelength that causes an electron to transition from the ground state to a maximal energy level, termed the excited electronic singlet state(68–70). The fluorophore will undergo atomic structural changes releasing some energy, for example as heat, and the electron falls to a lower and more stable energy level, the singlet state. Return of the electron to ground state from singlet state involves the emission of residual energy (Figure 1.4). The surplus energy is then released as fluorescence(68,70). The emitted light is usually of lower energy than the absorbed light and is therefore of a longer wavelength (as the wavelength is inversely proportional to the energy of light)(68). Fluorescence will cease once the stimulating excitation source is removed, whereas phosphorescence will persist as an afterglow. The lifetime of a fluorophore is the average of the length of time between the excitation of the electron and its return to ground state(70). As long as the fluorophore is not damaged irreversibly in its excited state the process can be repeated. Photobleaching occurs when high intensity illumination degrades the fluorophore during its excited state where the molecular structure is unstable, irreversibly changing the structure so the fluorophore can no longer fluoresce(71,72).

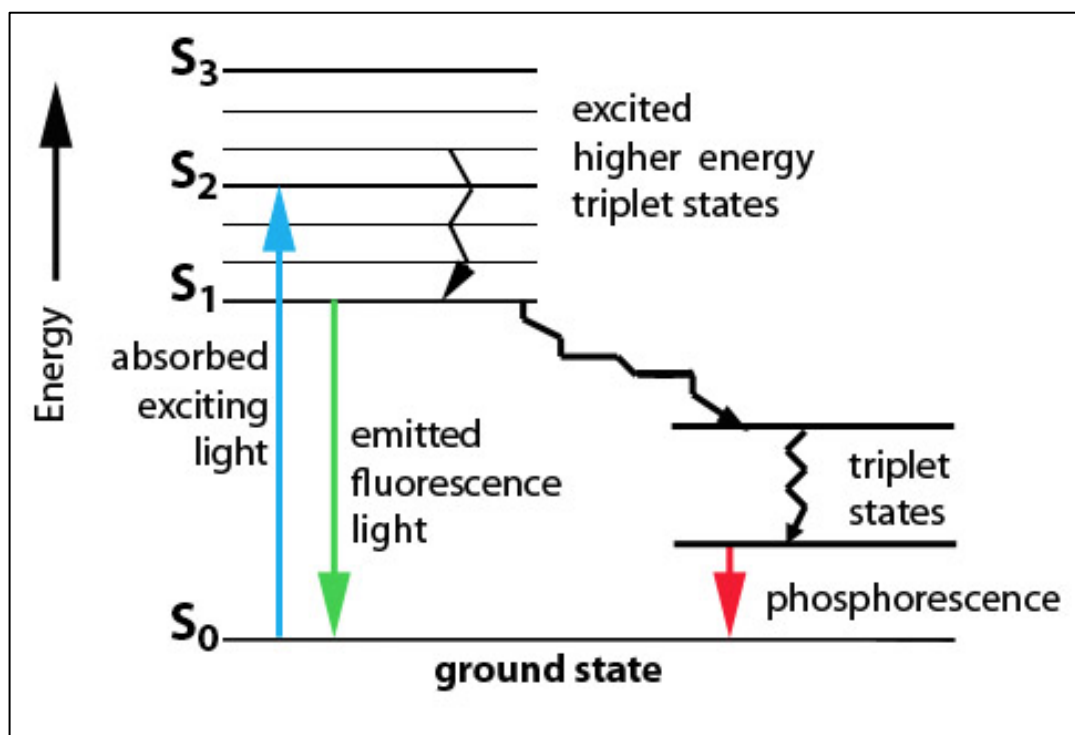


**Figure 1.4. Energy level diagram for fluorescence (Jablonski Diagram).** Taken from [https://gauravtiwari.org/jablonski-diagram/\(292\)](https://gauravtiwari.org/jablonski-diagram/(292)).  $S_0$  = resting ground state,  $S_1$  = excited electronic singlet state,  $S_2$  = second excited electronic singlet state. A Jablonski diagram illustrates the transition of a molecule through its electronic states following exposure to an excitation wavelength. When a fluorophore is exposed to light energy, it's excited to a higher vibrational energy level in the first excited state ( $S_1$ ) before relaxing to the lowest  $S_1$  energy level. Fluorescence represents the release of the surplus energy as the electron returns from the lowest  $S_1$  energy level back down to resting ground state,  $S_0$ .

If the emitted photon has less energy than the absorbed photon (as highlighted in Figure 1.4) the energy difference is termed the Stokes shift, after the Irish physicist George Gabriel Stokes. This can be represented as the difference between the peaks (band maxima) of the excitation and emission spectra of the fluorophore(73). An example of an approved fluorescent probe called Indocyanine Green is shown in Figure 1.5. The band maxima of the excitation and emission spectra are 788nm and 813nm respectively giving a Stokes shift value of 25nm.

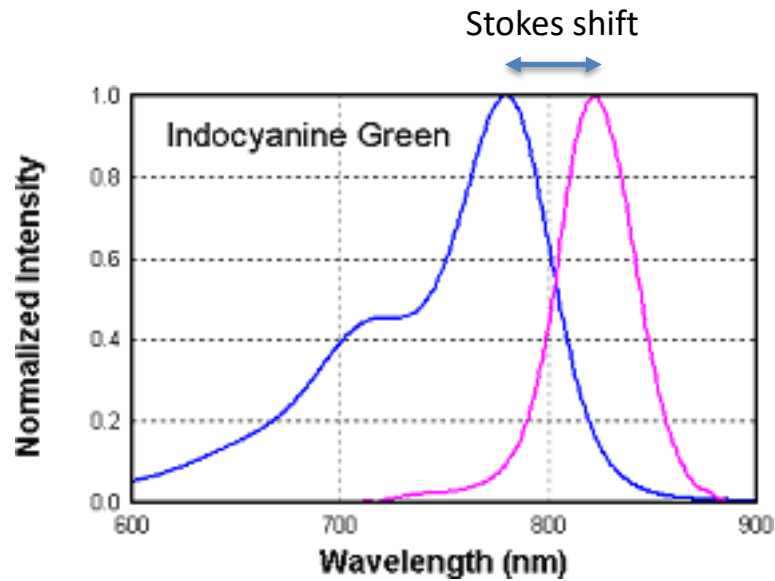


**Figure 1.5. Excitation and emission spectra of Indocyanine Green in water.** Taken from [www.iss.com](http://www.iss.com)(293). Blue = fluorescence excitation spectra, purple = fluorescence emission spectra. This excitation and emission spectra depict the change in the intensity of fluorescence of indocyanine green as a function of wavelength measured by a spectrofluorometer scanning across the desired wavelength range.

The brightness or intensity of a fluorophore is determined by the quantum yield and the extinction coefficient. Quantum yield in terms of fluorescence refers to the ratio of the number of photons emitted to the numbers of photons absorbed through fluorescence. Increasing the intensity of the exciting irradiation may increase the brightness of the emitted fluorescence, however this may impact on the photostability of the probe(74). The extinction coefficient is dependent on the fluorophores chemical and structural composition and is a value depicting how strongly the fluorophore absorbs light radiation at a particular wavelength. Therefore, increased intensity in the emission of photons from a fluorophore results in increased overall brightness. Anything that decreases the intensity of the fluorescence of a given fluorophore is a reversible process known as quenching. Photostability of a fluorophore refers to its resistance to reactions or processes that induce quenching(71) and can be measured as the time taken for 50% of the fluorescent brightness to dissipate.

Photodynamic diagnosis (PDD) utilises these properties of fluorophores to help identify and visually localise tumour tissue for diagnostic purposes. Photodynamic therapy (PDT) involves the administration of photosensitising agents which are taken up and retained within cells. Under non-light conditions these compounds possess negligible toxicity. However, upon exposure to light of a specific wavelength these compounds will generate reactive oxygen species, resulting in oxidative stress and cellular destruction(75). There are several clinical advantages that near infra-red (NIR) fluorescent probes hold over other fluorophores. This includes minimal tissue autofluorescence and light absorption; tissue autofluorescence is due to the presence of different fluorescent biological structures such as flavins, collagen and mitochondria, which absorb in the range of 355-488nm and emit in the range of 350-550nm(76). NIR wavelengths are also invisible to the human eye, with no visual impact on the surgical field and have deep tissue penetration (up to 1cm)(16,77,78).

Examples of photosensitising agents that are currently being utilised for PDT in clinics today include Photofrin and 5-ALA. Photofrin has been approved to treat many cancers including bladder, oesophageal and endobronchial cancers(79) and 5-ALA is in routine use for the treatment of dermatological malignancies(9,80). A drawback to many photosensitisers is their hydrophobicity which significantly reduces their clinical potential(69,81). This is in addition to being limited by their lack of tumour specificity, tendency to form aggregates, poor circulation pharmacokinetics, short half-lives and adverse cutaneous photosensitive reactions(9,82). These disadvantages have prompted the incorporation of photosensitisers within a nanomedicine system in order to overcome limitations and actively target the photosensitiser against the desired tumour tissue. A study by *Patel et al.*(83) encapsulated a fluorescent dye, indocyanine green, into poly(lactic-co-glycolic acid) nanoparticles (NPs) which were then conjugated to different targeting ligands (RGD-4C peptides, folic acid and R11 peptides). There was significant increase in uptake of the targeted dye-loaded NPs in the prostate cancer cell line, PC3,

as compared to the bare non-targeted NP, suggesting their potential for photodynamic therapy.

### **1.3.3.2 Indocyanine Green**

Indocyanine green (ICG) is a Food and Drug Administration (FDA) approved fluorescent probe which has previously been used for fluorescence-guided surgery. In comparison to the colorimetric dyes used for SLNM, ICG possess a safe toxicity profile. ICG accumulates within malignant tissue and is retained for a prolonged time as compared to benign and normal tissues(84). Activation of ICG with NIR light results in fluorescence in the malignant tissue with negligible fluorescence in surrounding tissues (Figure 1.6).

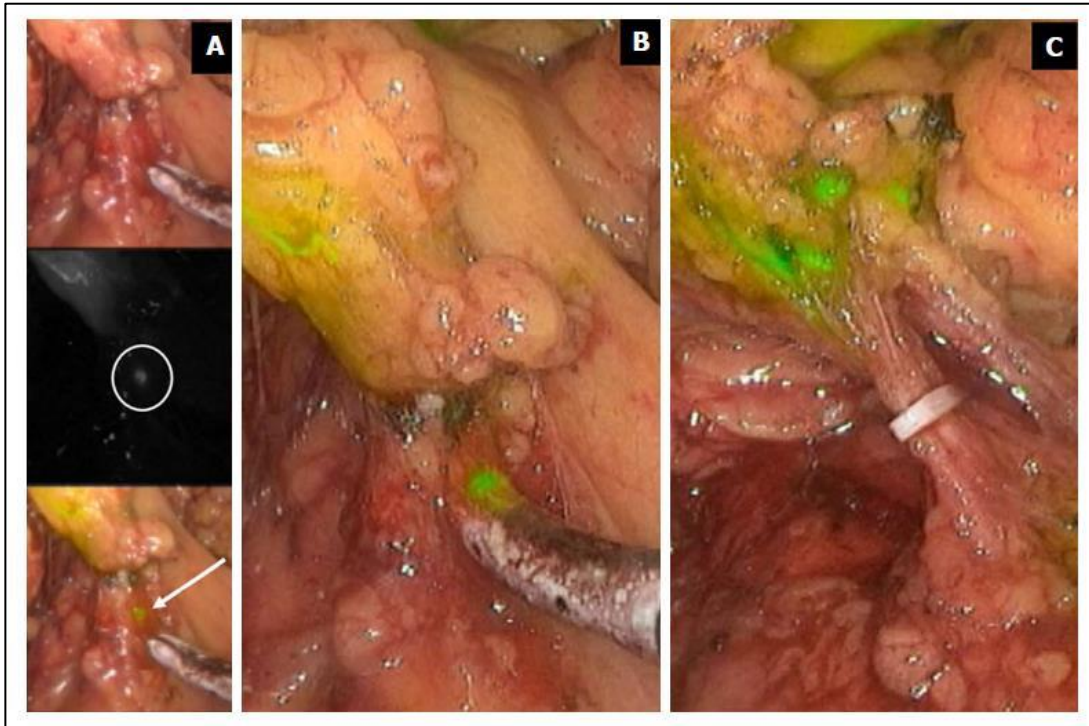


**Figure 1.6. ICG fluorescence during laparoscopic right hemicolectomy showing the position of regional lymph nodes within the mesentery.** Taken from Barocchi *et al.*(85). A – Laparoscopic visualisation of the ileocolic pedicle under white non-fluorescent light (top image), under fluorescence (middle image) and the composite overlay view of both white and fluorescent light (bottom image). B – Laparoscopic composite overlay view during dissection of the ileocolic pedicle demonstrating the presence of a fluorescent lymph node. C – Laparoscopic composite overlay view of the fully dissected ileocolic pedicle with lymph nodes visible within the mesocolic tissue due to ICG fluorescence.

Sentinel lymph node mapping using ICG has previously shown high identification rates of 83-100% with a low number of false-negatives (<6%) in patients with breast, gastric, anal and skin cancers(86–89). It has also been reported that the sensitivity of blue dye SLNM is affected by the patient's body mass index (BMI)(45), but this does not appear to be the case for ICG SLNM(90–92). Emile *et al.*(93) showed that the results of ICG SLNM were optimal when the ICG dose was calculated based on the patients weight as opposed to a standard dose. Limitations of ICG fluorescence includes the rapid clearance of the dye, meaning that training in the technique is essential to achieve high identification and accuracy rates(94).

Hirche *et al.*(12) presented data where ICG dye was used to identify and map the sentinel lymph nodes in 26 patients with colon cancer. Fifteen patients underwent open surgery whereas the remaining 11 patients had laparoscopic resections. The sentinel lymph node identification rate was 96%, with a sensitivity of 82% and a false-negative rate of 18%. The study was conducted by two surgeons experienced in fluorescence-guided surgery although exact details regarding their experience was not documented. The results appear promising and show that ICG fluorescence-guided surgery is technically feasible in colon cancer, however, the study population was small with only 26 patients. A further limitation is that the description of the method of peritumoural injection is unclear. It appears that two different methods were employed, which were not related to whether the patient had open or laparoscopic surgery. From the authors' discussion it may be that an *in vivo* and *ex vivo* technique was used for ICG SLNM as they have claimed that the two techniques were comparable in their study but have not given any subset data analysis to support this claim.

Cahill *et al.*(94) also investigated the use of ICG in the intraoperative identification of sentinel lymph nodes in laparoscopic colorectal cancer resections. In this study, 18 consecutive patients were included. Thirteen patients had localised colorectal cancer, four had endoscopically unresectable dysplasia, and the remaining patient had a polyp cancer. All patients demonstrated lymph node fluorescence, including four patients where fluorescent lymph nodes were identified outside the conventional field of resection indicating aberrant lymphatic drainage. None of the aberrant lymph nodes contained metastatic disease which is in keeping in with the fact that ICG fluorescence is not tumour specific.

Liberale *et al.*(84) have published initial data from a prospective trial investigating whether intravenously administration of ICG intraoperatively could detect LN metastases

in patients with colorectal cancer. They have reported the outcomes on their first two patients demonstrating that the technique is feasible and should be investigated further as the results are promising. With their first patient, *in vivo* fluorescence did not detect any SLNs. However, with an *ex vivo* technique three SLNs were detected, all of which contained metastatic disease. All remaining LNs were non-fluorescent. The second patient presented with recurrent disease following a previous right hemicolectomy and no evidence of LN involvement on CT or PET-CT imaging. *In vivo* and *ex vivo* fluorescent ICG imaging detected a single LN outside the planned resection margin which was found to be the only metastatic deposit in the specimen.

Intraoperative sentinel node mapping using ICG has also been evaluated in open, early stage gastric cancer surgery. It has been suggested that ICG fluorescent guided surgery might address the high rate of extended lymphadenectomy. Miyashiro *et al.*(38) conducted a study which comprised 241 patients with T1/2 N0 gastric cancer and found the technique accurately identified SLNs in 99.6% patients, with a false-negative rate of 10.3% and false-positive rate of 1.4%. Positives from this study are the high identification rates in a large patient cohort with no adverse reactions to ICG reported. Tajima *et al.*(89) had previously investigated ICG fluorescence-guided surgery in 77 patients undergoing surgery for early gastric cancer and evaluated the technique between open (39 patients) and laparoscopic (38 patients) groups. Similar detection rates were found between the laparoscopic (94.7%) and open (94.9%) groups. The accuracy and false-negative rates were 97.2% and 25% respectively in the laparoscopic group and 91.9% and 23.1% respectively in the open group. The higher false-negative rates in this study may be explained by the smaller patient sample. This study demonstrates the feasibility of ICG fluorescence-guided surgery in both the laparoscopic and open setting.

Yuasa *et al.*(95) described a novel approach for sentinel lymph node navigation in patients with superficial oesophageal cancer by combining ICG fluorescence with preoperative CT lymphography. This study consisted of a group of 20 patients who underwent endoscopic submucosal injection of a water-soluble iodine contrast medium surrounding the tumour 5 minutes prior to their routine staging CT, which enabled visualisation of the lymphatic drainage from the primary tumour. ICG was injected around the tumour during surgery and the lymphatic drainage was visualised intraoperatively. The detection rate of sentinel lymph nodes was 100% with CT lymphography and 95% with ICG fluorescence. In this study three out of the 20 patients had lymph node metastasis within sentinel lymph nodes that had been detected on both techniques with an accuracy of 95%. However, histopathology showed an additional malignant sentinel lymph node that both techniques missed.

None of the studies described above reported any adverse side-effects related to ICG occurring in any participating patient.

Accurate probes that can be used intraoperatively to predict nodal status would go a long way towards preventing unnecessary lymphadenectomy and reducing operative morbidity. However, ICG cannot currently be recommended for intraoperative nodal staging as part of standard practice due to the sub-optimal sensitivity and high false-negative rates.

### **1.3.3.3 5-aminolevulinic acid**

5-aminolevulinic acid (5-ALA), an endogenous compound within the human body, is metabolised within the cell mitochondria as part of the heme biosynthesis pathway to generate Protoporphyrin IX (PPIX), a precursor to heme. PPIX is a fluorescent molecule

which emits between 630 to 700nm when excited by blue-violet light (405nm) and is a potent photosensitiser. 5-ALA is taken up preferentially into malignant cells which have a higher metabolic rate than normal cells, altered levels of transporter molecules compared to normal cells and differences between the concentrations of the opposing catalytic enzymes porphobilinogen deaminase and ferrochelatase to normal cells. This typically allows generation of large amounts of PPIX within the cell. Under normal physiological conditions a negative feedback mechanism is triggered by the production of heme to prevent an excess production of endogenous 5-ALA and subsequent PPIX(80). This phenomenon is exploited in fluorescent-guided surgery, whereby exogenous 5-ALA is administered which can override the negative feedback mechanism and increase the production of intracellular PPIX. The excess PPIX cannot be quickly converted to heme and therefore this photosensitiser remains within the cell for a prolonged period of time, up to 48 hours(9). Upon irradiation with blue-violet light, cells with excessively accumulated intracellular PPIX levels will fluoresce allowing detection of malignant cells enabling photodynamic diagnosis(80) (Figure 1.7). When administered in high doses and exposed to the appropriate wavelength 5-ALA is cytotoxic to cells exhibiting a photodynamic therapeutic effect. However, in lower doses it can be used for purely photodynamic diagnostic purposes.

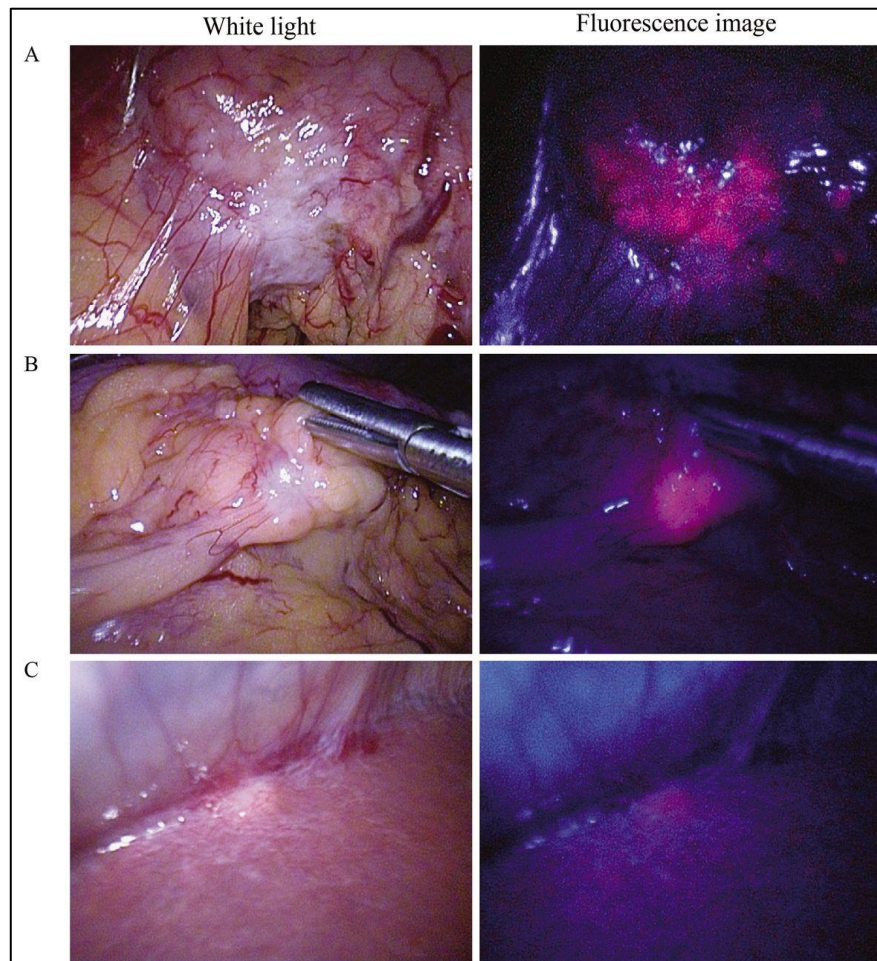


**Figure 1.7. 5-ALA fluorescence of colonic tumour and lymph node metastases within mesentery.** Taken from Andrew *et al.*(9). A + B – Laparoscopic visualisation of a caecal tumour during a right hemicolectomy under white light (left hand images) and under fluorescence (right hand images). C – Laparoscopic intraoperative visualisation of a pericolic D1 lymph node during the resection under white light (left hand image) and under fluorescence (right hand image).

Side-effects reported with the use of 5-ALA include photosensitivity, nausea, vomiting, tachycardia, hypotension and elevated liver function tests. However, no safety concerns or serious adverse effects have been documented in any published clinical studies(80).

There have been several clinical studies investigating the use of 5-ALA as a photodynamic diagnostic agent in fluorescence-guided surgery for bladder transitional cell carcinoma(96–98), detection of endometriosis(99) and peritoneal metastases in ovarian cancer(100). Neurosurgeons have also used exogenous 5-ALA to improve

tumour detection and clearance of resection margins in glioma tumours(101–103). In addition, there have been several studies advocating the use of 5-ALA for the detection of colorectal tumours and metastases(11,104–108). Interest in the use of 5-ALA as a photodiagnostic agent also extends to the detection of colon cancer and its ability to accurately detect lymph node metastases, which was investigated in the GLiSten clinical trial(9). This study included 41 patients, 19 of whom had nodal disease and compared two cohorts to assess the optimum dosage of administered 5-ALA (cohort 1 patients received a dose of 20mg/kg and cohort 2 patients received 30mg/kg). 5-ALA showed low sensitivity (11.1% and 0% for cohorts 1 and 2 respectively) and specificity (75% for both cohorts 1 and 2) for colonic tumours and their lymph node metastases. The trial report concluded that 5-ALA was not accurate enough to detect lymph node metastases and therefore could not be used for intraoperative staging of colon cancer.

## **1.4 Nanomedicine**

The increased understanding of the mechanisms and pathophysiology of diseases has resulted in progress in the development of novel treatments. In anti-cancer research there have been significant advancements in the production of new chemotherapy agents. Despite having improved mechanisms of action and being more efficacious than classical anti-cancer drugs, newer classes of drugs still possess many limitations(109). These include problems with drug-dose toxicities (narrow therapeutic index), lack of specificity and poor pharmacokinetics i.e. rapid clearance from systemic circulation mainly due to their low molecular weights. Traditionally chemotherapy agents are given systemically into the circulation and will affect rapidly proliferating cells and tissues, giving rise to potent adverse toxicities which can limit the dose administered and, in some cases, can result in the premature termination of treatment. Common unwanted side-effects of chemotherapy include hair loss, nausea and vomiting, anaemia, fatigue,

neurosensory toxicity, insomnia, immunosuppression, anorexia, mucositis and weight loss among others. Another disadvantage of chemotherapy is the development of acquired and multi-drug resistance to treatment in cancers, particularly within recurrent tumours(110).

The advantage of directly targeting treatment towards cancers would mean a reduction in the amount of anti-cancer drug given and reduction in adverse toxicities in healthy normal tissue. Ultimately this would reduce the side-effects experienced by the patient and increase the efficacy of the treatment(110).

The first example of a targeted drug therapy to be used clinically is Tamoxifen, however, it was not initially developed or intended as a treatment for breast cancer. Tamoxifen was created as part of an antifertility project to discover a new non-steroidal anti-oestrogen oral contraceptive in the 1960s by a pharmaceutical company now known as AstraZeneca(111). Tamoxifen showed promising results in murine studies, but had the opposite effect in humans and improved fertility. The development of Tamoxifen transitioned into breast cancer treatment with potential for its application in antagonising the hormone oestrogen, which is involved in the growth of breast cancers. Tamoxifen inhibits the binding of oestradiol to oestrogen receptors which appears to block the transcription of growth factor genes (for example HER-2) within breast tumour cells(112), thereby reducing the rate of cell proliferation. Clinical trials(113–116), the first beginning in the 1970s, have supported its use in the treatment of advanced breast cancer patients.

Nanomedicine refers to the use of nanotechnology in clinical applications for diagnosing or treating diseases such as cancer(117). Nanomedicine formulations are submicrometer-sized carriers(118) that are being investigated to overcome the

pharmacokinetic limitations of these novel chemotherapy agents by prolonging their retention within systemic circulation and improving delivery of the drug to the specific target site.

Nanoparticles are of interest in nanomedicine formulations due their inherent advantages of size and physical-chemical properties. NPs currently being investigated for clinical use include quantum dots, polymeric NPs or micelles, gold NPs, liposomes, dendrimers as well as carbon nanotubes and nanofibers(119). NPs can range from 20nm to 200nm in size which is large enough to avoid clearance through the renal excretion system, enabling prolonged circulating time while being small enough to travel across cell membranes(119). NPs can be designed to incorporate hydrophilic, hydrophobic, amphiphilic compounds as well as those that are negatively or positively charged enabling them to be present in environments where they would normally be rendered inactive. For instance, many chemotherapy agents are hydrophobic and are difficult to dissolve in solution however encapsulating these hydrophobic or positively charged compounds within NPs can improve their solubility and increase drug dose delivery(120). NPs can also be created to be structurally large and flexible enough so that different compounds can be encapsulated within the NP resulting in high drug loading, as well as allowing the development of combination therapy(121,122). NPs can be internalised into cells by endocytosis effectively bypassing mechanisms of resistance to drug delivery(123).

The surface of NPs can also be modified to allow conjugation of chemotherapy agents or targeting molecules. Functionalising the surface of NPs with targeting or recognition molecules such as antibodies, peptides, DNA or RNA affimers is of great interest as this would allow specific delivery of the NP, with either its diagnostic or therapeutic abilities, to the target tissue thereby increasing the efficacy of the nanomedicine formulation. NPs

can also be designed to aid in diagnosis of disease as well as improving the efficacy of imaging modalities(110).

## **1.4.1 Targeting of tumour**

### **1.4.1.1 Passive targeting**

Passive targeting of tumours exploits the pathophysiological mechanism termed the enhanced permeability and retention (EPR) effect, which was originally described by Matsumura and Maeda in 1986(124). Malignant tumours develop more aggressively than normal tissues and many advanced tumours can induce angiogenesis. However, this often results in a poorly structured vascular network which is hyperpermeable and allows the leakage of fluid and macromolecules from systemic circulation(125–127). NPs can extravasate from the micro vessels and into the interstitial spaces within the tumour microenvironment. Under normal physiological conditions the lymphatic system drains interstitial fluid back into the systemic circulation and eliminates any macromolecules that may have leaked out. However, within the tumour microenvironment improper lymphatic drainage coupled with the leakiness of tumour vasculature means that macromolecules (such as NPs) can accumulate and are retained, resulting in an elevated interstitial fluid pressure(128). This elevated pressure reduces the transport of macromolecules(129) and diffusion is hindered by the dense extracellular matrix(130). Passive targeting of tumours uses the EPR effect to increase the concentration of the NPs in the peritumoural area (Figure 1.8).

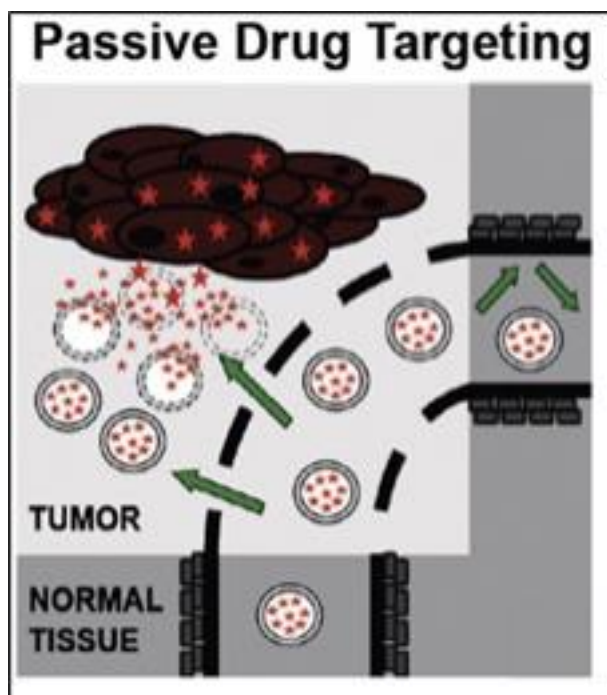


**Figure 1.8. Diagram illustrating Passive drug targeting.** Taken from Lammers *et al.*(118). The leaky vessels in the tumour microenvironment can allow macromolecules such as NPs to passively extravasate and accumulate within the interstitial spaces and increase the concentration of NPs in the tumour vicinity. Grey spheres represent the NP drug delivery system with the therapeutic drug depicted as red stars.

Kim *et al.*(131) utilised the EPR effect to treat SCC7 (murine head and neck carcinoma cell line) xenografts *in vivo*, using cisplatin-loaded glycol chitosan NPs. Using a NIR non-invasive imaging technique they were able to demonstrate improved localisation of fluorescence within the tumour xenografts as compared to free cisplatin control. As a result, cisplatin-loaded glycol chitosan NPs showed better anti-tumour efficacy and lower adverse toxicity than free cisplatin. Another study by Cho *et al.*(132) developed sodium deoxycholate-heparin NPs to target tumours *in vivo* using the EPR effect. Athymic BALB/c-nu/nu female nude mice were used with a KB (human epidermoid carcinoma cell line) xenograft. The study showed that overall tumour volume was reduced in the group treated with the NPs as compared to the control group that received saline only. Chytil *et al.*(133) used a murine lymphoma model to determine the effect of doxorubicin-HPMA co-polymer micelle conjugate which targets the tumour via passive targeting and the

EPR effect. Their study demonstrated increased antitumour activity, slower blood clearance and enhanced tumour accumulation of the drug-copolymer conjugate compared to free doxorubicin.

Despite a large number of studies advocating the use of the EPR effect for passive targeting of tumours, clinical studies have shown no advantage or increased efficacy(130,134). Maeda *et al.* suggest that inadequately vascularised tumours, such as prostatic or pancreatic tumours, will naturally display a lower tendency for the EPR effect. They also argued that the EPR effect may be affected by obstruction within the vascular supply due to thrombus formation which could potentially account for the lack of increased efficacy within clinical studies(135). The EPR effect was discovered using murine models and has been well documented in other small animal studies. However, murine models may not translate well into humans(124). Human clinical cancers have significant differences, particularly in the tumour microenvironment, as compared to murine models (Figure 1.9). This is in part due to the accelerated tumour development in murine models. Tumours are induced in immunocompromised mice allowing them to develop large tumours in as little as 2 weeks, in addition to causing a change in tumour-to-body weight ratio(110). These features are not representative of clinical tumour growth thereby resulting in disparities in the ability of macromolecules to utilise the EPR effect between murine and human cancers. The rapid growth of the murine tumour compared to human cancers could potentially result in poorer development of the tumoural vasculature with increased hyperpermeability due to increased fenestrations with the endothelium and poorer pericyte coverage(118). In human tumours, varying fenestrations in the vascular endothelium results in a heterogenous distribution of hyperpermeability or extravasation of the macromolecules(130). The EPR effect can also vary largely with intra- and inter-heterogeneity between different pre-clinical tumour models and also between clinical cancers(118).

Further heterogeneity within human tumours is also demonstrated by the presence of hypoxic areas (Figure 1.9) resulting from the proliferation of malignant cells at sites away from the nearest supplying blood vessel(130). The poor vascularity of the core compared to the periphery means that any nanomedicine is required to diffuse across large distances and pass through multiple layers of cells and extracellular matrix in order to access all areas of the tumour. Blood flow within the tumour vasculature is also noted to be transient due to their inherent abnormal and poor development, limiting the supply of oxygen and exacerbating the hypoxic effect(136).

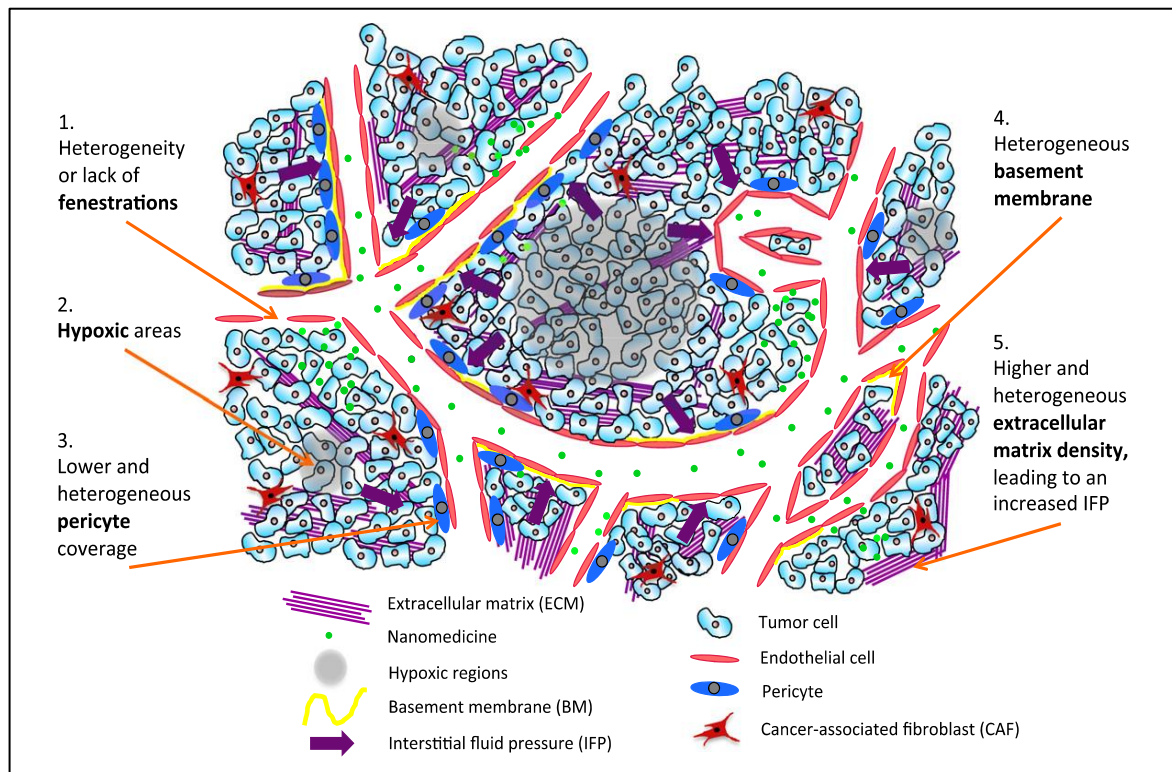


**Figure 1.9. Representative diagram of the tumour micro-environment and passive targeting of a nanomedicine system using the EPR effect.** Taken from Danhier *et al.*(130). The tumour microenvironment consists of different stromal cells (fibroblasts, endothelial cells, pericytes), the extracellular matrix, tumour vasculature and the tumour, differing markedly from murine models: 1 – heterogenous distribution of fenestrations within human tumour vasculature, 2 – human solid tumours tend to contain hypoxic areas due to heterogenicity of blood flow through the tumour, 3 – the pericyte coverage and degree of attachment varies throughout a human tumour whereas all tumour vasculature has low and loose pericyte coverage in murine models, 4 – the morphology of the basement membrane varies within a single tumour, 5 – the extracellular matrix is more dense and thick in human tumours compared with murine models.

The tumour micro-environment in human cancers differs from murine models (Figure 1.9). Examples of such differences include the level of pericyte coverage on the endothelial cells, differences within the basement membrane (BM), and differences in the composition and density of the extracellular matrix (ECM). The BM is a specialised form of the ECM and is composed of layers of laminin and type IV collagen that anchors epithelial cells to the underlying connective tissue and separates it from the endothelium. The density of the BM and the number of layers within it vary and form a barrier to extravasation of nanomedicines(137–139). The endothelial cells composing tumour vasculature in clinical cancers are covered with a layer of smooth muscle cells and

pericytes to varying degrees of coverage(140). The neo-vasculature in colorectal cancers generally has a thinner layer of pericyte coverage, as compared to glioblastoma for example, and heterogeneity in pericyte coverage is also observed between different types of colorectal cancers(130). A higher level of pericyte coverage means that there is a thicker layer for macromolecules to permeate through before reaching the tumour tissue. The ECM represents the last barrier that nanomedicines have to cross before reaching their target tissue.

Interstitial fluid allows the exchange of oxygen, nutrients and waste products between cells and systemic circulation. Interstitial fluid pressure refers to the hydrostatic and colloid osmotic pressures exerted by the interstitial fluid and is affected by the EPR effect, which increases the pressure due to the increased concentration of macromolecules present in the interstitial fluid(128). Diffusion and convection are the main molecular transport mechanisms across the ECM, and elevated interstitial fluid pressure will hinder larger sized nanomedicine compounds, reducing the effectiveness of the EPR effect(109,141). In human cancers the ECM is more abundant than tumours in murine models and this reduces the ability of large nanomedicines to penetrate through to the target tissue(140).

In summary, the EPR effect has shown great promise in numerous studies and many nanomedicines that have been developed rely upon this mechanism. However, there are several factors that affect the efficacy of EPR in clinical cancers hindering the translation of pre-clinical results into clinical practice. Indeed, despite the complexity of nanomedicine preparations within the literature, very few have been approved by the FDA and those that have been are relatively simple in design(142).

#### **1.4.1.2 Active targeting**

Active targeting of nanomedicines refers to the concept whereby functionalising the nanomedicine with a recognition agent, such as an antibody, will enable the nanomedicine to selectively bind to the desired target site (antigen) thereby improving the efficacy of treatment(118). Passive targeting increases the accumulation of the nanomedicine within the peritumoural area and active targeting aims to improve uptake of the nanomedicine within the target cancer cell (Figure 1.10). Active targeting of tumours uses one of two approaches; the first being to exploit the specific biochemical interactions between a ligand and its corresponding target molecule and the second approach taking advantage of either internal or external signals(126) such as pH or enzymatic reactions. Tumours are known to induce the upregulation of specific cell surface markers, for example the carcinoembryonic antigen (CEA) is upregulated in colorectal tumours(143). Therefore, functionalising a nanomedicine with a CEA-targeting ligand will actively target cells overexpressing CEA thereby increasing the intracellular uptake of the nanomedicine with little to no effect on non-CEA expressing cells. The development of molecular probes that actively target tumours for diagnostic and therapeutic purposes constitutes a large area of current anti-cancer research.

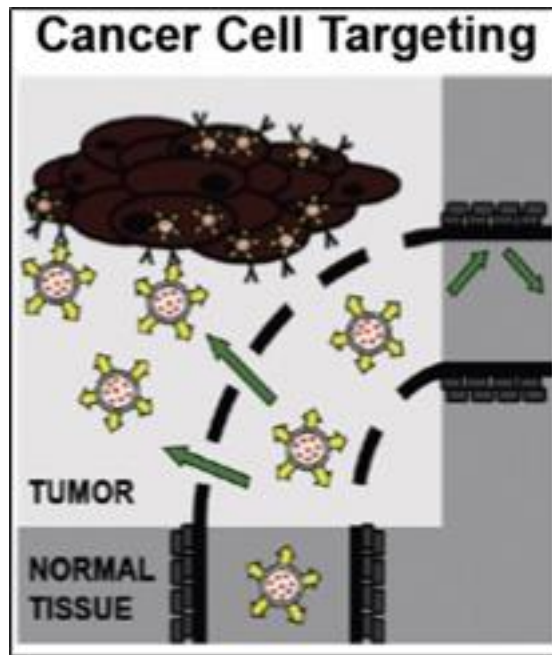


**Figure 1.10. Diagram illustrating Active drug targeting.** Taken from Lammers *et al.*(118). The leaky vessels in the tumour micro-environment can allow macromolecules such as functionalised NPs to passively extravasate and accumulate within the interstitial spaces. The targeting ligands conjugated to the NPs can recognise and bind to tumour cell specific antigens, thereby increasing the uptake of NP into cells. Grey spheres represent the NP drug delivery system, the therapeutic drug depicted as red stars with the yellow arrows representing the targeting ligand.

The aim of modifying the surface of nanomedicines with recognition molecules is to promote accumulation, internalisation and retention of the macromolecule within the tumour. However, active targeting also relies upon the EPR effect in order for the targeted nanomedicine to accumulate within the region of the tumour, and therefore suffers from similar limitations as passive targeting(118,134). In order to target cancers actively, the recognition molecule must be conjugated to the nanomedicine. Most of the biochemical conjugation systems used are based upon covalent bonds. Commonly used conjugation reactions use carbonyl reactive groups, amine reactive groups or Click Chemistry(144,145). Another commonly used high affinity conjugation reaction is the non-covalent interaction between (strept)avidin and biotin(144).

### 1.4.2 Recognition molecules

Recognition molecules or targeting agents include but are not limited to small molecules, peptides, proteins, whole antibodies, antibody fragments, and NPs(121,129). The recognition molecule on its own or conjugated to a nanomedicine can be considered as a form of a molecular probe. The ideal characteristics of an effective molecular probe are summarised in Table 1.2.

<b>Table 1.2. Ideal characteristics of a molecular probe</b>
High binding affinity to target
High specificity to target
High sensitivity to detect the biochemical process of disease
High contrast ratio
High stability in vivo
Low immunogenicity and toxicity
Feasible and economical production

In the 1960s there was interest within the research community to explore unique cancer cell surface antigens that could identify malignant from benign tissue for the purposes of diagnosis and therapy(146,147). This followed the discovery that the cell surface membrane is highly differentiated with different types of cells exhibiting a profile of cell surface markers that enabled differentiation(148). Following extensive resections to surgically remove colorectal tumours, healthy colorectal tissue can be harvested from the same patient providing a control to the tumour tissue. The disparity in expression of cell surface markers between healthy and tumour tissue could potentially be exploited. Animal studies using rabbits compared benign and malignant colonic tissues from the

same animal using immunologic tolerance and absorption techniques(146) and found a single unique antigen present in higher concentrations in colonic malignant tissue than benign tissue; carcinoembryonic antigen (CEA). CEA has subsequently been shown to be upregulated in all tumours originating from the endoderm of the digestive system as compared to their corresponding normal healthy tissue(149). CEA is therefore one of several cell surface antigens being investigated as potential targeting agents for colorectal tumours.

#### **1.4.2.1 Antibodies**

Antibodies (also known as immunoglobulins) are the most common recognition molecules used for active targeting. Monoclonal antibodies have been used extensively to actively target tumours due to their high affinity and specificity(119). Initially, monoclonal antibodies were generated from mouse hybridoma technology(150). However, this produced an immunogenic reaction upon introduction into a human host. This reaction resulted in the rapid clearance of the murine monoclonal antibody from the circulation thereby greatly reducing its clinical efficacy. Chimeric (a combination of sequences from different species, most commonly human and murine) and fully humanised monoclonal antibodies have subsequently been developed that exhibit lower immunogenicity(150,151).

Antibodies have a basic structure composed of two heavy and two light polypeptide chains held together by disulphide bonds(152) forming a Y-shape as shown in Figure 1.11. Immunoglobulin G (IgG) antibodies are approximately 150KDa with each heavy chain approximately 50KDa and the light chains being 25KDa. The antigen recognition and binding fragment of the antibody (Fab) is formed by the interaction of the two identical domains, comprised of the whole of the light chain and half of the heavy chain. This interaction folds the Fab fragment into a complex globular structure and is highly

specific giving antibodies their high affinity and specificity properties(153). The Fab fragment contains the three hypervariable amino acid domains (variable domains) which give the antibody its specificity.

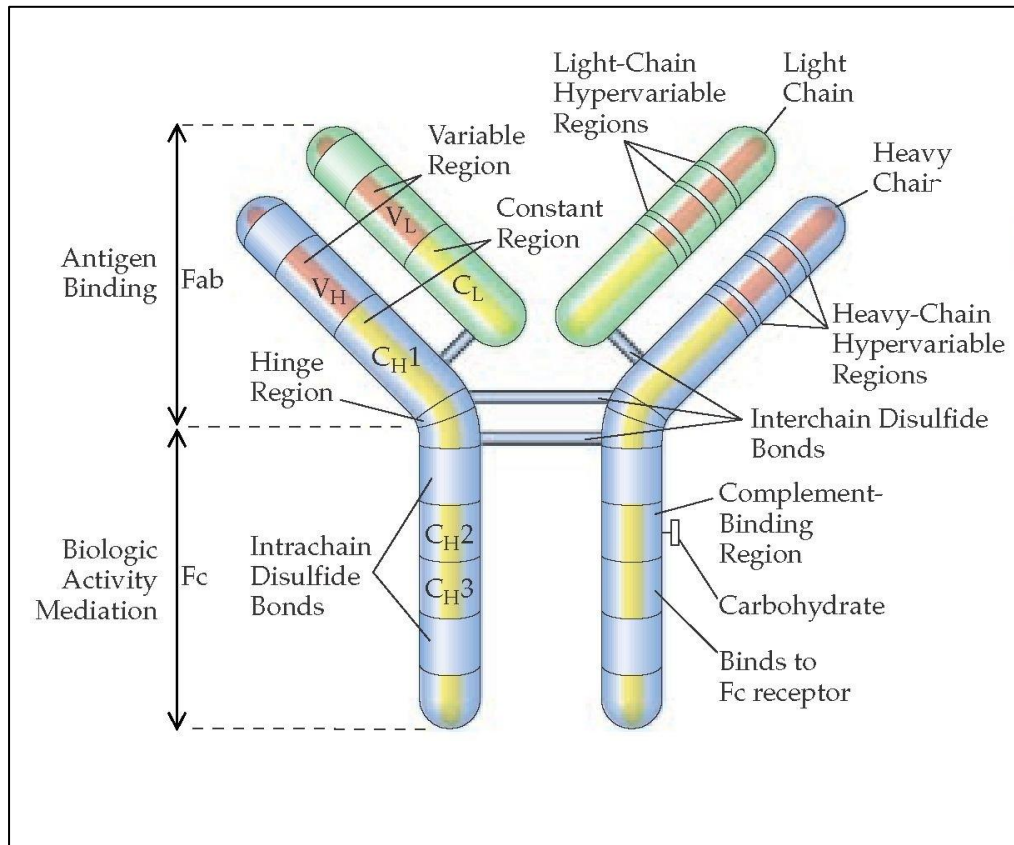


**Figure 1.11. A schematic representation of the structure of an IgG monoclonal antibody.** Taken from what-when-how.com(154). The antibody is composed of four polypeptide chains, two heavy chains and two light chains attached together by disulphide bonds, creating a Y-shaped protein. Blue squares depict intrachain disulphide bonds, blue bars depict interchain disulphide bonds. Each polypeptide chain has constant regions (yellow) whose amino acid sequences are unvarying as well as variable regions (red). These variable regions on both the heavy and light chains fold to create a specific recognition site (antigen binding site).

Antibodies can be reduced into different fragments which can be of clinical use(155).

These fragments include monovalent IgG (“half-antibody”), single chain Fv antibody fragments (consisting of the variable regions of the heavy and light chains bound by a disulphide bond), diabodies, triabodies and minibodies (Figure 1.12). These smaller

antibody fragments can penetrate cells more quickly than the larger whole monoclonal antibodies and have been shown to be less immunogenic(152,156,157).

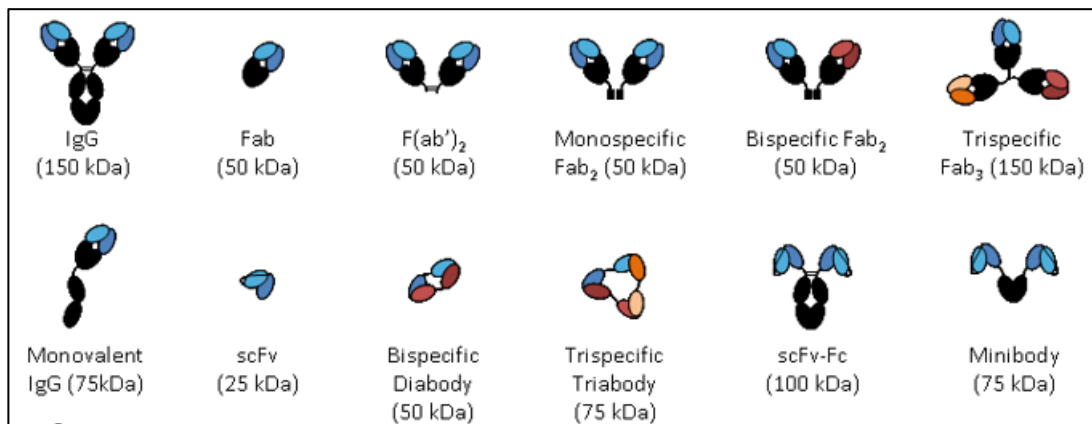


**Figure 1.12. Examples of different antibody fragments formed from an IgG monoclonal antibody.** Taken from [www.absoluteantibody.com](http://www.absoluteantibody.com)(158). The polypeptide IgG monoclonal antibody is modular and can be reduced into its separate domains, or combination of domains, producing a variety of different antibody fragments. Antibody fragments possess altered physiochemical features of the original antibody that can be exploited for clinical purposes. For instance, the smaller size of the Fab fragment allows penetration into tissues not accessible to the full-sized IgG antibody molecule(159).

Monoclonal antibodies can exert a therapeutic effect on tumour cells through mechanisms such as binding to and inhibiting receptors on cell membranes or by disrupting intracellular signalling pathways. This suppresses further cell growth, inhibits angiogenesis or induce apoptosis(156). The epidermal growth factor receptor (EGFR) and vascular endothelial growth factor (VEGF) signalling pathways have both been highlighted as important therapeutic targets for colorectal cancer(156). Cetuximab and panitumumab are examples of anti-EGFR monoclonal antibodies which are approved by the FDA for the treatment of colorectal cancer, as is Bevacizumab, an anti-VEGF monoclonal antibody to treat metastatic colorectal cancers(160). Use of monoclonal antibodies as stand-alone therapeutic agents have shown limited therapeutic effects, which could be attributed in part to the host immunogenic reaction(160).

Currently, monoclonal antibodies are used as targeting agents in haematological malignancies, such as Non-Hodgkin's lymphoma (the first monoclonal antibody approved for clinical therapy was for NHL; Rituximab), Hodgkin's lymphoma and chronic lymphocytic leukaemia, and solid tumours including those affecting the lung, renal tract, brain, breast and prostate in addition to colorectal cancer(150).

The disadvantages of monoclonal antibodies include their high molecular weights, limited tissue penetration, instability, expense (high production costs), requirements for large doses to achieve clinical efficacy and potential immunogenicity(156,161–163). Monoclonal antibodies targeting immune checkpoint molecules have been reported to have adverse effects similar to those experienced with chemotherapy agents(164). A phase I clinical trial(165) investigating an anti-CD28 monoclonal antibody was found to affect T-cells with severe side-effects secondary to a cytokine storm. The trial was subsequently ended, and further development of the antibody was abandoned.

A phenomenon known as the binding site barrier(162) can also reduce tissue penetration. Once bound, high affinity antibodies will not dissociate from their antigens. This means that all the antigens in the tumour periphery have to be saturated before unbound antibody will penetrate deeper into the tumour. In contrast, molecules with moderate binding affinity are released and are able to penetrate and bind to antigens deeper within the tumour, ultimately leading to higher tumoural uptake. Antibody engineering and antibody fragments are undergoing further research to overcome these limitations of monoclonal antibodies.

#### 1.4.2.1.1 Studies using monoclonal antibodies as recognition molecules

A particular antibody of interest in colorectal cancer nanomedicine research is the monoclonal anti-CEA antibody. Although there are numerous cell surface proteins, such as tumour-associated glycoprotein-72 (TAG-72), folate receptor- $\alpha$  (FR $\alpha$ ) and EGFR, that are upregulated on the cell membrane of colorectal cancer cells, CEA has been shown to be the most reliable biomarker(143). Tiernan *et al.*(16) successfully conjugated a humanised anti-CEA monoclonal antibody to a glycolated iodoacetamide dye-doped (NIR-664) silica NP. This study showed strong CEA-specific targeting of colorectal tumour cells *in vitro*, as well as revealing positive tumour-specific fluorescence *in vivo* using a murine tumour xenograft model. Campos da Paz *et al.*(166) also showed the conjugation of an anti-CEA antibody to a meso-2,3-dimercaptosuccinic acid (DMSA) functionalised magnetic NP. The authors demonstrated an increased uptake into LS174T cells, a cell line expressing high levels of cell membrane CEA, as compared to HCT116 cells, a cell line with low levels of CEA expression.

Cohen *et al.*(72) developed a cyanine dye-based NIR albumin NP system that was actively targeted to colon cancers using an anti-CEA antibody. Three human colorectal adenocarcinoma cells lines (LS174T, SW480 and HT29) were used in a chicken embryo model. LS174T and HT29 tumours were developed on the chorioallantoic membrane of the chicken embryos with differing cell membrane expression levels of CEA between the different cell lines (HT29 has lower CEA expression as compared to LS174T). The authors observed a 6-fold increase in NIR fluorescence in embryos with LS174T tumours as compared to embryos with HT29 tumours when treated with the anti-CEA antibody conjugated NIR albumin NP. No difference was seen between the two cell lines when tumours were exposed to bare non-functionalised NIR albumin NPs.

A humanised monoclonal anti-CEA antibody was conjugated to a fluorophore with similar excitation and emission profiles to ICG, and the ability of the antibody-targeted fluorophore to bind specifically to colorectal cancer cells was observed in a murine model(167). The study sample was small (n=3) however, the antibody targeted fluorophore showed good specificity for the tumour xenograft. It was noted that there was significant accumulation of the antibody-conjugated fluorophore in the liver and kidneys. This was presumed to be secondary to rapid clearance from the circulation due to the hydrophobic nature of the fluorophore used.

Cho *et al.*(168) conjugated the chimeric monoclonal antibody Cetuximab (anti-EGFR), which is licensed for use in advanced colorectal cancers, to silica-coated iron-oxide NPs. This antibody-NP conjugate system was then tested in a murine HCT116 colon cancer xenograft model and accumulation of iron-oxide NPs was observed through MRI imaging. The authors demonstrated a decrease in MRI signalling in xenografts exposed to the Cetuximab-conjugated NP compared to non-functionalised NPs. The decrease in the MRI signal represents increased intracellular uptake of the NP and therefore successful targeting of the tumour xenografts.

A single chain Fv (scFv) antibody fragment which targets CEA (sm3E) was used as the recognition molecule to actively target superparamagnetic iron oxide NPs (SPIONs) and improve MRI imaging of colorectal cancers(157). SPIONs with different coatings were conjugated to the anti-CEA scFv forming separate conjugate systems. These were tested against a CEA positive colorectal cancer cell line (LS174T) and a CEA negative melanoma cell line (A375M). The coatings were dextran only and a dextran-PEG coating. Bare unfunctionalised SPIONs of each specification were used as controls. An ELISA assay demonstrated that the functionalised NPs specifically bound to the CEA antigen, and binding of the bare non-functionalised NP was not detected. *In vitro* studies

confirmed that all 3 specifications (uncoated, dextran only and dextran-PEG) of scFv-functionalised SPIONs showed specific binding to the CEA positive cell line compared to the control cell line and bare non-functionalised SPIONs. The dextran-coated 50nm SPIONs showed clear internalisation into the LS174T cell line with no apparent binding to the A375M cell line. However, there was evidence to suggest that PEGylation of SPIONs enhanced non-specific binding of the NPs to the A375M cell line, in addition to the increased cellular uptake mediated by the recognition molecule. This may have been due to a negative surface charge created by the carboxylated PEG chain terminals.

Similarly, other studies have explored the use of different cell surface receptors for the targeting of colorectal cancer cells. Fay *et al.*(169) investigated the use of Conatumumab, a human antibody that binds to the cell surface receptor DR5 (part of the TNF receptor superfamily), and can initiate apoptosis through the activation of Caspase 8(170). The study found that Conatumumab-conjugated camptothecin (a chemotherapy agent) loaded NPs were able to incite cell death via apoptosis in addition to delivering a payload of camptothecin. Hsieh *et al.*(171) created an anti-VEGF antibody-conjugated dextran-coated iron oxide NP that actively targets the vascular endothelial growth factor (VEGF), which is an important signalling protein involved in angiogenesis. The conjugated magnetic NPs were specifically taken up into murine colorectal cancer models *in vivo* and increased MRI contrast intensity as compared to unconjugated (bare) magnetic NPs.

#### **1.4.2.2 Affimers**

Affimers (also known as aptamers) are short single-stranded RNA or DNA oligonucleotides that bind with high affinity and specificity to target molecules and are of interest as an alternative to antibodies for the active targeting of tumours(144,172). They are a type of non-immunoglobulin protein scaffold(161) which are chemically synthesised. Their primary sequences are usually 20-80 nucleotides in length and this

determines the 3-dimensional tertiary shape of the affimer (173), similar to the structural conformation of an enzyme. The binding clefts formed through their 3-D conformation enables affimers to bind to their specific targets with a specificity rivalling monoclonal antibodies(174). This is achieved through a combination of van der Waals, hydrogen bonding, hydrophobic and electrostatic interactions(175).

Ellington and Tuerk(176,177) were the first to develop affimers through a complex but powerful purification method termed Systematic Evolution of Ligands by Exponential Enrichment (SELEX). A library consisting of a large pool of short oligonucleotides of random sequences is initially incubated with the target molecule. This incubation process is used to isolate the nucleic acid sequences which bind to the target molecule. Once isolated the nucleic acid sequences are eluted and then amplified, by either reverse transcription polymerase chain reaction (RT-PCR) for RNA or simply just PCR for DNA. This process of incubation, elution and amplification is repeated until the pool has reduced to a small but enriched size of nucleic acid sequences with a high affinity to bind to the target molecule. These high affinity sequences (affimers) are then tested against the target molecule and their binding affinities are compared to determine potential affimer candidates for further investigation (Figure 1.13).

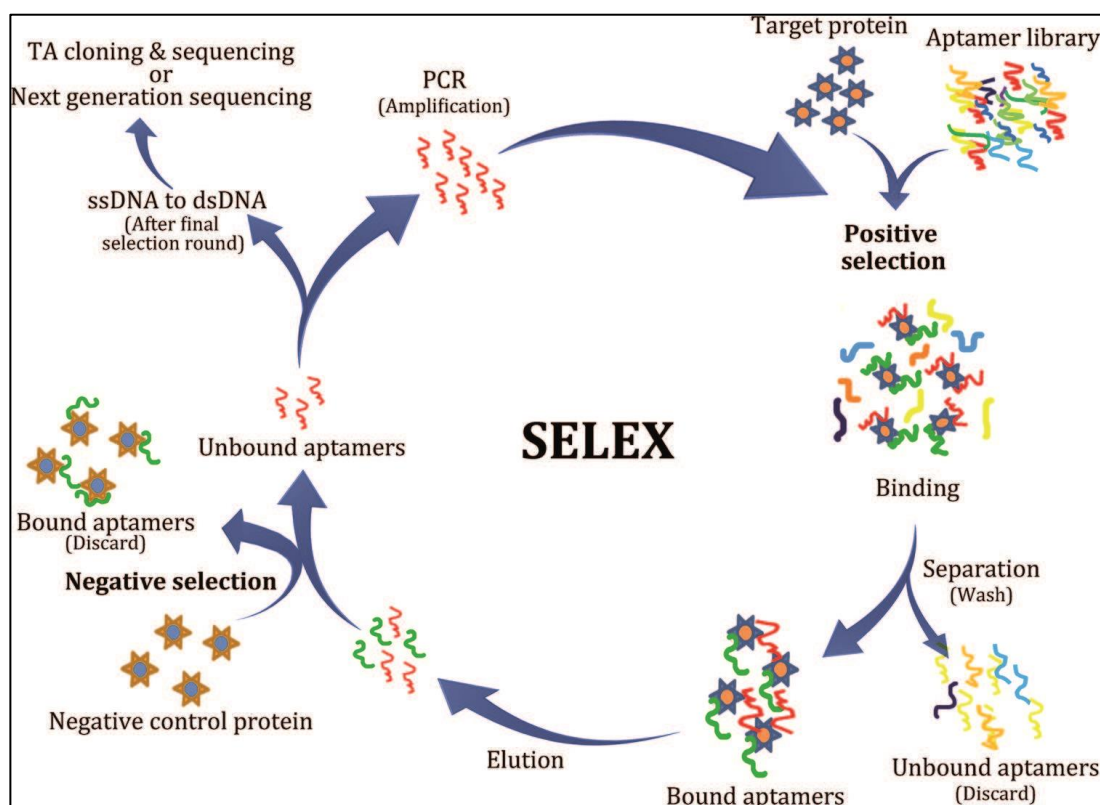


**Figure 1.13. Diagram depicting the process of Systematic Evolution of Ligands by Exponential Enrichment (SELEX).** Taken from Ellington *et al.*(178). Initially different oligonucleotides (affimer or aptamer library) are incubated with target protein (represented by the blue stars with orange centre); affimers bound to the target protein are separated and the unbound affimers are discarded (positive selection). Bound affimers are released from the target protein and then incubated with the negative control protein. Affimers binding to the negative control protein are discarded and the unbound affimers are recovered (negative selection). These affimers are amplified and subjected to repeated positive and negative selection followed by amplification until the final selection cycle where the affimers are sequenced.

The advantages affimers exhibit over antibodies are that they are of a much smaller size, promoting higher levels of tissue penetration and are rapidly cleared by the renal system. Higher levels of tissue penetration with rapid clearance from the circulation is desirable for diagnostic applications, however, high tissue accumulation and prolonged circulating time is preferable for therapeutic purposes(156,161). Affimers lack immunogenicity(173,179) and can be used to recognise both intracellular and extracellular targets whereas antibodies are designed for extracellular targets(173). They can also easily be modified, produced at low cost with little variability between batches

and are stable over prolonged periods of time(172,179). Monoclonal antibodies and whole humanized monoclonal antibodies can induce an immunogenic reaction with the generation of T-cell dependent neutralising antibodies. This could precipitate resistance against treatment with monoclonal antibodies in relapsed patients. Currently, there is no evidence suggesting that similar neutralising antibodies are induced against affimers(163). However, they can be unstable within serum environments(175) as they are susceptible to enzymatic degradation leading to a reduced circulation time. This coupled with the fact that they are rapidly cleared by the renal system means their clinical efficacy could be limited(141).

Affimers can be modified following post-sequencing to promote bioavailability, improve their biocompatibility profile or for conjugation to other molecules such as fluorescent NPs. Affimer-conjugated NPs have been shown to enhance the uptake and retention of therapeutic agents in tumours(179), although modifying the affimer may also alter the conformational structure potentially reducing the binding affinity and specificity(141).

Ahmadzadeh-Raji *et al.*(180) attached an anti-CEA affimer on to gold NPs, which were electrodeposited on to indium tin oxide, to create a biosensing device capable of detecting colorectal cancer cells. *In vitro* studies were performed, and the anti-CEA functionalised gold NPs were tested against HCT116 (colorectal cancer, CEA positive) and HEP-2 (laryngeal cancer, CEA negative) cell lines. The study demonstrated that the affimer-NP system was more sensitive in detecting HCT116 cells compared to HEP-2 cells.

Li *et al.*(181) conjugated an EpCAM affimer on to mesoporous silica NPs loaded with the chemotherapy agent DM1 or Mertansine (anti-mitotic tubulin inhibitor). EpCAM is a transmembrane glycoprotein overexpressed in epithelial cancers such as colorectal

tumours(182). The authors demonstrated increased uptake of the NPs in the human colorectal adenocarcinoma cell line, SW480, expressing high cell surface levels of EpCAM, as compared to low and negligible EpCAM expressing cell lines. The affimer-NP system effectively delivered its chemotherapy payload. Similar findings have been shown with curcumin-loaded lipid-polymer hybrid NPs conjugated to an EpCAM affimer(183).

MRI is a common used imaging modality in colorectal cancers, however, the conventional MRI contrast agent gadolinium diethylenetriaminepentaacetic acid has a short circulation time in addition to high toxicity(171). Supermagnetic NPs are of interest in MRI imaging as they can be used as contrast enhancement and signal amplification agents without the disadvantages of gadolinium(166). Iron-based magnetic NPs are particularly useful as their surface can be chemically modified to bind recognition molecules and promote active targeting to the desired tissue(166). A 5TR1 affimer, which targets the MUC-1 cell surface marker on epithelial tumours such as colorectal cancer, has previously been conjugated to a superparamagnetic iron oxide NP(184) containing the chemotherapy agent epirubicin to act as a nanomedicine with theranostic applications. This study demonstrated that the 5TR1 affimer-conjugated superparamagnetic iron oxide nanomedicine improves MRI imaging in addition to inducing targeted toxicity within colorectal tumours.

Affimers can also be used as stand-alone therapeutic agents as they typically become internalised via endocytosis after binding to their target molecule. The commercially available RNA affimer, Pegaptanib (Macugen), has been shown to have a high affinity for the vascular endothelial growth factor isoform (VEGF-165). VEGF-165 is responsible for pathological ocular neovascularisation and vascular permeability seen in conditions such as age-related macular degeneration and diabetic macular oedema, in addition to

tumours(185). Ng *et al.*(185,186) showed that Pegaptanib binds and inactivates VEGF-165 demonstrating significant clinical benefit following intravitreal injection in several clinical trials. Due to the inhibitory effects on endothelial cells Pegaptanib was investigated as an anti-angiogenesis agent for cancer therapy in malignant brain tumours. However, the impressive results seen with ocular conditions were not replicated (179). Direct conjugation of affimers to chemotherapy agents has been shown to facilitate the internalisation and increase the efficacy of the drug. Taghdisi *et al.*(187) demonstrated targeted delivery of epirubicin to prostate cancer cells *in vitro* using a PEGylated prostate-specific membrane antigen affimer. Affimers are also being investigated as photodynamic therapy agents after conjugation to photosensitisers. Mallikaratchy *et al.*(188) successfully conjugated an affimer that specifically targets a Burkitt lymphoma cell line to a photosensitiser and induced selective cell death in this cell line when treated with light radiation. Similar results have been demonstrated using affimer conjugated photosensitiser systems in breast(189,190) and lung cancer(172).

### **1.4.3 Nanoparticles**

As described in 1.4.1.1, NPs are designed to accumulate in tumour tissue due to the EPR effect(191,192). EPR (193) refers to the combination of rapid tumour growth, hyperpermeable tumour neovasculature and ineffectual development of lymphatics, enabling the passive extravasation and retention of NPs within the tumour. Yuan *et al.*(194) demonstrated that particles up to 400nm can pass into solid tumours due to the enhanced permeability of tumours. Other studies(195,196) have equally demonstrated that particles  $\leq 200$ nm accumulate within tumours more effectively. In cancer-related nanomedicine, NPs are usually designed to be given intravenously. The macromolecule travels through the systemic circulation prior to arriving at the site of tumour growth. Therefore, there are many steps and obstacles involved before a nanomedicine is able to achieve its effect(110). These involve travelling extensively through systemic

circulation, extravasation within the tumour micro-environment, accumulation into the interstitial fluid and uptake into cancer cells.

#### **1.4.3.1 Opsonization and the Mononuclear phagocyte system**

Some of the challenges faced by nanomedicine whilst in human systemic circulation are opsonization, the mononuclear phagocyte system (MPS) and clearance by either the liver or kidney. Even NPs that have been functionalised to actively target tissues will be present in non-targeted organs, particularly the liver and spleen.

NPs can have very high surface areas due to their surface-to-volume ratio which can lead to their aggregation. Aggregation will significantly increase the size of the NP and potentially have adverse effects on its biodistribution(197,198). Upon introduction into systemic circulation, serum proteins can adhere to the NP creating a corona (known as non-specific adsorption) which not only promotes aggregation but also promotes uptake within macrophages and will affect extravasation of the NP, thereby reducing cell uptake(110). Adsorption of proteins on to the surface of the nanomedicine may also interfere with its function(199). Blood serum proteins have an enhanced affinity for adsorption on to hydrophobic particles and opsonization of these particles has been shown to occur more quickly compared to hydrophilic particles(200,201). Opsonization is the term referring to the binding of certain proteins to the surface of a foreign body, such as a NP, rendering it more visible to phagocytic cells(202). The phagocyte then proceeds to engulf the bound NP complex leading to the destruction and removal of the NP from the circulation. The proteins which mediate opsonization are known as opsonins, the most common of which are complement proteins C3-5 and immunoglobulins(202).

The MPS, also termed the reticulo-endothelial system (RES), refers to a system of specialised macrophages (phagocytes), usually Kupffer cells, most prominently located in the liver and spleen(110). These macrophages do not directly detect foreign NPs, however they recognise specific opsonin proteins which become bound to the surface of the NP as described above. This is the main mechanism by which foreign particles present within the circulation that are too large to be excreted via the kidney are removed. Following opsonization the foreign particle is phagocytosed into the specialised macrophages. Firstly, the macrophage must attach to the opsonin protein via one of three different mechanisms and then engulf the particle into itself(202). The first and simplest mechanism is non-specific adherence of the bound opsonin protein to the phagocyte. This typically occurs due to the association of opsonins with more hydrophobic particle surfaces. The second mechanism involves the foreign particle-bound opsonin protein to undergo conformational changes. This activates the protein and allows it to interact with specialised receptors found on the cell membranes of macrophages. The final mechanism is through complement activation either through the classical, alternative or lectin pathways. Once the foreign particle has been attached to the phagocyte, via the bound opsonin protein, the phagocyte ingests the particle via endocytosis. The particle is then broken down by various enzymes and oxidative-reactive chemicals such as nitric oxide and hydrogen peroxide. If the NP cannot be degraded by these processes then they become sequestered within one of the MPS organs such as the liver or spleen, unless they are of a small enough size to be excreted via the kidney(202). Particles with a molecular weight of less than 5000g/mol can be excreted via renal clearance(202).

#### **1.4.3.2 PEGylation**

The ability to modify the surface of NPs has an inherent advantage in trying to reduce aggregation and opsonization. The surface of the NP can be altered to contain long

hydrophilic polymer chains which extend into the media, forming a barrier that blocks the adhesion of opsonin proteins and can therefore shield hydrophobic or charged particles from the MPS(202). These polymer chains are also usually charge neutral lessening the effect of electrostatic interactions. This method of avoiding or reducing opsonization creates what is thought of as 'stealth NPs' due to their ability to evade the MPS-mediated elimination. The most commonly used polymer is an FDA-approved reagent(145) called poly(ethylene glycol) (PEG). NPs are readily excreted from the human body, via the MPS, and generally have a relatively short circulation time. However, incorporating PEG chains on to the surface of a NP can provide protection and reduce aggregation(53,199). This reduces the clearance of the NP from the blood by the MPS thereby prolonging the circulation time(170,191,202) and allowing increased accumulation of the NP in tumour tissue(126). Non-PEGylated NPs by contrast can be excreted within minutes. Choi *et al.*(203) compared outcomes including circulation time between non-PEGylated hyaluronic acid NPs and a PEGylated version. Their results suggested that PEGylation of the NPs reduced uptake within the liver and increased the circulation time compared to non-PEGylated NPs. It is also possible to PEGylate affimer molecules which increases their half-life within the circulation(172), but may alter their conformational structure reducing their binding affinity.

A key factor in the application of nanomedicine is the biocompatibility profile. Concerns have been raised regarding the use of heavy metals such as gold or iron oxide NPs (inorganic NPs), as they have relatively prolonged circulation times and very few studies on the effects of exposure have been conducted(204–207). Sadauskas *et al.*(204) showed a reduction in the number of Kupffer cells after exposure to gold NPs potentially indicating damage to these cells taking up the inorganic NP and being removed by phagocytosis. Hanini *et al.*(206) investigated the effects of iron oxide NPs on endothelial cells and showed convincing evidence that exposure of endothelial cells to iron oxide NPs, even at low doses, caused a severe drop in cell viability after 24 hours. PEGylated

NPs show decreased immunogenicity *in vivo* compared to non-PEGylated NPs(53) as the PEG chains reduce the interaction between the highly charged NP surface and the cell membrane which potentially disturbs the cells lipid bilayer(208). There are less inherent concerns regarding the biocompatibility of organic NPs as the metabolites formed from the breakdown of these nanomedicines are readily excreted(110).

PEG also has the advantage of being easily modifiable so that a wide range of different ligands can be attached at the terminal end of the PEG chain enabling conjugation to targeting agents(209). Attaching the ligand at the terminal end of the polymer chain reduces steric hindrance between the targeting moiety and the PEG chain. PEG is a hydrophilic compound meaning that it is water soluble; PEGylation of a NP can, in addition to conferring protection from the MPS, render an insoluble NP soluble within an aqueous environment such as the human circulatory system(126). It has to be noted that PEG can also potentially induce an immunogenic response and formation of antibodies, particularly after repeated administrations which can accelerate the clearance of the PEGylated nanomedicine from the circulation(210). A recent Phase III clinical trial, investigating an anti-IX coagulation factor PEGylated affimer, demonstrated significant toxic side-effects in a small number of patients (10 out of 1605) with one fatality which was initially thought to be due to the affimer(211). However, after analysis(212) it was found that the toxicity observed in these patients was secondary to a PEG allergy as evidenced by the presence of anti-PEG antibodies.

#### **1.4.3.3 Fluorescent nanoparticles**

NPs make effective imaging agents for clinical purposes due a number of inherent features such as their small size, enabling the NP to utilise the EPR effect for tumour targeting. The surfaces of these NPs are also amenable to modification allowing the conjugation of recognition molecules and enabling the NP to be used to actively target

tissue. They have a capacity to deliver a large payload of therapeutic agents in addition to tunable biodistribution properties and multi-modal signalling capacities(213). The field of fluorescent NPs is of particular interest as these can potentially overcome the limitations associated with traditional fluorescent dyes or proteins(74,214) used for imaging purposes, specifically photostability and brightness. Due to the aforementioned surface modification and drug internalisation properties they have therapeutic potential in addition to diagnostic applications. However, the use of fluorescent NPs as fluorescent probes does impose restrictions on their properties such as size, biocompatibility and surface chemistry(74).

Fluorescent NPs can be designed to emit wavelengths in the NIR region ( $>780\text{nm}$ )(16) which makes them ideal for intraoperative imaging. This is due to the deeper penetration of light at long wavelengths ( $>600\text{nm}$ ), through multiple layers of cells and tissue.

Fluorescent probes which emit in the NIR region have good tissue penetration and also reduced autofluorescence(16,215). Other features of an ideal probe includes bright fluorescence with good tissue penetration, negligible photobleaching and quenching, stability(53,215,216), high degree of sensitivity and specificity for the target tissue and biocompatibility(217).

Quantum dots (QDs) have been extensively investigated, in addition to other inorganic fluorescent NPs. Quantum dots are fluorescent nanocrystals whose emission spectrum can be altered by adjusting their size and composition. Other advantages of quantum dots over conventional dyes include high quantum fluorescent yield, superior brightness in addition to a broader spectrum of excitation, photostability and resistance to photobleaching(75). However, there are inherent limitations with these inorganic NPs as there is less flexibility with surface modification, their lack of biodegradability, inadequate

*in vivo* stability due to their hydrophobic nature and concerns regarding toxicity following their accumulation within organs of the MPS(74,75,172).

One clinical use that QDs are being investigated for is in sentinel lymph node biopsies in breast cancer surgery and have shown early promise. However, this has been limited by the inherent toxicity of the heavy metal ions, particularly Cadmium, which has traditionally been used to produce QDs. Cadmium-free QDs have been developed for clinical translation which do not exhibit toxicity to tissues. Yaghini *et al.*(218) developed a water-soluble heavy metal ion free QD with an emission range of 500-700nm for lymphatic mapping applications. Cell toxicity tests did not show any significant difference between cells exposed to various concentrations of the QD over 24 and 48 hours compared with controls, although the study acknowledges that further long-term toxicity studies need to be completed. Their animal model, however, showed promising results with the QDs accumulating in the regional lymph nodes from the injection site (subcutaneous injection of QDs into rat paws) and demonstrating stable fluorescence, with only trace amounts of the QD being detectable in other tissues.

Fluorescent NPs composed of organic materials can offer more flexibility than inorganic NPs as their constituents can be altered and modified to control their properties such as brightness, size and surface chemistry. These include dye NPs (comprised of small organic dyes) and lipid or polymer NPs that have encapsulated fluorescent dyes within their cores. A balance for the latter type of organic NP needs to be achieved as the brightness of the fluorescent probe is dependent on the number of dye molecules (fluorophores) within the core. Increasing the number of fluorophore molecules present should theoretically increase the brightness of the probe. However, the structure of the fluorophore encourages aggregation of the dye molecules leading to quenching(74). The aggregation of fluorophores with subsequent quenching decreases the quantum yield

and brightness of the fluorescent dye-loaded NP. Permanent encapsulation of the dye must also be assured as leaching of the dye from the probe could affect its ability to complete accurately its intended diagnostic function.

#### **1.4.3.3.1 Semiconducting polymer nanoparticles**

Semiconducting polymer NPs (SCNPs) are composed of electronically and optically active polymers which render them of interest in applications such as sensors, electronic devices and as fluorescent probes for molecular imaging(213,219–222). Inherent properties within SCNPs include large absorption co-efficients, tunable optical properties, surface properties, excellent photostability and oxidative tolerance(223–225). SCNPs are usually found to exhibit higher levels of fluorescence compared with organic dyes(145). The optical properties of SCNPs are influenced by their component polymers(199) and, unlike quantum dots, the size of the NP does not affect the emitted fluorescence(213). SCNPs can be designed to have a small diameter making them effective for tumour penetration(223) as well as having a suitable Stokes shift(226). Furthermore, SCNPs are primarily composed of biologically inert organic materials unlike heavy metal dependant quantum dots, making them biocompatible(74,213).

Pu *et al.*(213) performed *in vivo* SCNPs biocompatibility studies on murine models with fully functioning immune systems. The control group were injected with saline whereas the study group were injected with a SCNP comprised of a copolymer of poly(styrene) and poly(ethylene glycol). No observable behavioural differences were observed between the control and study groups, nor was there evidence of acute or chronic toxicity. However, there was evidence of a transient inflammatory response (decrease in mean corpuscular volume, increase in neutrophils and elevated hepatic enzymes), that was attributed to the normal immune response of a host to foreign material. The study did acknowledge the small murine population (n=5 for both study and control groups)

used for the study but concluded that it was a pilot study demonstrating positive results that could warrant further investigation on a larger sample size.

SCNPs are synthesised from hydrophobic conjugated polymers and therefore require either formulation with a hydrophilic polymer or chemical modification in order to be stable within an aqueous environment(198). Where the NP contains both hydrophobic and hydrophilic polymers, the core of the SCNP is comprised of the hydrophobic polymer which surrounds itself via hydrophobic interactions with the hydrophilic polymer. The sizes of these self-assembling polymer NPs can be controlled by altering the size of the hydrophobic and hydrophilic constituents of the NP(145).

It is this outer layer of hydrophilic polymer that determines how the SCNP interacts with substances within a biological environment, such as aqueous media. Proteins have a tendency to adhere to the surface of these NPs by non-specific adsorption(199), although PEG has been shown to reduce protein attachment which is a further advantage of PEGylation. This is of particular importance for clinical translation as protein adsorption to the surface of the SCNP has been shown to cause quenching(227).

One method of producing SCNPs is reprecipitation which is also known as nanoprecipitation or post-polymerization. The constituent amphiphilic polymers (a polymer with both hydrophobic and hydrophilic parts(145)) are dissolved in an organic solvent and are then mixed with a second solvent, for example water, in which they have poor solubility. Usually the SCNPs are dispersed via ultrasound waves and the initial solvent is then evaporated(145). This method has been used to create many fluorescent SCNPs as it is a relatively simple process, of low cost and has a high yield of SCNPs. A second strategy of SCNP is via mini-emulsion. This is essentially the same process as

nanoprecipitation; the difference between the two processes is that the solvent used in nanoprecipitation is miscible with water but immiscible for mini-emulsion(228).

Surface modification of SCNPs to allow conjugation of recognition molecules and enable active targeting for clinical applications can be achieved by several methods. One strategy is to use amphiphilic polymers that already possess a functional group and coprecipitate with the semiconducting polymers to form a functionalised SCNPs. Although these functional groups are non-covalently bound to the amphiphilic polymer and therefore may become dissociated once exposed to a complex biological environment(145).

Ding *et al.*(223) fabricated a fluorescent folic acid conjugated SCNPs to target cancer cells that overexpress folate receptors. The SCNPs were ~80nm in diameter as determined by dynamic light scattering (DLS) measurements. The SCNPs were incubated with MCF-7 breast cancer cells with a high expression of folate receptors on their cell surface membranes and NIH/3T3 fibroblasts cells which were used as a negative control. Fluorescent imaging confirmed that SCNPs specifically targeted the breast cancer cells in comparison to the control. *In vivo* experiments were performed in tumour-bearing murine models using hepatic H22 cancer cells. The control group were injected with bare non-functionalised SCNPs and the study group received functionalised folic acid conjugated SCNPs. Both groups showed tumour fluorescence indicating the presence of the SCNPs within tumour tissue regardless of whether it possessed the functional recognition molecule folic acid. This was attributed to the EPR effect (passive targeting). However, the intensity of fluorescence was higher at the site of the tumour in the study group. This suggested that functionalisation of the SCNPs allowed greater accumulation of the NP within tumour tissue due to the active targeting effects of the folic acid.

Combining the advantages of SCNPs with NIR fluorescence for the purposes of biomedical imaging would be ideal given their high brightness, excellent photostability and biocompatibility(229). Hydrophobic low molecular weight NIR dyes have been encapsulated within the core of a SCNP (“dye-doping”) enabling emission of NIR fluorescence. Unfortunately, the systems that have manufactured these fluorescent NIR SCNPs have produced low yields, leakage of the dye from the SCNP core, a broad spectrum of emission and poor stability(229). Another limitation of using a fluorescent dye with a SCNP is that excessive aggregation of dye molecules within the core can lead to quenching(145).

The NP I propose to use in this research project is a fluorescent organic SCNP PEG-shell dye-doped NP manufactured via a nanoprecipitation method. The fluorescent core is comprised of poly(2,5-di(hexyloxy)cyanoterephthalylidene) (CNPPV), a red-emitting conjugated polymer which is hydrophobic but exhibits bright fluorescence and stability(229)(Figure 1.14).



glycol) methyl ether-block-poly(lactide-co-glycolide)(PLGA-PEG). This is a biodegradable diblock co-polymer composed of units of PEG and PLGA. The PLGA end of the co-polymer is hydrophobic whereas the PEG end is highly hydrophilic. When these components are placed within an aqueous environment the polymer chains associate with the hydrophobic segment facing inward and the hydrophilic segment projects outwards. This minimises the contact between the hydrophobic PLGA and the aqueous media. As CNPPV is also hydrophobic it becomes incorporated within the centre of the NP. This means the NP can self-assemble with the CNPPV and PLGA in a hydrophobic core surrounded by a hydrophilic shell of PEG in an aqueous environment. This manufacturing process yields an increased amount of PEGylated NIR fluorescent SCNP(229).

Kemal *et al.*(229) showed that the hydrodynamic diameter of this specific CN-PPV dye-doped SCNP ranged from 110-140nm, and an increase in size correlated to an increase in the proportion of PLGA-PEG used in the SCNP. However, increasing PLGA-PEG content was also associated with increased emission intensity and reduced quenching. Quenching has been shown to be reduced with the use of PEGylated polymers(145). Normalised absorption and emission spectra comparing CN-PPV SCNPs versus CN-PPV dye-doped PLGA-PEG SCNPs showed no differences in the emission profiles, therefore incorporating the NIR dye into a SCNP core does not affect its fluorescent properties.

## 1.5 Summary

Colorectal cancer presents a huge clinical burden to healthcare with over 40,000 new patients diagnosed per year and representing 10% of all cancer deaths annually in the UK. Surgical resection of the tumour is the basis for curative treatment however, there

are limitations in the ability to accurately stage the involvement of the regional lymph nodes. This creates differences in the treatment of patients whereby node-negative patients are unnecessarily exposed to the risks of an extensive resection and node-positive patients may potentially have residual disease left behind in unresected D3 lymph nodes. This latter group of patients receive adjuvant chemotherapy which poses its own profile of toxicities and adverse effects. There is a clear need to improve the staging of patients prior to removal of the tumour enabling the extent of surgical resection to be tailored to the patient. Sentinel lymph node mapping and biopsy is a potential solution which has been used successfully in the treatment of other types of tumours, particularly in breast cancer. However, the excellent results seen in breast cancer surgery have not translated to colorectal cancer surgery. These poor results have shown that traditional SLNM cannot be recommended in colorectal cancers and there is a need for a more appropriate and specific probe.

Near infra-red fluorophores are of interest as they exhibit good tissue penetration and reduced rates of autofluorescence. Several studies investigating NIR fluorophores as SLN probes in colonic cancer have been conducted. However, findings from these studies have shown below acceptable levels of sensitivity and accuracy in addition to high false-negative rates. The main limitation for these fluorophores is that they do not specifically target colorectal cancer cells.

NPs have many advantages for clinical applications such as prolonged circulating time, their ability to cross through the cell surface membrane and the potential for modification allowing active targeting of a tissue or encapsulation of hydrophobic drugs. Therefore, it is unsurprising that NIR fluorescent NPs conjugated to a ligand capable of accurately targeting colorectal cancer cells represents a large area of current clinical research. Monoclonal antibodies are an effective ligand for targeting specific receptors on cell

surface membranes in addition to exhibiting a therapeutic effect on the tumour cells. Semi-conducting organic fluorescent NPs are also of particular interest in clinical imaging applications due to their biocompatibility, ability for surface modification with recognition molecules, tunable optical properties as well as their brightness and photostability.

## 1.6 Aims and Objectives

The aim of my research is to create and evaluate a fluorescent probe which can be used intra-operatively to target colorectal cancers. This will help identify the position of the tumour as well as any potential lymph node metastases.

The objectives of my research are as follows:

- Evaluate 5-ALA, as an example of a small drug fluorophore, for use in colorectal cancer fluorescent guided surgery
- Fabrication and characterisation of a semiconducting polymer NP
- *In vitro* evaluation of anti-CEA antibody as a targeting molecule for colorectal cancer
- Optimise methods for conjugating anti-CEA antibody to NP
- Evaluate *in vitro* binding of anti-CEA NP conjugate to colorectal cancer cell lines

# **Chapter Two**

## **Materials and Methods**

## **2 Materials and Methods**

### **2.1 Next Generation intraoperative Lymph node staging for Stratified colon cancer surgery**

#### **2.1.1 Trial protocol**

The Next Generation intraoperative Lymph node staging for Stratified colon cancer surgery (GLiSten) trial was a bi-centre, multi-national feasibility study. The primary aim of this study was to determine the optimum dose of the fluorescent photosensitiser, 5-aminolevulinic acid (5-ALA) (Photonamic GmbH & Co. KG, Pinneberg, Germany), to detect lymph node (LN) metastases during laparoscopic surgery. Pre-operative CT reporting of LN status, intra-operative fluorescence and quality of surgical resection with D3 lymphadenectomy were secondary aims. Safety data was also collated. This study was conducted with approval from the Medicines and Healthcare Products Regulatory Agency and IRAS ethics committees (reference number: ISRCTN79949827) from both hospital sites involved in the trial (St James's University Hospital, Leeds, UK and The Mater Misericordiae University Hospital, Dublin, ROI). Funding for the trial was obtained from the Efficacy and Mechanism Evaluation programme; a Medical Research Council and National Institute for Health Research partnership. The trial registration number is ISRCTN79949827 and the EudraCT number is 2012-002623-15.

Adult patients with locally advanced right-sided and sigmoid colon tumours, as identified using the Fluoropyrimidine, Oxaliplatin and Targeted-Receptor pre-Operative Therapy (FOxTROT) trial criteria(230), undergoing elective laparoscopic resection of colon tumours with extended D3 lymphadenectomy and meeting the inclusion criteria (Table 2.1) were recruited across the two sites. The FOxTROT trial criteria defined locally

advanced colonic adenocarcinomas as T3/4 disease with extramural depth  $\geq 5$ mm on preoperative CT imaging.

**Table 2.1. Inclusion and exclusion criteria**

Inclusion Criteria	Exclusion Criteria
<ul style="list-style-type: none"> <li>• Able to give informed consent and willing to follow trial protocol</li> <li>• Aged over 18 years</li> <li>• Patients with cancers of the right and sigmoid colon amenable to laparoscopic resection incorporating D3 lymphadenectomy, as agreed by MDT discussion following histopathological confirmation of cancer diagnosis and radiological staging.</li> <li>• Patients with distant metastatic disease will be eligible, provided laparoscopic resection of the cancer is part of routine clinical care.</li> <li>• Fit for standard laparoscopic resection</li> <li>• American Society of Anaesthesiologists (ASA) classification <math>\leq 3</math></li> <li>• Normal hepatic and renal function on most recent blood tests (to be within 30 days prior to surgery). For the purposes of the trial, normal hepatic and renal function were defined as:</li> </ul>	<ul style="list-style-type: none"> <li>• Patients with cancers of the transverse and left colon, due to difficulty in defining D3 lymphadenectomy in these anatomical locations</li> <li>• Past history of hypersensitivity reactions to 5-ALA or colorimetric dye</li> <li>• Acute or chronic porphyria or a family history of the same</li> <li>• Patients with synchronous colonic or rectal cancer (but patients with synchronous benign polyps are eligible)</li> <li>• Patients with co-existent inflammatory bowel disease, such as Crohn's disease, ulcerative colitis or active diverticulitis, which may influence the lymphatic uptake of 5-ALA</li> <li>• Pregnant (positive pregnancy test) or breast feeding</li> <li>• Received an investigational medicinal product at any dose within 28 days before registration</li> <li>• Poorly controlled or serious medical or psychiatric illness that, in the</li> </ul>

<ul style="list-style-type: none"> <li>a. Total bilirubin within normal institutional limits</li> <li>b. AST/ALT &lt; 2.5 X institutional upper limit of normal</li> <li>c. GFR <math>\geq</math> 60 ml/min/1.73m<sup>2</sup> or Creatinine within 10% of upper value for normal institutional limits</li> </ul>	<p>Investigator's opinion, was likely to interfere with participation and/or compliance in this clinical trial.</p>
--	---

Recruited patients were administered 5-ALA shortly before undergoing laparoscopic surgery and any intra-operative fluorescence of the primary tumour and/or any lymph nodes or aberrant tumour deposits was documented. In the subsequent histopathological examination of their specimen patients were identified as node positive if metastatic disease was detected in at least one lymph node and node negative if no metastatic disease was detected in the lymph nodes. Assessment of the accuracy of 5-ALA to detect metastases was based on whether fluorescence correctly distinguished between node positive and node negative patients. The sensitivity and specificity of 5-ALA was based on whether 5-ALA fluorescence detected an involved lymph node. A positive diagnosis was categorised by the identification of metastatic disease in a lymph node as characterised by PPIX fluorescence.

The primary aim of this trial was to determine the optimal dosage of 5-ALA therefore the trial was designed to assess an initial cohort of patients receiving a single dose of 20mg/kg of oral 5-ALA, which is the most commonly administered dose of 5-ALA taken from previous studies(9). Reaching 10 patients with post-operative histopathological confirmation of positive lymph node disease at a dose of 20mg/kg marked the end of recruitment to Cohort 1. The dose of 5-ALA administered to a second cohort was dependent on the results from Cohort 1 and would either increase to 30mg/kg or

decrease to 10mg/kg (Figure 2.1). As pre-operative CT staging cannot accurately predict the lymph node status of colorectal tumours it was anticipated that more than 10 patients would be recruited per cohort to achieve the required number of patients with post-operative histopathological confirmation of positive lymph node disease.

The dose of 5-ALA that correctly identified the most number of patients with lymph node positive disease via fluorescence would be further evaluated in a developmental phase of the trial, with a set minimum of 2 correctly identified patients from a single cohort. The developmental phase would treat a third cohort of 10 patients with the optimal dose to confirm the validity of the technique. The trial ended if an optimal dose was not correctly identified by a minimum of two patients from either cohort.

All patients underwent standard pre-operative assessments, including a pre-operative staging CT of the thorax, abdomen and pelvis. Oral doses of 5-ALA were calculated based on the weight of the patient. 5-ALA was reconstituted in water to a stock concentration of 30mg/ml. 5-ALA was administered to patients between 1-6 hours before surgery.

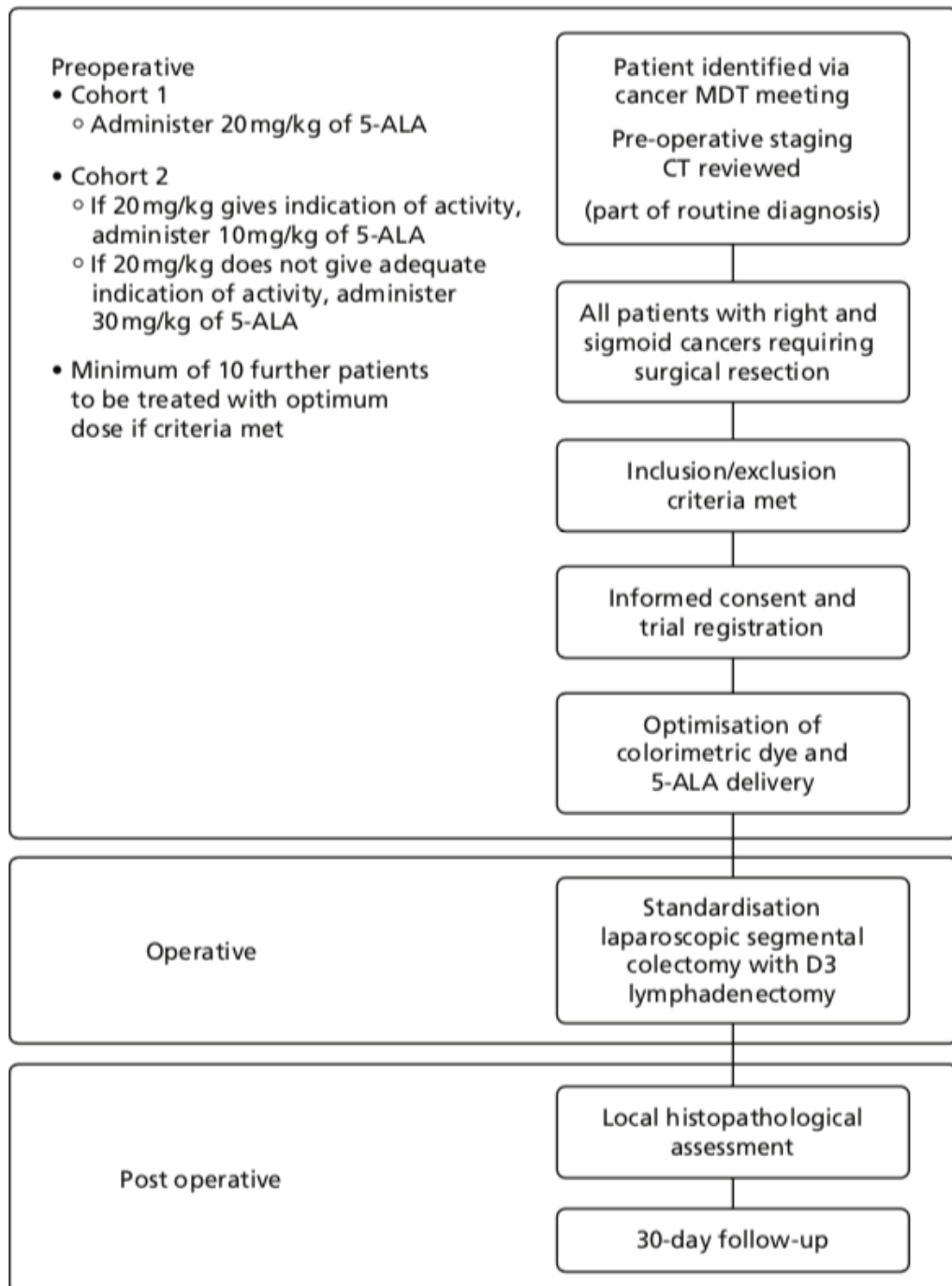


**Figure 2.1. GLiSten trial flow diagram.** Taken from Andrew *et al.*(9). Eligible patients meeting the inclusion and exclusion criteria were identified at the local colorectal MDT meeting at trial sites and approached by trial research personnel. Patients consenting to participation in the GLiSten trial were prescribed the appropriate dose of 5-ALA according to their weight and trial cohort on the morning of their surgery. Patients underwent fluorescence guided laparoscopic segmental colectomy with D3 lymphadenectomy with the specimen examined within the local histopathology department. All patients were followed up in clinic 30 days following their surgery.

The intraoperative fluorescence detecting system used to assess the tumour and draining lymphatic field was the Storz D-Light Laparoscopic System (KARL STORZ GmbH & Co. KG; Tuttlingen, Germany). This infrared laparoscopic camera has a blue-light setting emitting light from 380-440nm. The location of fluorescent lymph nodes was documented and marked with surgical clips to allow identification during histopathological examination.

Patients underwent segmental colectomy with D3 lymphadenectomy and tissue specimens were subjected to standard histopathological examination(231). In addition, identified fluorescent lymph nodes underwent step-sectioning to identify micrometastatic disease.

To determine the sensitivity and specificity of pre-operative CT reporting in this study CT reports were compared to histopathological examinations.

Resection specimens were examined for oncological quality, including the plane and completeness of mesocolic resection and the extent of lymphadenectomy.

Following surgery patients received standard post-operative care with additional monitoring for any adverse effects due to 5-ALA, such as cutaneous photosensitivity. To reduce the risk of photosensitivity reactions all patients skin and eyes were protected from the theatre operating lights and were kept out of direct sunlight on the ward for at least the first 48 hours following surgery. Patients were monitored for any 5-ALA related adverse effects in addition to the normal complications of major colorectal cancer surgery and general anaesthesia such as anastomotic leak, conversion to open surgery

and venous thromboembolism. Any adverse side effects or complications in the first 30 postoperative days were recorded. All patients were followed up at 30 days post-surgery.

## **2.1.2 Patient samples**

Paired normal and colonic tumour tissues were taken from each patient to allow further investigation of factors that could influence 5-ALA mediated fluorescence. Details regarding the use and storage of tissue samples were discussed with patients during the trial recruitment and consenting process.

### **2.1.2.1 Snap freezing specimens**

Following surgical resection, tissue samples were rapidly cooled to preserve tissue integrity and prevent the degradation of biological molecules such as proteins and RNA.

Biopsy samples were fixed on to cork discs using Optimal Cutting Temperature (OCT) compound (VWR International Ltd, Lutterworth, UK) ensuring the tissue samples were completely embedded into the OCT compound. The cork board were then submerged into liquid nitrogen cooled iso-pentane. For long-term storage, samples were stored at -80°C .

### **2.1.2.2 Cryoscrolling and cryosectioning snap frozen specimens**

Snap frozen tissue samples were cryoscored (RNA extraction) and cryosectioned (histopathological examination) by mounting the cork board containing the snap frozen specimens onto a chuck using OCT. Sections were cut using a Leica CM3050 S Research Cryostat (Leica Microsystems (UK) Ltd, Milton Keynes, UK) that was set to -20°C. For RNA extraction, specimens were sectioned at 10µm and 30µm and the cryoscored samples were collected. For histopathological examination, 10µm sections

were cut and fixed onto SuperFrost™ Microscope Glass Slides (Thermo Fisher Scientific Inc., Waltham, Massachusetts, USA).

### **2.1.2.3 H&E staining of sectioned tissue specimens**

Cryosectioned samples on glass slides were initially stained with Mayer's Haematoxylin solution then rinsed in running water for 1 minute. The slides were washed in Scott's Tap Water for 1 minute before being rinsed in running water for a 1 minute. Slides were counterstained with Eosin for 1 minute before being rinsed in running water for 1 minute. Slides were then dehydrated in ethanol, rehydrated in xylene and mounted on to coverslips using DePeX Mounting Medium (Sigma Aldrich, Gillingham, UK).

Slides were assessed by an experienced gastrointestinal histopathologist to identify samples with the highest percentage of malignancy to allow a reasonable comparison between fluorescent and non-fluorescent tumours. Six specimens from the fluorescent tumours and six non-fluorescent tumour specimens were selected for RNA analysis.

### **2.1.2.4 Extraction of RNA from snap frozen specimens**

Three different RNA extraction methods were compared to identify the most effective protocol. The first and second protocols utilised the PureLink™ RNA Mini Kit (Thermo Fisher) and the third protocol utilised the RNeasy Mini Kit (Qiagen, Manchester, UK) for RNA extraction. A single cryoscored sample (as described in 2.1.2.2) of normal colonic tissue was randomly selected and used for each protocol.

#### **2.1.2.4.1 RNA separation using PureLink™ RNA Mini Kit – Protocol 1**

In the first protocol, 20x cryosections of 30µm thick tissue were transferred into a PureLink™ RNA Mini Kit 1.5ml RNA/DNA free cartridge. 500µl of TRIzol reagent (Thermo Fisher) was then added into the cartridge. Repetitive pipetting using RNA/DNA free pipette tips was performed to lyse the cells and the solution transferred into a PureLink™ RNA Mini Kit 2ml RNase-free cartridge. After 5 minutes at room temperature, 100µl of chloroform was added and the cartridge was agitated for 15 seconds. The solution was left for a further 3 minutes at room temperature before being centrifuged for 15 minutes at 12,000g at 4°C. This separates the solution into a lower red phenol-chloroform phase, an interphase, and a colourless upper aqueous phase. The upper phase contains the RNA fragments and 400µl of this phase was transferred into a fresh RNase-free cartridge and mixed with 400µl 70% ethanol.

#### **2.1.2.4.2 RNA separation using PureLink™ RNA Mini Kit – Protocol 2**

For the second protocol, 20x cryosections of 30µm thick tissue were transferred into a PureLink™ RNA Mini Kit 1.5ml RNA/DNA free cartridge. 700µl of TRIzol reagent was then added into the cartridge. Repetitive pipetting using RNA/DNA free pipette tips was performed to lyse the cells and 140µl of chloroform was immediately added. The cartridge was then agitated for 15 seconds. The solution was left for a further 3 minutes at room temperature before being centrifuged for 15 minutes at 12,000g at 4°C. The upper aqueous phase was transferred to a fresh RNase-free cartridge and an equal volume of 70% ethanol was added.

#### **2.1.2.4.3 RNA extraction using PureLink™ RNA Mini Kit**

Following RNA separation utilising the PureLink™ RNA Mini Kit, the subsequent steps were identical for both protocol 1 and 2. The RNA-ethanol mixtures were transferred into a spin cartridge with a collection tube and centrifuged at 12,000g for 15 seconds at room temperature. The flow-through was discarded and the spin cartridge reinserted. 700µl Wash Buffer I was added to the spin cartridge and centrifuged again at 12,000g for 15 seconds at room temperature. Both the flow-through and collection tubes were discarded at this point and the spin cartridge placed into a new collection tube. 500µl Wash Buffer II with ethanol was added to the spin cartridge and centrifuged at 12,000g for 15 seconds at room temperature. The flow-through was discarded and this wash step with Wash Buffer II was repeated once more. The flow-through was again discarded and the spin cartridge was centrifuged at 12,000g for one minute at room temperature. The spin cartridge was then placed in the recovery tube and 30µl RNAase-free water was added and left to incubate at room temperature for a further minute. RNA fragments were recovered by centrifuging the spin cartridge at room temperature for two minutes at 12,000g.

#### **2.1.2.4.4 RNA extraction using RNeasy Mini Kit – Protocol 3**

For the third protocol, 30x cryoscrolls of 10µm thick tissue were harvested and transferred into a RNeasy Mini Kit RNA/DNA free cartridge. 10µl of β-mercaptoethanol (β-ME) was added to 1ml RNeasy Mini Kit Buffer RLT and 350µl of this solution was added to the cryoscrolls prior to centrifuging at 15,000g for 3 minutes at room temperature. The supernatant was removed using an RNA/DNA free pipette tip into a sterile micro-centrifuge tube and an equal volume of 70% ethanol was added and thoroughly mixed. The lysate was then added to a RNeasy spin column within a 2ml collection tube and centrifuged at 8,000g for 15 seconds at room temperature. The flow-through was discarded and 700µl of Buffer RW1 was added to the same spin column.

This was then centrifuged at 8,000g for 15 seconds at room temperature and the flow-through discarded. RNeasy Mini Kit Buffer RPE was diluted at 1 in 5 with 96-100% ethanol and 500µl added to the same spin column. This was then centrifuged at 8,000g for 15 seconds at room temperature and the flow-through discarded. A further 500µl of the diluted Buffer RPE was again added to the same spin column, which was centrifuged at 8,000g for two minutes at room temperature. The spin column was placed in a new collection tube and 50µl RNAase-free water was added directly to the membrane. Elution of the RNA was achieved by centrifuging at 8,000g for one minute at room temperature.

#### **2.1.2.4.5 Analysing the quality of extracted RNA**

Following extraction of RNA from the samples using the three different protocols, the quality of RNA was assessed. Quality assessment was based on:

1. The concentration of extracted RNA
2. RNA integrity number (RIN) value

##### **2.1.2.4.5.1 – Determining RNA concentration**

The concentration of RNA was determined by calculating the ratio between the optical density absorbance values between 260nm and 280nm using a NanoDrop 1000 Spectrophotometer (Thermo Fisher). The Nanodrop was initially calibrated using deionised water. The absorption spectrum of RNase-free water was measured as a blank control to normalise RNA absorption spectra. RNA absorption was mapped out between 200nm and 350nm. Absorption values at 260nm and 280nm were recorded and the ratio between these values was used to determine RNA concentration.

#### **2.1.2.4.5.2 – Determining RIN value**

RIN values were determined using the RNA ScreenTape Assay (Agilent Technologies, Waldbronn, Germany). Firstly, a running ladder was prepared by mixing 5µl RNA Sample Buffer with 1µl RNA Ladder. All extracted RNA samples were prepared by mixing 5µl RNA Sample Buffer with 1µl extracted RNA sample. The ladder and all samples were then heated at 72°C for 3 minutes after which they were placed on ice for 2 minutes. Samples were then loaded and analysed in an RNA ScreenTape 2200 TapeStation (Agilent Technologies).

#### **2.1.2.5 Gene expression analysis**

RNA was extracted from selected fluorescent and non-fluorescent tumours using the optimal RNA extraction protocol. Gene expression analysis was carried out to identify any underlying factors that could be responsible for the differences in observed tumour fluorescence. The analysis was performed by Fios Genomics Ltd (Edinburgh, UK).

## **2.2 Recognition molecules**

### **2.2.1 Immunofluorescence**

#### **2.2.1.1 Cell lines**

LoVo (metastatic colorectal), HEK293 (renal epithelial) and EA.hy926 (endothelial) cell lines were obtained from the European Collection of Authenticated Cell Cultures (Salisbury, UK). LoVo cells were cultured in Ham's F-12 Nutrient Mixture Medium (Life Technologies™, Paisley, UK) supplemented with 10% heat-treated foetal calf serum (FCS) (Sigma Aldrich). HEK293 and EA.hy926 cells were cultured in Dulbecco's Modified Eagle Medium (DMEM) + GlutaMAX™ (Life Technologies, Paisley, UK)

medium supplemented with 10% heat-treated FCS. All three cell lines were cultured in 75cm<sup>2</sup> tissue culture flasks (Corning Inc., New York, USA) and incubated at 37°C, 5% CO<sub>2</sub> and 95% Relative Humidity (RH).

### **2.2.1.2 Passaging cell lines**

Upon 70% confluency, cell cultures were washed with Dulbecco's Phosphate-Buffered Saline (DPBS) (Life technologies, Paisley, UK) and incubated for 5 minutes with 0.05% (v/v) trypsin and 0.5% (v/v) ethylenediaminetetraacetic acid (Life technologies, Paisley, UK) in DPBS. FCS-supplemented cell media was then added to the flasks, cell suspension was collected and centrifuged for 5 minutes at 400g. The supernatant was discarded and the pelleted cells were resuspended in fresh medium and re-seeded into 75cm<sup>2</sup> tissue culture flasks at 1:10 to 1:3 dilutions. Excess cells were used for experiments or subsequently discarded.

### **2.2.1.3 Fixing cells**

For immunofluorescence, 2ml of a 1:15 dilution of cells in appropriate cell media were seeded onto sterile glass cover slips in 6-well plates (Corning, New York, USA) and incubated for 48 hours at 37°C, 5% CO<sub>2</sub> and 95% RH. Cell media was discarded and cells were washed with DPBS. Cells were then fixed with 4% paraformaldehyde (Sigma Aldrich) for 10 minutes at room temperature then washed twice with DPBS. For long-term storage the plates were stored at 4°C.

### **2.2.1.4 Immunofluorescence protocol**

Fixed cells were washed with PBS for 5 minutes and blocked using 0.5% skimmed milk solution (Marvel, Premier Foods Group, London, UK) in PBS for another 5 minutes. A 1:10 dilution of primary anti-CEA antibody (A5B7, Biotherapeutics Development Unit,

Cancer Research UK, Clare Hall Laboratories, Potters Bar, UK) in the blocking solution was centrifuged for 5 minutes at 13,000g. 100µl of the diluted primary antibody was then added to the fixed cells and left to incubate at room temperature for 1 hour. Cells were then subjected to three wash cycles lasting 5 minutes each with PBS. A fluorescent secondary goat anti-mouse Alexa Fluor® 488 antibody (Thermo Fisher) was diluted in the blocking solution to a concentration of 1 in 300 and similarly centrifuged. 100µl diluted secondary antibody was then added to the cells and incubated at room temperature for 30 minutes and protected from light. Another three wash cycles with PBS were performed before the cover slips were removed from the wells and mounted onto glass slides using Prolong Gold Antifade reagent with DAPI (Thermo Fisher). Slides were sealed with ethyl acetate and cured overnight at room temperature whilst protected from light and then imaged at x63 magnification using a Zeiss Axioimager fluorescent microscope (Carl Zeiss, Herts, UK).

## **2.2.2 Antibodies**

Recombinant chimeric anti-CEA monoclonal IgG antibody A5B7 (supplied by Cancer Research UK Biotherapeutics Development Unit, UK) that was raised against purified human CEA from human metastatic colon tumour tissue was used as the primary targeting antibody. Monoclonal mouse anti-human anti-CD31 IgG antibody clone JC70A (Dako, Glostrup, Denmark) was selected as the control antibody. CD31 is a type 1 transmembrane glycoprotein known as platelet endothelial cell adhesion molecule-1(232). Both these antibodies were tested against all three cell lines.

### **2.2.2.1 Reduction of antibody**

Reducing agents break the disulphide bonds holding the light and heavy chains of the antibody together, exposing a free cysteine (sulfhydryl) group for conjugation(233). A

half antibody fragment is created when the disulphide bond holding the two heavy chains together is broken, but the antigen recognition site created by the folding of the heavy and light chain remains intact. This means that there is a free cysteine group available on the heavy chain of the antibody with an intact antigen recognition site. A half antibody fragment should allow orientation of antibody when bound to the functionalised NP.

Three reducing agents were tested on the target antibody in an attempt to identify the optimal agent to produce the largest proportion of half antibody fragments:-

1. Tris(2-carboxyethyl)phosphine (TCEP) (Thermo Fisher)
2. 2-mercaptoethanol (2-ME) (Sigma Aldrich)
3. 2-mercaptoethylamine-HCl (2-MEA) (Sigma Aldrich)

The target anti-CEA antibody described in 2.2.2 was added separately at a concentration of  $0.44\mu\text{g}/\mu\text{l}$  to 10mM TCEP, 0.1M 2-ME and 0.18M 2-MEA and incubated at  $37^{\circ}\text{C}$  for 90 minutes.

### **2.2.2.2 Gel electrophoresis**

5 $\mu\text{l}$  of non-reducing buffer dye was added to 10 $\mu\text{l}$  of each reduced target antibody. Each reduced antibody-dye complex was added separately to a column in a Mini-Protean TGX Precast gel cartridge (Bio-Rad, Watford, UK) with a Spectra Multicolour Broad Range Protein ladder dye (Thermo Fisher) to enable reading of the size of the bands. The cartridge was then placed into a gel electrophoresis tank (Bio-Rad) which ran for 1 hour at 120V and 20mA. The gel was then removed from the cartridge and incubated with Instant Blue Commassie stain (Generon, Maidenhead, UK) for 1 hour. The gel was rinsed with distilled water to remove excess dye before exposure and imaged using a G:Box (Syngene, Cambridge, UK).

### 2.2.2.3 Dot blotting

Dot blotting was used to identify any potential glycoprotein side chains from the heavy chains of the anti-CEA antibody.

4.2mg sodium meta-periodate (Sigma Aldrich) was added to 1ml Glycolink Coupling Buffer (Thermo Fisher). 1ml of 2mg/ml target antibody solution was added to the sodium meta-periodate solution and incubated at room temperature for 30 minutes whilst protected from light. Excess sodium meta-periodate was removed by gel filtration through a 50K Amicon Ultra centrifugal filter (Merck Millipore Ltd, Cork, Ireland) that had been equilibrated with the Glycolink Coupling Buffer. The filtrate was recovered and made up to a volume of 2ml using the buffer producing an oxidised antibody solution at a concentration of 1mg/ml.

The presence of any oxidised glycoprotein was tested by labelling with a biotin group. This was done by adding 200 $\mu$ l 5mM hydrazine-biotin (Sigma Aldrich) to 1.8ml oxidised 1mg/ml target antibody and incubating for 1 hour at room temperature. The resulting solution was filtered using the same centrifugal filter to remove any excess hydrazine-biotin and the recovered filtrate was made up to a 1mg/ml concentration by dilution in PBS. This oxidised and biotinylated antibody solution was used in subsequent dot blotting and western blotting. Untreated target antibody was used as a control.

2 $\mu$ l biotinylated target antibody and 2 $\mu$ l untreated target antibody were spotted onto two separate nitrocellulose membranes which were allowed to air dry for 15 minutes before blocking with a 5% non-fat milk solution for 1 hour at room temperature. The milk blocking solution was removed and 10 $\mu$ l streptavidin-HRP (Sigma Aldrich) was added to 10ml 5% non-fat milk solution. 5ml streptavidin-HRP-milk solution was incubated with

each membrane for 1 hour at room temperature. Two wash steps were performed with PBS containing 0.1% tween-20 (PBST) (Acros Organics, Geel, Belgium) with another wash in PBS. The membrane was subsequently exposed using a Pierce™ ECL Western Blotting Substrate Kit (Thermo Fisher) according to the manufacturer's protocol and imaged using a G:Box (Syngene, Cambridge, UK).

#### **2.2.2.4 Western blotting**

Biotinylated and untreated target antibodies were mixed with a reducing dye buffer containing dithiothreitol (DTT) (Sigma Aldrich) and incubated at 90°C for 10 minutes. 15µl of each antibody-dye mixtures were loaded into a nitrocellulose gel and resolved for 60 minutes at 120V and 20mA. The gel was removed from the cartridge, assembled between felt pads and a nitrocellulose membrane in a transfer cassette and placed into a Western Blot gel tank (Bio-Rad) containing transfer buffer for 1 hour at 120V. Following the transfer of proteins, the membrane was blocked in 5% bovine serum albumin (BSA) (Thermo Fisher) for 30 minutes, then incubated with 10ml 5% BSA containing 10µl streptavidin-HRP for 1 hour at room temperature. The membrane was then washed with PBST twice followed by another wash in PBS. The membrane was subsequently exposed using a Pierce™ ECL Western Blotting Substrate Kit (Thermo Fisher) according to the manufacturer's protocol and imaged using a G:Box.

#### **2.2.2.5 Oxidation of antibody**

Both target and control antibodies underwent oxidation of the glycoprotein side chains to enable conjugation to the functionalised NP. The control antibody was diluted in a solution containing BSA which needed to be extracted prior to oxidation. This was an additional step not required for the target antibody. This was achieved by filtering the control antibody through a 100K Amicon Ultra centrifugal filter (Merck Millipore Ltd, Cork,

Ireland) that had been equilibrated with Glycolink Coupling Buffer (Thermo Fisher). All subsequent steps were the same for both antibodies.

4.2mg sodium meta-periodate (Sigma Aldrich) was added to 1ml Glycolink Coupling Buffer. Equal volumes of the sodium meta-periodate solution and 2mg/ml antibody were allowed to incubate for 30 minutes at room temperature whilst being protected from the light. Excess sodium meta-periodate was removed by gel filtration through a 50K Amicon Ultra centrifugal filter that had been equilibrated with the Glycolink Coupling Buffer. The filtrate was recovered and made up to the original volume of solution filtered using the buffer producing an oxidised antibody solution at a concentration of 1mg/ml. Both the oxidised target and oxidised control antibodies were then tested against fixed cell lines using the immunofluorescence technique described in 2.2.1.4.

#### **2.2.2.6 Biotinylation of antibody**

Oxidation of the target and control antibodies was performed as described in 2.2.2.5 and then labelled with biotin. This was achieved by adding 5mM hydrazine-biotin to the filtered antibody solution followed by the addition of aniline and mixed for 1 hour at room temperature. Using the same desalting column as the oxidation process the antibody-biotin solution was centrifuged at 10,000g for 1 minute to remove any unreacted biotin. The filtrate was recovered and made up to the original volume of solution and filtered using PBS producing a biotinylated antibody solution at a concentration of 1mg/ml.

The three cell lines were prepared and fixed in 6-well plates as described in 2.2.1.3. If cells on glass slides had been stored at 4°C prior to use cells were rehydrated in PBS for 5 minutes. The PBS was then discarded and an avidin-containing reagent (Vector Laboratories Ltd, Peterborough, UK) was added to the wells and incubated at room

temperature for 15 minutes. Following a rinse with PBS a biotin solution (Vector Laboratories Ltd, Peterborough, UK) was added to the wells and incubated at room temperature for 15 minutes. A blocking solution containing 0.1% bovine serum albumin was then added to the cells for 30 minutes. This blocking solution, in addition to the original antibodies, were used as controls to be compared to the biotinylated antibodies. 1 in 100 solutions of the controls and biotinylated antibodies were added to the wells and incubated at room temperature for 1 hour. The cells were subjected to three wash cycles lasting 5 minutes each with PBS (Sigma Aldrich). A fluorescent secondary goat anti-mouse Alexa Fluor® 488 antibody (Invitrogen, Oregon, USA) was diluted in the blocking solution to a concentration of 1 in 300 and similarly centrifuged. 100µl diluted secondary antibody was added to the cells and incubated at room temperature for 30 minutes protected from light. Another three wash cycles with PBS were performed before the cover slips were removed from the wells, mounted onto glass slides, cured and imaged as described in 2.2.1.4.

### **2.2.3 Biotinylation of affimer**

The anti-CEA affimer used in this project was kindly supplied by the Department of Biotechnology (School of Molecular and Cellular Biology, Faculty of Biological Sciences, University of Leeds, UK).

Reduction of 155µl anti-CEA affimer at a concentration of 0.82mg/ml was performed using a TCEP Disulfide Reducing Gel. 4µl of PBS with 50mM EDTA was added to the prepared gel prior to the affimer being added. This was incubated for one hour at room temperature on a rotator at 20rpm. The gel was then centrifuged at 1,000g for 1 minute and the clear supernatant containing the reduced affimer was recovered. This was immediately mixed with 44.28µl 2mM biotin-maleimide and incubated for 2 hours at room

temperature. The biotinylated affimer solution was then filtered through a prepared Zebra spin desalting column 7K MWC to remove any unbound biotin.

The three cell lines were prepared and fixed in 6-well plates as described in 2.2.1.3. If cells on glass slides had been stored at 4°C prior to use cells were rehydrated in PBS for 5 minutes. The PBS was removed, an avidin-containing reagent added to the wells and incubated at room temperature for 15 minutes. Following a rinse with PBS, Biotin was added to the wells and incubated at room temperature for 15 minutes. A blocking solution containing 0.1% bovine serum albumin was then added to the cells for 30 minutes. A 1 in 100 dilution of the biotinylated affimer in the blocking solution was incubated with the cells in addition to a control of plain blocking solution. This was left to incubate overnight at 4°C. The cells were subjected to three wash cycles lasting 5 minutes each with PBS. A fluorescent protein that binds to biotinylated proteins, Streptavidin Dylight 488, was diluted in the blocking solution to a concentration of 1 in 300. 100µl diluted Streptavidin Dylight 488 was added to the cells and incubated at room temperature for 1 hour protected from light. Another three wash cycles with PBS were performed before the cover slips were removed from the wells, mounted onto glass slides, cured and imaged as described in 2.2.1.4.

## **2.3 Nanoparticle**

### **2.3.1 Fabrication of nanoparticles**

The semiconducting organic polymer NP is comprised of a fluorescent core, poly(2,5-di(hexyloxy)cyanoterephthalylidene) (CN-PPV) (Sigma-Aldrich, Dorset, UK), encapsulated in a shell of poly(ethylene glycol) methyl ether-block-poly(lactide-co-glycolide) (PLGA-PEG) (Sigma-Aldrich, Dorset, UK). The average molecular weight (Mn) for PLGA was 55,000Da and 5,000Da for the PEG component of the polymer.

A 2.5mg/ml solution of CN-PPV and a 5.56mg/ml solution of non-functionalised PLGA-PEG in tetrahydrofuran (THF) (Fisher Scientific, Loughborough, UK) were created. 900µl PLGA-PEG solution was added to 100µl CN-PPV solution. 5ml distilled water was then added slowly and sonicated for 15 minutes in an ice water bath using a Bandelin Sonorex (Bandelin Electronic, Berlin, Germany). This mixture was then continuously stirred for 24 hours in a fume cupboard to allow the THF to evaporate. These non-functionalised NPs were then stored in the dark at 4°C.

PLGA-PEG with a functional terminal maleimide group (Akina Inc., Indiana, USA) with a Mn of 30,000Da and 5,000Da respectively was used to form a maleimide functionalised NP using a similar method. The maleimide functionalised PLGA-PEG was dissolved in THF at a concentration of 5.56mg/ml. Maleimide functionalised NPs were then created with different ratios of the functional group in increments of 25% as detailed below. This was done by combining different volumes of the PLGA-PEG-Maleimide and standard PLGA-PEG (total volume equal to 900µl).

- 25% MNP: 675µl non-functionalised PLGA-PEG, 225µl maleimide functionalised PLGA-PEG and 100µl CNPPV solution
- 50% MNP: 450µl non-functionalised PLGA-PEG, 450µl maleimide functionalised PLGA-PEG and 100µl CNPPV solution
- 75% MNP: 225µl non-functionalised PLGA-PEG, 675µl maleimide functionalised PLGA-PEG and 100µl CNPPV solution
- 100% MNP: 0µl non-functionalised PLGA-PEG, 900µl maleimide functionalised PLGA-PEG and 100µl CNPPV solution

NPs with a shorter PEG component were also fabricated for conjugation applications.

The Mn values for PLGA was 11,500Da and 2,000Da for the PEG component of the

polymer in these NPs. Both non-functionalised and maleimide functionalised NPs with this shorter PEG component were fabricated and stored as described above.

For the purposes of this thesis, non-functionalised NPs are NPs that have been formed using PLGA-PEG that does not possess the maleimide functional group and functionalised NPs are NPs whose PLGA-PEG possess a functional terminal maleimide (MNP) or streptavidin (SNP) group. Bare NPs refer to non-functionalised and functionalised NPs that have not been conjugated to a recognition molecule.

### **2.3.2 Characterisation of nanoparticles**

All non-functionalised and maleimide functionalised NPs were characterised by the following methods. Serial characterisation was also performed over the course of up to 12 weeks to establish bench life of these NPs.

#### **2.3.2.1 Characterisation of nanoparticle sizes**

The hydrodynamic diameter of all NPs and MNPs was established using dynamic light scattering via a Malvern Zetasizer Nano ZSP (Malvern Instrument, Worcestershire, UK) at 25°C in micro UV-Cuvettes (Brand GmbH & Co., Wertheim, Germany). The z-average is the intensity weighted mean hydrodynamic diameter measured by dynamic light scattering and this measurement is what was used to characterise the size of the NPs over time. The polydispersity index was also measured; this represents the heterogeneity of the hydrodynamic diameters of the NPs in a single sample. The back scattering angle used was 173° for all measurements taken with dynamic light scattering.

### **2.3.2.2 Characterisation of the nanoparticle absorption and emission profiles**

The absorption spectrum was measured using a Perkin Elmer UV/Vis/NIR Spectrophotometer (Perkin Elmer GmbH, Uberlingen, Germany) using a slit width of 2nm and an absorption range between 300nm and 800nm. The emission spectrum was tested using a Jobin Yvon Horiba FluoroMax-3 spectrofluorimeter (Jobin Yvon Ltd, Stanmore, UK) using a slit width of 2nm and an emission range between 300nm and 800nm. Emission spectra were tested at 4 different excitation wavelengths; 380nm, 425nm, 440nm and 470nm. Both the absorption and emission spectrum of non-functionalised NP and MNP solutions at an optimal dilution were measured using a High Precision Cell Quartz Suprasil 10mm cuvette (Hellma Analytics, Germany).

#### **2.3.2.2.1 Determining optimum dilution for testing absorption and emission profiles**

Standard non-functionalised NPs were produced as described in 2.3.1. To determine the optimum NP dilution for testing emission spectra, non-functionalised NPs were diluted in distilled water in 0.25µg/ml increments to form a series of dilutions ranging from 3µg/ml to 5µg/ml CN-PPV. The absorption and emission spectra for all dilutions was measured as described in 2.3.2.2.

### **2.3.3 Testing the effect of centrifugation on nanoparticle characterisation**

The conjugation between the recognition molecule and the maleimide functionalised NP initially required the MNP to undergo chemical modifications. Therefore, investigations were conducted to determine whether these modifications would have any effect on the hydrodynamic diameter or fluorescent emission of the MNP.

To investigate the effect of centrifugation on the MNP, two series of 1500µl optimal dilution bare 25% maleimide functionalised NP were centrifuged from 1,000g to 10,000g at increments of 1,000g at room temperature. The supernatant was discarded and MNPs resuspended in 1500µl distilled water. Series 1 was centrifuged for 5 minutes, whereas series 2 was centrifuged for 30 minutes. Following resuspension, the MNPs were characterised as per 2.3.2.1 and 2.3.2.2. The control was 1500µl of optimal dilution bare 25% maleimide functionalised NP that had not been subjected to centrifugation.

### **2.3.3.1 Testing effects of repeated centrifugation on nanoparticle characterisation**

To investigate the effect of repeated centrifugation on MNPs, 1500µl optimal dilution bare 25% maleimide functionalised NP was centrifuged at 6,000g for 30 minutes at room temperature and the supernatant discarded. The MNPs were resuspended in 1500µl distilled water and characterised as per 2.3.2.1 and 2.3.2.2. The MNPs were then centrifuged for a further 30 minutes at room temperature, the supernatant discarded and the MNPs resuspended in 1500µl distilled water. This process was then repeated twice. Following each round of centrifugation and resuspension the MNP was characterised as per 2.3.2.1 and 2.3.2.2.

### **2.3.4 Cell viability after exposure to bare maleimide functionalised nanoparticle**

#### **2.3.4.1 Cell counting for seeding 96-well plates**

LoVo, HEK293 and EA.hy926 cells were passaged as described in 2.2.1.2 and 10µl of cell suspension solutions were mixed with 10µl Trypan blue (Life Technologies Europe, Bleiswijk, Netherlands). 10µl of this solution was placed into an Invitrogen cell counting

slide (Life Technologies Europe, Bleiswijk, Netherlands) and the cell concentration was determined using a Countess II Automated Cell Counter (Life Technologies, Carlsbad, California, USA). A concentration of  $2.5 \times 10^4$  cells/ml was then created and 100  $\mu$ l of cells in suspension were then added to each well in 96-well plates and placed into incubation.

#### **2.3.4.2 MTT Assay**

LoVo, HEK293 and EA.hy926 cells were prepared in 96-well plates (Corning Inc., New York, USA) as described in 2.3.4.1. After 24 hours, total cell media was exchanged with cell media containing 10-fold dilutions of bare 25% maleimide functionalised NPs and left for either 24, 48 or 72 hours. Plates also contained a media only control. After 24, 48 or 72 hours, the media was replaced with a 1 mg/ml solution of 3-(4,5-dimethylthiazol-2-yl)-2,5-diphenyltetrazolium bromide (MTT) (Sigma-Aldrich, MO 63103, USA) in cell media and incubated for 4 hours. Excess unmetabolised MTT solution was discarded and formazan crystals were completely dissolved in propan-1-ol (Fisher Scientific, Loughborough, UK). Dissolved formazan absorbance values were determined at 570nm using a Mithras LB 940 Microplate Reader (Berthold Technologies Ltd., Harpenden, UK).

#### **2.3.5 Testing for non-specific binding of nanoparticle to cell lines**

LoVo, HEK293 and EA.hy926 cells were prepared in 96-well plates as described in 2.3.4.1. A control of appropriate cell media was compared against diluted bare non-functionalised NP and the different ratios of diluted maleimide functionalised NPs (25%, 50%, 75% and 100% MNP) in appropriate cell media. 100  $\mu$ l of either control, diluted non-functionalised NP or diluted MNP were added to wells and plates were incubated for 24 hours at 37°C and 5% CO<sub>2</sub>. Cell media was then removed and the plates were subjected to three wash cycles lasting 5 minutes each with PBS (Sigma-Aldrich, MO

63103, USA). Plates were left overnight at room temperature protected from light. 200µl 10% sodium dodecyl sulfate (SDS) was added to each well for 2-3 minutes and then centrifuged at room temperature for 5 minutes at 400g. 150µl of the supernatant from the wells were transferred into a new plate and fluorescence was measured (Excitation: 470nm, Emission: 650nm) on the microplate reader.

This method was repeated with the addition of cysteine to investigate whether blocking the unoccupied maleimide functional group had any impact on non-specific binding of the MNP to cells. A 10mM solution of cysteine was created in appropriate cell media and used to dilute the bare non-functionalised NP and different ratio bare maleimide functionalised NPs. The control, NP and different ratio MNP dilutions were left in the 10mM cysteine cell media solution for an hour prior to adding to the wells to allow the cysteine to block the maleimide functional groups.

## **2.4 Conjugation**

### **2.4.1 Conjugating anti-CEA antibody to heterobifunctional crosslinker**

To confirm the conjugation of oxidised antibodies through binding of aldehyde groups to hydrazide functional groups on the heterobifunctional crosslinker, a fluorescent sulfhydryl-reactive dye was used. Dylight™ 488 Maleimide (ThermoFisher Scientific, Rockford, USA) is a maleimide activated fluorescent dye that labels unoccupied sulfhydryl groups.

#### **2.4.1.1 Testing antibody – dye labelled crosslinker conjugate against cell lines using 0.5% skimmed milk as the blocking agent**

Dylight™ 488 Maleimide and PDPH were dissolved in dimethyl sulfoxide (DMSO) to concentrations of 1.6mg/ml and 2.4mg/ml respectively. 250µl of each solution were mixed together and incubated for 2 hours at room temperature, protected from light, allowing the dye to label the crosslinker. The anti-CEA antibody was oxidised as per the protocol described in 2.2.2.5 and 500µl mixed with 280µl of the dye-labelled crosslinker. This mixture was incubated in the dark for an hour at room temperature. Excess reagents were extracted from the antibody-dye-labelled crosslinker conjugate by gel filtration through a PBS-equilibrated 50K Amicon Ultra centrifugal filter. The filtrate was recovered and diluted in 780µl PBS. The antibody-dye-labelled crosslinker conjugate was then tested on LoVo, HEK293 and EA.hy926 cell lines using the immunofluorescence protocol described in 2.2.1.4. 0.5% skimmed milk blocking and unconjugated oxidised antibody served as controls. Due to the presence of the fluorescent Dylight 488 molecules a secondary fluorescent antibody was not needed.

#### **2.4.1.2 Testing antibody – dye labelled crosslinker conjugate against cell lines using 0.1% bovine serum albumin as blocking the agent**

The protocol described above in 2.4.1.1 was repeated using a different blocking method (Avidin/Biotin blocking). LoVo, HEK293 and EA.hy926 cell lines were prepared and fixed in 6-well plates as described in 2.2.1.3. Cells were rehydrated in PBS for 5 minutes. The PBS was then discarded and an avidin-containing reagent (Vector Laboratories Ltd, Peterborough, UK) was added to cells and incubated at room temperature for 15 minutes. Cells were then washed with PBS and a biotin solution (Vector Laboratories Ltd, Peterborough, UK) was added to cells and incubated at room temperature for 15 minutes. A blocking solution containing 0.1% bovine serum albumin was then added to the cells and incubated for 30 minutes. The following steps were conducted as described

in 2.2.1.4. 0.1% bovine serum albumin blocking and unconjugated oxidised antibody served as controls. Due to the presence of the fluorescent Dylight 488 molecules a secondary fluorescent antibody was not needed for experiments.

#### **2.4.1.3 Testing components of antibody – dye labelled crosslinker conjugate**

To identify components which may potentially be responsible for non-specific binding to cell lines each of the following components were tested against LoVo, HEK293 and EA.hy926 cell lines using the immunofluorescence technique as described in 2.4.1.2 with the additional control of unmodified PDPH:

- Oxidised anti-CEA antibody
- PDPH
- Dye labelled PDPH
- Unblocked Dylight™ 488 Maleimide dye
- Blocked Dylight™ 488 Maleimide dye

To block the Dylight™ 488 Maleimide the dye was added to a 10mM cysteine solution and left to incubate for an hour to allow the cysteine to block maleimide functional groups.

#### **2.4.2 Conjugation of antibody recognition molecule to maleimide functionalised nanoparticle**

Conjugation of the anti-CEA antibody to the 25% maleimide functionalised NP through the use of the heterobifunctional crosslinker, PDPH, was investigated. For subsequent experiments the non-functionalised PLGA-PEG used in the NP system was the 2KDa PEG chain length.

#### **2.4.2.1 Conjugating heterobifunctional crosslinker to maleimide functionalised nanoparticle**

To ascertain the length of time for the heterobifunctional crosslinker to bind to the maleimide functional group on the MNP, the following binding assay was performed.

LoVo cells were passaged as per 2.2.1.2 and seeded into 96-well plates as per 2.3.4.1. The plates were incubated overnight at 37°C, 5% CO<sub>2</sub> and 95% Relative Humidity (RH).

Equal volumes of 0.1mg/ml PDPH and 25% bare maleimide functionalised NP were mixed for 30 minutes, 1 hour and 2 hours at room temperature. Excess PDPH was removed by gel filtration through a 50K Amicon Ultra centrifugal filter that had been equilibrated with distilled water. The anti-CEA antibody was oxidised and filtered as per 2.2.2.5.

The oxidised anti-CEA antibody and each PDPH-NP conjugate were mixed at a ratio of 20:1 for 1 hour at room temperature. Excess oxidised anti-CEA antibody was removed from each solution by centrifuging the mixture at 6,000g for 30 minutes, carefully removing the supernatant and resuspending in an original volume of PBS.

1 in 100 dilutions of bare 25% maleimide functionalised NPs, 30 minute anti-CEA antibody-NP conjugate, 1 hour anti-CEA antibody-NP conjugate and 2 hour anti-CEA antibody-NP conjugate were created in appropriate cell media. Cell media in the 96-well plates was exchanged with 100µl cell media of either the bare 25% maleimide functionalised NP or the various anti-CEA antibody-NP conjugates. Plates also contained a media only control. Plates were incubated for 24 hours at 37°C, 5% CO<sub>2</sub> and 95% Relative Humidity (RH).

Cell media was then removed and the plates were subjected to three wash cycles lasting 5 minutes each with PBS. Plates were left overnight at room temperature protected from light. 200µl 10% sodium dodecyl sulfate (SDS) was added to each well for 2-3 minutes and then centrifuged at room temperature for 5 minutes at 400g. 150µl of the supernatant from the wells were transferred into a new plate and fluorescence was measured (Excitation: 470nm, Emission: 650nm) on the microplate reader.

#### **2.4.2.2 Testing anti-CEA antibody – nanoparticle conjugate against LoVo cell line**

LoVo cells were passaged as per 2.2.1.2 and seeded into 96-well plates as per 2.3.4.1. The plates were incubated overnight at 37°C, 5% CO<sub>2</sub> and 95% Relative Humidity (RH).

The anti-CEA antibody was oxidised and filtered as per 2.2.2.5. Equal volumes of 0.1mg/ml PDPH and 25% bare maleimide functionalised NP were mixed for 30 minutes at room temperature. Excess PDPH was removed by gel filtration through a 50K Amicon Ultra centrifugal filter that had been equilibrated with distilled water. The filtrate was recovered and made up to the 50% of the original volume of solution filtered using distilled water so that the MNP concentration did not alter.

Equal volumes of the oxidised anti-CEA antibody and PDPH-MNP conjugate were mixed for 1 hour at room temperature. Excess oxidised anti-CEA antibody was removed by centrifuging the mixture at 6,000g for 30 minutes, carefully removing the supernatant, and resuspending in an original volume of PBS.

Cell media in the 96-well plates was exchanged with 100µl cell media containing either bare non-functionalised, bare 25% maleimide functionalised or anti-CEA antibody-

conjugated MNPs; each a 1 in 100 dilution. Plates also contained a media only control. Plates were incubated for 24 hours at 37°C, 5% CO<sub>2</sub> and 95% Relative Humidity (RH).

Cell media was then removed and the plates were subjected to three wash cycles lasting 5 minutes each with PBS. Plates were left overnight at room temperature protected from light. 200µl 10% sodium dodecyl sulfate (SDS) was added to each well for 2-3 minutes and then centrifuged at room temperature for 5 minutes at 400g. 150µl of the supernatant from the wells were transferred into a new plate and fluorescence was measured (Excitation: 470nm, Emission: 650nm) on the microplate reader.

The anti-CEA antibody-conjugated NP was also tested against the target cell line, LoVo, as described in 2.2.1.4.

#### **2.4.2.3 Testing target (anti-CEA) and control (anti-CD31) antibody – nanoparticle conjugates against target and control cell lines**

LoVo, HEK293 and EA.hy926 cell lines were passaged as per 2.2.1.2 and seeded into 96-well plates as per 2.3.4.1. Plates were incubated overnight at 37°C, 5% CO<sub>2</sub> and 95% Relative Humidity (RH).

Both the target (anti-CEA) and control (anti-CD31) antibodies were oxidised and filtered as per 2.2.2.5. Equal volumes of 0.1mg/ml PDPH and 25% bare maleimide functionalised NPs were mixed for 30 minutes at room temperature. Excess PDPH was removed by gel filtration through a 50K Amicon Ultra centrifugal filter that had been equilibrated with distilled water. The filtrate was recovered and made up to the original volume of 25% bare maleimide functionalised NP using distilled water to maintain MNP concentrations. Equal volumes of the oxidised target and control antibodies were mixed

with PDPH-MNP conjugates for 1 hour at room temperature. Excess oxidised target and control antibodies were removed by centrifuging mixtures at 6,000g for 30 minutes. The supernatants were carefully removed and antibody-NP conjugates resuspended in PBS to the original volume.

Cell media in the 96-well plates was exchanged with 100µl cell media in the following conditions:

- i. Cell media only
- ii. Bare 25% maleimide functionalised NPs
- iii. Target antibody
- iv. Control antibody
- v. Target antibody-conjugated NPs
- vi. Control antibody-conjugated NPs

All reagents were made up to 1 in 100 dilution in cell media. Cells were incubated with the different conditions for 24 hours at 37°C, 5% CO<sub>2</sub> and 95% Relative Humidity (RH). Cell media was then removed and plates were subjected to three wash cycles with PBS for 5 minutes each. Plates were then left overnight at room temperature protected from light. 200µl 10% SDS was added to each well for 3 minutes and then centrifuged at room temperature for 5 minutes at 400g. 150µl of the supernatant from the wells were transferred into fresh 96-well plates and fluorescence intensities were measured (Excitation: 470nm, Emission: 650nm) using the microplate reader.

The target and control antibody-conjugated NPs were also tested against fixed target and control cell lines as described in 2.2.1.4.

### **2.4.3 Optimising the protocol for conjugating antibodies to maleimide functionalised nanoparticle**

Different aspects of the antibody-NP conjugation process were investigated to optimise the work flow system. The following methods (categorised into steps) are based on the master protocol described in 2.4.2.3 and detail the aspects of the protocol that had been altered. For optimisation protocols only the target (anti-CEA) antibody was tested against LoVo, HEK293 and EA.hy926 cell lines.

#### **2.4.3.1 Optimisation step 1: Comparing different extraction techniques to remove excess antibody from antibody-nanoparticle conjugates**

The protocol in 2.4.2.3 was followed with the only alteration being the method for extracting excess oxidised antibodies from antibody-NP conjugates. Cell media in the 96-well plates was exchanged with 100µl cell media in the following conditions:

- i. Cell media only
- ii. Bare 25% maleimide functionalised NPs
- iii. Target antibody-NP conjugates with no extraction of excess antibodies
- iv. Target antibody-NP conjugates with extraction of excess antibodies by centrifugation
- v. Target antibody-NP conjugates with extraction of excess antibodies by dialysis
- vi. Target antibody-NP conjugates with extraction of excess antibodies by magnetism

##### **2.4.3.1.1 Extraction of excess antibody by dialysis**

A 1ml Spectra/Por® Float-A-Lyzer® G2 dialysis tube (Merck KGaA, Darmstadt, Germany) was used to extract excess oxidised antibodies from antibody-NP conjugates through dialysis. The Float-A-Lyzer® G2 membrane was primed using 10% ethanol and then flushed with distilled water. After allowing the oxidised antibody and the magnetic PDPH-MNP conjugate to mix for 1 hour, the mixture was carefully placed at the bottom of the

membrane and the dialysis tube was placed in PBS. The PBS dialysate buffer was refreshed at 2 hours, 6 hours and 10 hours then left overnight. Antibody-NP conjugates were then retrieved from the dialysis tube.

#### **2.4.3.1.2 Extraction of excess antibody by magnetism**

A magnetic CN-PPV/FeO<sub>4</sub> lipid NP was kindly supplied by the Department of Physics (Photonics & Nanotechnology Group, Faculty of Natural and Mathematical Sciences, Kings College London, UK).

After allowing the oxidised antibody and the magnetic PDPH-NP conjugate to mix for 1 hour, the mixture was placed into a DynaMag™-2 Magnet (ThermoFisher Scientific, Rockford, USA) (Figure 2.2) and left overnight at 4°C. The supernatant was removed and antibody-NP conjugates resuspended in PBS to the original volume.

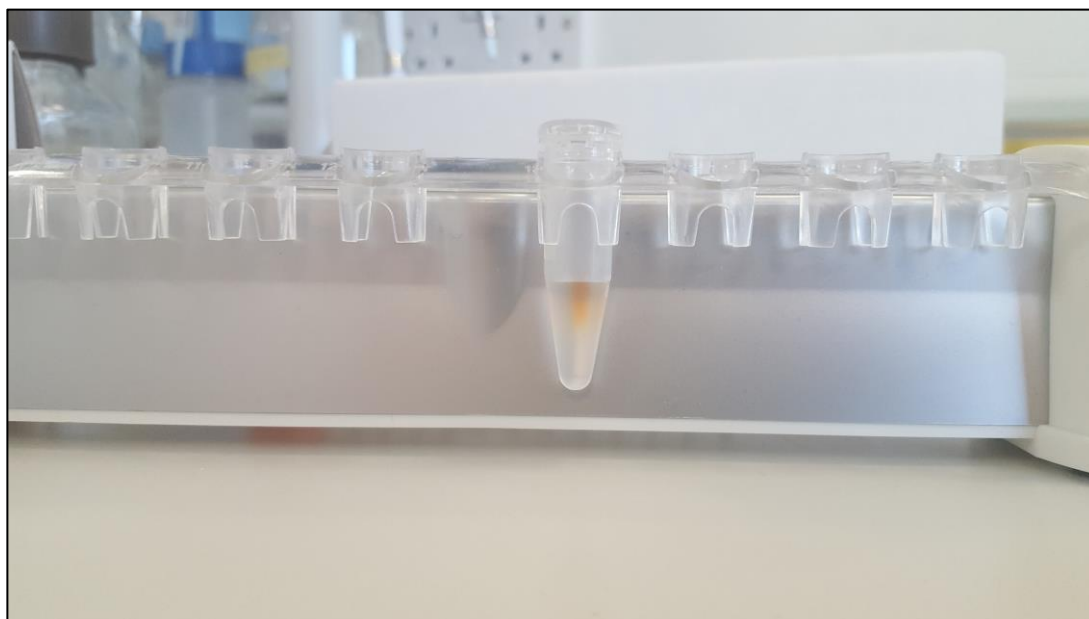


**Figure 2.2.** Image showing separation of magnetic maleimide functionalised NP from solution using DynaMag™-2 Magnet magnetic separator. Orange sediment represents magnetic maleimide functionalised CNPPV/PLGA-PEG NP that has been separated from distilled water using the magnetic separator.

### **2.4.3.2 Optimisation step 2: Galactose-mediated blocking of unoccupied hydrazide groups on crosslinker**

The monosaccharide, Galactose, can be oxidised to block unoccupied hydrazide functional groups on the heterobifunctional crosslinker, PDPH. Galactose was therefore chosen as a blocking agent. Cell media in the 96-well plates was exchanged with 100 $\mu$ l cell media in the following conditions:

- i. Cell media only
- ii. Bare 25% maleimide functionalised NPs
- iii. PDPH - 25% maleimide functionalised NP conjugates
- iv. PDPH - 25% maleimide functionalised NP conjugates with galactose
- v. Target antibody-NP conjugates
- vi. Target antibody-NP conjugates with galactose

2mg galactose was dissolved into 1ml Glycolink Coupling Buffer solution. 2.1mg sodium meta-periodate (Sigma Aldrich) was added to 500 $\mu$ l Glycolink Coupling Buffer solution. Equal volumes of the sodium meta-periodate and 2mg/ml galactose solutions were mixed and incubated for 30 minutes at room temperature whilst being protected from the light. Equal volumes of the oxidised galactose were added to PDPH - 25% maleimide functionalised NP conjugates and anti-CEA antibody-NP conjugates. These mixtures were left for 1 hour at room temperature, to allow galactose to block unoccupied hydrazide groups on PDPH. Excess oxidised galactose was removed by gel filtration through a 50K Amicon Ultra centrifugal filter that had been equilibrated with the Glycolink Coupling Buffer solution. The filtrate was recovered and made up to the original volume of conjugate using PBS.

### **2.4.3.3 Optimisation step 3: Assessing the effect of conjugation time between oxidised antibody and PDPH-MNP conjugate**

Oxidised anti-CEA antibodies and the PDPH-maleimide functionalised NP conjugates were incubated at room temperature for different lengths of time. Cell media in the 96-well plates was exchanged with 100 $\mu$ l cell media in the following conditions:

- i. Cell media only
- ii. Bare 25% maleimide functionalised NPs
- iii. Target antibody-NP conjugates – 1 hour incubation
- iv. Target antibody-NP conjugates – 2 hour incubation
- v. Target antibody-NP conjugates – 4 hour incubation
- vi. Target antibody-NP conjugates – 8 hour incubation

### **2.4.3.4 Optimisation step 4: Investigating the effect of increasing the amount of Target (anti-CEA) antibodies incubated with PDPH-MNP in conjugation reactions**

The amount of oxidised target antibody mixed with the PDPH – maleimide functionalised NP conjugates was increased and compared to the original ratio. PDPH-blocking with galactose and filtration of the excess galactose were also examined. Cell media in the 96-well plates was exchanged with 100 $\mu$ l cell media in the following conditions:

- i. Cell media only
- ii. Bare 25% maleimide functionalised NP
- iii. Target antibody-NP conjugate – 1x Ab in reaction
- iv. Target antibody-NP conjugate – 2x Ab in reaction
- v. Target antibody-NP conjugate – 2x Ab in reaction with blocking agent
- vi. Target antibody-NP conjugate – 2x Ab in removal with extraction of blocking and oxidising agents

#### **2.4.3.5 Optimisation step 5: Investigating optimum dilution of maleimide functionalised nanoparticle in conjugation reaction**

Prior to conjugation with the oxidised target antibody different concentrations of the PDPH-maleimide functionalised NPs were created using PBS as the diluent. The target antibody-NP conjugates (of different MNP concentration) were tested against the cell lines as per 2.4.2.3. Cell media in the 96-well plates was exchanged with 100µl cell media in the following conditions:

- i. Cell media only
- ii. Bare 25% maleimide functionalised NP
- iii. Undiluted target antibody-NP conjugate
- iv. 90% dilution target antibody-NP conjugate
- v. 80% dilution target antibody-NP conjugate
- vi. 70% dilution target antibody-NP conjugate

#### **2.4.3.6 Optimisation step 6: The influence of wash cycles following the incubation of cells with conjugates**

As per the protocol described in 2.4.2.3, cells were subjected to three wash cycles lasting 5 minutes each with PBS after 24 hours incubation with conjugates. Therefore, the impact of multiple wash cycles was investigated (2-4 wash cycles). Cell media in the 96-well plates was exchanged with 100µl cell media in the following conditions and plates subjected to 2-4 wash cycles:

- i. Cell media only
- ii. Bare 25% maleimide functionalised NP
- iii. Target antibody-NP conjugate

#### **2.4.3.7 Optimisation step 7: Investigating the different parameters of incubation**

Different parameters (time and temperature) of incubation for the target antibody-NP conjugates on cells were investigated to determine the optimum incubation settings. Cell media in the 96-well plates was exchanged with 100µl cell media in the following conditions and plates incubated for either 1 hour or overnight at 4°C, room temperature or 37°C:

- i. Cell media only
- ii. Bare 25% maleimide functionalised NP
- iii. Target antibody-NP conjugate
- iv. Blocked target antibody-NP conjugate

#### **2.4.4 Testing target and control antibody – nanoparticle conjugates against target and control cell lines using streptavidin functionalised nanoparticle**

The streptavidin functionalised variant of the CNPPV/PLGA-PEG NP was kindly supplied by the Department of Physics (Photonics & Nanotechnology Group, Faculty of Natural and Mathematical Sciences, Kings College London, UK). LoVo, HEK293 and EA.hy926 cell lines were passaged as per 2.2.1.2 and seeded into 96-well plates as per 2.3.4.1. Plates were incubated overnight at 37°C, 5% CO<sub>2</sub> and 95% Relative Humidity (RH). Both the target and control antibodies were biotinylated and filtered as per 2.2.2.6. Equal volumes of the biotinylated target and control antibodies were mixed with the streptavidin functionalised NPs for 1 hour at room temperature. Excess biotinylated target and control antibodies were removed by centrifuging at 6,000g for 30 minutes. The supernatants were carefully removed and antibody-SNP conjugates resuspended in PBS to the original volume. Cell media in the 96-well plates was exchanged with 100µl cell media in the following conditions:

- i. Cell media only
- ii. Bare streptavidin functionalised NPs
- iii. Target antibody
- iv. Control antibody
- v. Target antibody-streptavidin functionalised conjugated NPs
- vi. Control antibody-streptavidin functionalised conjugated NPs

All reagents were made up to 1 in 100 dilution in cell media. Cells were incubated with the different conditions for 24 hours at 37°C, 5% CO<sub>2</sub> and 95% Relative Humidity (RH). Cell media was then removed and plates were subjected to three wash cycles with PBS for 5 minutes each. Plates were then left overnight at room temperature protected from light. 200µl 10% SDS was added to each well for 3 minutes and then centrifuged at room temperature for 5 minutes at 400g. 150µl of the supernatant from the wells were transferred into fresh 96-well plates and fluorescence intensities were measured (Excitation: 470nm, Emission: 650nm) using the microplate reader.

## **2.4.5 Conjugation of anti-CEA affimer to maleimide functionalised nanoparticle**

### **2.4.5.1 Preparing anti-CEA affimers**

The control and anti-CEA affimers used in this project were kindly supplied by the Department of Biotechnology (School of Molecular and Cellular Biology, Faculty of Biological Sciences, University of Leeds, UK). Two anti-CEA affimers, anti-CEA II and anti-CEA III, were assessed. A yeast SUMO-binding affimer (ySUMO) was used as the control affimer.

Concentration of affimers was determined by calculating the optical density absorbance value at 280nm using a NanoDrop 1000 Spectrophotometer (Thermo Fisher). The value obtained was the divided by the extinction coefficient of that specific affimer. The

Nanodrop was initially blanked and calibrated using elution buffer as described in 2.1.2.4.5.1. Once concentrations of affimers were determined, elution buffer was added to affimer samples so the concentrations of control and anti-CEA affimers were equal.

#### **2.4.5.2 Testing variants of anti-CEA affimer-maleimide functionalised nanoparticle conjugates**

Target (LoVo) and control (HEK293) cell lines were passaged as per 2.2.1.2 and seeded into 96-well plates as per 2.3.4.1. Plates were incubated overnight at 37°C, 5% CO<sub>2</sub> and 95% Relative Humidity (RH).

Initially, both target and control affimers were reduced using immobilised TCEP Disulfide Reducing Gel (ThermoFisher Scientific, Rockford, USA) making cysteine functional groups available for conjugation to maleimide functionalised NPs. The immobilised TCEP Disulfide Reducing Gel was prepared using Eppendorf LoBind protein microcentrifuge tubes (Merck KGaA, Darmstadt, Germany) and centrifuged at 1,000g for 1 minute. The supernatant was removed and the gel was washed three times with PBS supplemented with 1mM ethylenediaminetetraacetic acid (EDTA). 4µl PBS with 50mM EDTA was added to the immobilised TCEP Disulfide Reducing Gel. Each affimer was added to double the volume of prepared immobilised TCEP Disulfide Reducing Gel and incubated for 1 hour at room temperature on a centrifuge tube rotator. Reduced affimer was recovered by centrifuging at 1,000g for 1 minute and extracting the clear supernatant containing the affimer.

Affimer conjugated NPs were prepared by mixing equal volumes of reduced affimer and 25% bare maleimide functionalised NPs and incubated overnight at room temperature. Excess affimer was removed by gel filtration through a 50K Amicon Ultra centrifugal filter

that had been equilibrated with elution buffer. The filtrate was recovered and resuspended in PBS to the original volume of reduced affimer and 25% bare maleimide functionalised NP. Cell media in the 96-well plates was exchanged with 100µl cell media in the following conditions:

- i. Cell media only
- ii. Bare 25% maleimide functionalised NPs
- iii. Control affimer-conjugated NPs
- iv. Anti-CEA II affimer-conjugated NPs
- v. Anti-CEA III affimer-conjugated NPs
- vi. Equal mixture of anti-CEA II and anti-CEA III affimer-conjugated NPs

All reagents were made up to 1 in 100 dilution in cell media. Cells were incubated with the different conditions for 24 hours at 37°C, 5% CO<sub>2</sub> and 95% Relative Humidity (RH). Cell media was then removed and plates were subjected to three wash cycles with PBS for 5 minutes each. Plates were then left overnight at room temperature protected from light. 200µl 10% SDS was added to each well for 3 minutes and then centrifuged at room temperature for 5 minutes at 400g. 150µl of the supernatant from the wells were transferred into fresh 96-well plates and fluorescence intensities were measured (Excitation: 470nm, Emission: 650nm) using the microplate reader.

#### **2.4.5.3 Comparing different incubation settings for affimer-conjugated nanoparticle**

Different parameters (time and temperature) of incubation for the target (anti-CEA) affimer-NP conjugates on LoVo cells were investigated to determine the optimum incubation settings. The protocol described in 2.4.5.2. was followed, however, differences in incubation conditions of 96-well plates containing cells exposed to affimer-conjugated NPs were made. Cell media in the 96-well plates was exchanged with 100µl

cell media in the following conditions and plates incubated for either 2 hours or overnight at 4°C or room temperature:

- i. Cell media only
- ii. Bare 25% maleimide functionalised NP
- iii. Target anti-CEA II/III affimer-NP conjugate

#### **2.4.5.4 Testing target and control affimer – nanoparticle conjugates against target and control cell lines**

The protocol described in 2.4.5.2 was followed with the exception that once the target and control affimer-conjugated NPs had been added to target and control cell lines the 96-well plates were incubated overnight at room temperature. Cell media in the 96-well plates was then exchanged with 100µl cell media in the following conditions:

- i. Cell media only
- ii. Bare 25% maleimide functionalised NPs
- iii. Control affimer-NP conjugates
- iv. Target anti-CEA II/III affimer-NP conjugates

The target and control affimer-conjugated NPs were also tested against fixed target and control cell lines as described in 2.2.1.4.

## 2.5 Statistical analysis

Statistical analysis was performed using Graphpad Prism 8 (Graphpad Software Inc, California, USA). One-way ANOVA and student's *t*-test were used for statistical analyses. P-values equal to and less than 0.05 ( $p \leq 0.05$ ) are considered to show statistically significant differences. The statistical methods used for gene expression analysis were principal component analysis and hierarchical clustering; analysis was conducted by an external agent, Fios Genomics.

**Chapter Three**

**Next Generation of**

**Laparoscopic intraoperative**

**Lymph node staging for**

**Stratified colon cancer surgery**

**(GLiSten) clinical trial**

### **3 Next Generation of Laparoscopic intraoperative Lymph node staging for Stratified colon cancer surgery (GLiSten) clinical trial**

#### **3.1 Introduction**

A major limitation in the current standards of colorectal cancer surgery is the tendency to unnecessarily overtreat lymph node (LN) negative patients and undertreat LN positive patients(9). This is attributed to the inability to accurately predict and stage the presence of metastatic disease in LNs prior to surgical resection(31,33,34). Consequently, radical surgery will expose LN negative patients to unnecessary increased surgical risks (29), whilst LN positive patients will be at risk of disease progression if resection is not radical enough. This is an unmet clinical need and advances need to be made to accurately identify the presence of metastatic disease in LNs prior to surgical resection.

As discussed in 1.3.3, fluorescence guided surgery is a potential option to improve disease-free survival following colorectal cancer surgery through fluorescence-mediated intraoperative identification of the tumour and LN metastases(11,12,94,96–102,104–108,234,235). Various fluorescent dyes and probes, including indocyanine green (ICG) and 5-aminolevulinic acid (5-ALA), have been investigated across different surgical specialties for their efficacy in intraoperatively identifying tumour location and the presence of metastatic disease.

Exogenously administered 5-ALA is metabolically converted intracellularly in the mitochondria into the fluorescent photosensitiser, PPIX. The Next Generation intraoperative Lymph node staging for Stratified colon cancer surgery (GLiSten) study(9) was designed to determine the feasibility of potentially using PPIX from exogenous 5-

ALA as a fluorescent probe to detect the presence of LN metastases in colon cancer. The use of PPIX as a fluorescent marker to detect and identify the location of colonic tumours and the presence of LN metastases is a novel approach that has not been previously explored.

The trial design is outlined in 2.1.1. The primary objective of the study was to determine the optimal dosage of 5-ALA for the intraoperative detection of metastases in LNs in adult colon cancer patients undergoing elective surgery. As a pre-defined criteria, a minimum of 2/10 (20%) patients in a single cohort needed to be accurately identify with metastatic LN to confirm the optimal dose of 5-ALA.

The secondary objectives of this study were to establish a repeatable and consistent methodology by the standardisation of:

- I) Pre-operative computerised tomography (CT) LN reporting
- II) Laparoscopic segmental colonic resection with D3 lymphadenectomy
- III) Histopathological examination of resected specimens

In addition to the primary and secondary objectives, data was collated relating to the incidence of surgical complications and side-effects potentially due to administration of 5-ALA.

## 3.2 Results

### 3.2.1 GLiSten study results

A total of 44 patients were recruited to the GLiSten study and no patients withdrew. 18/44 participants were assigned to cohort 1 and 26/44 to cohort 2. 26 male and 18 female patients participated in the trial with a mean of 72 years (range: 52-88 years). The mean BMI was 27.3 (range: 19.1-37.8) with a median ASA grade of 2. There were no significant differences in the baseline characteristics between the two cohorts (Table 3.1).

<b>Table 3.1. Patient Demographics</b>		Cohort 1	Cohort 2
Number of participants (n)		18	26
Sex (ratio of male : female)		10 : 8	16 : 10
Age (years) [Mean (range)]		69.3 (52 - 85)	71.8 (53 - 88)
BMI (kg/m <sup>2</sup> ) [Mean (range)]		26.1 (21 - 35)	28 (19 - 38)
ASA Grade	I	9	5
	II	8	13
	III	1	8

In cohort 1, patients were treated with a dose of 20mg/kg of 5-ALA. The identification of at least 2 patients with LN positive disease, as observed through fluorescence at 20mg/kg of 5-ALA, was not achieved. Subsequently, cohort 2 received a higher dosage (30mg/kg) of 5-ALA.

41/44 (93.2%) patients underwent blue-light laparoscopy. From these, 40/41 (97.6%) patients also had subsequent histopathological examination of the specimen. One patient (1/41) who underwent blue-light laparoscopy was found to have irresectable

disease at the time of surgery and no oncological specimen was taken for histopathological examination. 3/44 (6.8%) patients did not undergo blue-light laparoscopy as 2/3 patients were cancelled on the planned day of surgery and the fluorescent laparoscopic equipment was unavailable for 1/3 patients.

### 3.2.2 Primary objective: Diagnostic accuracy of intraoperative 5-ALA fluorescence

Of the 41 patients who underwent blue-light laparoscopy, 13/41 (31.7%) had fluorescent primary tumours and 7/13 (53.8%) of these patients also had fluorescent LN (Table 3.2). In either cohort, fluorescent LNs were observed in addition to fluorescent primary tumours. No fluorescent LNs were observed in the absence of fluorescent tumours.

#### 3.2.2.1 Cohort 1

In cohort 1, 17/18 (94.4%) patients received blue-light laparoscopy. One (1/18) operation was cancelled. All 18 patients received 20mg/kg of 5-ALA. 6/17 (35.3%) patients had a fluorescent primary tumour and 3/6 (50%) of these patients had additional fluorescent LN (Table 3.2).

<b>Table 3.2. Fluorescence results in Cohort 1</b>	✓	✗
Received blue-light laparoscopy	17	1
Fluorescent primary tumour observed	6	11
Fluorescent primary tumour AND fluorescent LN observed	3	3

Of the 3 patients with both fluorescent primary tumour and LN in cohort 1, one (1/3) patient had confirmed metastatic disease in the LN as confirmed by standard histopathological examination. Therefore, 1/17 (5.88%) patient in cohort 1 who received

5-ALA and blue-light laparoscopy had confirmed fluorescent LN positive disease. Cohort 1 did not meet the success detection criteria of 5-ALA, which is defined as histopathology confirmed metastatic disease in fluorescence LN in at least 2 for every 10 node positive patients (20%).

Equations 3.1A and 3.1B were used to calculate the sensitivity and specificity rates of 5-ALA mediated fluorescence respectively.

$$A. \text{Sensitivity } (\%) = \left( \frac{\text{No. of fluorescent positive AND histopathology positive LN}}{\text{Total no. of histopathology positive LN}} \right) \times 100$$

$$B. \text{Specificity } (\%) = \left( \frac{\text{No. of fluorescent negative AND histopathology negative LN}}{\text{Total no. of histopathology negative LN}} \right) \times 100$$

**Equation 3.1. Determining 5-ALA mediated fluorescence sensitivity and specificity**

In cohort 1, 5-ALA mediated fluorescence demonstrated a sensitivity of 11.1% and specificity of 75% for determining the pathological outcome of LN assessment (Table 3.3).

Table 3.3. Comparison of fluorescence and histopathology LN results in Cohort 1		Histopathology		Total
		POSITIVE	NEGATIVE	
Fluorescence	POSITIVE	1	2	3
	NEGATIVE	8	6	14
Total		9	8	17

As shown in Table 3.3, 9 patients in cohort 1 were identified with disease in the LNs, instead of the required 10, as per the trial protocol outlined in 2.1.1. This is due to the accuracy of 5-ALA mediated fluorescence being determined by LN status on the basis of individual patients rather than the individual LN. Two patients in cohort 1 that were observed with fluorescent positive LNs were found to have benign disease (histology negative) upon standard histopathological examination of the fluorescent LN (Table 3.3) (false positive). Of these two patients, the first patient had no malignant LNs in their specimen including the fluorescent LN i.e. all LNs were found to be benign. The second patient was found to have six histopathology confirmed positive LNs in non-fluorescent LNs (false negative), out of a total of 23 LNs examined within the pathological specimen. However, the fluorescent LN did not contain any metastatic disease upon standard histopathological examination. This patient could therefore be placed in either the fluorescence positive & histopathology negative group (false positive), OR fluorescence negative & histopathology positive group (false negative). As the primary outcome of this study was to determine the accuracy of fluorescence in predicting LN involvement this patient was placed in the former (fluorescence positive & histopathology negative) group for data analysis. Therefore, the total number of patients in cohort 1 with histopathology positive LNs is calculated to show 9, instead of 10.

#### Summary of findings from cohort 1:

1. 18 patients were treated with a dose of 20mg/kg 5-ALA
2. 17/18 received blue-light laparoscopy
3. 6/17 (35.3%) patients showed fluorescence within the tumour
4. 9/17 (52.9%) patients were found to be histopathology confirmed LN positive
5. 1/9 (11.1%) of these patients had correctly identified node positive disease via fluorescence
6. Cohort 1 did not meet the pre-defined criteria for acceptable 5-ALA sensitivity (*actual*: 1/9, 11.1% vs *pre-defined*: 2/10, 20%).

7. The sensitivity for the detection of involved LNs was inadequate and, therefore, as per the study protocol cohort 2 received the increased dose of 30mg/kg 5-ALA.

### 3.2.2.2 Cohort 2

In cohort 2, 24/26 (92.3%) patients underwent blue-light laparoscopy. Two (2/26) patients did not undergo blue-light laparoscopy. All 26 patients received 30mg/kg of 5-ALA. One (1/24) patient who underwent blue-light laparoscopy was found to have irresectable disease. Excluding this one patient, 23/24 patients who underwent surgery had histopathological examination of their specimens. As summarised in Table 3.4, of the patients who underwent blue-light laparoscopy surgery 7/24 (29.2%) patients had a primary fluorescent tumour and 4/7 also had fluorescent LNs.

<b>Table 3.4. Fluorescence results in Cohort 2</b>	✓	✗
Received blue-light laparoscopy	24	2
Fluorescent primary tumour observed	7	17
Fluorescent primary tumour AND fluorescent LN observed	4	3

None of the patients with fluorescent LNs were found to contain metastatic disease upon standard histopathological examination (Table 3.5). In cohort 2, 5-ALA mediated fluorescence demonstrated a sensitivity of 0% and specificity of 75% for determining the pathological outcome of LN assessment (Table 3.5).

Table 3.5. Comparison of fluorescence and histopathology results in Cohort 2		Histopathology		Total
		POSITIVE	NEGATIVE	
Fluorescence	POSITIVE	0	4	4
	NEGATIVE	7	12	19
<b>Total</b>		<b>7</b>	<b>16</b>	<b>23</b>

In cohort 2, 9 patients had histopathology confirmed metastatic LN disease. 4 patients had fluorescent positive LNs but none of the fluorescing LNs were found to contain metastatic disease (false positive). 2/4 had no histopathology confirmed evidence of metastatic disease in any LNs. The other 2/4 patients had metastatic disease found in non-fluorescent LNs and the fluorescent LN were found to contain benign disease upon histopathological examination. This is similar to the observations seen in cohort 1. Therefore, the latter two patients were placed in the fluorescence positive & histopathology negative group for of data analysis. Hence the total number of patients with histopathology positive LNs in cohort 2 is calculated to show 7, instead of 9.

Summary of findings from cohort 2:

1. 26 patients were treated with a dose of 30mg/kg of 5-ALA
2. 24/26 received blue-light laparoscopy
3. 7/24 (29.2%) patients showed fluorescence within the tumour
4. 7/26 (26.9) patients were found to be histopathology confirmed LN positive
5. 0/4 (0%) patients had correctly identified node positive disease via fluorescence
6. Cohort 2 did not meet the pre-defined criteria for acceptable 5-ALA sensitivity (*actual*: 0/4, 0% vs *pre-defined*: 2/10, 20%).

### 3.2.3 Secondary objectives: Preoperative CT imaging

Surgical resection with blue-light laparoscopy was performed in 41/44 patients. Pre-operative CT imaging and pathology staging was compared in these patients. Pre-operative CT imaging was in concordance with histopathological findings in reporting non-involved (N0) and involved (N1/2) LN in 23/41 (56.1%) patients. Pre-operative CT reported over-staged and under-staged LN status in 11/41 (26.8%) and 7/41 (17.1%) patients respectively (Table 3.6).

Table 3.6. Preoperative CT prediction of LN stage compared with histopathology		LN staging in histopathology		Total
		N1/2	N0	
LN staging in CT	N1/2	13	11	<b>24</b>
	N0	7	10	<b>17</b>
Total		<b>20</b>	<b>21</b>	<b>41</b>

Equations 3.2A and 3.2B were used to calculate the sensitivity and specificity rates in preoperatively predicting LN stage using CT imaging.

$$A. \text{Sensitivity (\%)} = \left( \frac{\text{No. of CT N1/2 AND histopathology N1/2}}{\text{Total no. of histopathology N1/2}} \right) \times 100$$

$$B. \text{Specificity (\%)} = \left( \frac{\text{No. of CT N0 AND histopathology N0}}{\text{Total no. of histopathology N0}} \right) \times 100$$

#### Equation 3.2. Determining preoperative CT imaging sensitivity and specificity for LN staging

The sensitivity and specificity of preoperative CT imaging, to predict LN staging were 65% and 47.6% respectively.

Pre-operative CT imaging, as confirmed by histopathology examination, was also conducted to detect for the presence of extramural vascular invasion (EMVI). EMVI is defined as the invasion of tumour cells into the veins beyond the muscularis propria(236). In colon cancer patients, EMVI is an indicator of poor prognosis and the presence of EMVI positively correlates with potential recurrence of disease(237). In this study EMVI was detected in 14/41 (34.1%) patients using histopathology. 27/41 (65.9%) patients were accurately identified as EMVI positive or negative on preoperative CT scan (Table 3.7).

Table 3.7. Preoperative CT prediction of EMVI compared with histopathology		Presence of EMVI in histopathology		Total
		POSITIVE	NEGATIVE	
Presence of EMVI in CT	POSITIVE	14	5	19
	NEGATIVE	9	13	22
Total		23	18	41

Equations 3.3A and 3.3B were used to calculate the sensitivity and specificity rates in preoperatively detecting EMVI using CT imaging.

$$A. \text{Sensitivity } (\%) = \left( \frac{\text{No. of CT positive EMVI AND histopathology positive EMVI}}{\text{Total no. of histopathology positive EMVI}} \right) \times 100$$

$$B. \text{Specificity } (\%) = \left( \frac{\text{No. of CT negative EMVI AND histopathology negative EMVI}}{\text{Total no. of histopathology negative EMVI}} \right) \times 100$$

**Equation 3.3. Determining preoperative CT imaging sensitivity and specificity for detecting EMVI**

The sensitivity and specificity of preoperative CT detection for the presence of EMVI were 60.9% and 72.2% respectively.

For the purpose of this study, patients were selected for recruitment on the basis of having suspected locally advanced disease as defined by FOxTROT pre-operative CT imaging criteria (see 2.1.1). Pre-operative CT imaging accurately identified tumour invasion beyond the muscularis propria (T3/4) in 33/41 (80.5%) patients (Table 3.8).

<b>Table 3.8.</b> <b>Preoperative CT prediction of T stage compared with histopathology</b>		T stage in histopathology				
		T0/1	T2	T3	T4	<b>Total</b>
Pre-operative CT T stage	T2	1	0	0	1	<b>2</b>
	T3	0	6	16	9	<b>31</b>
	T4a	0	1	2	4	<b>7</b>
	T4b	0	0	0	1	<b>1</b>
	<b>Total</b>	<b>1</b>	<b>7</b>	<b>18</b>	<b>15</b>	<b>41</b>

### 3.2.4 Secondary objectives: Histopathology

Forty-one patients underwent blue-light laparoscopy. From these, only 1 patient was found to have unresectable cancer and a specimen for histopathological examination was not taken. 40 patients who underwent blue-light laparoscopy also had subsequent histopathological examination of the resected specimen. Quality of the resected specimens were judged on the plane of resection. In total, 26/40 (65%) specimens were resected in the mesocolic plane with a larger proportion of mesocolic resections performed in cohort 2 (18/24, 78.2%) as compared to cohort 1 (8/17, 47.1%) (Table 3.9).

<b>Table 3.9. Comparison of resection procedures between cohorts</b>		Cohort 1 (n=17)	Cohort 2 (n=24)
Resection plane	Mesocolic	8	18
	Intramesocolic	8	5
	Muscularis propria	1	0
	Missing data	0	1

### **3.2.5 Complications relating to surgery and 5-ALA administration**

Known risks of 5-ALA administration in humans include photosensitivity reactions, derangement of liver function tests, nausea, vomiting, tachycardia and hypotension. In addition to these specific risks relating to 5-ALA administration, patients were also counselled regarding the normal risks of major colorectal surgery and general anaesthesia (Table 3.10).

<b>Table 3.10. Major risks associated with major laparoscopic colorectal surgery</b>
<ul style="list-style-type: none"> <li>• Venous thromboembolism</li> <li>• Bleeding</li> <li>• Infection including chest, wound, urine etc</li> <li>• Myocardial infarction or cerebral vascular accident</li> <li>• Conversion to open surgery</li> <li>• Injury to intra-abdominal structures such as intra-abdominal organs, major blood vessels, bowel, ureter, nerve etc</li> <li>• Anastomotic leak</li> <li>• Death</li> <li>• Formation of stoma</li> <li>• Ileus</li> </ul>

There were no serious adverse events related to 5-ALA in the trial however, minor side effects were observed in eight patients. Two patients experienced mild self-limiting

photosensitivity reactions beginning within 48 hours of surgery and resolving by the fifth postoperative day. This was thought to be related to their planned postoperative admission to a high dependency unit which has brighter ambient lighting than the general surgical ward. No intervention was required other than topical skin emollient cream. Mild derangement of liver function was noted in four patients within the immediate postoperative period and all four cases resolved within 3 days. The final two patients were both noted to have slight derangement of their renal function however, this could have been related to other factors such as their surgery and cannot be definitely attributed to receiving 5-ALA. Both patients renal function returned to normal without any intervention.

Risks of major colorectal surgery are highlighted in Table **3.10**. The anastomotic leak rate and conversion rate from laparoscopic to open surgery within the trial was 4.5% and 14.2% respectively. One incidence of organ perforation (stomach) occurred within the trial with two incidences of major intra-abdominal haemorrhages (*inferior vena cava* and a peripancreatic vessel), one of which required conversion to open surgery. These figures should be considered in context of the patient selection process where patients with advanced disease were recruited for the trial and are therefore likely to be at a higher risk of a more difficult procedure increasing the risk of complications such as leak and conversion. Two patients were managed for postoperative ileus. Three patients were readmitted to hospital within 30 days of their discharge home; one for a chest infection, one for an acute kidney injury and one for a post-operative ileus. None of these complications requiring readmission were felt to be related to 5-ALA administration.

There was a single death within 30 days of surgery in the GLiSten trial which was reviewed by the Data Monitoring and Ethics Committee (DMEC) and Trial Steering Committee (TSC), both of whom felt that 5-ALA was not implicated in the cause of death.

This individual was a high-risk surgical candidate with multiple co-morbidities and suffered an anastomotic leak with subsequent myocardial infarction and multi-organ failure, from which he succumbed.

### **3.2.6 Gene expression analysis**

In addition to resecting tumour specimens for histopathology, normal and malignant colonic mucosa was also taken from resected specimens for further analysis and preserved as described in 2.1.2.1.

Tumour samples were processed and cryosections produced and stained for further analysis as described in 2.1.2.2 and 2.1.2.3. This was done to identify tumours with high yields of malignant cells making them suitable for gene microarray analysis. 12 patient samples were selected; 6 from cohort 1 and 6 from cohort 2. Patient demographics were kept as close as possible between both fluorescent and non-fluorescent groups (Table 3.11). 6 fluorescent and 6 non-fluorescent tumours were selected and were equally distributed between both cohorts. The proportion of malignant cells in each tumour sample was at least 60% (Table 3.11).

<b>Table 3.11. Patient demographics of selected samples for gene microarray</b>		Non-fluorescent tumours	Fluorescent tumours
Number of samples (n)		6	6
Sex (ratio of male : female)		5:1	3:3
Age (years) [Mean (range)]		65 (53-77)	76.8 (68-83)
BMI (kg/m <sup>2</sup> ) [Mean (range)]		26.35 (22-35)	26.75 (24.7-28)
ASA Grade	I	2	1
	II	2	4
	III	2	1
Tumour Site (Right : Left colon)		4:2	5:1
Tumour differentiation	Well/Moderate	6	4
	Poor	0	1
	Mucinous	0	1
T stage	3	5	4
	4	1	2
M stage	0	1	1
	X	5	4
Yield of malignant cells (%) [Mean (range)]		76.7 (60-85)	76.7 (60-90)

Prior to extracting RNA from specimens, the optimal RNA extraction technique was determined. Cryosections were taken from a single randomly selected benign tissue specimen and three different RNA extraction protocols were compared and evaluated as described in 2.1.2.4. The protocol that produced the best quality RNA was used to extract RNA from the 12 selected patient samples.

### 3.2.6.1 Comparison of RNA extraction techniques

The RNA integrity number (RIN) is an algorithm-based method for determining the degree of degradation of RNA extracted from samples and has been identified as the preferred method of assessing RNA quality(238). Samples are assigned a number from 1 to 10 (1 = Most degraded and 10 = Least degraded). The RIN and concentration of RNA were used to compare the outcomes of the three protocols (Figure 3.1).

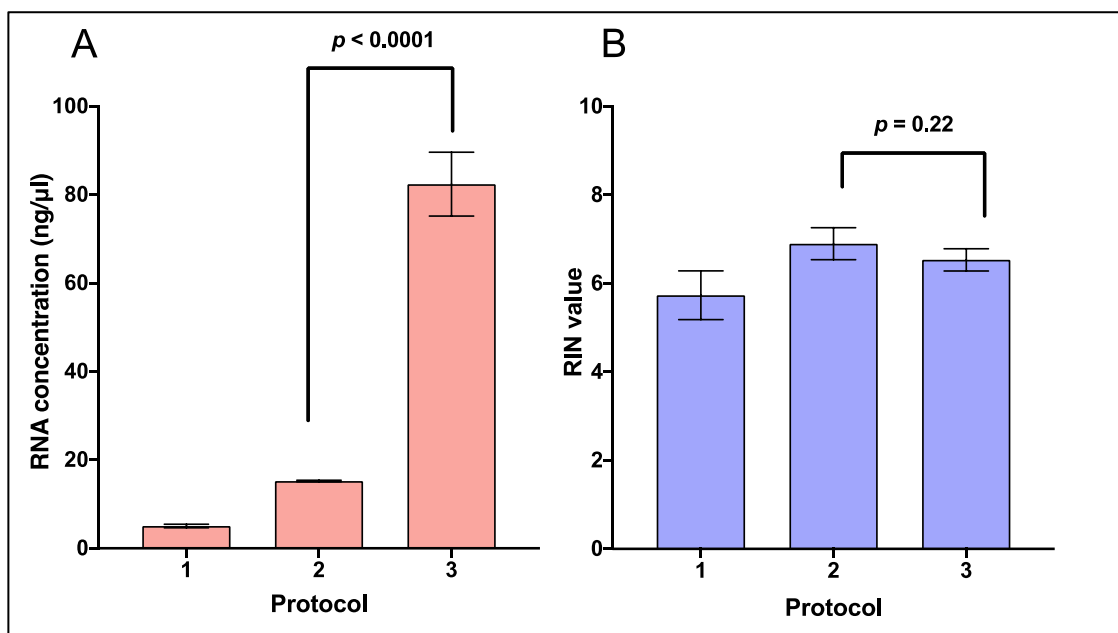


**Figure 3.1. Comparison of the quality of RNA extraction from GLiSten trial specimens. A)** The concentrations of RNA extracted from the tissue using the three different protocols. **B)** The RIN values of RNA extracted using the three different protocols. Data represents means with standard deviation of 3 independent experiments. See 2.1.2.4 in Materials and Methods for detailed protocols. Protocol 3 gave the highest RNA concentration whereas Protocol 2 produced the highest RIN value.

Using the three different RNA extraction protocols, Protocol 3 (see 2.1.2.4.4 in Materials and Methods for the detailed protocol) using the Qiagen RNeasy Mini Kit gave the highest concentration of RNA (*Protocol 3*: 82.37ng/μl vs. *Protocol 2*: 15.22ng/μl,  $p < 0.0001$ ) (Figure 3.1A). Protocol 2 was found to have the highest RIN value but the

difference in comparison to Protocol 3 was not significant (*Protocol 3: 6.5 vs. Protocol 2: 6.9,  $p = 0.22$* ) (Figure 3.1B).

### **3.2.6.2 Gene expression analysis report**

Gene expression analysis was performed to identify differentially expressed genes between fluorescent and non-fluorescent tumours after the administration of 5-ALA. Extracted RNA samples using the protocol described in 2.1.2.4.4 were processed and hybridised to the Affymetrix Human Transcriptome Array (HTA) 2.0. All 12 samples passed quality control measures and were used for analysis.

Data from gene micro-array was assessed to identify any associations between biological and technical factors. Exploratory analysis using principal component analysis (PCA) and hierarchical clustering showed a partial difference based on gender however, no clear difference in gene expression between the fluorescent and non-fluorescent tumours was found (Figure 3.2). Due to the potential confounding effect based on gender, any probes located on the sex chromosomes were then removed from statistical analysis. A single-factor comparison was then performed to identify any significant differences in expression levels between fluorescent and non-fluorescent tumours.

Figure 3.2 shows that the RIN value (technical factor) had the strongest effect on the gene expression data and this would have no influence on the observed fluorescence or non-fluorescence of the tumour sample. Figure 3.2 also shows that gender, tumour differentiation, the T and M stage of the tumour were all associated with either the second or third principal component indicating these biological factors may have some influence on the data variance. However, given the small sample size (Table 3.11) any disparity in the patient demographics will bias the results.

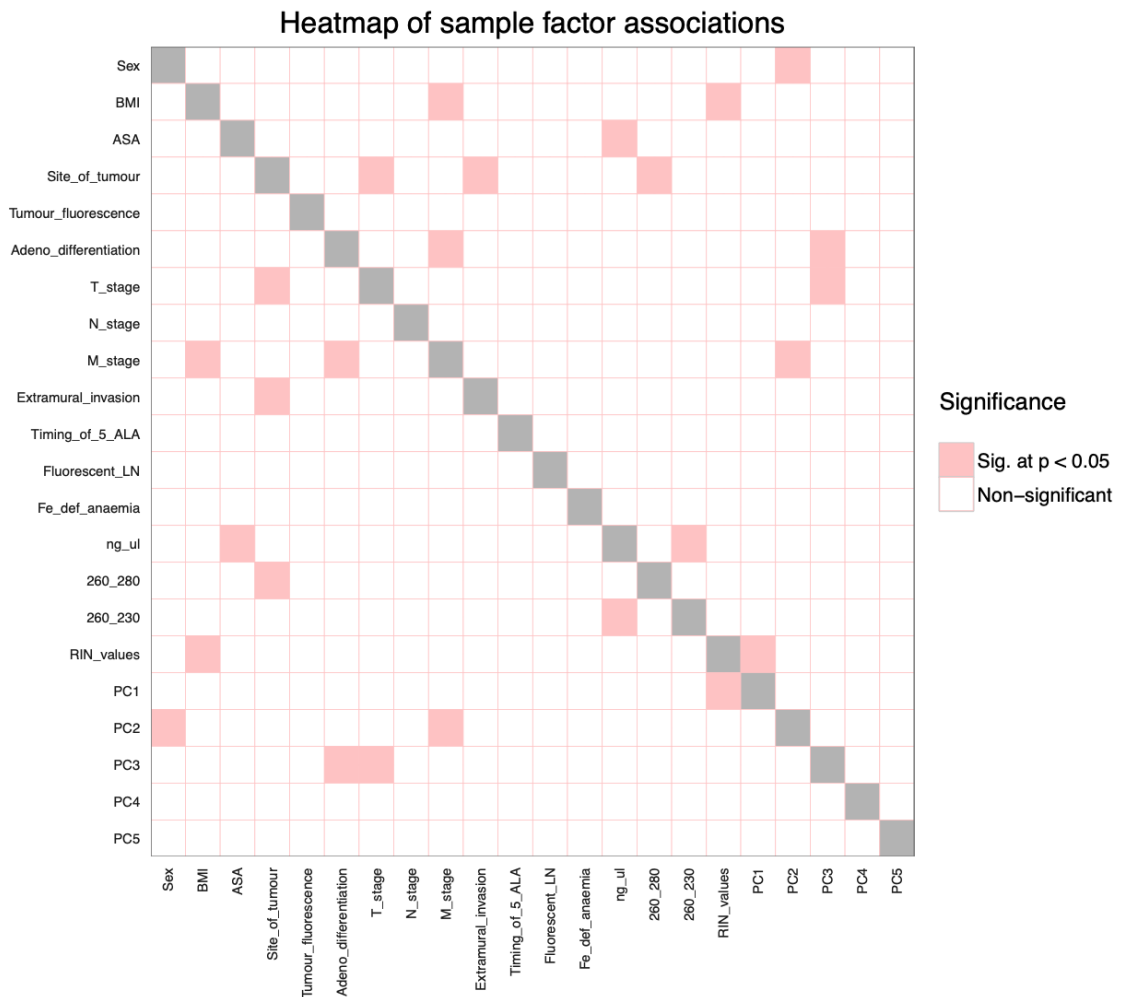


**Figure 3.2. Heatmap showing the strength of association between technical and clinical factors within the study samples.** Taken from Tendeng *et al.*(239). Biological and technical factors within the experimental design were tested using a single-factor comparison to identify any significant differences between fluorescent and non-fluorescent tumours. Entries were considered significant at  $p < 0.05$ . RIN value (PC1), gender (PC2), tumour differentiation (PC3), T-stage (PC3) and M-stage (PC2) were found to be have statistically significant different levels of expression between fluorescent and non-fluorescent tumours.

Using single-factor comparison with the recommended statistical threshold of  $p < 0.05$ , no significant markers were identified. Relaxing the threshold to  $p < 0.01$  with fold-change cut off  $\geq 1.3$  to enable pathway analysis identified 217 differentially expressed genes comparing fluorescent verses non-fluorescent tumour samples. However, relaxation of the threshold increases the rates at which false-positives are highlighted. Therefore the 217 genes identified should be validated using independent experimental techniques.

Pathway analysis using the relaxed threshold criteria, identified the upregulation of genes in the fluorescent group, that were primarily associated with the immune response system (Figure 3.3) and in particular olfactory transduction. Down-regulated genes that were identified, were mainly involved in cellular metabolic processes eg. Glycerolipid, lipoprotein or amino acid metabolism (Figure 3.3).

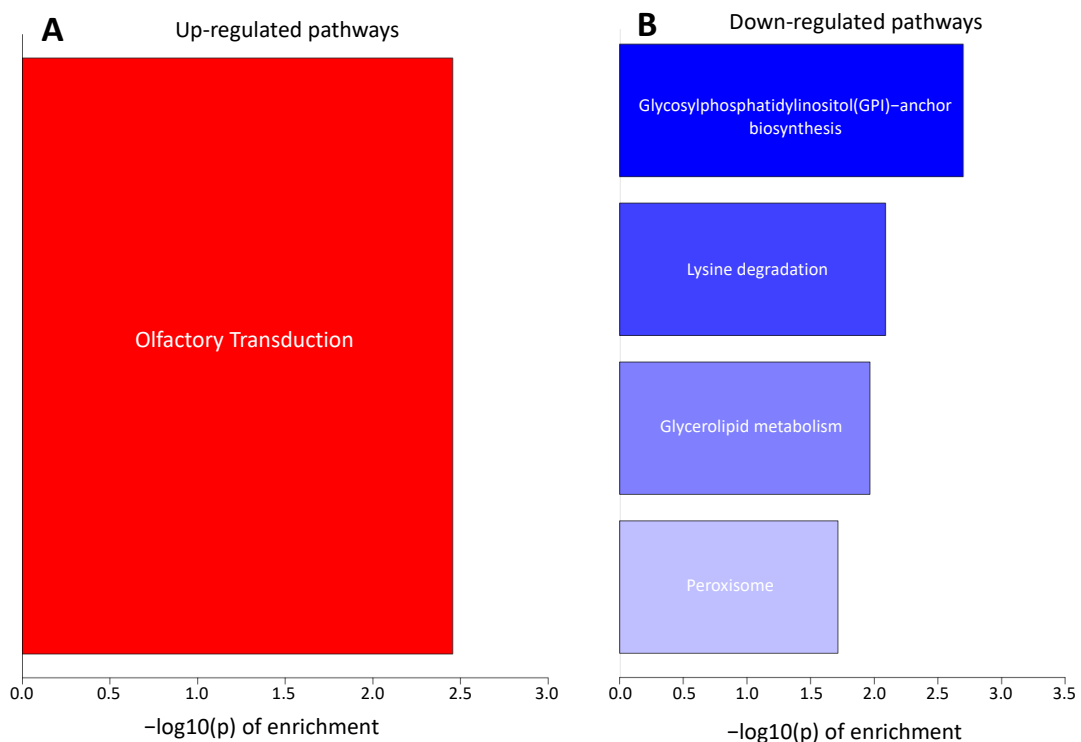


**Figure 3.3. KEGG Enrichment Analysis of A) upregulated and B) downregulated enriched KEGG pathways.** Taken from Tendeng *et al.*(239). Only KEGG pathways with an enrichment  $p < 0.05$  are included in this figure. Up- and downregulated enrichments are shown separately as different components of a given KEGG pathway could be up- and downregulated within a single comparison. Colour (red for upregulated and blue for downregulated) is assigned based on the enrichment  $p$ -value, with white implying less significant enrichment. Genes associated with olfactory transduction were upregulated and those associated with cellular metabolic processes were downgraded in the fluorescent tumours on pathway analysis.

### 3.3 Discussion

The GLiSten study is the first human clinical trial of intraoperative 5-ALA mediated fluorescence-guided surgery in colon cancer. A total of 44 patients were recruited, 41 patients had intra-operative blue-light laparoscopy and of these, 13 primary tumours (31.7%) showed intraoperative fluorescence. 6 fluorescing tumours in cohort 1 (35.3%) and 7 fluorescing tumours in cohort 2 (29.2%) (Table 3.3). Seven out of 19 patients with LN positive disease exhibited LN fluorescence, 3 in cohort 1 (17.6%) and 4 in cohort 2 (16.7%). All patients with fluorescent LN also had fluorescent tumours. Only one patient with fluorescent positive LN was found to have LN metastases. Neither dose of 5-ALA (20mg/kg and 30mg/kg) demonstrated adequate accuracy and sensitivity to support further investigation for the use of 5-ALA as an intraoperative fluorescent probe for LN staging in colorectal cancer surgery. Therefore, the trial did not proceed to a subsequent evaluation phase. Following surgery, patients received standard post-operative care and continued to receive routine follow-up and surveillance as per NICE guidelines(240).

Similar to the GLiSten study, Kondo *et al.*(241) attempted to evaluate the use of 5-ALA mediated fluorescent diagnosis of peritoneal metastases in colon cancer patients. In this study, 12 patients were recruited on the basis of suspected peritoneal disease upon CT examination. 8/12 (66.7%) patients showed accurate fluorescence in the peritoneum confirming metastatic disease. This study did not comment on fluorescence of the primary tumour, LNs or any non-peritoneal metastatic deposits. Therefore, a direct comparison with the findings from our study is not possible. Nakamura *et al.*(106) evaluated 5-ALA mediated fluorescence in guiding endoscopic resections of early stage gastric and colorectal tumours. Of the 3 patients in this study with colorectal cancerous lesions only one showed fluorescence (33.3%). It is not possible to draw a strong conclusion between the GLiSten study and this study given that the latter only recruited three patients with colorectal tumours. To date, there are no additional studies that can

be compared to the GLiSten study evaluating the use of 5-ALA mediated fluorescence diagnosis in patients with colonic cancer.

Aside from colorectal cancers, 5-ALA mediated fluorescence has been evaluated for the detection of other cancers. A study by Rink *et al.* assessing the use of 5-ALA in non-muscle invasive bladder cancer surgery found that the sensitivity of tumour detection ranged between 76-97% with a specificity of 56%(96). It was suggested that 5-ALA fluorescence diagnosis might reduce the risk of residual disease. As detailed in chapter 1, neurosurgeons use exogenous 5-ALA to improve tumour detection and clearance of resection margins in brain tumours. A Cochrane review by Barone *et al.*(235) reviewing the use of visual assistance and guidance during neurosurgery for brain tumours found that the evidence supporting the use of 5-ALA fluorescence assisted neurosurgery is possibly not as strong as previously expected. However, there was a significant improvement in complete tumour resection rates when using 5-ALA mediated fluorescence (65%) as compared to standard resection procedures (36%).

In comparison to other malignancies, such as urological and neurological cancers, 5-ALA appears to be less sensitive for the fluorescent detection of colorectal tumours. Although the timing and doses of 5-ALA administration in the GLiSten study were similar to other published studies with similar patient characteristics, different factors could have potentially influenced the findings. This includes i) autofluorescence of the surrounding tissue (false positive)(108,241,242), ii) quenching(108) and iii) photobleaching of the tumour by white light laparoscopy performed at the beginning of the procedure, reducing the intensity of fluorescence over time(96).

Of the 41 patients that underwent blue-light laparoscopic resection, 19 patients had LN disease and 7/19 (36.8%) of these patients exhibited intra-operative 5-ALA/PPIX

fluorescence of the LN. Only one fluorescent LN was found to contain metastatic disease, suggesting non-specific fluorescence in the other fluorescent LNs. Clinical studies evaluating 5-ALA mediated fluorescent diagnosis in other malignancies have not focused on the detection of LN metastases, and currently the only studies for comparison are pre-clinical *in vivo* studies using animal models.

Kato *et al.* conducted a study using murine models of colorectal cancer(11) that were administered intraperitoneal 5-ALA. Of the 10 mice that were treated, 3/10 (30%) mice exhibited fluorescent LN and all fluorescent LN contained metastatic disease as confirmed by histopathological examination. Histopathological examination of mice without fluorescent LN was not performed and sensitivity and specificity values were not obtained. A study by Harada *et al.* investigated 5-ALA mediated fluorescence in detecting LN metastases in freshly excised colonic tumour resections from 14 patients(108). The study used a spectral unmixing method to reduce the autofluorescence from collagen masking true PPIX fluorescence. 12/14 patients had stage III disease and 9/14 patients were found to have LN positive disease. No fluorescent benign LNs were observed in this study and the sensitivity and specificity for detecting LN metastatic disease were 88.3% and 92% respectively, which is comparably higher than sensitivity and specificity rates from the GLiSten study. However, in this study 5-ALA fluorescence was examined *ex-vivo* and further details of LN fluorescence, including any non-fluorescent LNs containing metastatic disease, was not reported. In addition, the only reported patient demographic was the age range, not permitting the direct comparison of baseline characteristics with the GLiSten study.

The GLiSten study found that although 5-ALA can be administered without serious adverse effects, it is not sensitive enough to detect LN metastasis and is not to be recommended for intra-operative fluorescence mediated staging of colonic cancers. The

results from this study suggest that 5-ALA mediated fluorescence in colonic cancers is not as effective as previously expected. To date, this is the only study that has clinically examined 5-ALA for intra-operative fluorescent diagnosis of colonic LN metastases. Another outcome of this study is that the application of intraoperative fluorescence in clinical practice is feasible and a viable strategy for intraoperative LN staging. For future applications, a fluorescent probe and/or photosensitising agent with high sensitivity and specificity for colorectal cancers would be highly beneficial.

In this study, the sensitivity and specificity for detecting colorectal metastatic LN using pre-operative CT imaging were 65% and 47.6%, respectively (Table 3.6). This is comparable to the sensitivity (64-70%) and specificity (53-78%) for detecting colorectal metastatic LN using pre-operative CT imaging as reported in other studies (33,34). Based upon the findings from this study, 5-ALA fluorescence diagnosis did not demonstrate an improved ability to detect LN metastases as compared to pre-operative CT imaging.

A clinical study by Dighe *et al.* evaluated the accuracy of CT imaging in stratifying patients into different prognostic groups (33). The presence of EMVI was examined as a potential prognostic marker. The sensitivity and specificity were 61% and 79% respectively. These results are similar to the sensitivity and specificity for EMVI detection on pre-operative CT imaging in the GLiSten study, which were 60.9% and 72.2% (Table 3.7) respectively. The authors of the study argue that preoperative CT imaging is ineffective for detecting EMVI due to the poor sensitivity. This is potentially due to the subjective evaluations of pathologists creating discrepancies between CT imaging and pathological examinations. EMVI is still being reviewed as a clinical marker of prognosis in colon cancer patients and will benefit from simultaneous improvements in both the standards of CT imaging and pathological examination.

In the GLiSten study, 5-ALA fluorescence was observed in ~30% of the primary tumours which may be indicative of differences in the pharmacokinetics (uptake and clearance), metabolism of 5-ALA, and production of PPIX by different tumours(243–245). Given the low rates of tumour fluorescence observed, the tumour biology was investigated in an attempt to further explain the findings. Gene microarray analysis was performed to identify any differences at a gene expression between different colonic tumours, which might explain the differences that were observed in fluorescence of the primary tumour. From the 3 methods that were evaluated to extract RNA, Protocol 3 (Qiagen RNeasy Mini Kit ) produced the highest concentration of RNA per sample (Figure 3.1A). It also had the second highest RIN value of 6.5 (Figure 3.1B) which shows moderate degradation of the RNA within the sample(238). This was, therefore, the protocol selected to extract RNA from the tumour samples that were selected for gene expression analysis.

Principal component analysis simplifies complex data whilst retaining patterns within the data set without knowledge of the different groups being compared(246). It transforms the data into fewer dimensions and projects onto lower dimensions called principal components to find the best summary of the data. In essence it is a data analysis tool that identifies the main axes of variance in a data set as well as understanding the key variables and spotting outliers. There are limitations with this data analysis tool however, the data must be linear, highly correlated patterns may not be identified as the principal components are uncorrelated and may miss clusters(246). On statistical analysis using single-factor comparison with the recommended threshold of  $p < 0.05$ , no significant differences in gene expression were identified between the fluorescent and non-fluorescent tumours.

In summary, the GLiSten study was unable to support the use of 5-ALA/PPIX mediated fluorescence for intraoperative LN staging during colon cancer surgery. This study did show that 5-ALA fluorescence-guided surgery is an acceptable intervention to improve the outcomes of treatment in colon cancer patients.

# **Chapter Four**

## **Cancer targeting agents**

## 4 Cancer targeting agents

### 4.1 Introduction

Monoclonal antibodies are one of the most commonly used recognition molecules used to actively target cancers(119). This is due to their high binding affinity and specificity for target antigens. The cell membrane marker, CEA, is commonly overexpressed in colorectal cancer cells(143,146,149) and, therefore, for this research project an anti-CEA antibody was chosen as the targeting agent. The recombinant chimeric IgG murine monoclonal anti-CEA antibody, A5B7, as described in 2.2.2, was used. A similar chimeric murine monoclonal antibody, CD31, was chosen as the control antibody. CD31 is a single chain transmembrane protein that is expressed on endothelial cells(232).

Affimers are short single-stranded RNA or DNA oligonucleotides that have been developed and are of interest as an alternative to monoclonal antibodies as active targeting agents(144,161,172,174). Given the overexpression of CEA in colorectal cancer cells an anti-CEA affimer was chosen for comparison as a targeting agent against the anti-CEA antibody. The anti-CEA affimer described in 2.2.3 was used for experiments described in this chapter.

The three cell lines chosen for this project were LoVo, EA.hy926 and HEK293. LoVo cells are derived from a human metastatic colonic adenocarcinoma and are known to have high expression levels of CEA(247) on their cell surface membrane with negligible expression of CD31. The EA.hy926 cell line originates from primary human umbilical vein cells and is an endothelial cell line. EA.hy926 cells have high expression levels of

CD31(248) with a low expression levels of CEA. HEK293 is an epithelial cell line derived from human embryonic renal tissue and does not express either CEA or CD31(249).

## **4.2 Results**

### **4.2.1 Antibody testing on fixed cells**

The three cell lines were cultured as described in 2.2.1.1 - 2.2.1.2 and prepared for immunofluorescence as described in 2.2.1.3.

#### **4.2.1.1 Testing target and control antibodies on fixed cells**

To demonstrate anti-CEA and anti-CD31 targeting on LoVo, EA.hy926 and HEK293 cells, immunofluorescence was performed as described in 2.2.1.4. As shown in Figure 4.1, green fluorescence was observed when LoVo cells were incubated with the anti-CEA antibody and no fluorescence was observed when incubated with the anti-CD31 antibody, suggesting that the LoVo cell line was an appropriate choice for the target cell line. For EA.hy926 cells, green fluorescence was only observed when incubated with the anti-CD31 antibody, suggesting that this cell line is an appropriate cell line to demonstrate that the anti-CD31 is correctly binding and as a control for the anti-CEA antibody. No green fluorescence was observed in HEK293 cells incubated with either antibody indicating that HEK293 cells are an appropriate control cell line for both the anti-CEA and anti-CD31 antibodies.

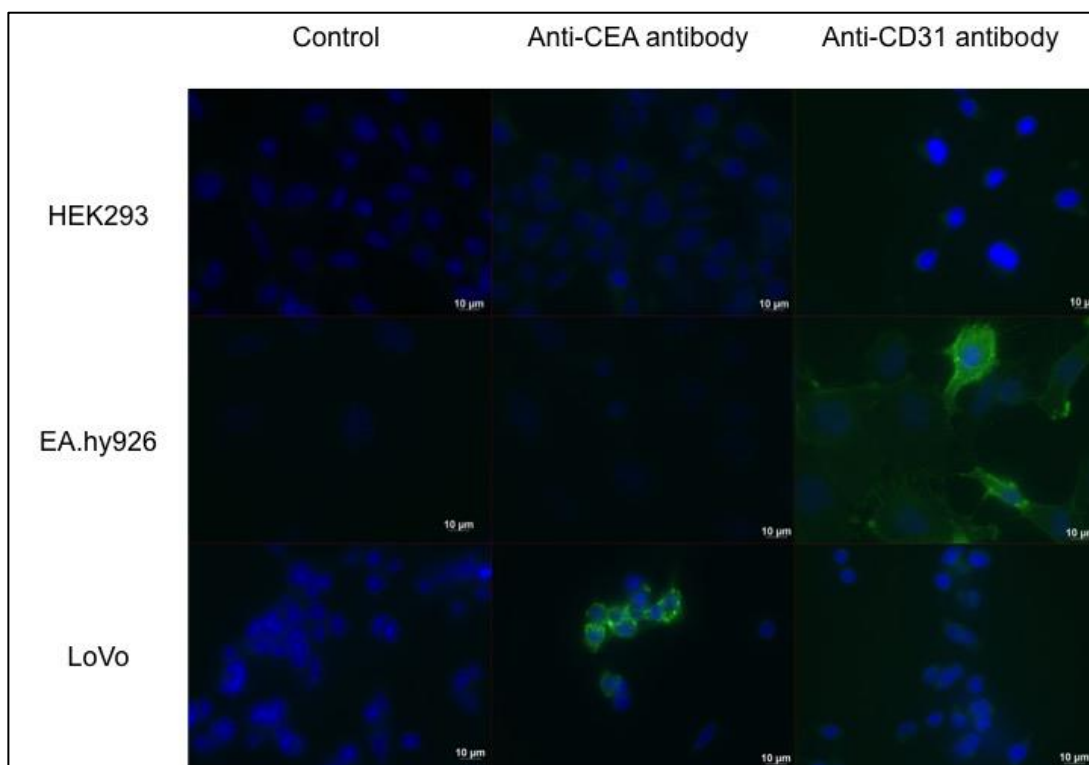


**Figure 4.1. Binding of target and control antibodies on target and control cell lines using immunofluorescence on fixed cells.** Blue fluorescence is DAPI. Green fluorescence is Alexa Fluor® 488 using FITC filter. Magnification x63. Scalebar = 10 µm. 0.5% skimmed milk blocking served as the control. Images in this figure are representative of at least 3 independent experiments. See 2.2.1.4 of Materials and Methods for the detailed protocol. The target anti-CEA antibody binds selectively to the LoVo cell line and the control anti-CD31 antibody binds selectively to the EA.hy926 cell line. Neither the target nor the control antibody bind selectively to the HEK293 cell line.

#### 4.2.1.2 Testing oxidised antibodies on fixed cells

Antibodies underwent an oxidative process to enable conjugation to the MNP as described in 2.2.2.5. To investigate whether oxidising the anti-CEA and anti-CD31 antibodies changed their affinities and specificities for their target cell surface markers, the oxidised antibodies were prepared and tested as described in 2.2.1.4. Green fluorescence was only observed when EA.hy926 and LoVo cell lines were incubated with the oxidised anti-CD31 and anti-CEA antibodies respectively. No fluorescence was detected in HEK293 cells incubated with either oxidised antibodies (Figure 4.2). This

suggests that the oxidation process did not influence the binding of either antibodies to their respective cell surface markers.

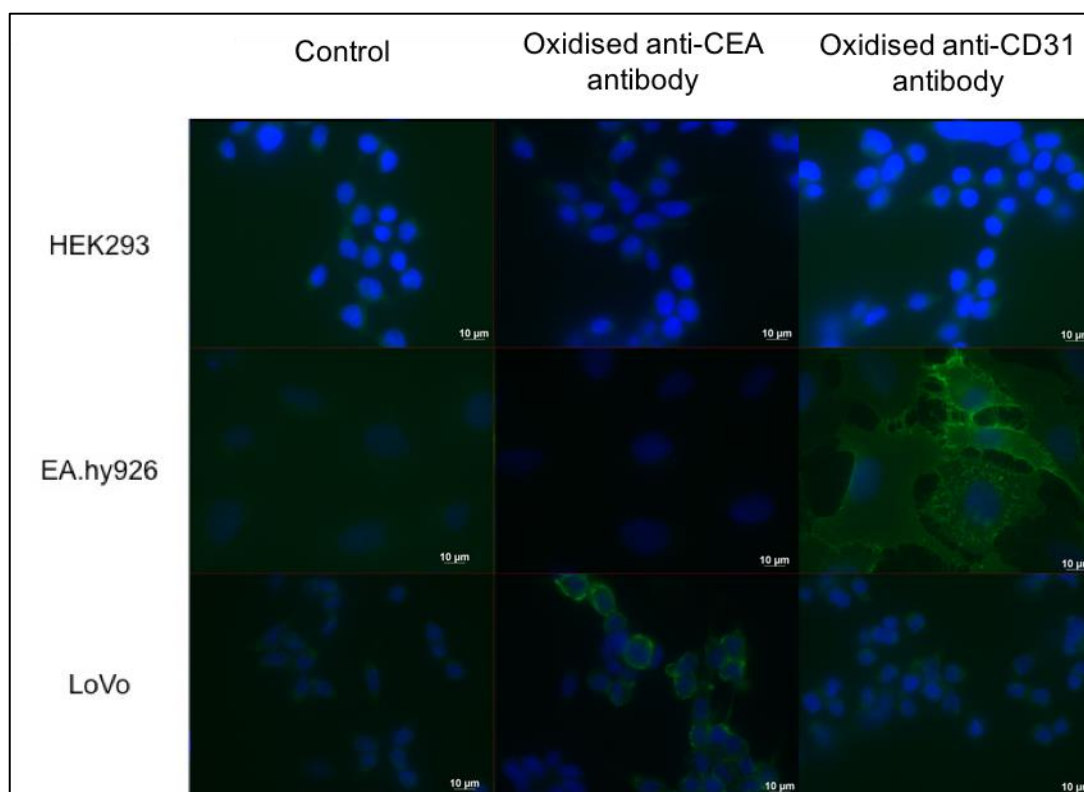


**Figure 4.2. Binding of oxidised target and control antibodies on target and control cell lines using immunofluorescence on fixed cells.** Blue fluorescence is DAPI. Green fluorescence is Alexa Fluor® 488 using FITC filter. Magnification x63. Scalebar = 10 µm. 0.5% skimmed milk blocking served as the control. Images in this figure are representative of at least 3 independent experiments. See 2.2.1.4 of Materials and Methods for the detailed protocol. The oxidised target anti-CEA antibody binds selectively to the LoVo cell line and the oxidised control anti-CD31 antibody binds selectively to the EA.hy926 cell line. Neither the oxidised target nor the oxidised control antibody bind selectively to the HEK293 cell line.

#### 4.2.1.3 Testing biotinylated antibodies on fixed cells

Biotinylation of both antibodies was performed as described in 2.2.2.6. This was performed to identify this technique as a potential alternative conjugation route for binding the antibodies to the MNP. To investigate whether biotinylation had an impact on antibody binding, biotinylated antibodies were prepared and tested as described in 2.2.1.4. Green fluorescence was only observed when EA.hy926 and LoVo cell lines were incubated with the biotinylated anti-CD31 and anti-CEA antibodies respectively. No

fluorescence was detected in HEK293 cells incubated with either biotinylated antibodies (Figure 4.3). This suggests that the biotinylation process did not influence the binding of either antibodies to their respective cell surface markers.

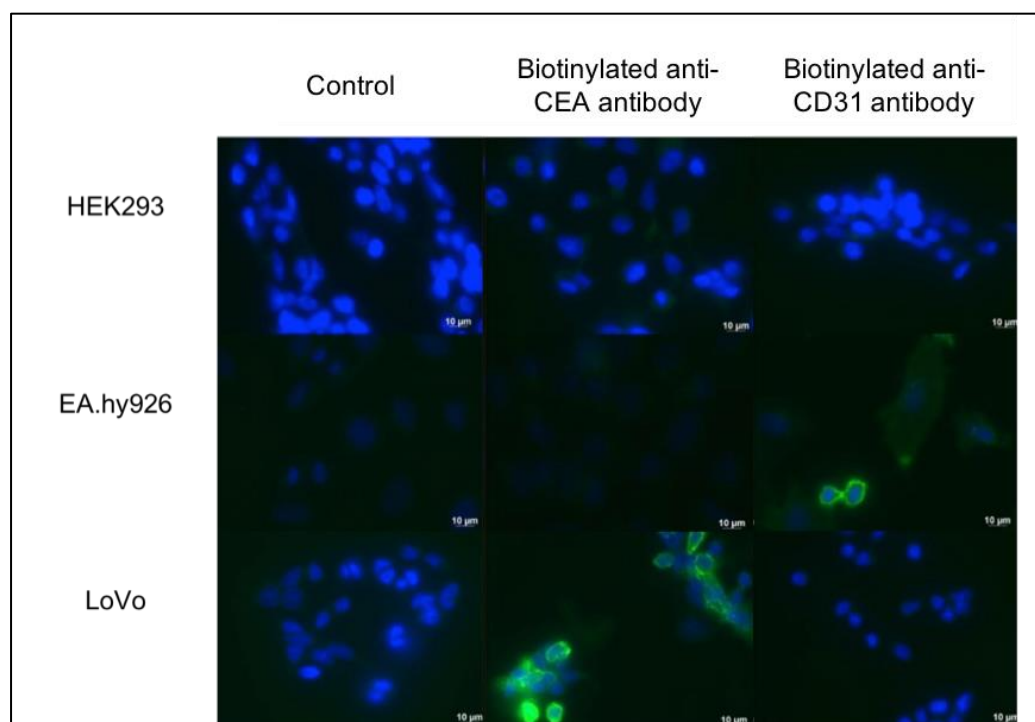


**Figure 4.3. Binding of biotinylated anti-CEA and anti-CD31 antibodies on target and control cell lines using immunofluorescence on fixed cells.** Blue fluorescence is DAPI. Green fluorescence is Alexa Fluor® 488 using FITC filter. Magnification x63. Scalebar = 10 μm. 0.5% skimmed milk blocking served as the control. Images in this figure are representative of at least 3 independent experiments. See 2.2.1.4 and 2.2.2.6 in Materials and Methods for the detailed protocols. The biotinylated target anti-CEA antibody binds selectively to the LoVo cell line and the biotinylated control anti-CD31 antibody binds selectively to the EA.hy926 cell line. Neither the biotinylated target nor the biotinylated control antibody bind selectively to the HEK293 cell line.

#### 4.2.2 Gel electrophoresis of reduced antibody

To create the antibody-NP conjugate, a half-antibody fragment was created by cleaving the di-sulphide bonds between the two heavy chains of the antibody in order to control its orientation in the conjugate. The half-antibody fragment would then be conjugated to the MNP via cysteine-maleimide conjugation chemistry. It was therefore important to

determine the most appropriate reducing agent as well as confirming the presence of a half-antibody fragment with an available cysteine group following reduction of the anti-CEA antibody. Three reducing agents (TCEP, 2-ME and 2-MEA) were investigated using the protocol described in 2.2.2.1 and gel electrophoresis was performed on the reduced target antibody as described in 2.2.2.2 to identify the presence of half-antibody fragments following reduction. The molecular weight of the half-antibody fragment should be ~75kDa. As shown in Figure 4.4, no band was seen at 75kDa following TCEP reduction (Lane 2). Following 2-ME and 2-MEA mediated reduction of the anti-CEA antibody, bands were observed at 75kDa (Lanes 3 and 4).

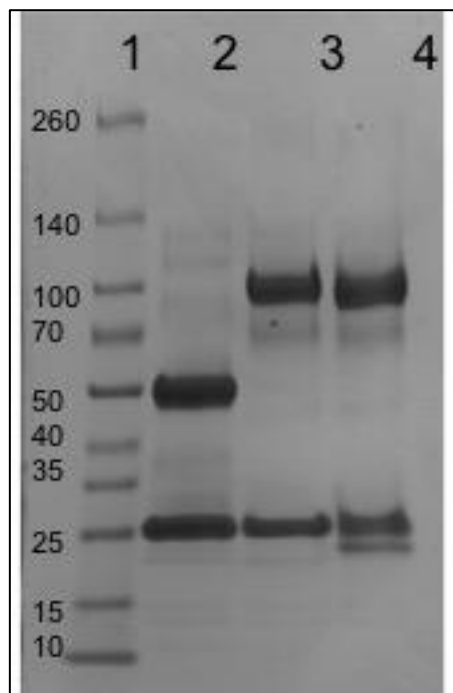


**Figure 4.4. Developed gel electrophoresis membrane depicting weights of antibody fragments following reduction with different reduction agents.** Lane 1 – Molecular weight Markers (kDa), Lane 2 - TCEP, Lane 3 - 2-ME, Lane 4 - 2-MEA. Images in this figure are representative of at least 3 independent experiments. See 2.2.2.1 and 2.2.2.2 of Materials and Methods for the detailed protocols. None of the three reducing agents produced a band at the 75kDa molecular weight indicating that low volumes of half-antibody fragments were produced with each reducing agent.

Densitometry analysis was performed on gels to estimate the percentage volume of the reduced antibody fragments in the total volume of antibody and summarised in Table 1. Densitometry analysis of the reduced antibody fragments revealed that reduction with TCEP produced negligible half-antibody fragments with no band detection around 75kDa. Reduction with 2-ME and 2-MEA were found to produce half-antibody fragments (Figure 4.4 and Table 4.1). Densitometry analysis showed that the overall volume was around 5% for 2-ME (combination of peaks at 69 and 73 kDa representing half-antibody fragments) and around 3% for 2-MEA (peak at 66kDa). This shows that reduction of the anti-CEA antibody to produce half-antibody fragments using TCEP, 2-ME or 2-MEA is inefficient and alternative conjugation techniques would need to be explored.

**Table 4.1. Densitometry analysis of the resulting anti-CEA antibody fragments following reduction with TCEP, 2-ME and 2-MEA.** Height represents the peak height above baseline for the signal and the raw volume is the area under the curve at the peak.

Reducing agent	Molecular weight (kDa)	Height	Raw volume	Total volume %
TCEP	113	1524	3180391	2
	49	21684	99368232	56
	26	20919	74281152	42
2-ME	93	18822	64296488	54
	73	2532	2067259	2
	69	2313	3017554	3
	25	20749	50056264	42
2-MEA	88	14913	43676720	47
	66	1260	2614556	3

	25	12041	38209272	41
	22	5644	8235290	9

#### 4.2.3 Testing for presence of glycoprotein on antibody

The use of a linker between the antibody and the MNP was explored. 3-(2-pyridyldithio)propionyl hydrazide (PDPH) is a heterobifunctional cross linker with sulfhydryl-reactive pyridyldithiol and carbonyl-reactive hydrazide groups. Many monoclonal antibodies contain glycoprotein side chains on their heavy chains. If this is present on the A5B7 anti-CEA antibodies then oxidising this glycoprotein on the antibody would allow for conjugation of PDPH via its hydrazide group. Dot blotting was performed to verify the presence of a glycoprotein side chain on the anti-CEA antibody as described in 2.2.2.3. Biotinylation of the oxidised anti-CEA antibody was successful confirming the presence of a glycoprotein chain that could be exploited as a site for conjugation to the MNP (Figure 4.5).

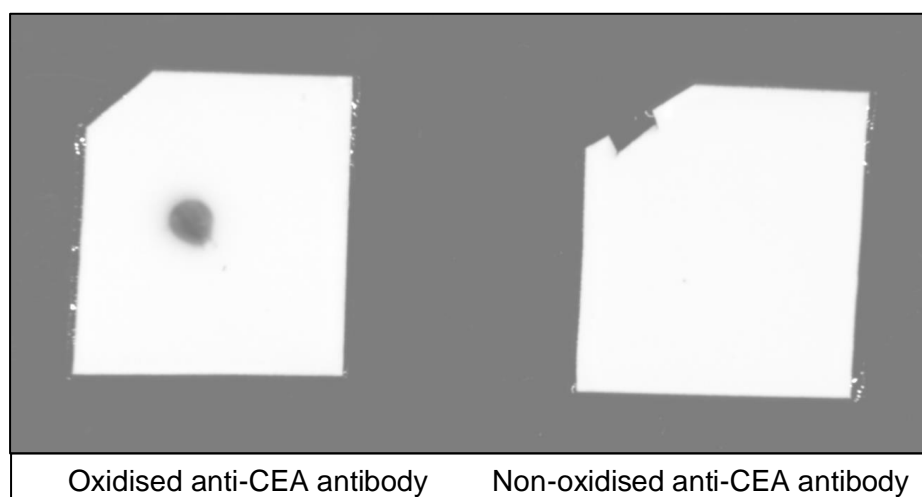


**Figure 4.5. Dot blot highlighting the biotinylation of oxidised anti-CEA antibody and non-oxidised anti-CEA antibody control.** Images in this figure are representative of at least 3 independent experiments. See 2.2.2.3 of Materials and Methods for detailed protocol. Biotinylation of the oxidised anti-CEA antibody was successful whereas biotinylation did not occur with the non-oxidised anti-CEA antibody indicating that the antibody does possess a glycoprotein side chain.

#### **4.2.3.1 Western blotting**

The configuration of an antibody, depicted Figure 1.13, shows the glycoprotein chain projecting out from the heavy chain. Western blotting of the biotinylated antibody was performed as per the protocol described in 2.2.2.4 to deduce the location of the glycoprotein chain. This was conducted in order to identify the orientation of the antibody after conjugation to the MNP. In agreement with Figure 4.5, Figure 4.6 shows that biotinylation of the untreated antibody was not detected (Lane 2). The largest band of reduced biotinylated antibody was detected around 35-40kDa (Figure 4.6. Lane 3). It is difficult to identify accurately which specific fragment of the anti-CEA antibody this band may represent and subsequently determine the location of the glycoprotein chain.

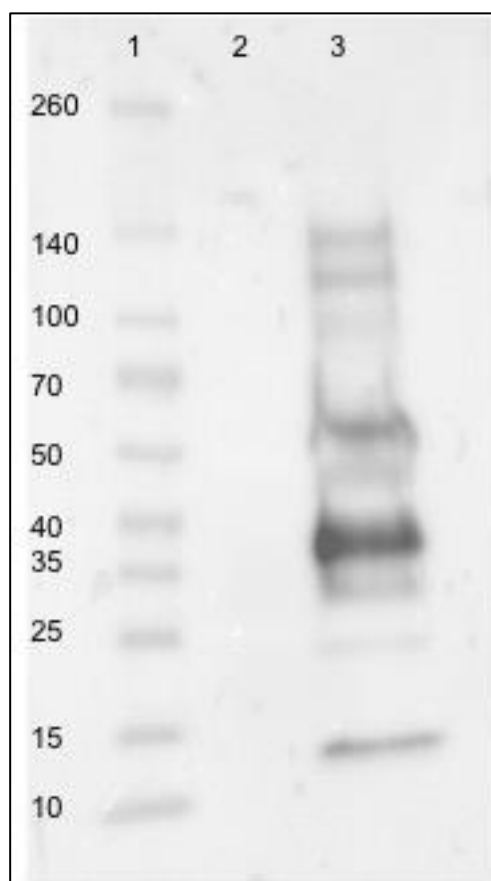


**Figure 4.6. Western Blot showing biotinylation of oxidised and non-oxidised anti-CEA antibody.** Lane 1 - Molecular weight Markers (kDa), Lane 2 - Untreated antibody, Lane 3 - Treated antibody. Images in this figure are representative of at least 3 independent experiments. See 2.2.2.4 of Material and Methods for the detailed protocol. The largest band occurred at a molecular weight of 35-40kDa.

#### 4.2.4 Testing biotinylated affimers

Following the unsuccessful characterisation of the anti-CEA antibody, an anti-CEA affimer was subsequently evaluated as a potential targeting agent. To assess the binding of the anti-CEA affimer, it was biotinylated as described in 2.2.3 and immunofluorescence was performed on LoVo, EA.hy926 and HEK293 cells. The affimer was designed with a free cysteine (sulfhydryl) group at the base enabling conjugation through cysteine-maleimide chemistry. In order to confirm that the anti-CEA affimer bound specifically to the target cell line only a biotin-maleimide dye was conjugated to the affimer resulting in biotinylation. The biotin was therefore available for binding to the

fluorescent protein, Streptavidin Dylight 488. As shown in Figure 4.7, noticeable green fluorescence was observed in anti-CEA affimer treated LoVo cells.

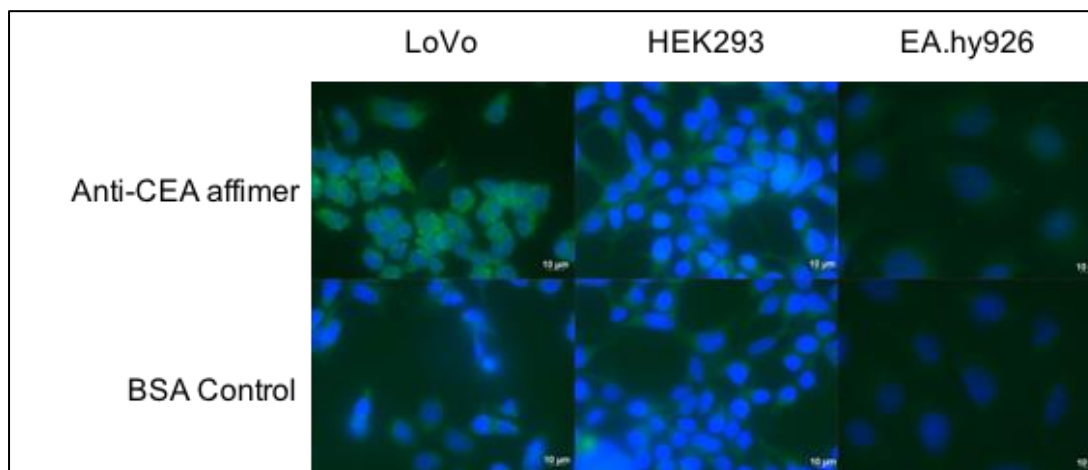


**Figure 4.7. Binding of biotinylated anti-CEA affimer on target and control cell lines compared to BSA control using immunofluorescence on fixed cells.** Blue fluorescence is DAPI. Green fluorescence is Streptavidin Dylight 488 using FITC filter. Magnification x63. Scalebar = 10  $\mu\text{m}$ . 0.1% bovine serum albumin blocking served as the control. Images in this figure are representative of at least 3 independent experiments. See 2.2.3 of Materials and Methods for the detailed protocol. The target anti-CEA affimer binds selectively to the LoVo cell line.

### 4.3 Discussion

Antibodies are commonly used as recognition molecules and affimers are of increasing interest for targeting. For my research project, I had to identify a suitable anti-CEA targeting candidate that could be used to functionalise the MNP and improve the targeting of colorectal cancers in addition to identifying an appropriate control recognition molecule. The anti-CEA (target) and anti-CD31 (control) antibodies were initially evaluated in this project for their suitability.

Immunofluorescence of both the target and control antibodies was performed on the three selected cell lines (Figure 4.1). The target antibody was found to selectively bind to

the target cell line, LoVo, which overexpresses the cell surface marker of interest (CEA). The control antibody was found to bind only to the control cell line, EA.hy926. Neither the target nor the control antibody was found to bind to the second control cell line, HEK293, which does not express either CEA or CD31. This demonstrated that the target and control cell lines, as well as the target and control antibodies, were suitable for further experiments.

Due to the unique structure of antibodies a variety of functional groups are available that can be exploited for conjugation(233). For this research project, the different conjugation methods via functional groups were considered as potential mechanisms for antibody conjugation to the NP. For example, free amine and carboxyl groups are commonly found on the tertiary structures of antibodies(233). However, exploiting these groups for conjugation could result in random orientation of the antibody on the NP and potentially affect the antigen-binding ability of the antibody-NP conjugate(155,250,251). Balevicius *et al.*(252) investigated the differences in the antigen-binding abilities of an antibody-based immunosensor. The antigen-binding abilities of fragmented antibodies was compared to whole non-fragmented intact antibodies. Whole intact antibodies were conjugated to the biosensors via covalent bonding of the free carboxyl groups and resulted in random orientation of the intact antibody once conjugated to the biosensors. Half-antibody fragments were formed through the reduction of whole intact antibodies using 2-ME as the reducing agent. Half-antibody fragments were conjugated to the biosensors using the free sulfhydryl groups (created through 2-ME mediated reduction) resulting in a more controlled orientation and conjugation of half-antibody fragments to the biosensors and without compromising the antigen-binding site. Half-antibody fragment-conjugated immunosensors were found to bind 2.5-fold higher to their respective antigens as compared to whole intact antibody-conjugated immunosensors. Findings from this study suggest that random orientation of antibodies could potentially compromise and decrease the antigen-binding abilities of the antibodies. Orientated

conjugation is where the chosen functional group to be used for conjugation is located at a specific site on the antibody and can preserve the ability of the antibody to bind specifically to its antigen(155,233,250,252,253). Dulay *et al.*(254) developed an antibody-based immunosensor for the diagnosis of the bacterial infectious disease, Tularemia. The authors compared whole intact antibodies against half-antibody fragments. Whole intact antibodies were conjugated using carboxyl groups resulting in random orientation of the antibodies and hindering the antigen-binding sites. Half-antibody fragments were correctly orientated and conjugated through sulfhydryl groups. The half-antibody fragment-conjugated immunosensors were found to be more sensitive in antigen-binding as compared to whole intact antibody conjugates. The authors attributed this difference in binding sensitivities to better presentation of the antigen-binding site enabling improved antigen binding.

Two commonly used orientated conjugation strategies are i) selective cleaving of antibodies into half-antibody fragments using a reducing agent(155,233) and ii) the oxidation of glycoprotein side chains on the heavy chain of antibodies and using a crosslinker to form the desired conjugate(233). Biotinylation of antibodies is also a common strategy used for antibody conjugation(233) as it takes advantage of the strong binding chemistry between avidin and biotin. Due to the proven track record of the chemical reduction, oxidation and biotinylation processes for facilitating antibody conjugation they were chosen and investigated in this project.

In order to conjugate the antibody to the NP, the antibody would initially undergo reduction or chemical modification. Monoclonal antibodies are susceptible to becoming inactivated through this process as the site of conjugation could potentially be located at the antigen binding site(155,233). Oxidation or biotinylation are methods of chemically modifying antibodies for conjugation and it was vital to identify whether these processes

altered the binding properties of both the target and control antibodies. Figure 4.2 and Figure 4.3 confirm that modifying the antibodies did not influence their antigen binding abilities. Modified target antibody only bound to LoVo cells and modified control antibody only bound to EA.hy926. After determining that oxidation and biotinylation did not affect the binding abilities of the antibodies these processes were investigated for forming antibody-NP conjugates.

Initially, it was proposed that half-antibody fragments would be ideal candidates as recognition molecules for conjugation. Half-antibody fragments have free cysteine groups formed through the cleavage of disulfide covalent bonds in the hinge region by a reducing agent(155,233). The cysteine groups are then available to bind to maleimide functionalised NPs. Antibodies would need to undergo chemical reduction first in order to produce half-antibody fragments. The ideal reducing agent as well as the quantity of half-antibody produced from this process was therefore investigated. Firstly, the reduction of the anti-CEA antibody was carried out using TCEP, 2-ME and 2-MEA, to identify which of these reducing agents would produce half-antibody fragments. These reducing agents were chosen as they possess varying potencies in reduction. 2-MEA is the mildest reducing agent, 2-ME has moderate reducing abilities and TCEP is the strongest reducing agent(155). All three reducing agents have previously been used successfully to produce half-antibody fragments as identified in the literature.

Dithiothreitol (DTT) is another strong and potent antibody reducing agent. However, DTT is known to possibly degrade structures and denature monoclonal antibodies(255).

As highlighted in Figure 4.4, the ideal reducing agent for producing half-antibody fragments for MNP conjugation was not successfully identified. Although reduction with 2-ME and 2-MEA did result in the production of half-antibody fragments, they constituted an inadequate fraction of the overall volume. Further optimisation of reducing conditions could potentially improve the production yield of half-antibody fragments. This was

suggested by Makaraviciute *et al.*(155), who, showed that optimisation of variables such as the type of reducing agent, concentration of reducing agent, pH, and also the type of antibody, can influence the production yields of half-antibody fragments.

The low volumes of anti-CEA half-antibody fragments produced through chemical reductions using 2-ME and 2-MEA means that large quantities of the anti-CEA antibody would be needed in order to generate adequate amounts of half-antibody fragments for MNP conjugation. Given that the anti-CEA antibody is not commercially available and had been gifted to our research laboratory by Cancer Research UK Biotherapeutics Development Unit, the total volume of antibody available for experiments was substantially limited. In addition, the same quantity of the control antibody would have also been required which was not financially feasible. This meant that reducing antibodies to produce half-antibody fragments was impractical and therefore not pursued further.

The use of a chemical linker between the glycoprotein side chain on the antibody and the MNP was then explored. A heterobifunctional crosslinker has different reactive groups at either end enabling conjugation to different functional groups(233). A carbonyl-reactive and sulfhydryl-reactive crosslinker would be an ideal choice for conjugating the antibody to the MNP and is discussed in more detail in Chapter 6. IgG monoclonal antibodies are typically glycosylated meaning they possess a polysaccharide glycoprotein side chain which protrudes from the heavy chain. The glycoprotein side chain on the antibody could be oxidised(233) creating a reactive aldehyde group. The aldehyde group formed would then bind to the carbonyl-reactive end of heterobifunctional crosslinkers, with the maleimide functionalised NP binding to the other end. PDPH is a heterobifunctional crosslinker that has a carbonyl-reactive hydrazide group and a sulfhydryl-reactive pyridyldithiol group on either ends. The pyridyldithiol

group is displaced by maleimide in its presence, subsequently allowing functionalised MNPs to bind to the linker and creating an antibody-NP conjugate. Other carbonyl-reactive and sulfhydryl-reactive crosslinkers which are commonly used include 4-(4-N-maleimidophenyl)butyric acid hydrazide (MPBH) and 4-(N-maleimidomethyl)cyclohexane-1-carboxyl-hydrazide ( $M_2C_2H$ ). Both of these crosslinkers utilise a maleimide functional group at the sulfhydryl-reactive end, which would not be compatible and would be unable to conjugate to the maleimide functionalised NP. PDPH was therefore selected as it has previously been used to conjugate antibodies(256).

The anti-CEA antibody used in this research project is not commercially available and the molecular structure of the antibody is unknown. Therefore, dot blotting was performed to confirm the presence of a glycoprotein side chain and western blotting to identify its location on the target antibody(Figure 4.6 and Figure 4.7). Dot blotting showed that the oxidised target antibody was biotinylated whereas the control non-oxidised target antibody was not biotinylated. This indicates the presence of a glycoprotein side chain on the antibody as suggested by successful oxidation and subsequent biotinylation. Western blotting was performed to identify the presence of the glycoprotein side chain which would have been expected to be located on the heavy chain fragment (refer to Figure1.13), producing a biotinylated band at 50kDa. As shown in Figure 4.6, the largest band of reduced biotinylated anti-CEA antibody was found to be between 35-40kDa. This does not correlate to a specific antibody fragment (refer to Figure 1.14), but could possibly represent a mixture of heavy and light chain fragments. Bands of heavy chain fragments are expected at ~50kDa and light chain fragments at ~25kDa. A possible explanation for this was the use of DTT as the reducing agent when preparing samples to be resolved via gel electrophoresis. As highlighted earlier, DTT is a strong reducing agent, which may have degraded the heavy chain fragment into further smaller partial fragments resulting in the band observed between 35-40kDa. Western blotting was therefore unable to identify the specific location of the glycoprotein side

chain on the oxidised target antibody. However, no discrete band was seen at 25kDa which is the expected weight for single light chain fragments, suggesting that the glycoprotein chain was not present on the light chains of the antibody. Therefore, using the glycoprotein chain to conjugate the antibody to the MNP should not interfere with the binding of the antibody to its target antigen.

An anti-CEA affimer that had been designed with a free cysteine group in the base of the scaffold that is available for binding was also investigated as an alternative to the anti-CEA antibody. This would eliminate the need for a linker in the conjugation of targeting agent to the MNP and rely on the cysteine-maleimide reaction chemistry. The targeting and binding properties of the anti-CEA affimer was evaluated. Figure 4.7 shows that FITC fluorescence was predominantly observed in LoVo cells incubated with the biotinylated anti-CEA affimer.

In summary, this chapter describes the work that was done in order to identify a suitable candidate that could be used as an anti-CEA targeting agent and conjugated to the MNP. Both the anti-CEA antibody and affimer were found to bind specifically to the target cell line (LoVo) and not to the control cell lines (EA.hy926 and HEK293). The anti-CD31 antibody was also identified as a suitable control antibody. Gel electrophoresis and densitometry analysis showed that generating half-antibody fragments of the anti-CEA antibody as targeting agents was not feasible. The presence of a glycoprotein side chain on the target antibody was identified that could potentially be oxidised and used for conjugation. Modifying both the anti-CEA and anti-CD31 antibodies by oxidation did not alter their ability to bind to their respective cell surface antigens. Although the precise location of the glycoprotein side chain was not determined on the anti-CEA antibody, it is unlikely to be located on the light chain fragment and therefore should not be present in the antigen-binding site. Therefore, using the glycoprotein side chain for conjugation to

the MNP should not alter the antibody's ability to bind to its target antigen. This was therefore the chosen mechanism for conjugating the antibody to the MNP.

# **Chapter Five**

## **Nanoparticles**

## 5 Nanoparticles

### 5.1 Introduction

Nanoparticles (NPs) and nanomedicines are versatile tools that can assist in the diagnosis and treatment of cancers. Due to the unique physiology of tumours and their microenvironments, NPs can utilise the EPR (see 1.1.4.1) effect to accumulate within the tumour vicinity (191,192) or be modified to specifically target and bind to cancers such as their application in fluorescence-guided cancer surgery. The ideal characteristics for NPs designed for fluorescent diagnosis, as detailed in 1.4.3.3, includes bright fluorescence, effective tissue penetration, negligible photobleaching and chemical/physical stability(53,215,216) with a high degree of sensitivity and specificity for the target tissue. Ideal fluorescent NPs have peak light emission within the near-infrared (NIR,  $\geq 650\text{nm}$ ) region thereby improving fluorescent emission through multiple layers of tissue and reduced autofluorescence(16,215,229). Semi-conducting organic polymer NPs, that emit in the NIR range, are potential candidates that can be applied for fluorescent diagnosis and fluorescent-guided surgery. These NPs are photostable, physically small in size (200nm) for effective tumour penetration, fluorescently bright, exhibit minimal cellular toxicity and large Stokes shift(226). A large Stokes shift is important because it improves the sensitivity of distinguishing fluorescent signals above non-specific background fluorescence, whereas a narrow Stokes shift can make it challenging to differentiate between true NPs fluorescent and background fluorescence i.e. tissue autofluorescence(257).

PEGylation involves the surface functionalisation of NPs with polyethylene glycol (PEG) polymer chains which helps them evade elimination via the mononuclear phagocyte system (MPS). PEGylation also allows NPs to be easily modified enabling the

conjugation of NPs to targeting moieties (170,191,209). PEGylation also reduces the 'clumping' and aggregation of NPs and decreases immunogenicity(53).

For this research project, a semi-conducting organic self-assembling NP was developed, comprised of a CN-PPV fluorescent core surrounded by a PLGA-PEG shell (Figure 5.1 and 1.14). CN-PPV is physically hydrophobic and the PLGA-PEG shell allows the NPs to be soluble in water (hydrophilic). As described above, the presence of PEG chains on the surface enables surface modification for conjugation to a targeting moiety for the active targeting of tumour tissue.

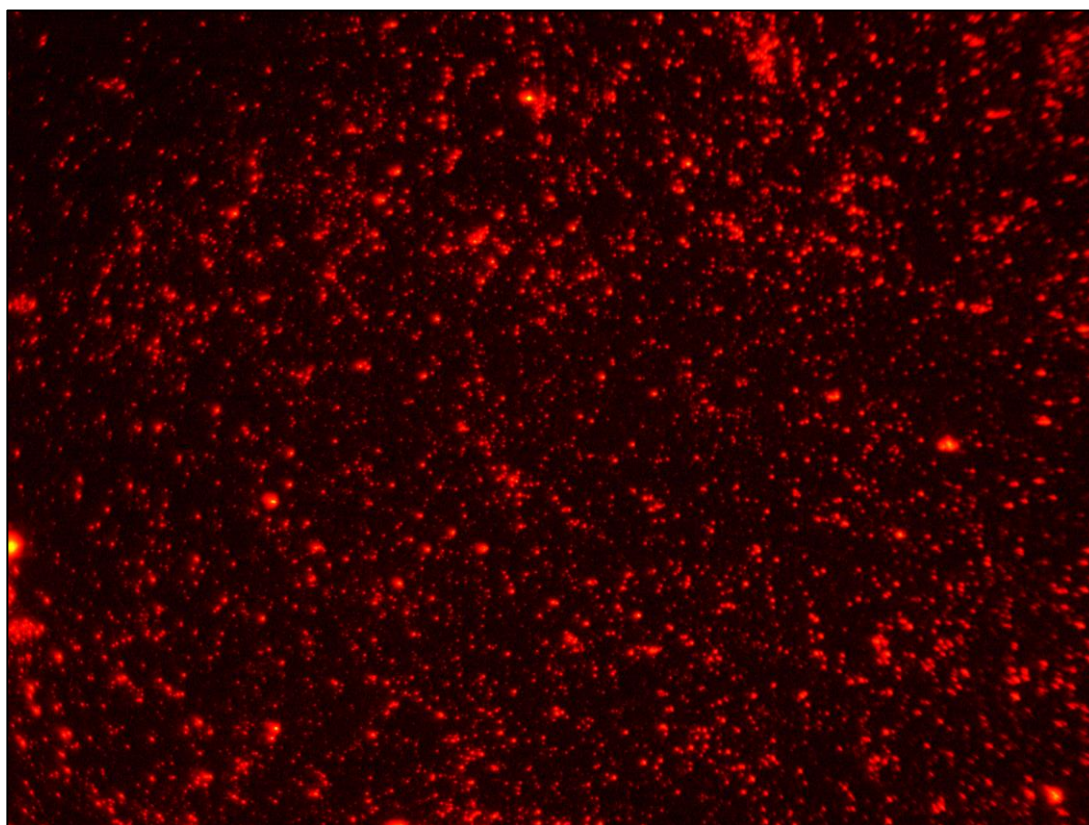


**Figure 5.1** Fluorescent imaging of NIR fluorescent CN-PPV dye-doped PLGA-PEG semiconducting polymer NP. This image shows the red emission of bare non-functionalised CN-PPV dye-doped PLGA-PEG NPs when exposed to an excitation wavelength of 405nm. Image in this figure is representative of 3 independent experiments using 3 independent batches of NPs.

## 5.2 Results

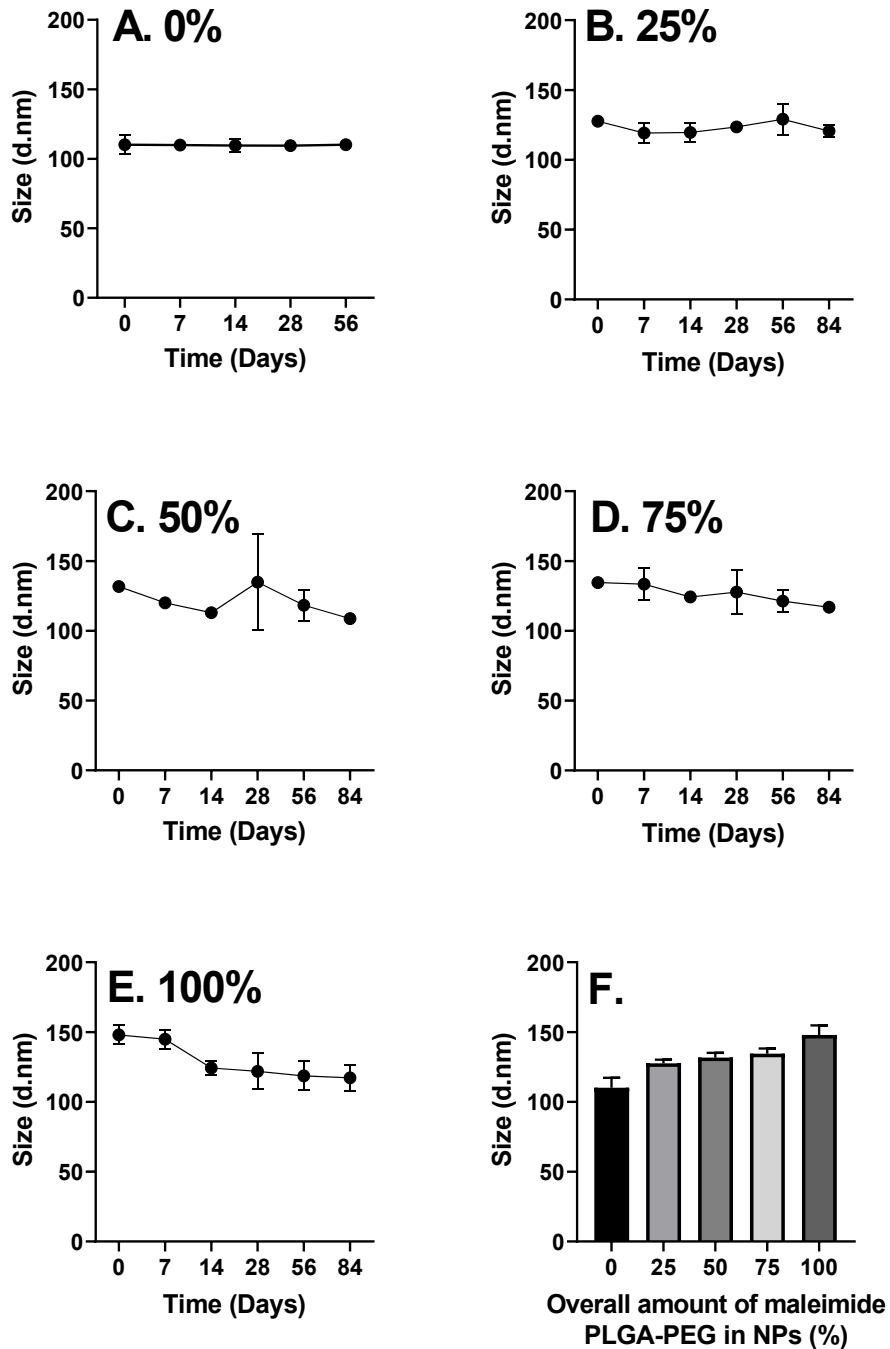
### 5.2.1 Nanoparticle characterisation

Bare non-functionalised (standard) and bare maleimide functionalised NPs were fabricated and characterised as described in 2.3.1 and 2.3.2 respectively.

#### 5.2.1.1 Characterisation of nanoparticle sizes

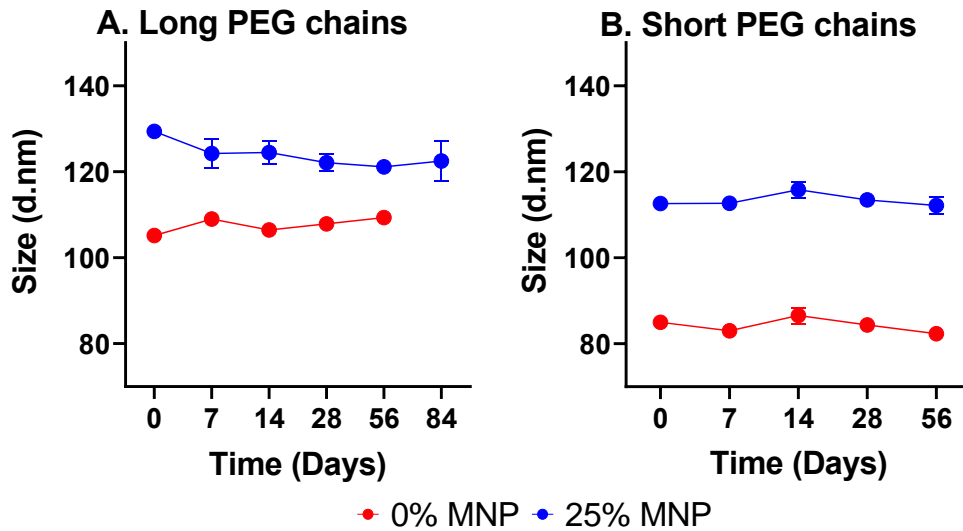
Characterisation of the sizes of NPs was carried out as described in 2.3.2.1. Figure 5.2 shows the sizes of CN-PPV/PLGA-PEG non-functionalised NPs and MNPs with varying amounts of maleimide PLGA-PEG that were stored in solution over time. Firstly, no significant changes in the hydrodynamic diameters of 0% ( $p=0.45$ ), 25% ( $p=0.24$ ), 50% ( $p=0.07$ ) and 75% ( $p=0.09$ ) maleimide functionalised NPs that were stored was observed over time (Figure 5.2A-5.2D). However, a 31d.nm reduction in hydrodynamic diameter was observed in 100% maleimide functionalised NPs when comparing sizes at Day 0 and Day 84 ( $p=0.002$ ) (Figure 5.2E). Increasing the overall amount of maleimide PLGA-PEG content within the MNPs resulted in increasing mean hydrodynamic diameters of the MNPs (Figure 5.2F).

Figure 5.3 shows sizes of non-functionalised and 25% MNPs with long (5,000 Da) and short (2,000) PEG polymer chains that were stored in solution over time. 25% maleimide functionalised CN-PPV/PLGA-PEG NPs with both long and short PEG polymer chains were found to be stable in size over time (long PEG chain:  $p=0.09$ , short PEG chain:  $p=0.1$ ). In addition, 25% maleimide functionalised NPs were found to have larger hydrodynamic diameters as compared to their non-functionalised counterparts. On Day 0, long PEG chains = 24d.nm increase in size,  $p<0.0001$  and short PEG chain = 28d.nm increase,  $p<0.0001$ .



**Figure 5.2. Mean hydrodynamic diameters of CN-PPV/PLGA-PEG NPs over time.**

**A)** Bare non-functionalised NP. **B)** Bare 25% maleimide functionalised NP. **C)** Bare 50% maleimide functionalised NP. **D)** Bare 75% maleimide functionalised NP. **E)** Bare 100% maleimide functionalised NP. **F)** Day 0 sizes of NPs with varying amounts of maleimide PLGA-PEG. Data represents means with standard deviation of 5 independent experiments. Experiments were performed in triplicate. See 2.3.2.1 of Materials and Methods for the detailed protocol. Hydrodynamic diameters of bare non-functionalised (0% MNP) and bare 25% - 75% maleimide functionalised NPs (MNPs) remained stable over time; There was a decrease in the hydrodynamic diameter of 100% MNP over time. Increasing the concentration of functionalised maleimide PLGA-PEG in the NP increased the hydrodynamic diameter.



**Figure 5.3. Mean hydrodynamic diameters of long and short PEG polymer chain functionalised CN-PPV/PLGA-PEG NPs. A)** NPs with long PEG chains (5,000Da) **B)** NPs with short PEG chains (2,000Da). Data represents means with standard deviation of 3 independent experiments. Experiments were performed in triplicate. See 2.3.2.1 of Materials and Methods for the detailed protocol. The hydrodynamic diameter of bare non-functionalised and bare 25% maleimide functionalised NPs with long and short PEG chains remained stable over time. The hydrodynamic diameter of both forms of 25% MNP was larger than both forms of 0% MNP.

Figure 4 shows the polydispersity index of non-functionalised NPs (0% MNP), MNPs with varying amounts of maleimide PLGA-PEG (25% - 100% MNPs) as well as non-functionalised (0% MNP) and 25% MNPs with long (5,000 Da) and short (2,000) PEG polymer chains over time. Values of below 0.2 are commonly deemed acceptable for polymer-based NPs.

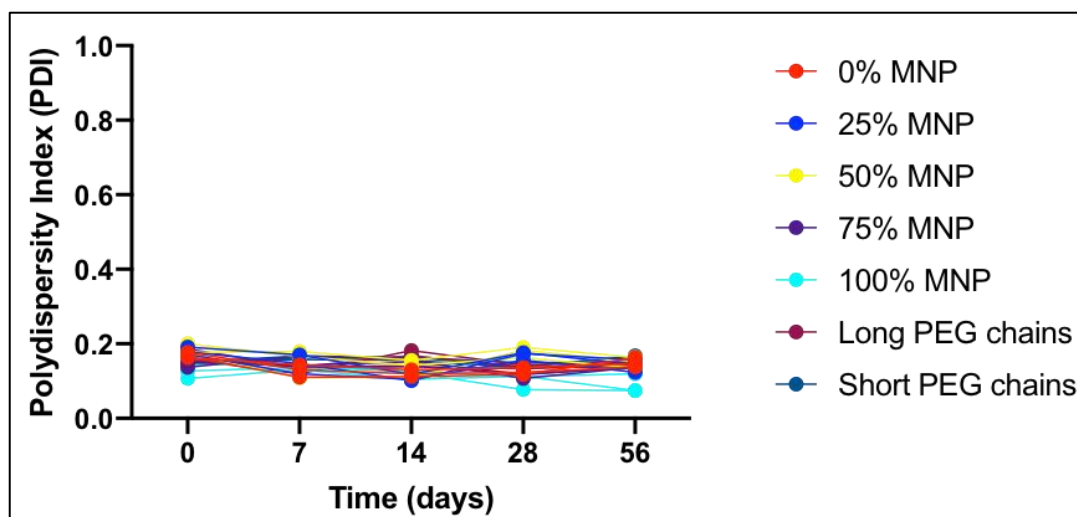


**Figure 4. Mean polydispersity index of CN-PPV/PLGA-PEG NPs over time.** Data represents means with standard deviation of 5 independent experiments. Experiments were performed in triplicate. See 2.3.2.1 of Materials and Methods for the detailed protocol. All different types of CN-PPV/PLGA-PEG NPs characterised over time showed polydispersity index values of less than 0.2.

### 5.2.1.2 Absorption and emission spectra

The absorption and emission spectra for non-functionalised NPs and all MNPs were mapped out as described in 2.3.2.2.

#### 5.2.1.2.1 Optimum dilution of nanoparticles

In order to deduce the optimal emission spectrum profile of NPs the concentration of NPs yielding a maximum absorbance of 0.1A.U. needs to be identified. There are two known factors that can influence the absorption and emission spectrum profiles when testing NPs using a spectrometer; scattering and reabsorption. On exposing NPs larger than 50nm to electromagnetic plane waves a phenomenon known as Mie scattering can contribute to the absorption spectrum profile. Mie scattering describes the scattering of light by a homogeneous sphere(258). The contribution from Mie scattering can be of the same magnitude or larger than the fluorescent material being studied. Reabsorption describes the effect of scattered light interacting with a second sample particle. If the

sample NP concentration was high, then light can interact with an initial NP, scatter but can then inadvertently interact and re-scatter from a second NP. The rescattered light could then potentially be detected by the spectrometer impacting on the spectrum profile. If the sample NP concentration is low enough then the scattered light from the interaction with the initial NP will be less likely to interact with a second NP and therefore the scattered light is not detected. The optimal concentration of NPs was therefore studied to determine the dilution/concentration that minimised strong contributions from Mie scattering in addition to reducing effects seen from reabsorption. A maximum absorption of 0.1A.U. is the empirical value used as absorbance at this peak seems to reduce these two factors across a wide range of NP systems. The absorption should be linearly proportional to the concentration of the NP, however this is not the case seen in Figure 5.5. There is increasing background at increased NP concentrations which would suggest that there is contribution to the spectrum profile from scattering.

Serial dilutions of non-functionalised CN-PPV/PLGA-PEG NPs were created and their absorption spectra were mapped out as described in 2.3.2.2.1. As shown in Figure 5.5, a maximal absorption of 0.1A.U. was achieved at 3.5 $\mu$ g CN-PPV/ml. For the other concentrations of non-functionalised NPs, the maximal absorption readings were - 5 $\mu$ g CN-PPV/ml: 0.1625A.U., 4.75 $\mu$ g CN-PPV/ml: 0.145A.U., 4.5 $\mu$ g CN-PPV/ml: 0.1375A.U., 4.25 $\mu$ g CN-PPV/ml: 0.1275A.U., 4 $\mu$ g CN-PPV/ml: 0.115A.U., 3.75 $\mu$ g CN-PPV/ml: 0.1075A.U., 3.25 $\mu$ g CN-PPV/ml: 0.0975A.U. and 3 $\mu$ g CN-PPV/ml: 0.0825A.U. Following this finding all NPs emission spectra profiles were generated at a dilution of 3.5 $\mu$ g CN-PPV/ml.

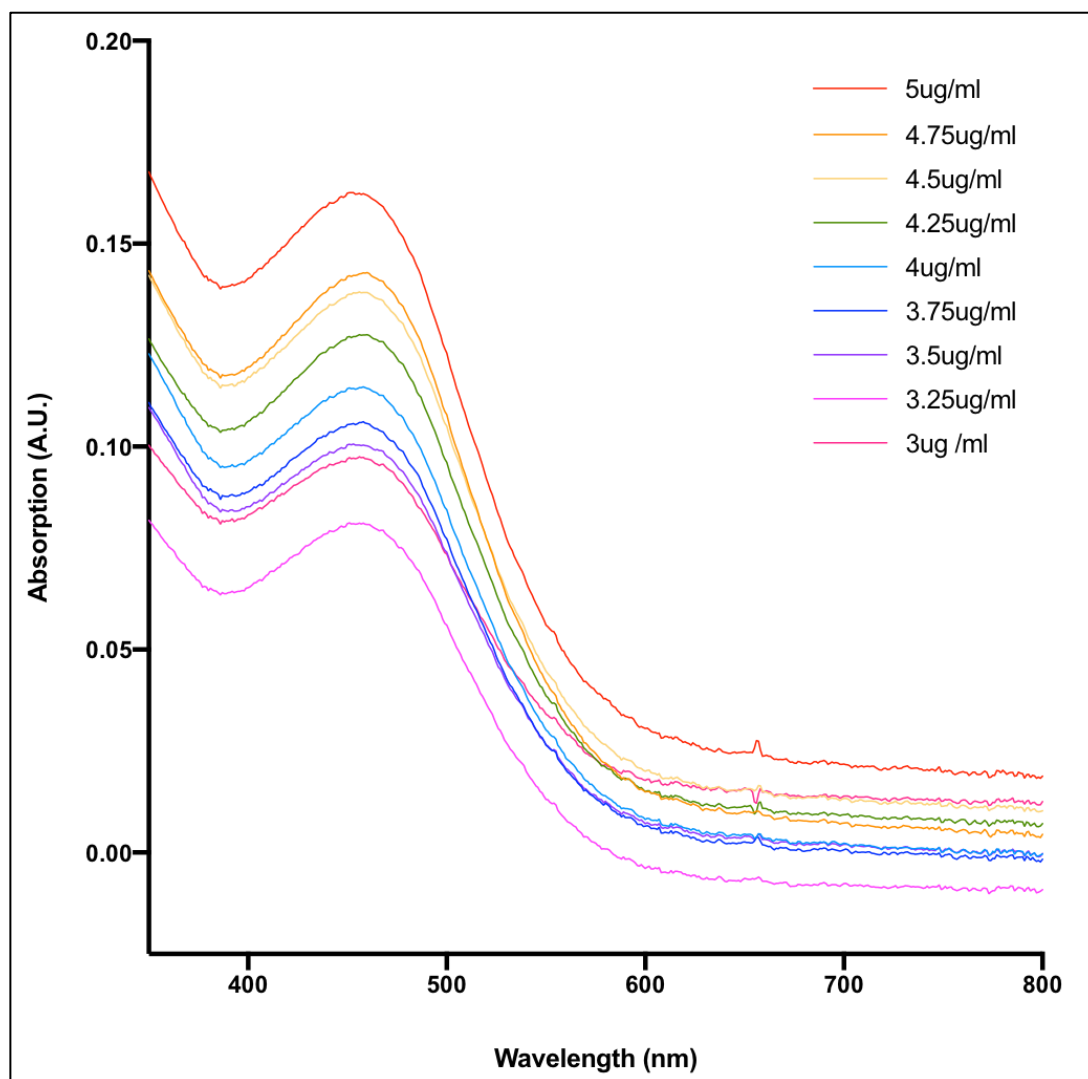


**Figure 5.5. Absorption profiles of serial dilutions of non-functionalised CN-PPV/PLGA-PEG NPs.** Data represents means with standard deviation of 3 independent experiments. Experiments were performed in triplicate. See 2.3.2.2.1 of Materials and Methods for the detailed protocol. An absorption of 0.1A.U. was achieved at 3.5µg CN-PPV/ml.

#### 5.2.1.2.2 Absorption and emission spectra for non-functionalised nanoparticles

Figure 5.6 illustrates the normalised absorption and emission spectra for non-functionalised NPs at 3.5µg CN-PPV/ml. Peak light absorption was found at the excitation wavelength of 470nm. Emission spectra was then mapped out at four different excitation wavelengths (380nm, 425nm, 440nm and 470nm) which all showed maximal

peak emission around 650nm. The absorption and emission spectra for the non-functionalised NPs did not appear to change over time.

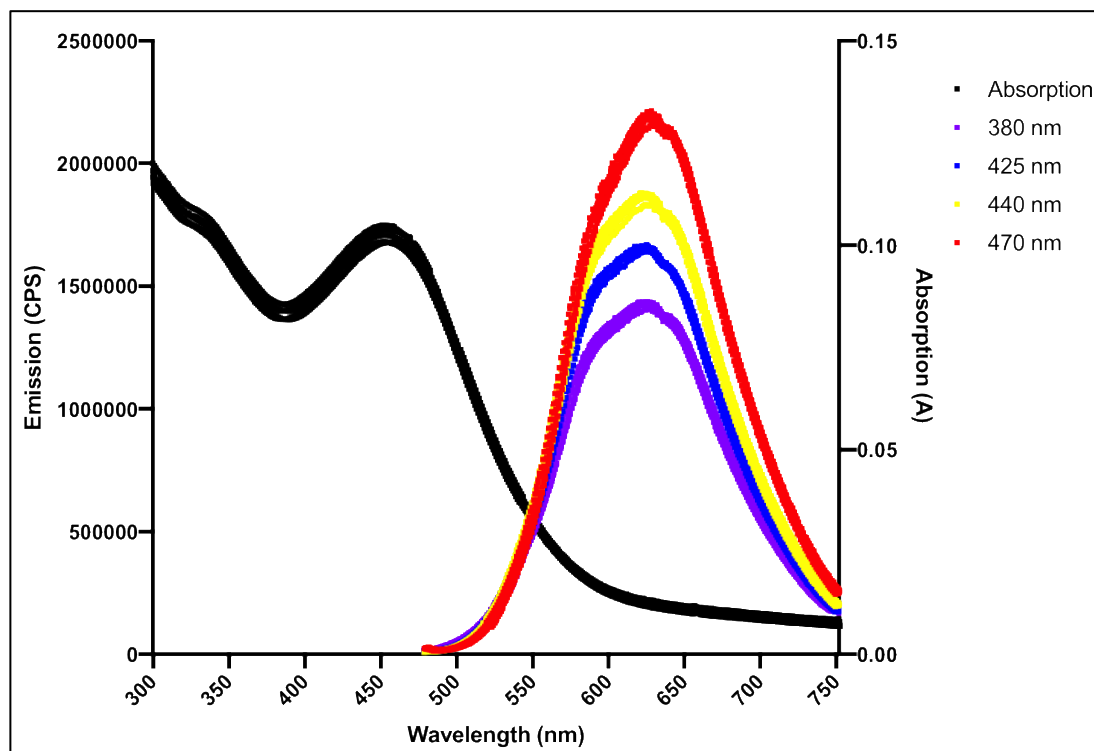


**Figure 5.6. Absorption and emission profiles of non-functionalised CN-PPV/PLGA-PEG NPs at optimum dilution over time.** Data represents means with standard deviation of 3 independent experiments. Experiments were performed in triplicate. See 2.3.2.2 of Materials and Methods for the detailed protocol. Peak absorption occurred at an excitation wavelength of 470nm. Peak emission occurred at 650nm at all four excitation wavelengths tested. The absorption and emission spectra for 0% MNP remained stable over time.

### 5.2.1.2.3 Absorption and emission spectra for maleimide functionalised nanoparticles

Figure 5.7 shows the normalised absorption and emission spectra for maleimide functionalised NPs. Peak light absorption was found at the excitation wavelength of 470nm. Emission spectra was then mapped out at four different excitation wavelengths (380nm, 425nm, 440nm and 470nm) which all showed maximal peak emission around

650nm. The absorption and emission spectra for all maleimide functionalised NPs remained comparable over time. These findings are similar to non-functionalised NPs.

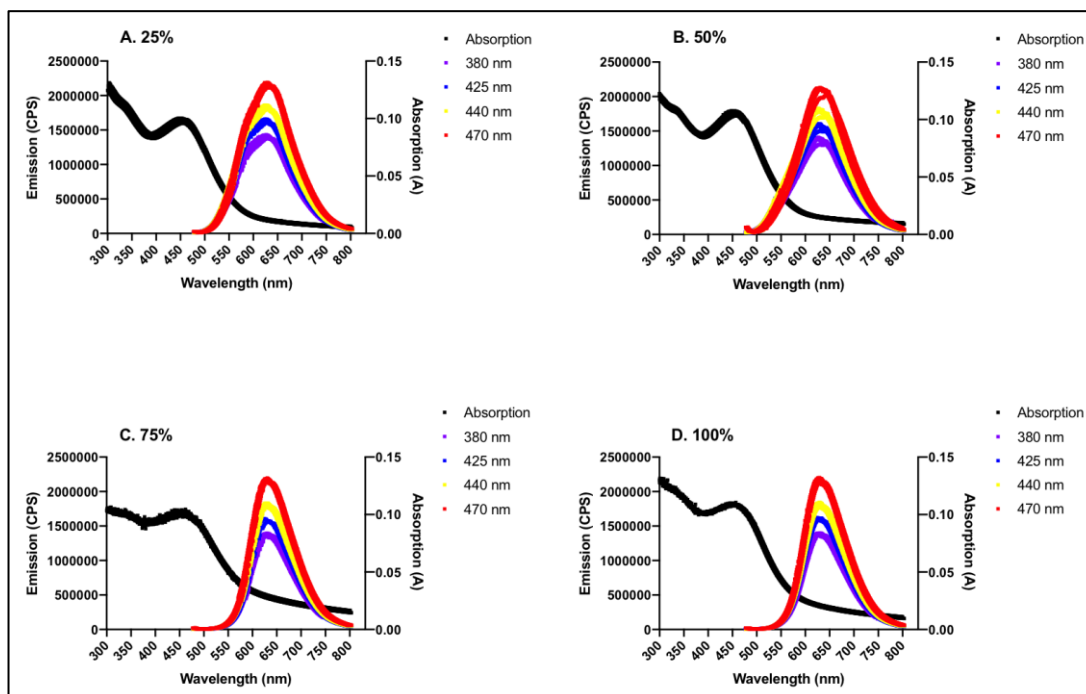


**Figure 5.7. Absorption and emission profiles for maleimide functionalised CN-PPV/PLGA-PEG NPs. A) Bare 25% maleimide functionalised NP. B) Bare 50% maleimide functionalised NP. C) Bare 75% maleimide functionalised NP. D) Bare 100% maleimide functionalised NP.** Data represents means with standard deviation of 3 independent experiments. Experiments were performed in triplicate. See 2.3.2.2 of Materials and Methods for the detailed protocol. Peak absorption occurred at an excitation wavelength of 470nm for all MNPs. Peak emission occurred at 650nm at all four excitation wavelengths tested for all MNPs. The absorption and emission spectra for all MNPs remained stable over time.

#### 5.2.1.2.4 Absorption and emission spectra for short PEG nanoparticles

The normalised absorption and emission spectra for the non-functionalised and maleimide functionalised short PEG NPs are illustrated in Figure 5.8. Peak light absorption was found at the excitation wavelength of 470nm. Emission spectra was mapped out at four different excitation wavelengths (380nm, 425nm, 440nm and 470nm) which all showed maximal peak emission around 650nm. The absorption and emission

spectra for these short PEG NPs and short PEG MNPs remained comparable over time.

These findings are similar to the non-functionalised and maleimide functionalised NPs.

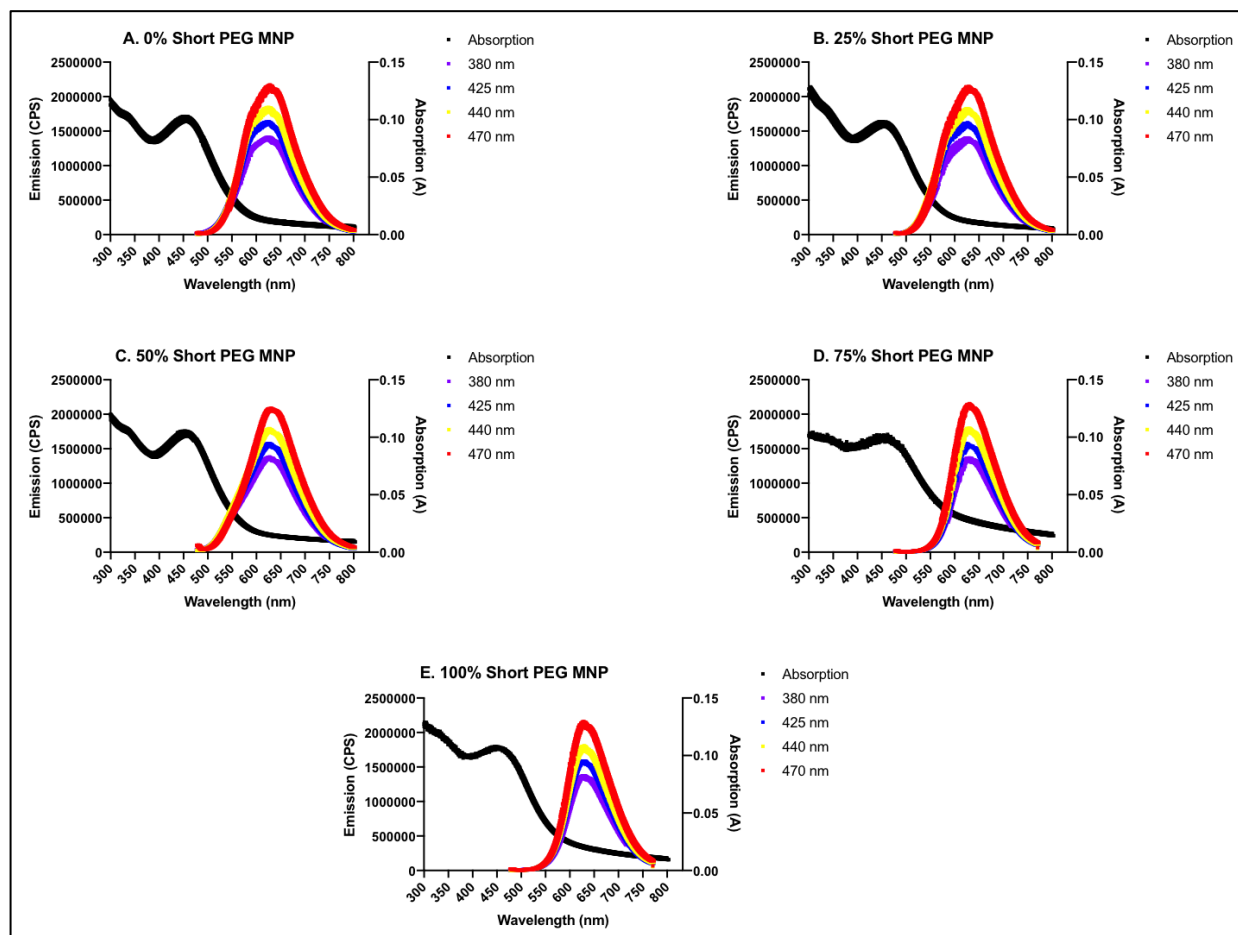
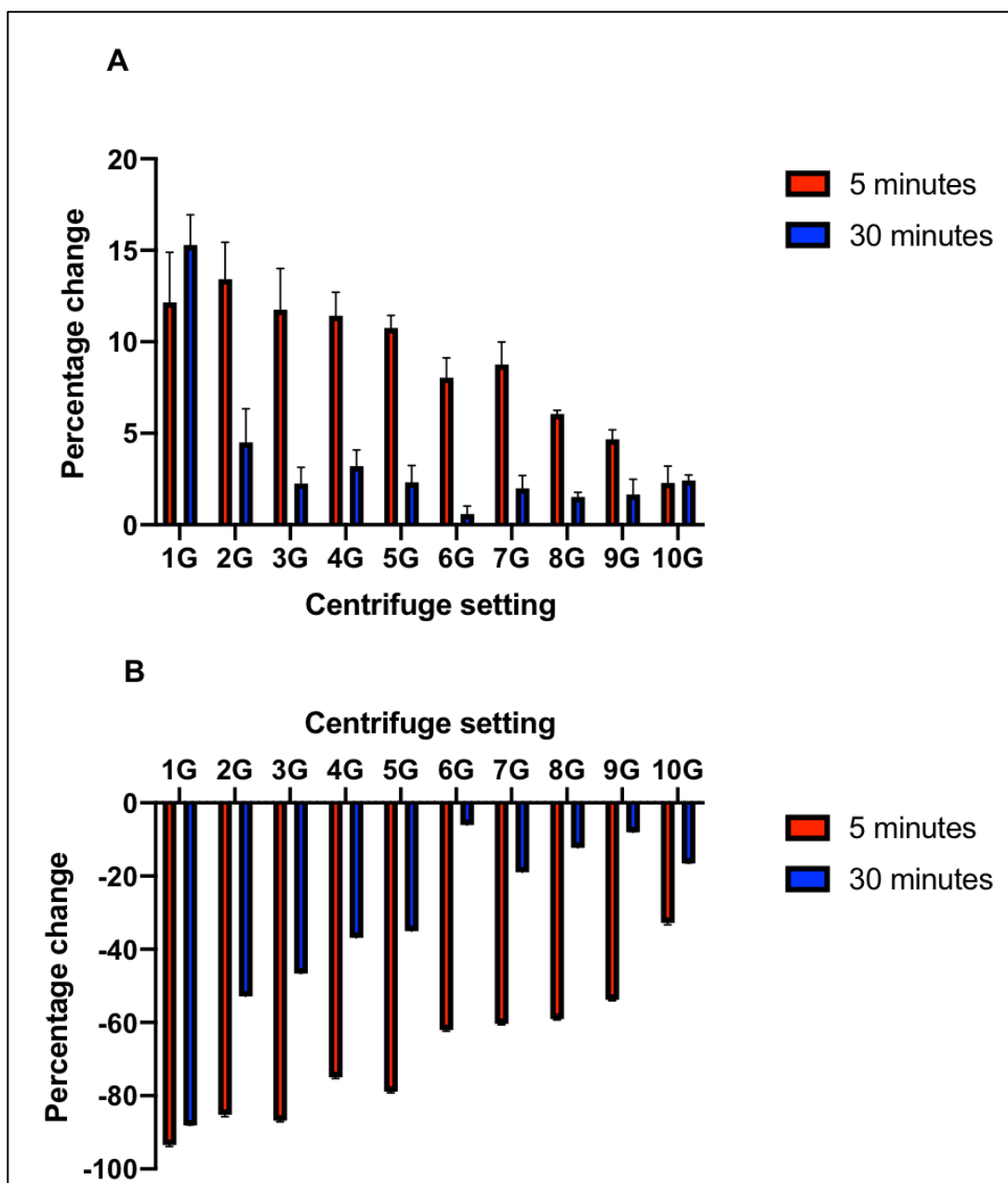


**Figure 5.8. Absorption and emission profiles for non-functionalised and maleimide functionalised short PEG CN-PPV/PLGA-PEG NPs. A)** Bare non-functionalised NP with short PEG chains. **B)** Bare 25% maleimide functionalised NP with short PEG chains. **C)** Bare 50% maleimide functionalised NP with short PEG chains. **D)** Bare 75% maleimide functionalised NP with short PEG chains. **E)** Bare 100% maleimide functionalised NP with short PEG chains. Data represents means with standard deviation of 3 independent experiments. Experiments were performed in triplicates. See 2.3.2.2 of Materials and Methods for the detailed protocol. Peak absorption occurred at an excitation wavelength of 470nm for all short PEG MNPs. Peak emission occurred at 650nm at all four excitation wavelengths tested for all short PEG MNPs. The absorption and emission spectra for 0% MNP remained stable over time for all short PEG MNPs.

### 5.2.1.3 Testing the effects of conjugation processes on nanoparticle characterisation

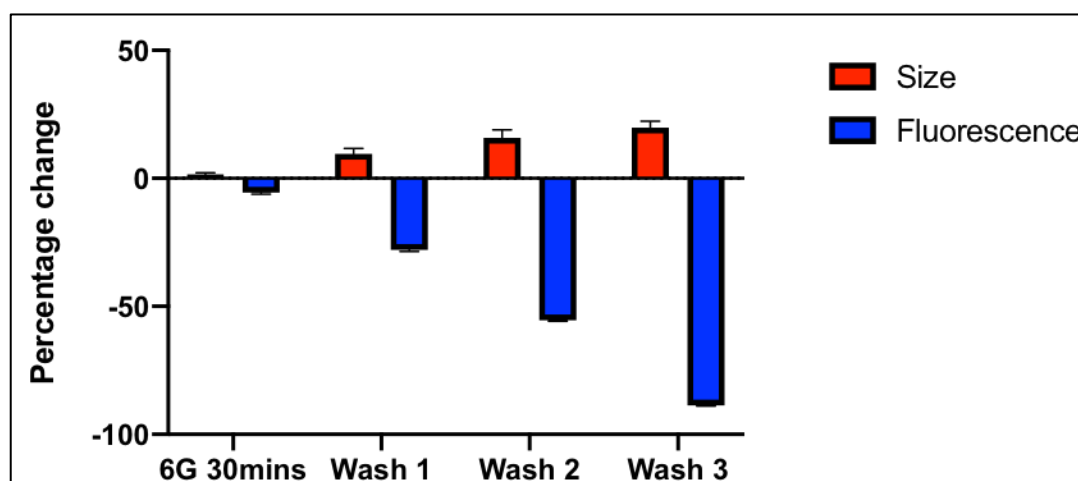
To form an efficient antibody-NP conjugate system the excess oxidised antibody must initially be removed from the solution. This procedure involves centrifuging the conjugate and it is important to determine the effects that centrifugation would have on the MNPs. The effects of different centrifuging parameters, such as G-force and time, were investigated and the results are shown in Figure 5.9.

Figure 5.9A shows that centrifuging for 5 minutes at lower centrifugal forces (2-8G) caused larger changes in the hydrodynamic diameters of the bare maleimide functionalised NPs as compared to bare maleimide functionalised NPs centrifuged for 30 minutes: 1G – 3.1% difference in hydrodynamic diameters ( $p=0.8957$ ), 2G – 8.9% ( $p<0.0001$ ), 3G – 9.5% ( $p<0.0001$ ), 4G – 8.2% ( $p<0.0001$ ), 5G – 8.4% ( $p<0.0001$ ), 6G – 7.5% ( $p<0.0001$ ), 7G – 6.8% ( $p<0.0001$ ), 8G – 4.5% ( $p=0.0178$ ), 9G – 3.0% ( $p>0.9999$ ), 10G – 0.1% ( $p>0.9999$ ). Figure 5.9B shows that centrifuging for 5 minutes decreased fluorescence emission of bare maleimide functionalised NPs more than centrifuging for 30 minutes: 1G - 5.4% reduction in fluorescent emission was observed between 5 and 30 minutes ( $p<0.0001$ ), 2G - 32.3% ( $p<0.0001$ ), 3G - 40.2% ( $p<0.0001$ ), 4G - 38.1% ( $p<0.0001$ ), 5G - 43.8% ( $p<0.0001$ ), 6G - 56.0% ( $p<0.0001$ ), 7G - 41.4% ( $p<0.0001$ ), 8G - 46.8% ( $p<0.0001$ ), 9G - 45.8% ( $p<0.0001$ ) and 10G - 16.3% ( $p<0.0001$ ).



**Figure 5.9. Effects of centrifugation on NPs** **A)** Changes in hydrodynamic diameter **B)** changes in the intensity of fluorescent emission of bare maleimide functionalised NPs. Data represents means with standard deviation of 3 independent experiments. Experiments were performed in triplicate and results are relative to non-centrifuged bare maleimide functionalised NPs control. Fluorescent excitation = 470nm and emission = 650nm). See 2.3.3 of Materials and Methods for the detailed protocol. Centrifugation of the NP increased the hydrodynamic diameter; centrifuging at 6G for 30 minutes caused the smallest increase in hydrodynamic diameter. Centrifugation of the NP reduced the emitted fluorescence; centrifuging at 6G for 30 minutes caused the smallest reduction in fluorescence emission.

Repeated wash steps as part of the protocols for synthesising antibody-conjugated NPs also involves centrifugation per wash. Therefore, the effects of repeated centrifugation at 6G per repeated wash step were investigated. Figure 5.10 shows that repeated centrifugation of MNPs after each wash step resulted in increasing hydrodynamic diameters of MNPs. 8% increase in the hydrodynamic diameter was observed after Wash 1 ( $p < 0.0001$ ), 14.3% after Wash 2 ( $p < 0.0001$ ) and 18.3% after Wash 3 ( $p < 0.0001$ ) as compared to non-centrifuged bare MNPs. Increasing reduction in fluorescent emission was also observed after each subsequent wash step; 22.3% reduction in fluorescence emission was observed after Wash 1 ( $p < 0.0001$ ), 49.8% after Wash 2 ( $p < 0.0001$ ) and 83.1% after Wash 3 ( $p < 0.0001$ ) as compared to non-centrifuged bare MNPs. It is possible that the reduction in fluorescence emission is due to the loss of NPs, and consequent dilution of NPs, during the repeated centrifugation and resuspension process.



**Figure 5.10. Effects of repeated centrifugation on hydrodynamic diameters and fluorescent emission on bare maleimide functionalised NPs.** Data represents means with standard deviation of 3 independent experiments. Experiments were performed in triplicate and results are relative to non-centrifuged bare maleimide functionalised NPs control. Fluorescent excitation = 470nm and emission = 650nm). See 2.3.3.1 of Materials and Methods for the detailed protocol. Repeated centrifugation of the NP at 6G increased the hydrodynamic diameter and reduced the emitted fluorescence.

## 5.2.2 Investigating cell viability after exposure to bare maleimide functionalised nanoparticles

Cell viability assays were performed on HEK293, EA.hy926 and LoVo cell lines after incubation with 10-fold dilutions of bare 25% maleimide functionalised NPs (for example, 1 in 10 refers to a dilution of 1ml of bare 25% maleimide functionalised NPs in 9ml of appropriate cell media, 1 in 100 refers to a dilution of 1ml of bare 25% maleimide functionalised NPs in 99ml of appropriate cell media etc) using the protocol described in 2.3.4. Cell viability measurements were taken at 24, 48 and 72 hours. Figure 5.11 shows cell viability after incubation with bare 25% maleimide functionalised NPs normalised to cell only (no MNPs) controls.

In HEK293 cells (Figure 5.11A), 26% ( $p=0.6635$ ) and 28% ( $p=0.7545$ ) reduction in cell viability (compared to cell media only) was observed at 1 in 10 MNPs (highest concentration) incubated for 24hrs and 72hrs respectively. HEK293 cell viability improved with further MNPs dilutions (1 in 100000 NPs: 3.7% ( $p>0.9999$ ) and 7.0% ( $p>0.9999$ ) reduction in cell viability (compared to cell media only) was observed at 24hrs and 72hrs respectively). In LoVo cells (Figure 5.11B), 3% ( $p>0.9999$ ) and 3% ( $p>0.9999$ ) reduction in cell viability was observed at 1 in 10 MNPs incubated for 24hrs and 72hrs respectively. In EA.hy926 cells (Figure 5.11C), 10% ( $p=0.0097$ ) and 16% ( $p<0.0001$ ) reduction in cell viability was observed at 1 in 10 MNPs incubated for 24hrs and 72hrs respectively.

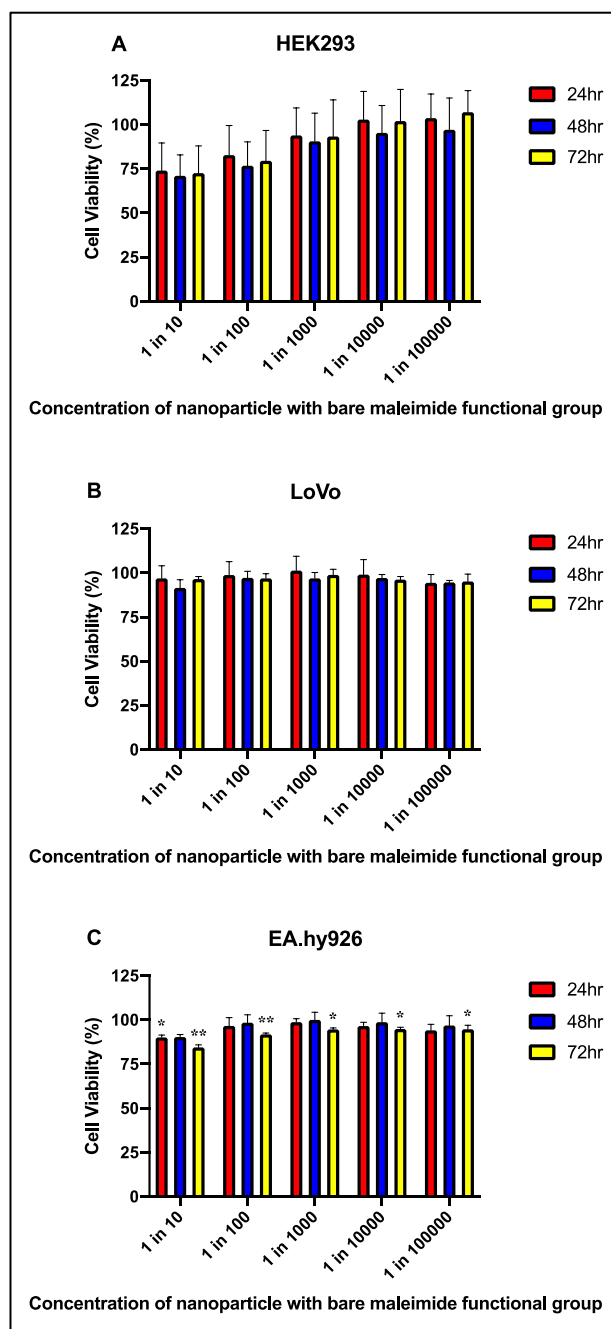


**Figure 5.11. Cell viability in cell lines after being exposed to varying concentrations of bare NPs containing the maleimide terminal group. A) HEK293 B) LoVo and C) EA.hy926 cell lines.** Data represents means with standard deviation of 3 independent experiments. Experiments were performed in triplicate.  $p < 0.05$  (\*) and  $p < 0.0005$  (\*\*). See 2.3.4 of Materials and Methods for the detailed protocol. Moderate toxicity was observed in HEK293 cells at the highest MNPs concentration (1 in 10). No major toxicities were observed in the HEK293 cell line at lower MNP concentrations. No major toxicities were observed in either the EA.hy926 and LoVo cell lines.

### 5.2.3 Non-specific binding of nanoparticles

To ensure that binding of antibody-conjugated NPs to target cells is mediated through active antibody targeting only, the non-specific binding of NPs was investigated. Bare non-functionalised and maleimide functionalised NPs were tested against HEK293, EA.hy926 and LoVo cell lines as described in 2.3.5. Figure 5.12 shows changes in fluorescent emission after cells were incubated with bare non-functionalised and maleimide functionalised NPs, as compared to cell only (no NPs) controls. No significant difference in fluorescent emission was observed in all cell lines with any dilution of the different bare non-functionalised NPs or bare maleimide functionalised NPs when compared to a media only control. 1 in 10 at **0%** MNP vs control: LoVo =  $p>0.9999$ , HEK293 =  $p>0.9999$  and EA.hy926 =  $p>0.9999$ . 1 in 10 at **100%** MNP vs control: LoVo =  $p>0.9999$ , HEK293 =  $p=0.9999$  and EA.hy926 =  $p>0.9999$ .

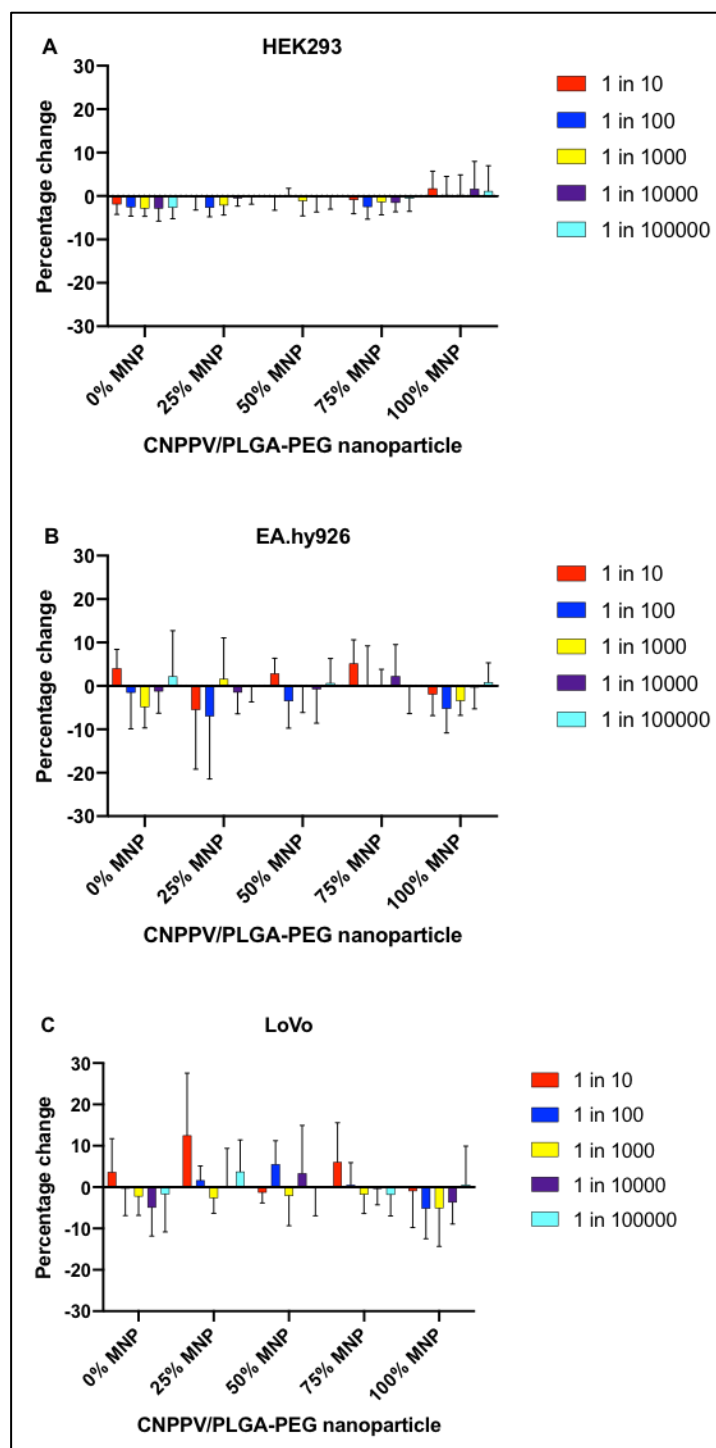


**Figure 5.12. Fluorescence in cell lines after incubation of bare non-functionalised (0% MNP) and maleimide functionalised NPs with varying concentrations of maleimide PLGA-PEG (25% MNP to 100% MNP). A) HEK293 B) EA.hy926 and C) LoVo cell lines. Data represents means with standard deviation of 8 independent experiments. See 2.3.5.1 of Materials and Methods for the detailed protocol. Non-functionalised and maleimide functionalised NPs exhibited very little non-specific binding to HEK293, LoVo and EA.hy926 cells.**

To determine whether blocking unoccupied maleimide functional groups on the NPs provided any additional benefit in reducing non-specific binding, cysteine was added as described in protocols 2.3.5. Figure 5.13 shows changes in fluorescent emission after cells were co-incubated with bare non-functionalised and maleimide functionalised NPs and maleimide-blocking cysteine, as compared to cell only (no NPs and cysteine) controls. No significant difference in fluorescent emission was seen in all cell lines incubated with any dilutions of the cysteine-blocked different bare non-functionalised NPs or bare maleimide functionalised NPs when compared to a media only control. 1 in 10 at cysteine-blocked **0%** MNP vs control: LoVo =  $p>0.9999$ , HEK293 =  $p>0.9999$  and EA.hy926 =  $p>0.9999$ . 1 in 10 at cysteine-blocked **100%** MNP vs control: LoVo =  $p>0.9999$ , HEK293 =  $p>0.9999$  and EA.hy926 =  $p>0.9999$ .

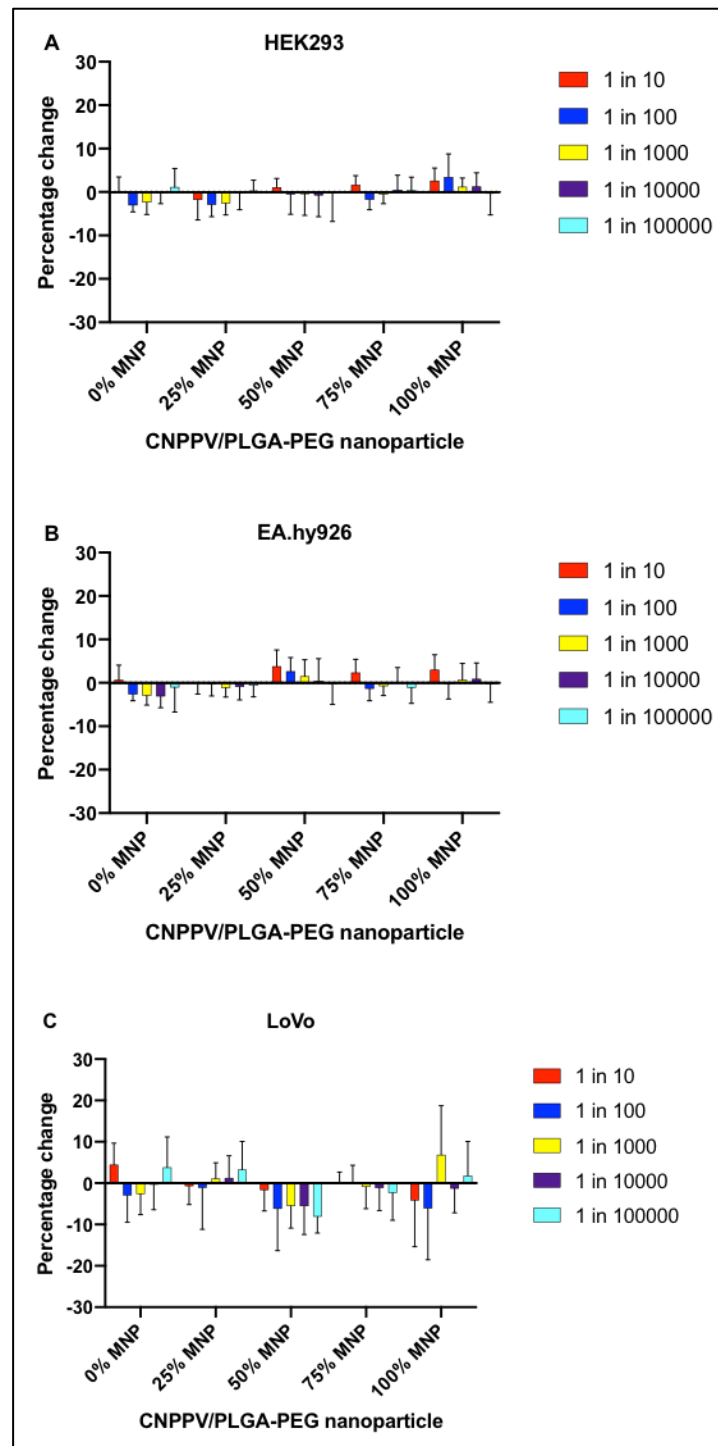


**Figure 5.13. Fluorescence in cell lines after incubation with varying concentrations of cysteine-blocked bare non-functionalised (0% MNP) and maleimide functionalised NPs with varying concentrations of maleimide PLGA-PEG (25% MNP to 100% MNP). A) HEK293 B) EA.hy926 and C) LoVo cell lines. Data represents means with standard deviation of 8 independent experiments. Experiments were performed in triplicate. See 2.3.5.1 of Materials and Methods for the detailed protocol. Cysteine-blocked non-functionalised and maleimide functionalised NPs exhibited very little non-specific binding to HEK293, LoVo and EA.hy926 cells.**

### 5.3 Discussion

The characterisation of the physical properties, specifically the stability of sizes, of both non-functionalised and maleimide functionalised NPs was conducted as part of this research project. Changes in NPs sizes over time, especially clinically-related nanomedicines, has previously been shown to influence their kinetics profiles and applications(259,260). Measurements of the hydrodynamic diameters of all NPs were recorded to highlight the physical stability of NPs and MNPs over extended periods of time. The hydrodynamic diameter of the non-functionalised NPs ranged between 103.3nm and 121.7nm. Over the course of 56 days the hydrodynamic diameter of the non-functionalised NPs remained stable in aqueous solution (Figure 5.2A). This is in concordance with previously published data regarding this self-assembling NP system. Kemal *et al.* (229) compared the hydrodynamic diameters of CN-PPV/PLGA-PEG NPs comprised of different ratios of CN-PPV to PLGA-PEG over time. The study found that the hydrodynamic diameters of NPs with varying ratios of CN-PPV:PLGA-PEG increased with increasing concentrations of PLGA-PEG in NPs. Overall diameters ranged between 110nm and 140nm. Differences in hydrodynamic diameters was primarily attributed to the 5,000Da long chain PEG. This study also compared the colloidal stability of CN-PPV-only NPs with 1:1 ratio CN-PPV/PLGA-PEG NPs by measuring the hydrodynamic diameters of both systems over 60 days. Similar to the findings in this research project, the authors found that the hydrodynamic diameters of both systems remained stable over 60 days.

As shown in Figure 5.2, the hydrodynamic diameters of the maleimide functionalised NPs remained stable over 84 days in aqueous solution. Maleimide functionalised NPs were found to be consistently larger than non-functionalised NPs and hydrodynamic diameters increased with increasing maleimide content within the NPs (Figure 5.2F). The hydrodynamic diameter of maleimide functionalised NPs ranged between 124nm and

158nm. On Day 0 (day of MNPs fabrication) the ranges of hydrodynamic diameters of maleimide functionalised NPs were:

- i. 25%: 124 – 131nm
- ii. 50%: 129 – 137nm
- iii. 75%: 130 – 140nm
- iv. 100%: 139 – 158nm

In this research project, the maleimide functionalisation of CN-PPV/PLGA-PEG NPs is a novel innovation. To date, no study has been conducted which can be used to draw comparisons on the physical properties of maleimide functionalised NPs. Following the characterisation of non-functionalised and maleimide functionalised NPs sizes over time, further experiments were conducted comparing non-functionalised and maleimide functionalised NPs. For these experiments 25% maleimide functionalised NPs (124.2nm – 130.6nm) were chosen as they were the closest in overall MNPs sizes to non-functionalised NPs (103.3nm - 121.7nm).

As discussed in 1.4.3.2, PEGylation is the most efficient strategy enabling NPs to evade MPS by inhibiting the adhesion of opsonin proteins(202,261). To achieve this, linear PEG chains block protein binding sites to shield the surfaces of NPs. The lengths and molecular weights of PEG chains that are used to block surface protein binding sites are important factors in PEGylation(197). Longer and heavier PEG chains have previously been shown to increase systemic circulation times of PEGylated NPs putatively indicating their evasion to MPS mediated elimination(262). However, excessive PEGylation can negatively affect NPs pharmacokinetics through hindering cellular uptake by interfering with the NPs ability to bind to targeted antigens(261). To highlight the influence of the length of PEG chains on NPs Pozzi *et al.*(261) conducted a study, investigating the effect of various lengths (and weights) of PEG chains in a liposomal drug delivery system. The authors compared non-PEGylated liposomes to PEGylated

liposomes functionalised with 1,000Da (short), 2,000Da (medium) and 5,000Da (long) PEG chains. The uptake of liposomes into the prostate cancer cell line, PC3, was evaluated between the four different liposomal formulations. The study found that the 1,000Da and 2,000Da PEGylated liposomes had higher cellular uptake as compared to non-PEGylated liposomes. The heaviest (5,000Da) PEGylated liposomes were found to have the lowest cellular uptake of all four liposomal formulations. The study also investigated the degree of protein binding to the surface of liposomes, and found that moderate PEGylation on the 2,000Da PEGylated liposomes provided the most effective shielding from protein adsorption. Therefore, in this project, to further enhance the binding to targeting moieties and reduce protein adsorption, a lighter and shorter PLGA-PEG (PEG 2,000Da) was used to create maleimide functionalised PLGA-PEG NPs. Figure 5.3 demonstrates that the hydrodynamic diameters of lighter and shorter PEG non-functionalised and maleimide functionalised NPs followed a similar trend in stability in sizes, as compared to their heavier and longer PEG counterparts. Overall, maleimide functionalised NPs remained heavier than non-functionalised NPs.

The ultimate application of the CN-PPV/PLGA-PEG NPs being investigated in this research project is optical medical imaging via fluorescent diagnosis. Characterising the light absorption and emission profiles of NPs is important to define their excitation and emission parameters during clinical application(74). The absorption and emission spectra profiles for both non-functionalised and maleimide functionalised NPs were found to be similar (Figure 5.6 and Figure 5.7). Both have peak absorption at 470nm which is optimal for clinical application(69,213,223). When excited at 470nm, both exhibit bright fluorescence at 650nm. Although this is not considered to be within the NIR, the emission of non-functionalised and maleimide functionalised NPs is within the deep-red region of the spectrum and is an emission wavelength that can be detected with existing laparoscopic equipment therefore this NP system represents good potential probes for fluorescence-guided surgery. An additional three excitation wavelengths were also

chosen to map out the emission spectra of NPs and MNPs. Endoscopic multispectral fluorescence camera system technologies such as the KARL STORZ D-Light P System and The Stryker ENV System, are commonly used in clinics as imaging platforms to assist in fluorescence-guided surgery and fluorescence angiography(83,263,264). These imaging platforms typically emit fluorescent light between 380nm and 440nm with peak at 425nm. Therefore, these three excitation wavelengths (380nm, 425nm and 440nm) were chosen in addition to the optimum excitation wavelength for the CN-PPV/PLGA-PEG NPs and MNPs, which is 470nm (Figure 5.6). Similar to the emission profile at 470nm excitation, the fluorescent emission profiles at the three additional wavelengths showed peaks in the near-infrared range positively indicating the suitability of the CN-PPV/PLGA-PEG NPs and MNPs with existing surgical and clinical imaging platforms.

As described earlier, multiple washing steps is performed as part of the protocols developed for creating antibody-conjugated NPs. Changes in the hydrodynamic diameters and fluorescence emission of NPs subjected to centrifuging has previously been reported in the literature(265–268). Biswas *et al.*(265) found that increasing the length of time that colloidal silicon NPs are subjected to centrifugation resulted in diminishing intensity of luminescence from NPs. The colour of luminescent emission also changed from white to blue/green. The authors also found that the sizes of silicon NPs reduced in correlation with the length of times under centrifugation. Another study investigating the effects of centrifugation on tin NPs found that increasing centrifugal force from 6,000g to 12,000g resulted in increasing agglomeration of NPs(266). Similar to this research project, Kemal *et al.*(229) investigated CN-PPV based semi-conducting NPs and found that low centrifugal forces caused irreversible aggregation of NPs. La Spina *et al.*(267) investigated the influence of repeated centrifugation on the surface chemistry of gold NPs. Centrifugation is used as a method for extracting sodium citrate, a stabilising agent used during the manufacturing of gold NPs. Sodium citrate impedes functionalisation of gold NPs. This study found that although the amounts of sodium

citrate had substantially reduced after three wash cycles (involving centrifugation), NPs had aggregated after the third wash. The authors also found decreasing intensity in near-infrared light absorbance of gold NPs with each subsequent centrifugation/wash cycle. Shi *et al.*(268) investigated the effect of repeated centrifugation on fluorescence emission of gold nanorods. Gold nanorods were centrifuged from 5,500g to 8,500g up to three times, and the authors found a reduction in the longitudinal peak wavelength of emission, i.e. a blue-shift. The shortening of the longitudinal peak wavelength of emission correlated with the number of centrifugation cycles and with increasing centrifugal forces.

To investigate the effects of centrifugation on our MNPs, they were subjected to a range of centrifugal forces ranging from 1,000g to 10,000g. The highest centrifugal force of 10,000g is used for the modification and extraction of excess antibodies. Therefore, this was the highest centrifugal force that the MNPs would be subjected to. Figure 5.9 shows that centrifugation induced changes in the hydrodynamic diameters and fluorescence emission (Excitation: 470nm) in maleimide functionalised NPs. It also demonstrates that the percentage change in these characteristics was dependent on time under centrifugation and the centrifugal force applied. Using these findings, it was decided that the MNPs would be centrifuged at 6,000g for 30 minutes when required during the conjugation process, as these settings yielded the smallest changes in size and fluorescent emission. Figure 5.10 demonstrates that repeated centrifugation also impacts the hydrodynamic diameter and emitted fluorescence of the bare maleimide functionalised NP. With each subsequent centrifugation the changes in size and fluorescence intensity got larger. Hence, it was decided not to perform serial wash steps after centrifuging MNPs at 6,000g for 30 minutes.

The biotoxicity of MNPs was investigated in different cell lines. Fluorescent NPs with specific medical imaging properties are designed with intent to be used as diagnostic agents. Adverse cytotoxicities induced by these NPs could ultimately lead to their failure during clinical trials with them being deemed unsafe for patient use(110,133,197,213). To investigate the cytotoxicities, MNPs were incubated with cells and cell viability was analysed. Moderate toxicity was observed in HEK293 cells at the highest MNPs concentration (1 in 10). However, cell viability improved with at lower MNPs concentrations. No major toxicities was observed in either EA.hy926 and LoVo cell lines (Figure 5.11). The findings from these results suggest that different cell lines have different levels of sensitivity to maleimide functionalised NPs. The optimal concentration of MNPs will need to be deduced which would yield the highest intracellular accumulation of MNPs and have negligible effects on cell viability.

Non-specific binding and non-specific interactions between cells and PEGylated NPs have been previously been shown in the literature. A study by Vigor *et al.* used active CEA targeting of superparamagnetic iron oxide NPs to improve MRI imaging of CEA-positive colorectal cancer cells. The authors found higher non-specific binding of NPs to control CEA-negative cell line, A375M (melanoma cell line) as compared to the LS174T CEA-positive cell line(157). This non-specific binding was also present with their bare unblocked NPs meaning that non-specific binding was not exclusively due to the targeting moiety used. The study also suggested that non-specific binding could be related to the negative surface charge of NPs produced by using negatively charged carboxylated PEG for conjugation purposes. Another study by Zhang *et al.*(269) found that by modifying their magnetite NPs by PEGylation reduced uptake into macrophage cells (part of the MPS) but also increased the non-targeted intracellular uptake of the NP into human breast cancer BT20 cells. They speculated that this increased uptake is due to the high solubility of PEG in the lipid bilayer of the cell surface membrane. In this research project, it was found that both bare (unblocked) and cysteine-blocked variants

of non-functionalised and maleimide functionalised NPs exhibited very little non-specific binding to HEK293, LoVo and EA.hy926 cells (Figure 5.12 and 5.13).

In summary, the semiconducting organic polymer CN-PPV NPs is an ideal fluorescent probe to assist in fluorescent diagnosis and imaging. As shown in this chapter, the peak intensity of fluorescent emission of both non-functionalised and maleimide functionalised NPs is around 650nm. In addition, maximum light absorption occurs in the blue-violet range (<500nm) conferring a wide Stokes shift, meaning there is clear separation between their maximal absorption and emission peaks. The blue-violet excitation range is currently achievable with commercially available laparoscopic equipment making the NP system compatible with existing surgical imaging platform. The non-functionalised and maleimide functionalised NPs have also exhibited physical stability over time in an aqueous solution and negligible adverse cytotoxic effects.

## **Chapter Six**

# **Conjugation and binding assays**

## 6 Conjugation and binding assays

### 6.1 Introduction

Active targeting, by conjugating tumour-specific targeting agents to nanomedicines, can improve the binding and uptake into tumours by (118,192). Antibodies have been extensively investigated and used in multiple studies as targeting agents for conjugation to NPs to improve delivery (150,166–168,270). Affimers are emerging as alternative targeting agents to antibodies, given their potential advantages (144,172). The increased cell membrane expression of the carcinoembryonic antigen (CEA) has been identified as an ideal antigen for targeting colorectal cancers(143). Therefore, for this research project a monoclonal IgG anti-CEA antibody and an anti-CEA affimer were selected as potential targeting agents for conjugation to CN-PPV/PLGA-PEG fluorescent NPs.

Conjugation of antibodies to NPs requires the availability of free functional groups to facilitate the conjugation process. PEG does not have functional groups to facilitate conjugation. One way this can be achieved is by using functionalised PEG that possesses free terminal groups, such as amine, carboxyl or maleimide. These functional groups allow multiple immunoglobulin antibody molecules to bind to a single NP, thereby increasing the binding affinity of NP-conjugates to target tumours(192,271). The 'cysteine-maleimide' reaction is a strong and reliable covalent bond, which has previously been investigated in pharmaceutical applications, specifically in developing antibody-drug conjugates(233). To this end, the CN-PPV/PLGA-PEG fluorescent NP was fabricated with maleimide terminal groups for conjugation to targeting agents via 'cysteine-maleimide' mediated bonding.

It was proposed that reducing the disulphide bonds in antibodies could make free cysteine groups available for binding(155,233). However, as discussed in 4.3, it became apparent that this was not a practical solution and an alternative pathway for conjugation of antibody to MNP was investigated. Oxidation of the antibody's glycoprotein side chain (specifically sialic acid) generates a reactive aldehyde group which interacts with hydrazide groups to form stable hydrazone bonds. This enables the possibility of conjugating the antibody through the glycoprotein side chain to the MNP via a crosslinker(233).

3-[2-pyridyldithio]propionyl hydrazide (PDPH) is a heterobifunctional crosslinker containing sulfhydryl-reactive pyridyldithiol and aldehyde-reactive hydrazide functional groups at either end of the molecule(272) (Figure 6.1). In the presence of maleimide, the pyridine-2-thione moiety in the sulfhydryl-reactive pyridyldithiol group is displaced allowing conjugation of maleimide to the heterobifunctional crosslinker. Through this reaction, PDPH is a suitable crosslinker between the reactive aldehyde group on the oxidised glycoprotein side chain of the antibody and maleimide terminal group on the NP.

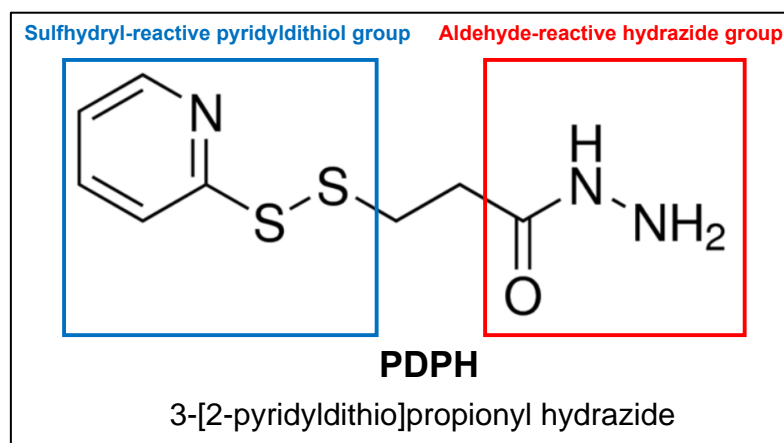


**Figure 6.1. Chemical structure of heterobifunctional 3-(2-Pyridyldithio)propionyl hydrazide (PDPH) crosslinker(273).** PDPH is a heterobifunctional crosslinker which contains a sulfhydryl-reactive pyridyldithiol group and an aldehyde-reactive hydrazide group. This crosslinker allows conjugation of glycoproteins to sulfhydryl-containing peptides or proteins.

## 6.2 Results

### 6.2.1 Conjugation of target (anti-CEA) antibody to heterobifunctional crosslinker

To demonstrate the conjugation of target (anti-CEA) antibody to the PDPH heterobifunctional crosslinker immunofluorescence was performed as described in 2.4.1.1. As shown in Figure 6.2, green fluorescence was observed when LoVo cells (target cell line for the anti-CEA antibody) were incubated with the anti-CEA antibody – DyLight™ dye labelled PDPH crosslinker conjugate. No fluorescence was observed when LoVo cells were incubated with the anti-CEA antibody alone. Green fluorescence was also observed when HEK293 and EA.hy926 cells were incubated with the anti-CEA antibody – DyLight™ dye labelled PDPH crosslinker conjugate, suggesting that the target antibody-dye conjugate was also binding to the two control cell lines.

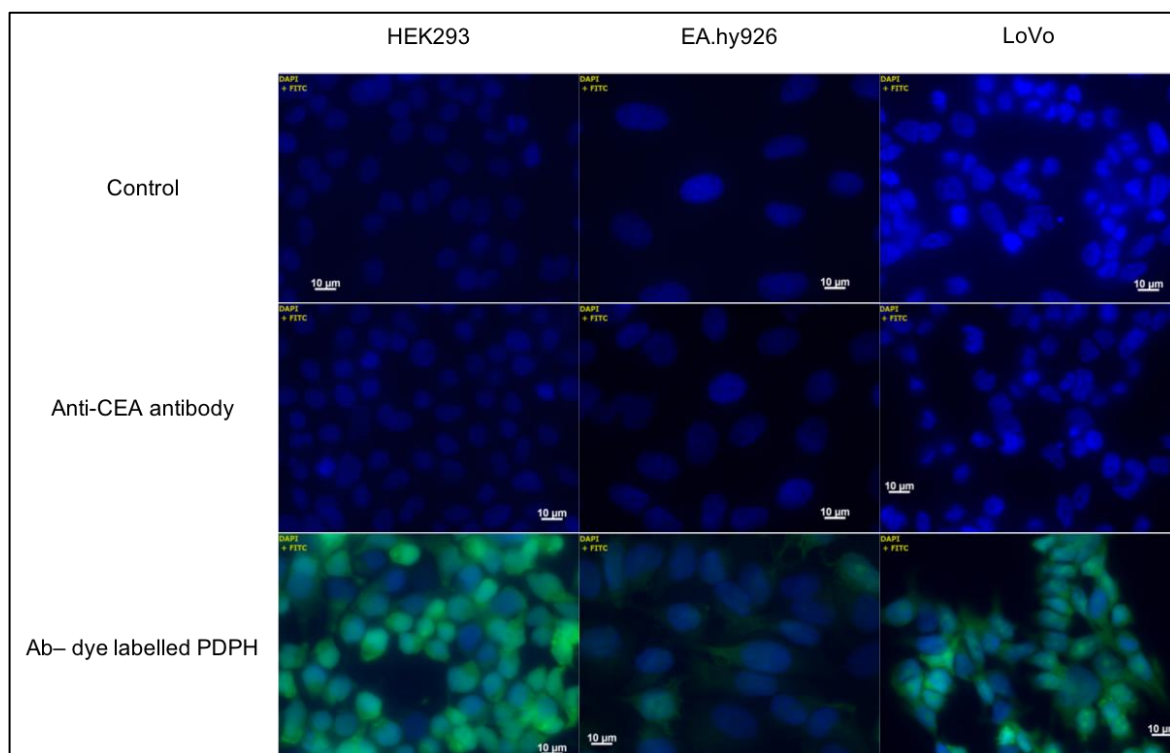


**Figure 6.2. Binding of target antibody and target antibody - dye labelled PDPH heterobifunctional crosslinker on target and control cell lines using immunofluorescence on fixed cells.** Blue fluorescence is DAPI. Green fluorescence is DyLight™ 488 using FITC filter. Magnification x63. Scalebar = 10  $\mu$ m. 0.5% skimmed milk blocking and unconjugated oxidised antibody served as controls. Due to the presence of the fluorescent DyLight 488 molecules, a secondary fluorescent antibody was not needed for experiments. Images in this figure are representative of at least 3 independent experiments. See 2.4.1.1 of Materials and Methods for the detailed protocol. The presence of green fluorescence in target (LoVo) and both control (EA.hy926 and HEK293) cell lines incubated with anti-CEA antibody–dye labelled PDPH conjugates suggests non-specific binding of conjugates to cells.

This experiment was repeated using bovine serum albumin as the blocking agent as described in 2.4.1.2. As shown in Figure 6.3, green fluorescence was observed when LoVo cells were incubated with the anti-CEA antibody – DyLight™ dye labelled PDPH crosslinker conjugate. No fluorescence was observed when LoVo cells were incubated with the anti-CEA antibody alone. Green fluorescence was seen when HEK293 and EA.hy926 cells were incubated with the anti-CEA antibody – DyLight™ dye labelled PDPH crosslinker conjugate. The results shown in Figure 6.2 and Figure 6.3 could represent non-specific binding of the target antibody-dye conjugate.

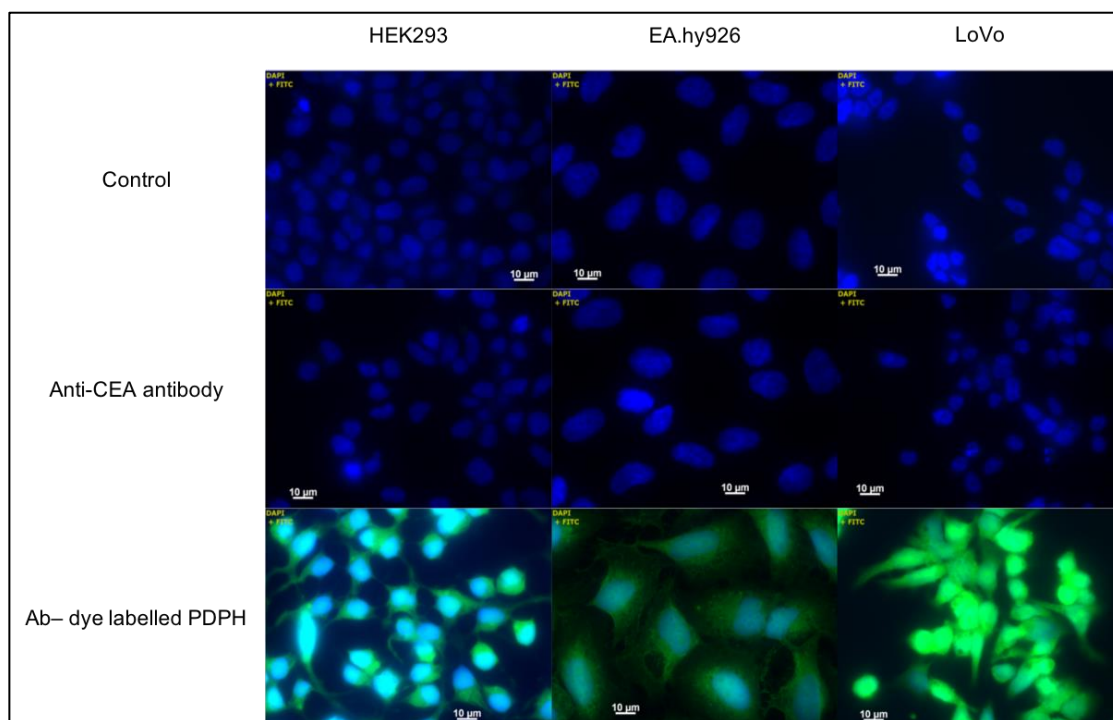


**Figure 6.3. Binding of target antibody and target antibody - dye labelled PDPH crosslinker on target and control cell lines using BSA blocking protocol on fixed cells.** Blue fluorescence is DAPI. Green fluorescence is DyLight™ 488 using FITC filter. Magnification x63. Scalebar = 10 μm. 0.1% bovine serum albumin and unconjugated oxidised antibody served as controls. Due to the presence of the fluorescent DyLight 488 molecules, a secondary fluorescent antibody was not needed for experiments. Images in this figure are representative of at least 3 independent experiments. See 2.4.1.2 of Materials and Methods for the detailed protocol. The presence of green fluorescence in target (LoVo) and both control (EA.hy926 and HEK293) cell lines incubated with anti-CEA antibody–dye labelled PDPH conjugates suggests non-specific binding of conjugates to cells despite blocking with BSA.

To identify the cause of non-specific binding seen in Figure 6.2 and Figure 6.3, the individual components of the anti-CEA antibody – dye labelled PDPH heterobifunctional crosslinker were investigated as described in protocol 2.4.1.3. Figure 6.4 shows that no green fluorescence was observed when LoVo, HEK293 or EA.hy926 cells were incubated with the oxidised anti-CEA antibody or the heterobifunctional crosslinker.

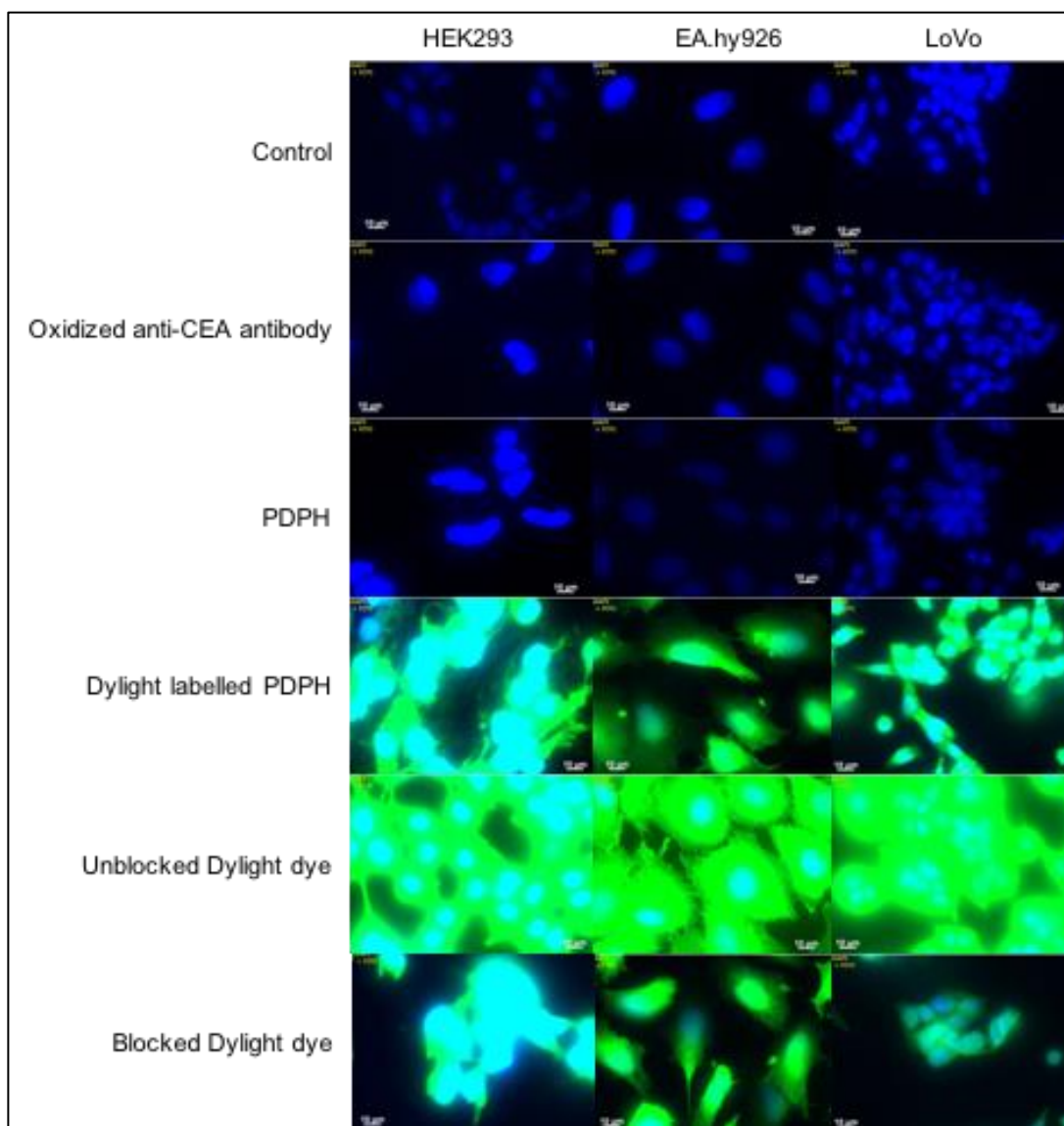


**Figure 6.4. Binding of different components of DyLight dye labelled anti-CEA antibody – PDPH heterobifunctional crosslinker conjugate on target and control cell lines using immunofluorescence on fixed cells.** Blue fluorescence is DAPI. Green fluorescence is DyLight™ 488 using FITC filter. Magnification x63. Scalebar = 10  $\mu$ m. 0.1% bovine serum albumin blocking, unconjugated oxidised antibody and unmodified PDPH served as controls. Due to the presence of the fluorescent DyLight 488 molecules, a secondary fluorescent antibody was not needed for experiments. Images in this figure are representative of at least 3 independent experiments. See 2.4.1.3 of Materials and Methods for the detailed protocol. Green fluorescence is seen on both the target and control cell lines in the presence of DyLight™ 488 Maleimide dye, even when the maleimide functional group is blocked by PDPH or cysteine. No green fluorescence is seen with the oxidised anti-CEA antibody or PDPH.

Green fluorescence in all three cell lines was observed when cells were incubated with the unblocked DyLight™ dye. Substantial fluorescence was also observed when all three

cell lines were incubated with the blocked DyLight™ dye and dye labelled PDPH. This could suggest that the DyLight™ 488 Maleimide dye is responsible for the non-specific binding of the target antibody-dye conjugate observed in Figure 6.2 and Figure 6.3.

## **6.2.2 Conjugation of antibody to maleimide functionalised nanoparticle using heterobifunctional crosslinker**

### **6.2.2.1 Conjugating heterobifunctional crosslinker to maleimide functionalised nanoparticles**

A binding assay was conducted as per 2.4.2.1 to determine the optimal length of incubation time to conjugate maleimide functionalised NPs to the heterobifunctional linker, PDPH (Figure 6.5). Target antibody-NP conjugates were incubated with the target cell line and fluorescence quantified, using bare maleimide functionalised NPs (MNP) as an additional control.

A significant difference in the fluorescence compared to cell media only treated cells was observed when the heterobifunctional crosslinker was incubated with the bare 25% maleimide functionalised NP for 30 minutes; 12% increase in fluorescence ( $p=0.0048$ ). No significant difference in fluorescence intensities were seen at 1 hour and 2 hours with 6% ( $p=0.3839$ ) and 7% ( $p=0.1868$ ) increase in fluorescence intensities respectively. The results shown in Figure 6.5 suggest that the optimal time for conjugation between the bare 25% maleimide functionalised NP and PDPH was 30 minutes and therefore this was used in all subsequent experiments.

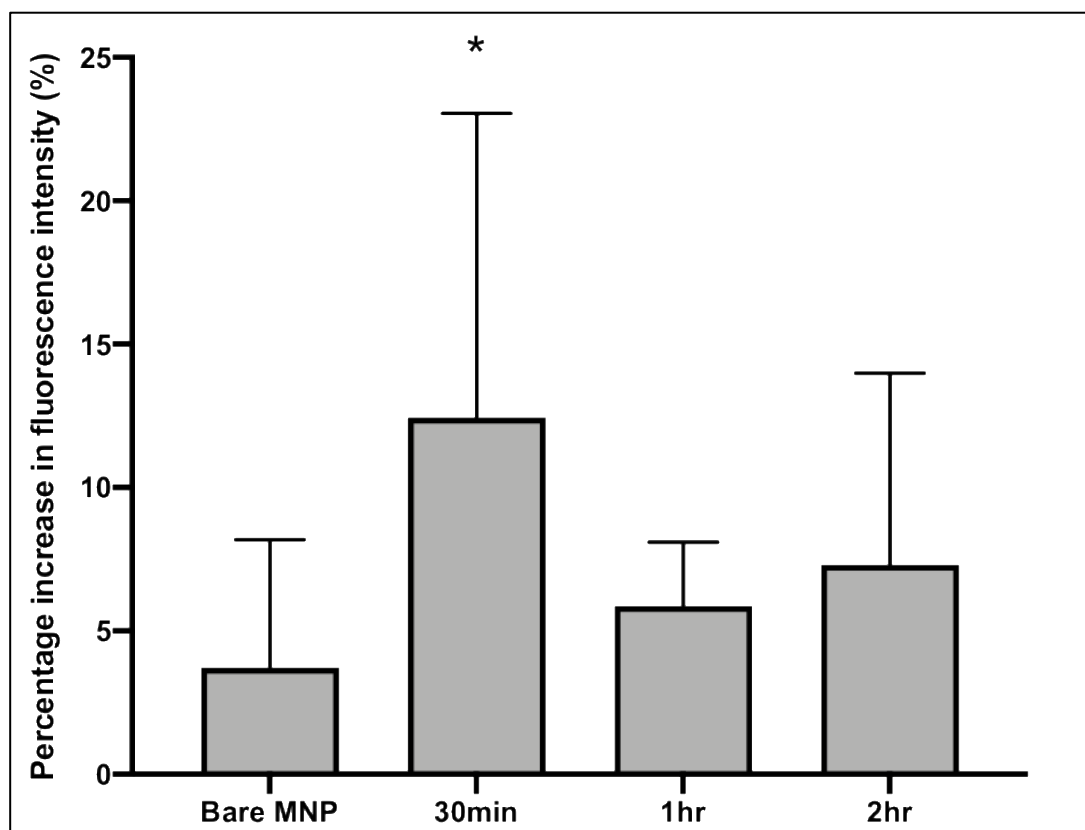


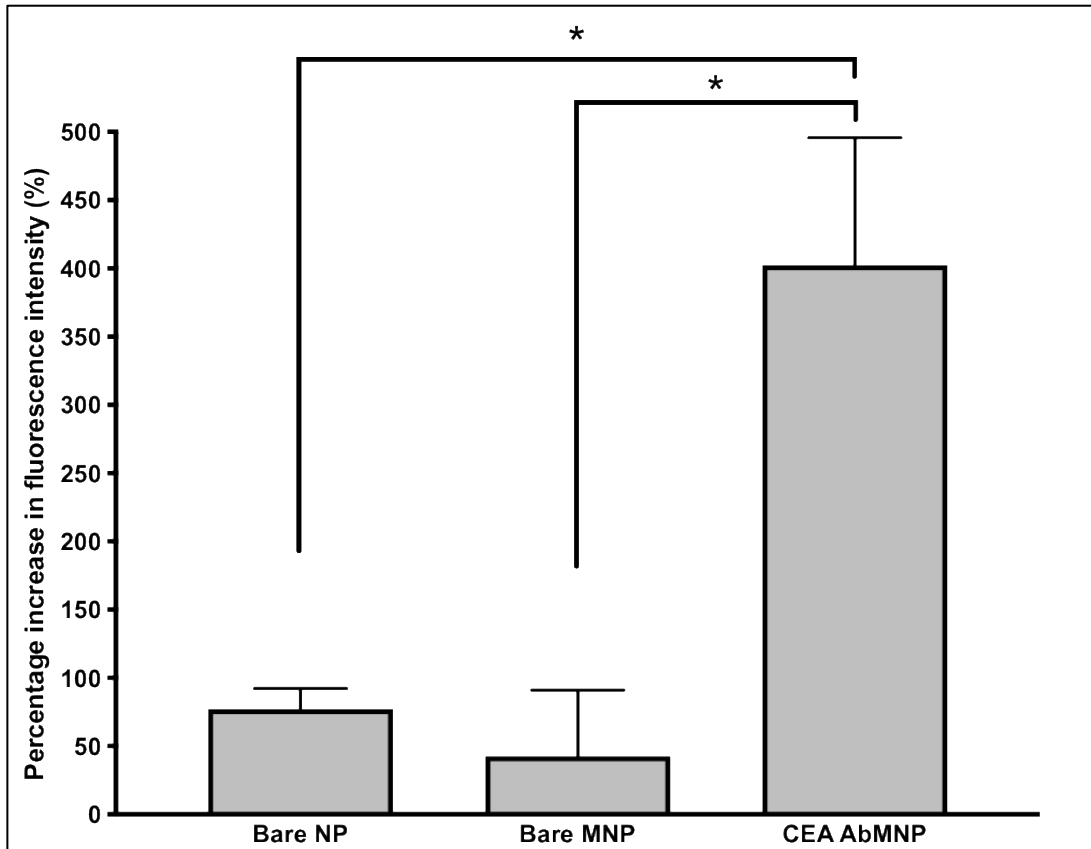
**Figure 6.5. Assessment of optimal incubation time for conjugation of maleimide functionalised NP (MNP) to heterobifunctional crosslinker.** Results represent mean values of at least 3 independent experiments with SD. Experiments were performed in triplicate. Statistically significant difference of fluorescence normalised to cell media only treated cells was considered at  $p < 0.05$  (\*). See 2.4.2.1 of Materials and Methods for the detailed protocol. A significant increase in the fluorescence intensity was observed when MNP was incubated with the heterobifunctional crosslinker for 30 minutes.

### 6.2.2.2 Testing anti-CEA antibody – nanoparticle conjugate against

#### LoVo cell line

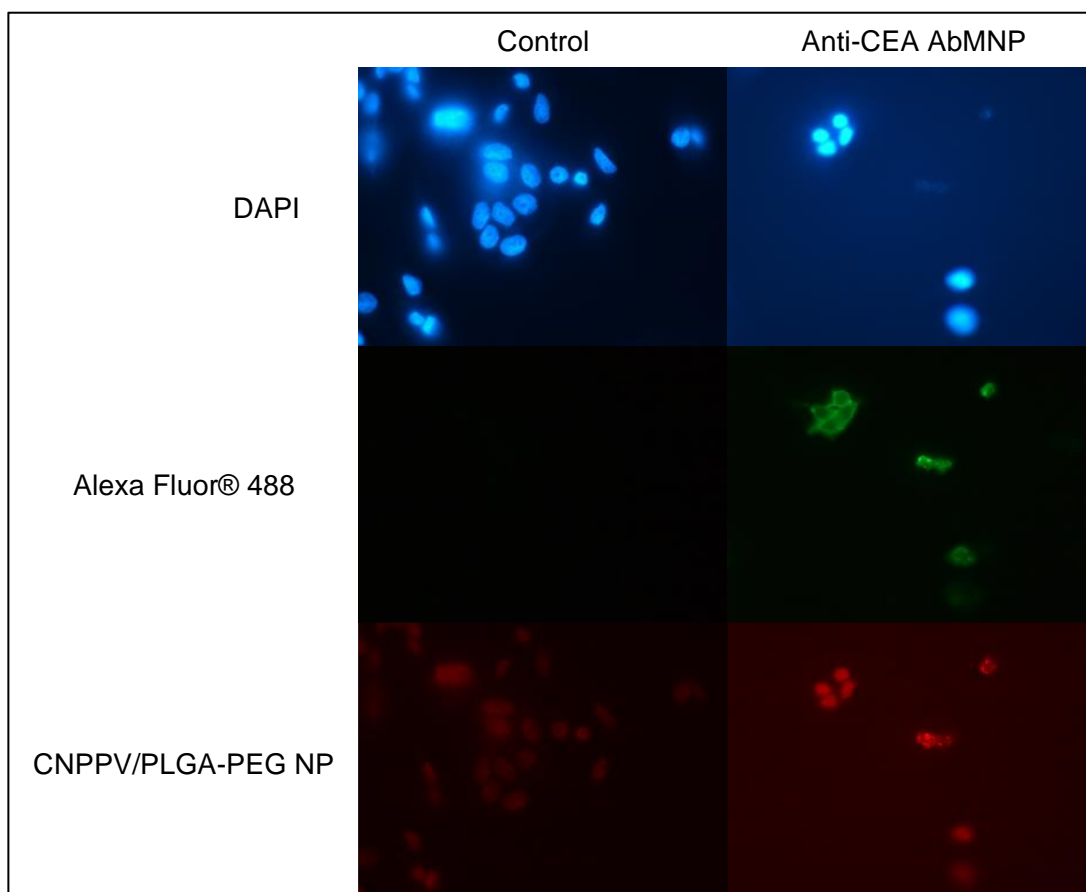
In order to confirm conjugation of the antibody to the maleimide functionalised NP, a binding assay and an immunofluorescence study on the target (LoVo) cell line were performed as described in 2.4.2.2. A 1 in 100 dilution of anti-CEA antibody-NP conjugate was chosen as this concentration of bare maleimide functionalised NP was the highest that also yielded minimal cytotoxicity (Figure 5.10).

Figure 6.6 shows that a 402% increase in fluorescence was observed when anti-CEA antibody-NP conjugates were incubated with LoVo cells, as compared to cell media only treated cells ( $p < 0.0001$ ). 77% ( $p = 0.6837$ ) and 42% ( $p > 0.9999$ ) increase in fluorescence was observed when bare non-functionalised and bare 25% maleimide functionalised NPs respectively were incubated with LoVo cells as compared to cell media only treated cells. This shows that there was a higher degree of binding of target antibody-NP conjugates to LoVo cells in comparison to bare NPs and bare MNPs. Comparing the different variants of NPs, a 325% increase in fluorescence was observed in target antibody-NP conjugates as compared to bare non-functionalised NPs ( $p = 0.0004$ ). A 360% increase in fluorescence was observed in target antibody-NP conjugates as compared to bare 25% maleimide functionalised NPs ( $p = 0.0002$ ) (Figure 6.6).



**Figure 6.6. Assessment of binding of bare NPs and antibody-NP conjugate (AbMNP) to LoVo cells.** Results represent mean values of at least 3 independent experiments with SD. Experiments were performed in triplicate. Statistically significant difference of fluorescence normalised to cell media only treated cells was considered at  $p < 0.05$  (\*). See 2.4.2.2 of Materials and Methods for the detailed protocol. A significant increase in the fluorescence intensity is seen when the target antibody-NP conjugate is incubated with LoVo cells compared to bare non-functionalised NPs and bare maleimide functionalised NPs.

Figure 6.7 shows that green fluorescence was observed when LoVo cells were incubated with target antibody–NP conjugates. Red fluorescence from CN-PPV/PLGA-PEG antibody-NP conjugates was also similarly observed in target LoVo cells. Taken together, this indicates successful binding of the target antibody to CN-PPV/PLGA-PEG MNPs and successful binding of target antibody-NP conjugates to the target cell line, supporting the findings in Figure 6.6.



**Figure 6.7. Binding of target antibody-NP conjugate (Anti-CEA AbMNP) on target cell line using immunofluorescence on fixed cells.** Blue fluorescence is DAPI using DAPI filter. Green fluorescence is Alexa Fluor® 488 secondary antibody using FITC filter. Red fluorescence is CN-PPV NP using 5-ALA filter. Magnification x63. Scalebar = 10  $\mu\text{m}$ . 0.5% skimmed milk blocking served as control. Images in this figure are representative of at least 3 independent experiments. See 2.4.2.2 of Materials and Methods for the detailed protocol. Green and red fluorescence is observed when the target antibody-NP conjugate is incubated with LoVo cells indicating successful conjugation of antibody to MNP.

### 6.2.2.3 Testing target and control antibody – nanoparticle conjugates against target and control cell lines

The binding abilities of both the target and control antibody-NP conjugates (CEA AbMNP and CD31 AbMNP respectively) against LoVo, HEK293 and EA.hy926 cell lines was investigated. The protocol used is described in 2.4.2.3.

Figure 6.8 shows that a 16% increase in fluorescence intensity was observed when target antibody-NP conjugates were incubated with the target cell line (anti-CEA antibody-NP conjugate against LoVo cell line) ( $p < 0.0001$ ). However, a 17% ( $p < 0.0001$ ) and 20% ( $p < 0.0001$ ) increase in fluorescence intensities were also observed when target antibody-NP conjugates were incubated with HEK293 and EA.hy926 control cell lines. An increase in fluorescence intensities was also observed when control antibody-NP conjugates were incubated with all three cell lines. *HEK293*: 18% ( $p < 0.0001$ ), *EA.hy926*: 17% ( $p < 0.0001$ ) and *LoVo*: 15% ( $p < 0.0001$ ).

No significant differences in fluorescence was observed between the binding of target antibody-NP conjugates and control antibody-NP conjugates on all three cell lines. *HEK293*: 1% difference in fluorescence ( $p = 0.9995$ ), *EA.hy926*: 2% ( $p = 0.8088$ ) and *LoVo*: 2% ( $p = 0.9208$ ). Figure 6.8 also shows a decrease in fluorescence when the two control cell lines were incubated with the bare 25% maleimide functionalised NP. *HEK293*: 9% ( $p = 0.0081$ ) and *EA.hy926*: 18% ( $p < 0.0001$ ). The anti-CEA antibody used to develop the target antibody-NP conjugates should preferentially bind to the CEA-positive LoVo cell line more than the control cell lines. However, no significant difference in fluorescence was found between LoVo and control cell lines when incubated with target antibody-NP conjugates. *HEK293* vs. *LoVo*: 1% ( $p > 0.9999$ ) and *EA.hy926* vs. *LoVo*: 4% ( $p = 0.4699$ ).

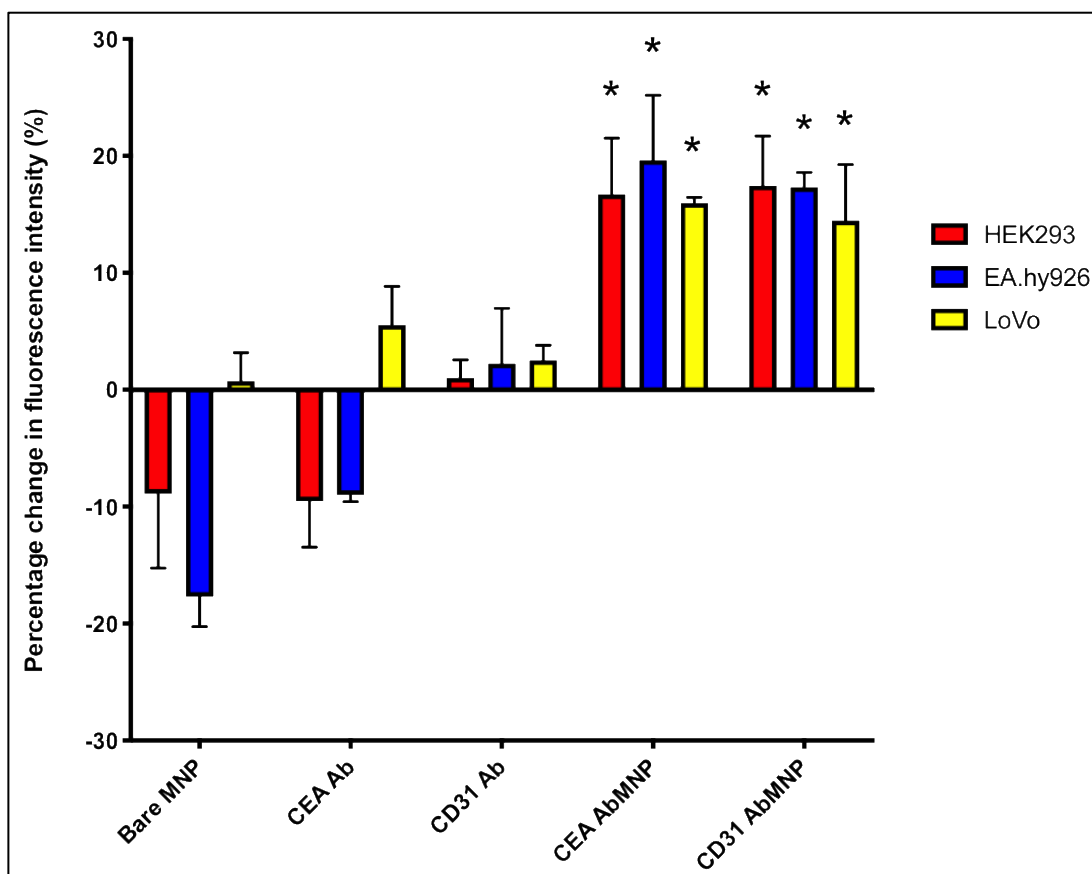


**Figure 6.8. Binding of target and control antibody-NP conjugates (AbMNP) against target and control cell lines.** Results represent mean values of at least 3 independent experiments with SD. Experiments were performed in triplicate. Statistically significant difference of fluorescence normalised to cell media only treated cells was considered at  $p < 0.0001$  (\*). See 2.4.2.3 of Materials and Methods for the detailed protocol. Significant increases in fluorescence intensity are seen with both the target and control antibody-NP conjugates to all cell lines indicating non-specific binding.

Figure 6.9 shows that green DyLight 448 fluorescence was observed when the target cell line, LoVo, was incubated with target (anti-CEA) antibody-NP conjugates. Red CN-PPV/PLGA-PEG NP fluorescence was also seen in anti-CEA AbMNP incubated LoVo cells. No green DyLight 448 fluorescence was observed when the target cell line was incubated with control (anti-CD31) antibody-NP conjugates. However, red fluorescence from CN-PPV/PLGA-PEG NPs was observed suggesting non-specific binding of control antibody-NP conjugates to LoVo cells. This supports the findings seen in Figure 6.8.

Green DyLight 448 fluorescence and red CN-PPV/PLGA-PEG NP fluorescence was also observed when the control cell line EA.hy926, was incubated with control antibody–NP conjugates (Figure 6.9). However, green DyLight 448 fluorescence was seen when EA.hy926 cells were incubated with target (anti-CEA) antibody – NP conjugates suggesting non-specific binding of target antibody-NP conjugates to EA.hy926 cells. Red fluorescence from CN-PPV/PLGA-PEG NPs was also seen when control antibody-NP conjugates were incubated with the second control cell line HEK293, suggesting non-specific binding.

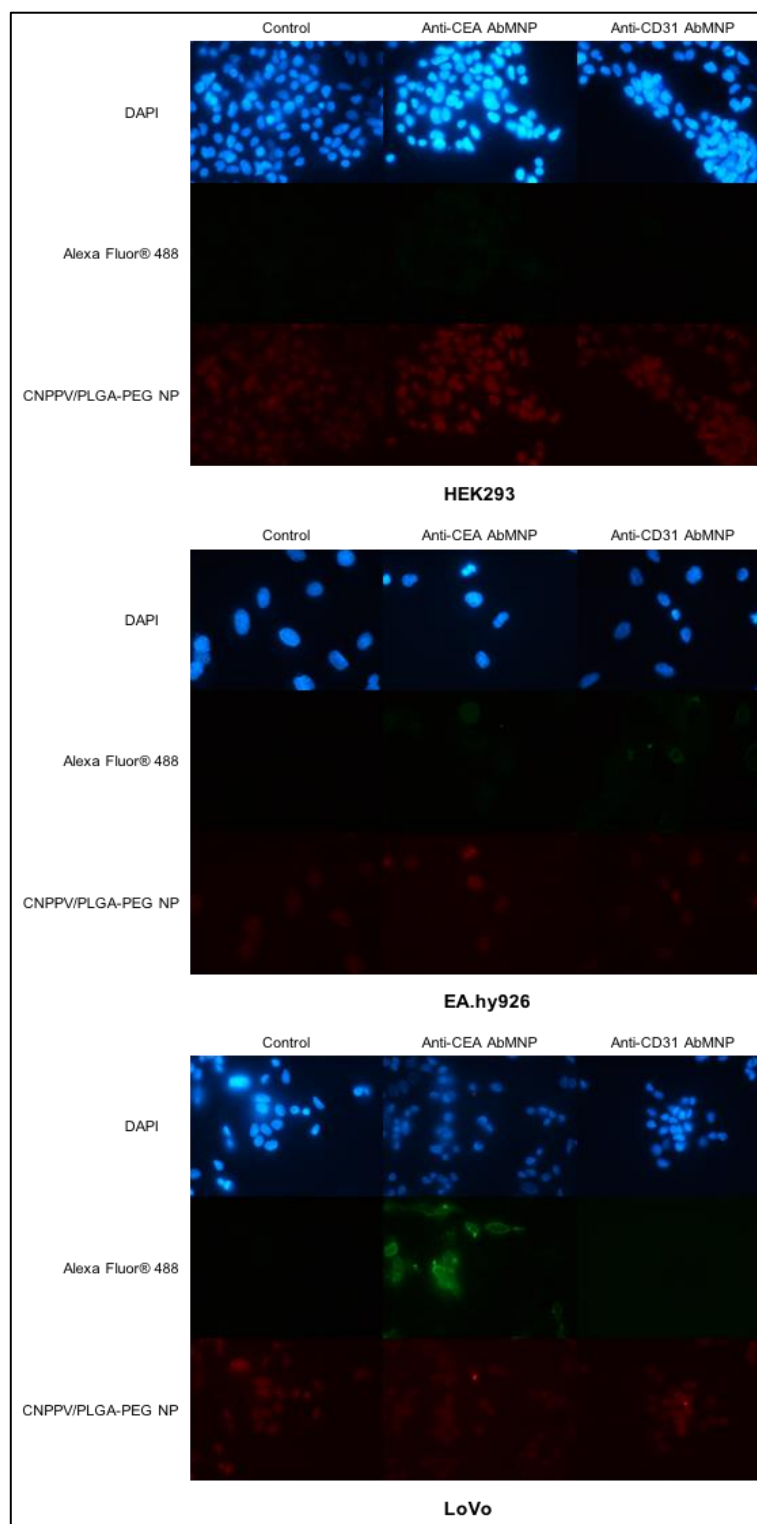


**Figure 6.9. Binding of target and control antibody-NP conjugates on target and control cell lines using immunofluorescence on fixed cells.** Blue fluorescence is DAPI using DAPI filter. Green fluorescence is Alexa Fluor® 488 secondary antibody using FITC filter. Red fluorescence is CN-PPV NP using 5-ALA filter. Magnification x63. Scalebar = 10  $\mu$ m. 0.5% skimmed milk blocking served as control. Images in this figure are representative of at least 3 independent experiments. See 2.4.2.3 of Materials and Methods for the detailed protocol. Green and red fluorescence is observed when both the target and control antibody-NP conjugates to all cell lines indicating non-specific binding.

## 6.2.3 Optimisation of antibody-nanoparticle conjugation

### 6.2.3.1 Optimisation step 1: Comparing different extraction techniques to remove excess antibody from antibody-nanoparticle conjugates

Excess oxidised antibody needs to be removed from antibody-NP conjugates to prevent free oxidised antibodies from binding and blocking target antigens. This would allow the antibody-NP conjugates only to bind and occupy the target antigens. Three different extraction methods were compared as per the protocol described in 2.4.3.1. Target antibody-NP conjugates were incubated with HEK293, LoVo and EA.hy926 cell lines and fluorescence quantified.

Centrifuging was found to be the most effective method in putatively removing free unconjugated antibodies. A 90% increase in fluorescence was found in centrifuged antibody-NP conjugate and free unconjugated antibodies mixture ( $p < 0.0001$ ). The use of magnetic forces to separate the mixture resulted in 24% increase in fluorescence ( $p = 0.0048$ ) and the use of a dialysis yielded 20% increase in fluorescence ( $p = 0.0251$ ) (Figure 6.10). When the three extraction methods are compared against no extraction, only centrifugation showed a significant difference in fluorescence. *Centrifugation*: 81.0% ( $p < 0.0001$ ), *Magnetism*: 15% ( $p = 0.2190$ ) and *Dialysis*: – 11% ( $p = 0.8559$ ). For all subsequent experiments, centrifugation was used to remove excess unconjugated antibodies.

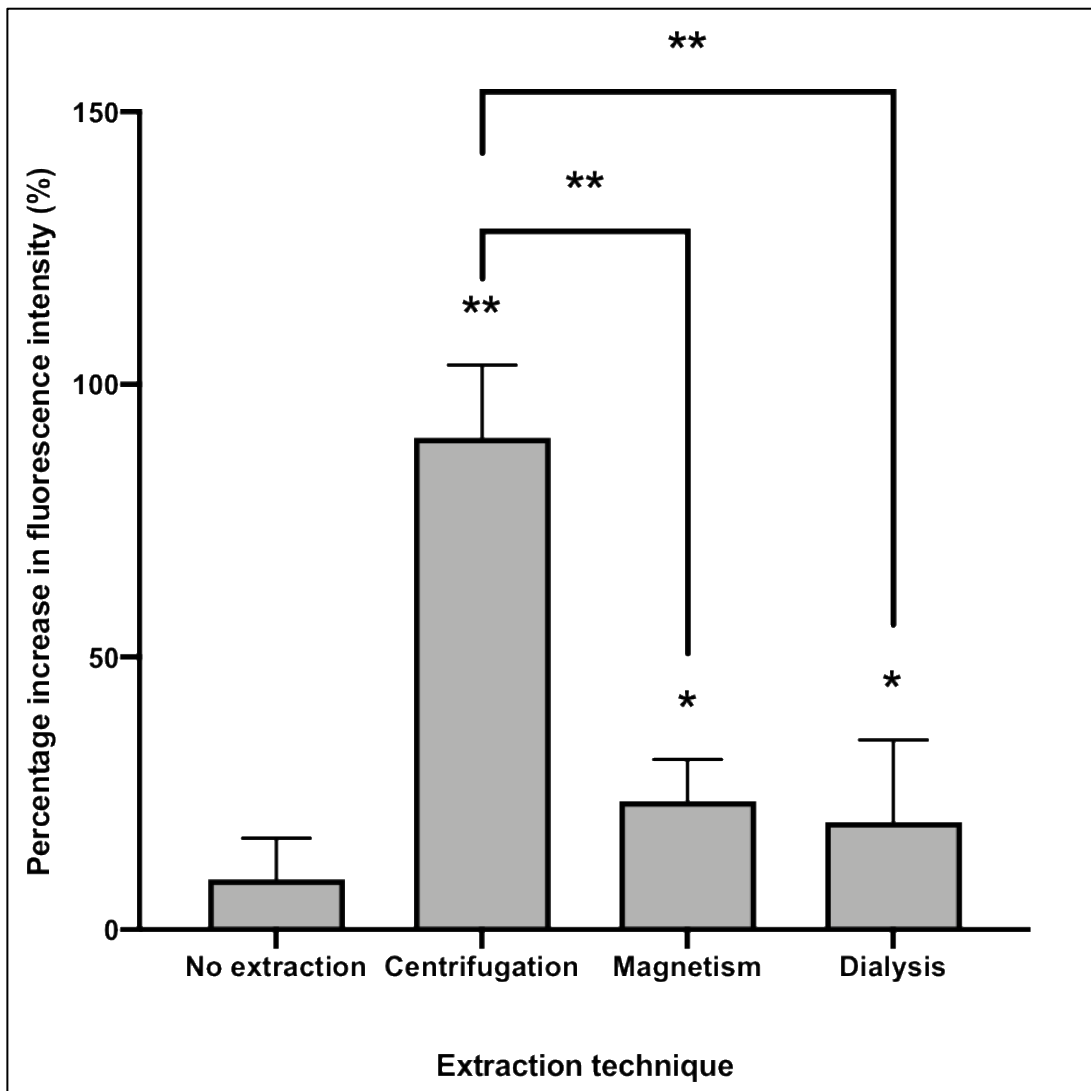


**Figure 6.10. Assessment of binding of target antibody-NP conjugate to LoVo cells using different extraction methods to remove excess oxidised target antibody.** Results represent mean values of at least 3 independent experiments with SD. Experiments were performed in triplicate. Statistically significant difference of fluorescence normalised to cell media only treated cells was considered at  $p < 0.05$  (\*) and  $p < 0.0001$  (\*\*). See 2.4.3.1 of Materials and Methods for the detailed protocol. These results show that centrifugation is the best extraction method to remove excess oxidised target antibody.

When comparing the different extraction methods, Figure 6.10 shows a statistically significant increase in fluorescence between extraction using centrifugation and both dialysis and magnetism. *Centrifugation vs. Magnetism*: 67% difference in fluorescence ( $p < 0.0001$ ), *Centrifugation vs. Dialysis*: 71% ( $p < 0.0001$ ), *Magnetism vs. Dialysis*: 4% ( $p > 0.9999$ ).

### 6.2.3.2 Optimisation step 2: Galactose-mediated blocking of unoccupied hydrazide groups on crosslinker

To reduce non-specific binding, the hydrazide functional groups on the heterobifunctional crosslinkers needs to be occupied by the aldehyde groups on oxidised antibodies or blocked by oxidised galactose. The blocking of unoccupied hydrazide functional groups by oxidised galactose was performed as per 2.4.3.2. Target antibody-NP conjugates were incubated with HEK293, LoVo and EA.hy926 cell lines and fluorescence quantified.

Figure 6.11 demonstrates that significant increases in fluorescence were observed in LoVo cells incubated with both target antibody-NP conjugates (AbMNP) and galactose-blocked target antibody-NP conjugate (Blocked AbMNP). *AbMNP*: 216% ( $p < 0.0001$ ) and *Blocked AbMNP*: 109% ( $p = 0.0066$ ).

However, increase in fluorescence was also observed when both AbMNP and Blocked AbMNP conjugates were incubated with HEK293 cells. *AbMNP*: 184% ( $p < 0.0001$ ) and *Blocked AbMNP*: 118% ( $p = 0.0001$ ). In EA.hy926 cells, a 98% ( $p = 0.0007$ ) and 49% ( $p = 0.0901$ ) increase in fluorescence was observed with AbMNP and Blocked AbMNP respectively. Comparing AbMNP and Blocked AbMNP, increased fluorescence was observed in all three cell lines incubated with AbMNP. *HEK293*: 65% ( $p = 0.0155$ ), *LoVo*: 106% ( $p = 0.0082$ ) and *EA.hy926*: 49% ( $p = 0.0921$ ).

Additionally, a 170% increase in fluorescence was also observed when PDPH-25% maleimide functionalised NP conjugates were incubated with HEK293 cells ( $p < 0.0001$ ) (Figure 6.11). To highlight the impact of galactose-mediated blocking of hydrazide functional groups, no significant differences in fluorescence were detected when blocked PDPH - 25% maleimide functionalised NP conjugates were incubated with all three cell

lines. *HEK293*: 22% increase in fluorescence ( $p=0.7604$ ), *EA.hy926*: 2% reduction ( $p>0.9999$ ) and *LoVo*: 47% increase ( $p=0.4156$ ) (Figure 6.11).

Similar to the results described in 6.2.2.3, no significant differences in fluorescence were observed between the *LoVo* and control cell lines incubated with blocked target (anti-CEA) antibody-NP conjugates. *HEK293* vs. *LoVo*: 9% ( $p>0.9999$ ) and *EA.hy926* vs. *LoVo*: 60% ( $p=0.2488$ ).

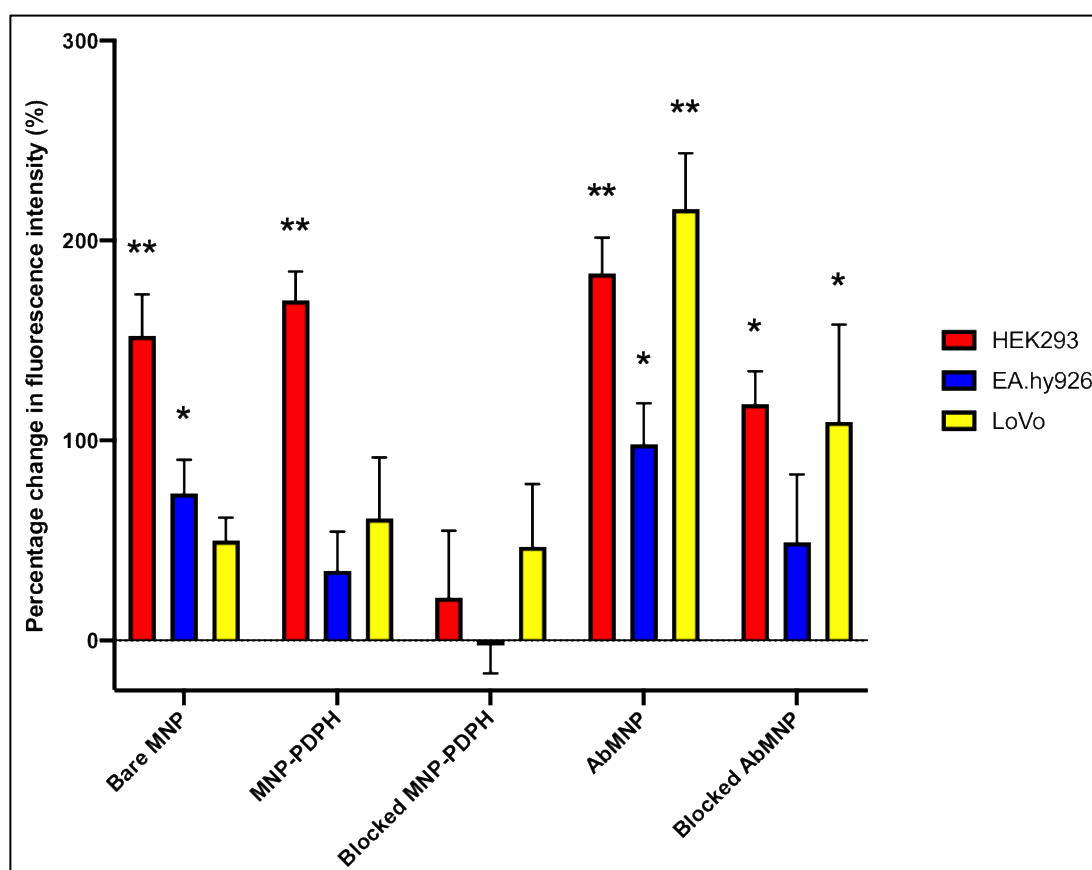


**Figure 6.11. Assessment of binding of target antibody-NP conjugate (AbMNP) against target and control cells using oxidised galactose to block unoccupied hydrazide functional groups on heterobifunctional crosslinker.** Results represent mean values of at least 3 independent experiments with SD. Experiments were performed in triplicate. Fluorescence was normalised to cell media only treated cells. Statistically significant difference of fluorescence normalised to cell media only treated cells was considered at  $p<0.05$  (\*) and  $p<0.0001$  (\*\*). See 2.4.3.2 of Materials and Methods for the detailed protocol. Galactose-mediated blocking of unoccupied hydrazide functional groups did not appear to prevent non-specific binding of the antibody-NP conjugate to control cell lines.

### 6.2.3.3 Optimisation step 3: Assessing the effect of conjugation time between oxidised antibody and PDPH-MNP conjugate

The oxidised anti-CEA antibody and PDPH-maleimide functionalised NP conjugates were incubated together for different time periods, to determine the optimum length of time for the conjugation reaction to occur as described in 2.4.3.3. Unconjugated anti-CEA (target) antibodies were then removed from mixtures and the target antibody-NP conjugates were incubated with HEK293, LoVo and EA.hy926 cell lines and fluorescence quantified.

Figure 6.12 shows that a significant increase (as compared to cell media only treated cells) in fluorescence intensities was found in all three cell lines that were incubated with target antibody-NP conjugates under conjugation reaction for all lengths of time (1, 2, 4 and 8 hours) ( $p < 0.0001$ ).

Comparing the different cell lines, it was found that LoVo cells had increased fluorescence as compared to control cell lines, when incubated with antibody-NP conjugates under reaction for 1 and 2 hours. **At 1hr** - HEK293 vs. LoVo: 138% ( $p < 0.0001$ ) and EA.hy926 vs. LoVo: 66% ( $p = 0.0001$ ). **At 2hr** - HEK293 vs. LoVo: 124% ( $p < 0.0001$ ) and EA.hy926 vs. LoVo: 68% ( $p = 0.0011$ ). However, when LoVo cells were incubated with antibody-NP conjugates that were under reaction for longer (4 and 8 hours), no significant increase in fluorescence was observed as compared to control cell lines. **At 4hr** - HEK293 vs. LoVo: 19% ( $p > 0.9999$ ) and EA.hy926 vs. LoVo: -20% ( $p = 0.9363$ ). **At 8hr** - HEK293 vs. LoVo: 9% ( $p > 0.9999$ ) and EA.hy926 vs. LoVo: 8% ( $p > 0.9999$ ).

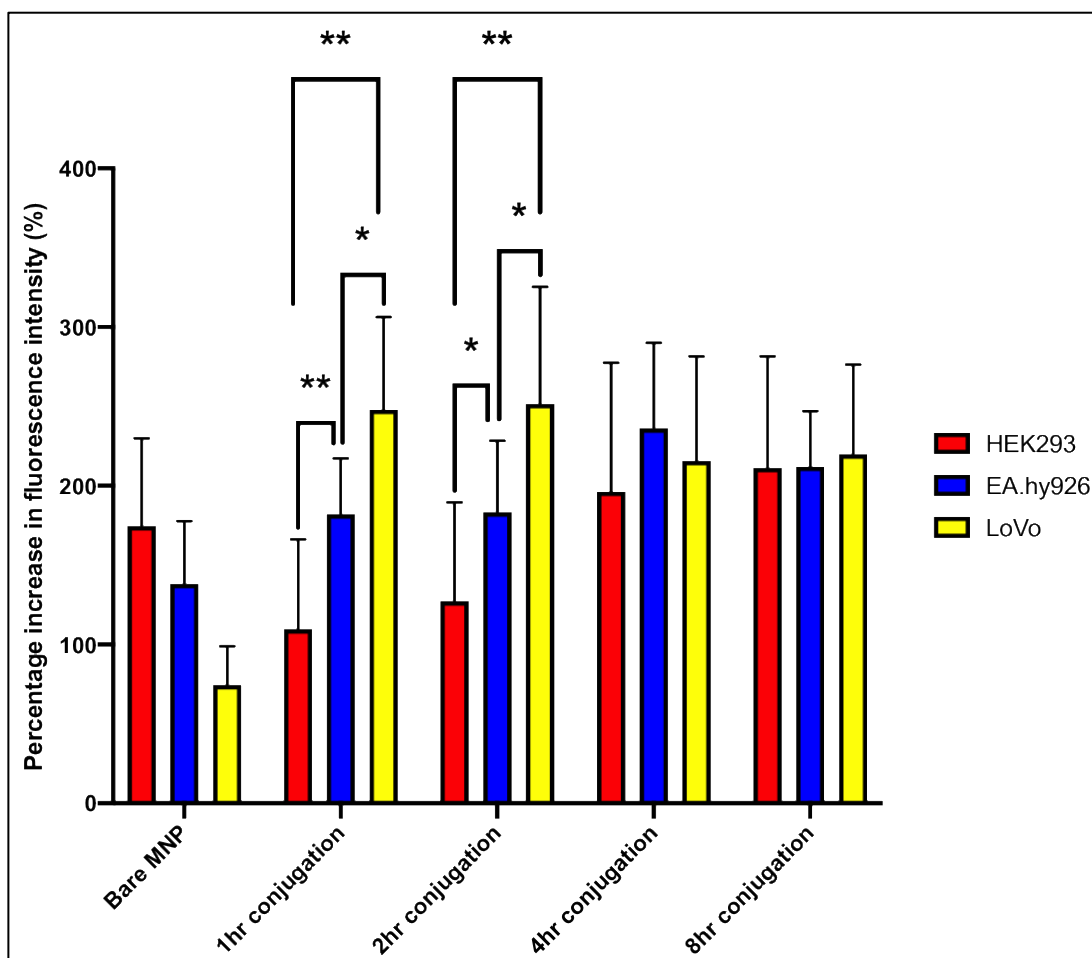


**Figure 6.12. Comparing binding of target antibody-NP conjugates where the antibody and PDPH-MNP have incubated for different time periods against target and control cell lines.** Results represent mean values of at least 3 independent experiments with SD. Experiments were performed in triplicate. Fluorescence was normalised to cell media only treated cells. Statistically significant difference of fluorescence between the target antibody-NP conjugates was considered at  $p < 0.05$  (\*) and  $p < 0.0001$  (\*\*). See 2.4.3.3 of Materials and Methods for the detailed protocol. Significant increases in fluorescence intensities was found in all three cell lines incubated with target antibody-NP conjugates at all incubation durations.

#### 6.2.3.4 Optimisation step 4: Investigating the effect of increasing the amount of Target (anti-CEA) antibodies incubated with PDPH-MNP in conjugation reactions

The amount of oxidised anti-CEA (target) antibody mixed with the PDPH – maleimide functionalised NPs was increased (Increased Ab:MNP) to determine whether this practical step could improve the efficiency of the antibody-NP system. Blocking of

increased Ab:MNP with galactose as well as the additional step of extracting excess blocking agent were also evaluated as per 2.4.3.4. Antibody-NP conjugates were incubated with HEK293, LoVo and EA.hy926 cell lines and fluorescence quantified.

Increase in fluorescence compared to cell media only treated cells was found when all three cell lines were incubated with increased Ab:MNP. *HEK293*: 31% ( $p=0.0104$ ), *EA.hy926*: 56% ( $p=0.0115$ ) and *LoVo*: 78% ( $p<0.0001$ ) (Figure 6.13). Similarly, increase in fluorescence was also observed when all three cell lines were incubated with AbMNP of normal amount of oxidised anti-CEA. *HEK293*: 61% ( $p<0.0001$ ), *EA.hy926*: 79% ( $p<0.0001$ ) and *LoVo*: 97% ( $p<0.0001$ ).

With the inclusion of galactose-mediated blocking of increased Ab:MNP, the increased fluorescence in cells was retained. *HEK293*: 64% ( $p<0.0001$ ), *EA.hy926*: 60% ( $p=0.0052$ ) and *LoVo*: 45% ( $p=0.0018$ ). However, when antibody-NP conjugates were filtered to remove excess galactose (blocking agent), fluorescence had reduced and no significant difference in fluorescence was observed as compared to cell media only treated cells. *HEK293*: 13% ( $p=0.7113$ ), *EA.hy926*: 18% ( $p=0.8753$ ) and *LoVo*: 18% ( $p=0.5981$ ) (Figure 6.13). The increased amount of oxidised anti-CEA antibodies in increased Ab:MNP mixtures was done to ensure that all PDPH-MNP were conjugated to antibodies, and therefore increase AbMNP binding to LoVo (CEA-positive) cells. However, a 19% reduction in fluorescence was observed in increased Ab:MNP treated LoVo cells compared to AbMNP treated cells ( $p=0.5487$ ). Galactose-mediated blocking reduced fluorescence by 52% ( $p=0.0002$ ) in increased Ab:MNP treated LoVo cells and galactose filtering reduced fluorescence by a further 27% ( $p=0.1864$ ).

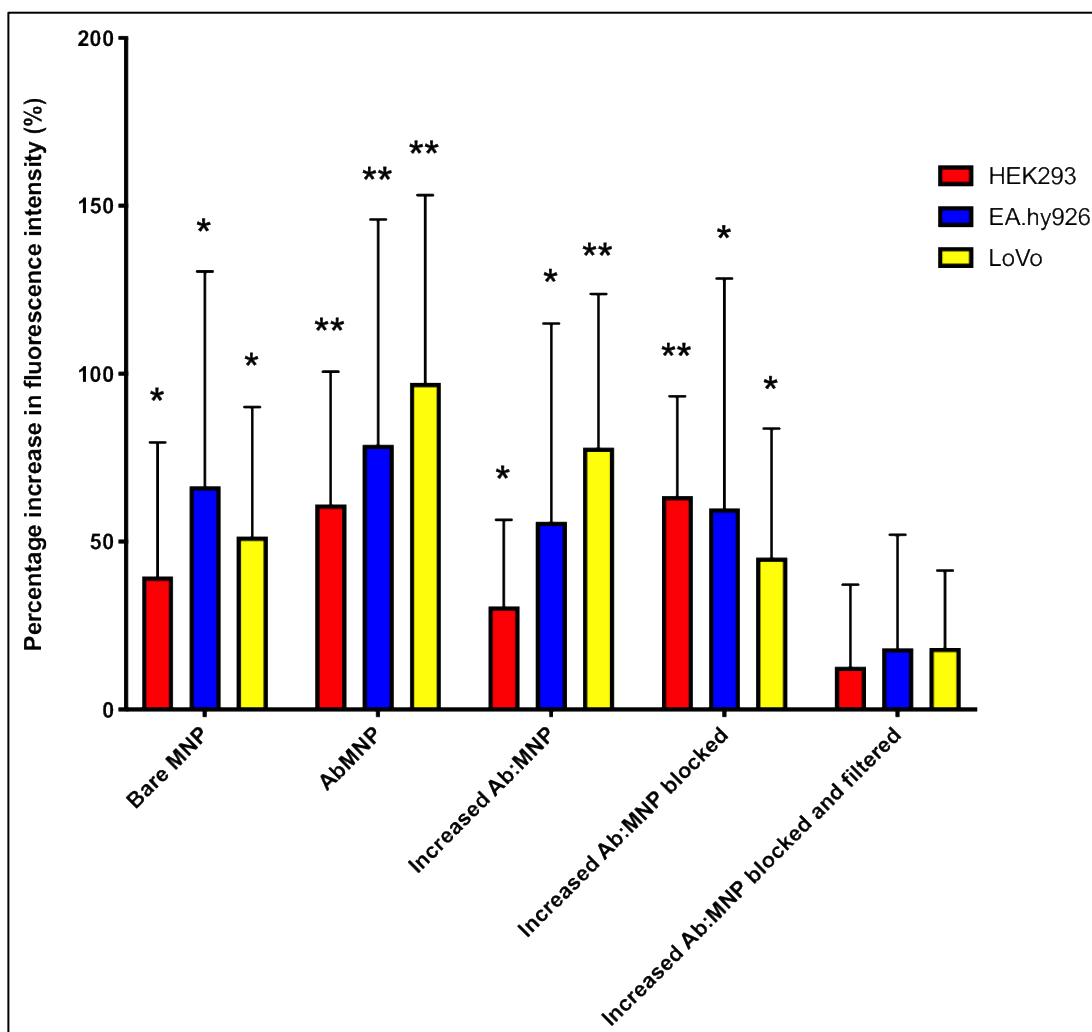


**Figure 6.13. Comparison of the binding of target antibody-NP conjugates (AbMNP) with different ratios of antibody to PDPH – maleimide functionalised NP conjugates and different post conjugation processes against target and control cell lines.** Results represent mean values of at least 3 independent experiments with SD. Experiments were performed in triplicate. Fluorescence was normalised to cell media only treated cells. Statistically significant difference of fluorescence normalised to cell media only treated cells was considered at  $p < 0.05$  (\*) and  $p < 0.0001$  (\*\*). See 2.4.3.4 of Materials and Methods for the detailed protocol. Increases in fluorescence intensity were seen when all three cell lines were incubated with increased concentration of antibody-NP conjugate.

### 6.2.3.5 Optimisation step 5: Investigating optimum dilution of maleimide functionalised nanoparticle in conjugation reaction

Bare maleimide functionalised NPs were diluted with phosphate buffered saline (PBS) prior to conjugation with oxidised target (anti-CEA) antibodies, as described in 2.4.3.5. AbMNP refers to standard target antibody-NP conjugates with no dilution of maleimide

functionalised NPs prior to conjugation. Antibody-NP conjugates were incubated with HEK293, LoVo and EA.hy926 cell lines and fluorescence quantified.

At all AbMNP dilutions, a significant increase in fluorescence was only observed in the CEA-positive LoVo cells as compared to cell media only treated cells. *No dilution*: 175% ( $p < 0.0001$ ), *90% dilution*: 185% ( $p < 0.0001$ ), *80% dilution*: 189% ( $p < 0.0001$ ) and *70% dilution*: 173% ( $p < 0.0001$ ) (Figure 6.14). No differences in fluorescence were observed in the control cell lines.

When comparing the different AbMNP dilutions, no significant differences in fluorescence were observed in LoVo cells. *No dilution vs. 90% dilution*: 10% difference in fluorescence ( $p = 0.9982$ ), *vs. 80% dilution*: 14% ( $p = 0.9901$ ), *vs. 70% dilution*: 2% ( $p = 0.9999$ ). *90% dilution vs. 80% dilution*: 4% ( $p > 0.9999$ ), *vs. 70% dilution*: 12% ( $p = 0.9960$ ). *80% dilution vs. 70% dilution*: 16% ( $p = 0.9830$ ).

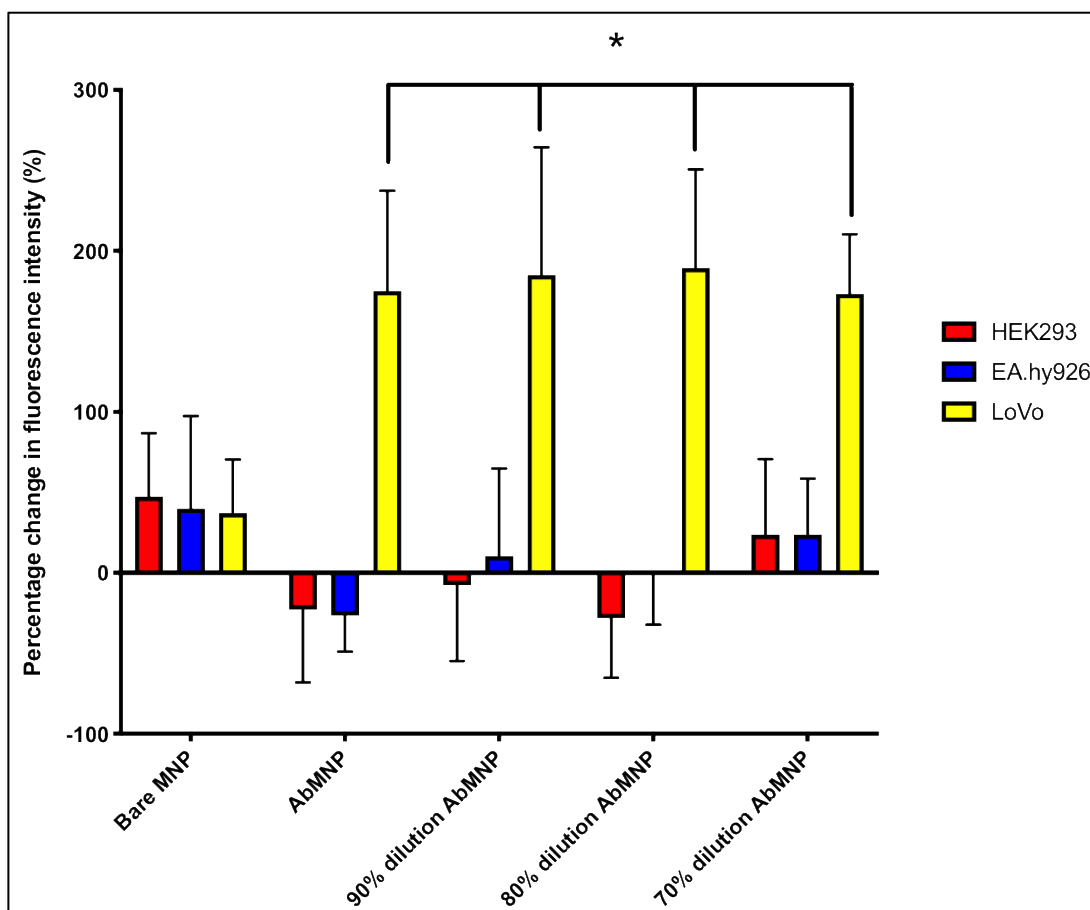


**Figure 6.14. Comparison of the binding of target antibody-NP conjugates (AbMNP) with different dilutions of maleimide functionalised NP used in the conjugation reaction against target and control cell lines.** Results represent mean values of at least 3 independent experiments with SD. Experiments were performed in triplicate. Fluorescence was normalised to cell media only treated cells. Statistically significant difference of fluorescence normalised to cell media only treated cells was considered at  $p < 0.0001$  (\*\*). See 2.4.3.5 of Materials and Methods for the detailed protocol. Significant increases in fluorescence intensity were only seen in target cell line with the target antibody-NP conjugate at all dilutions of MNP.

### 6.2.3.6 Optimisation step 6: The influence of wash cycles following the incubation of cells with conjugates

Plates of target (LoVo) and control (EA.hy926 and HEK293) cell lines were seeded as per 2.4.3.6 and subjected to different numbers of wash cycles with PBS from 2 cycles to 4 cycles. Antibody-NP conjugates were incubated with HEK293, LoVo and EA.hy926 cell lines and AbMNP fluorescence was quantified following PBS wash steps.

After 2 wash cycles, a 16% increase in fluorescence was observed in LoVo cells incubated with target antibody-NP conjugates (AbMNP) ( $p=0.0006$ ) as compared to cell media only treated cells. This increase in fluorescence (16%,  $p=0.0084$ ) was also observed in one other control cell line, HEK293 (Figure 6.15). Further PBS washes were found to mildly reduce the intensity of fluorescence in the target cell line. 2 wash cycles vs. 3 wash cycles: 9% ( $p=0.2950$ ). 2 wash cycles vs. 4 wash cycles: 8% ( $p=0.6094$ ).

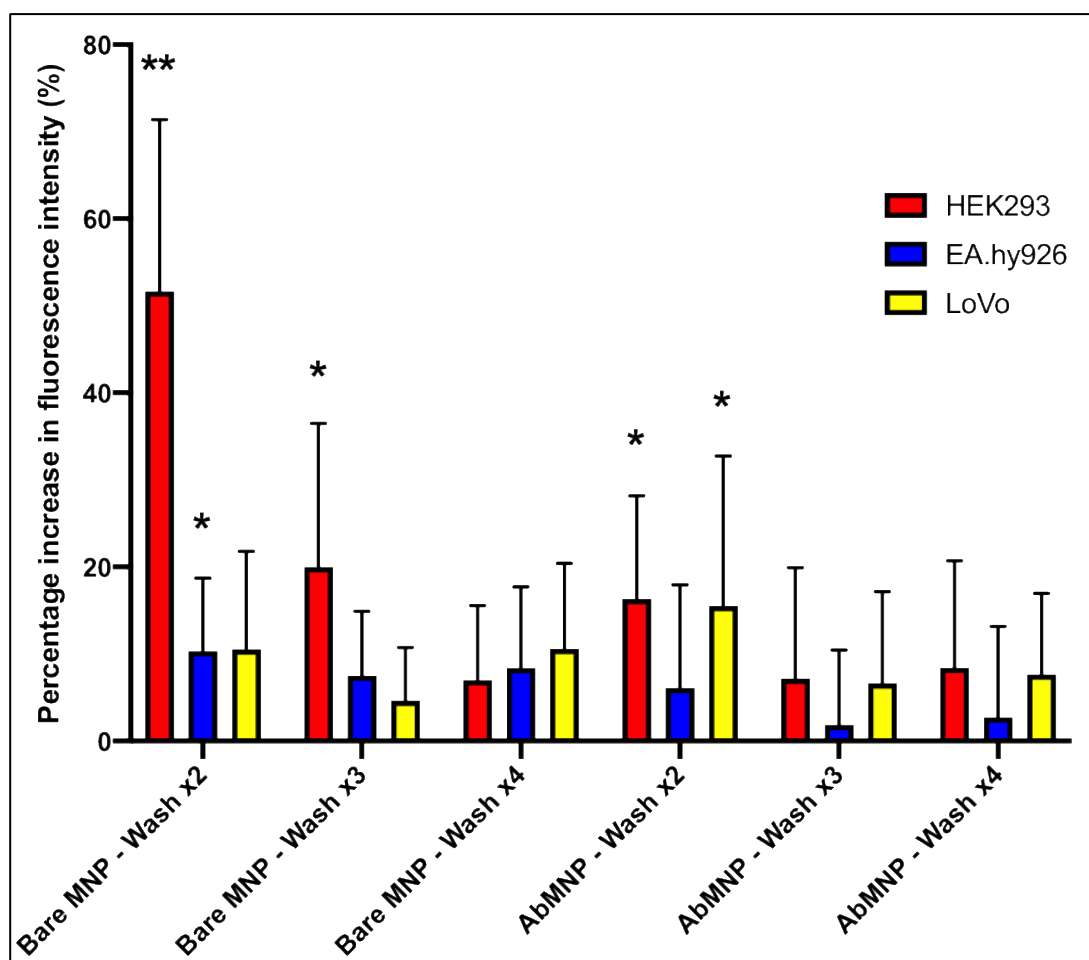


**Figure 6.15. Comparison of the binding of target antibody-NP conjugates (AbMNP) having undergone different numbers of wash cycles against target and control cell lines.** Results represent mean values of at least 3 independent experiments with SD. Experiments were performed in triplicate. Fluorescence was normalised to cell media only treated cells. Statistically significant difference of fluorescence normalised to cell media only treated cells was considered at  $p < 0.05$  (\*) and  $p < 0.0001$  (\*\*). See 2.4.3.6 of Materials and Methods for the detailed protocol. These results suggest that more than two wash cycles reduced fluorescence intensities in LoVo and both control cell lines.

### 6.2.3.7 Optimisation step 7: Investigating the different parameters of incubation

Target (LoVo) and control (EA.hy926 and HEK293) cell lines were seeded as per 2.4.3.7 and incubated under different conditions. Cells were either incubated for 1 hour or overnight at either 4°C, room temperature or 37°C. Antibody-NP conjugates were incubated with HEK293, LoVo and EA.hy926 cell lines and fluorescence quantified.

Overnight incubation at 37°C was found to yield optimal binding in LoVo cells incubated with both unblocked and galactose-blocked target antibody-NP conjugates (AbMNP), at 45% and 49% increase in fluorescence as compared to cell media only treated cells ( $p < 0.0001$  for both unblocked and galactose-blocked AbMNP) (Figure 6.16F). However, increased fluorescence was also observed in both control cell lines incubated overnight at 37°C with both unblocked and galactose-blocked AbMNP. *HEK293-unblocked AbMNP*: 39% ( $p = 0.0002$ ) and *HEK293-blocked AbMNP*: 46% ( $p < 0.0001$ ). *EA.hy926-unblocked AbMNP*: 27% ( $p = 0.0048$ ) and *EA.hy926-blocked AbMNP*: 30% ( $p = 0.0018$ ) (Figure 6.16F).

No significant differences in fluorescence intensities were observed for either AbMNP variations on the target cell line at any other incubation conditions (Figure 6.16A-E). *Unblocked AbMNP*: 1 hour at 4°C – 2% ( $p > 0.9999$ ), 1 hour at room temperature – 2% ( $p > 0.9999$ ), 1 hour at 37°C – 1% ( $p > 0.9999$ ), overnight at 4°C – 9% ( $p = 0.2744$ ) and overnight at room temperature – 1% ( $p > 0.9999$ ). *Galactose-blocked AbMNP*: 1 hour at 4°C – 0% ( $p > 0.9999$ ), 1 hour at room temperature – 5% ( $p > 0.9999$ ), 1 hour at 37°C – 0% ( $p > 0.9999$ ), overnight at 4°C – 5% ( $p > 0.9999$ ) and overnight at room temperature – 3% ( $p > 0.9999$ ).

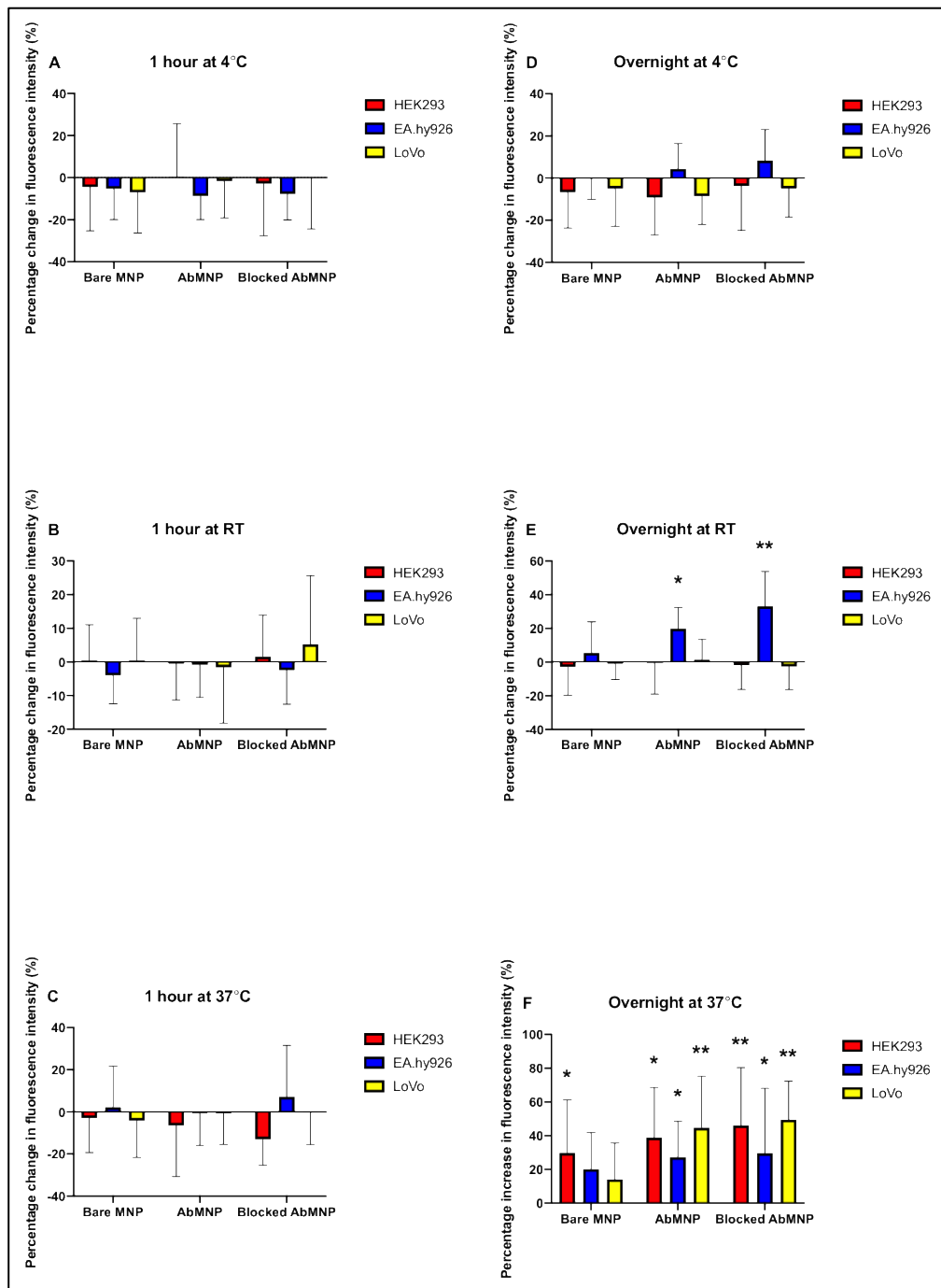


**Figure 6.16. Comparison of the binding of unblocked and blocked target antibody-NP conjugates (AbMNP) under different incubation conditions.** A) Incubation for 1 hour at 4°C, B) Incubation for 1 hour at room temperature, C) Incubation for 1 hour at 37°C, D) Incubation overnight at 4°C, E) Incubation overnight at room temperature, F) Incubation overnight at 37°C. Results represent mean values of at least 3 independent experiments with SD. Experiments were performed in triplicate. Fluorescence was normalised to cell media only treated cells. Statistically significant difference of fluorescence normalised to cell media only treated cells was considered at  $p < 0.05$  (\*) and  $p < 0.0001$  (\*\*). See 2.4.3.7 of Materials and Methods for the detailed protocol. Overnight incubation at 37°C is the best incubation condition for antibody-NP conjugates on cells although non-specific binding is still present and observed in both control cell lines, even with galactose-mediated blocking of unoccupied hydrazide functional groups.

In the control cell lines, a significant increase in fluorescence was only observed in EA.hy926 cells incubated with both unblocked and galactose-blocked AbMNP overnight at room temperature. *Unblocked AbMNP*: 20% ( $p=0.0006$ ) and *galactose-blocked AbMNP*: 33% ( $p<0.0001$ ) (Figure 6.16E). Apart from this, no significant differences in fluorescence was observed in control cell lines incubated with either AbMNP variants at the remaining incubation parameters (Figure 6.16).

#### **6.2.4 Testing target and control antibody – nanoparticle conjugates against target and control cell lines using streptavidin functionalised nanoparticle**

A different conjugation strategy utilising biotin – streptavidin conjugation chemistry was explored using streptavidin functionalised CN-PPV/PLGA-PEG NPs, supplied by KCL. Conjugation of the streptavidin functionalised NPs was achieved through biotinylated target (anti-CEA) and control (anti-CD31) antibodies. Biotinylation of the antibodies was carried out as per 2.2.2.6. The ability of this system to target the tissue of interest was investigated by testing both the target and control antibody-streptavidin functionalised NP conjugates (CEA AbSNP and CD31 AbSNP respectively) against LoVo, EA.hy926 and HEK293 cell lines as described in protocol 2.4.4.

As shown in Figure 6.17, a 37% increase in fluorescence was observed when CEA AbSNP was incubated with the target (LoVo, CEA-positive) cell line as compared to cell media only treated cells ( $p<0.0001$ ). However, increase in fluorescence was also observed when the control cell lines were incubated with CEA AbSNP. *HEK293*: 17% ( $p=0.8103$ ) and *EA.hy926*: 34% ( $p=0.0280$ ). No significant differences in fluorescence was found between target and control cell lines. *HEK293 vs. LoVo*: 20% ( $p=0.3557$ ) and *EA.hy926 vs. LoVo*: 3% ( $p>0.9999$ ).

Similarly, an increase (24%) in fluorescence was observed when LoVo cells were incubated with the control CD31 AbSNP ( $p=0.0044$ ). This increase was also observed in control cell lines incubated with CD31 AbSNP. *HEK293*: 19% ( $p=0.7350$ ) and *EA.hy926*: 31% ( $p=0.0486$ ) (Figure 6.17). No significant differences in fluorescence was found between target and control cell lines. *HEK293* vs. *LoVo*: 5% ( $p>0.9999$ ) and *EA.hy926* vs. *LoVo*: 7% ( $p>0.9999$ ).

A non-significant 13% increase in fluorescence was found between CEA AbSNP and CD31 AbSNP incubated LoVo cells ( $p=0.1682$ ).

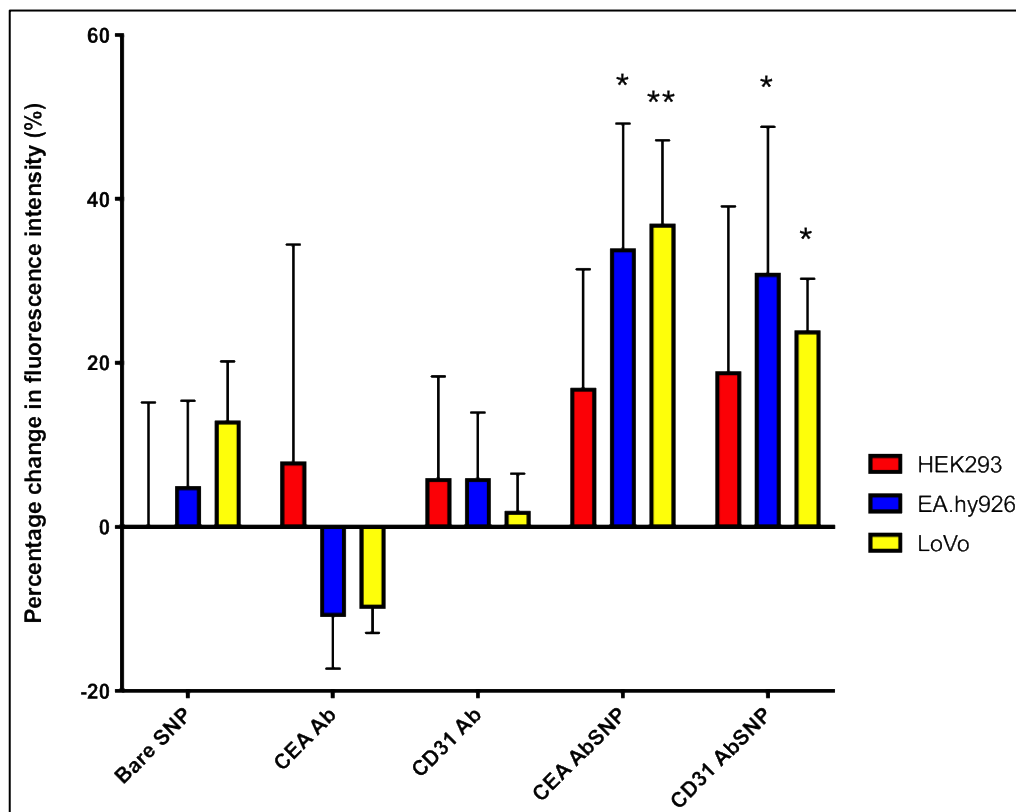


**Figure 6.17. Binding of target and control antibody-streptavidin functionalised NP conjugates (AbSNP) against target and control cell lines.** Results represent mean values of at least 3 independent experiments with SD. Experiments were performed in triplicate. Statistically significant difference of fluorescence normalised to cell media only treated cells was considered at  $p<0.05$  (\*) and  $p<0.0001$  (\*\*). See 2.4.4 of Materials and Methods for the detailed protocol. Significant increases in fluorescence intensity are seen with both the target and control AbSNPs to all cell lines indicating non-specific binding.

## **6.2.5 Conjugation of anti-CEA affimer to maleimide functionalised nanoparticle**

### **6.2.5.1 Testing target and control affimers on fixed cells**

Target (anti-CEA) and control ( $\gamma$ SUMO) affimers underwent biotinylation for the purpose of testing against target (LoVo) and control (HEK293) cell lines. Immunofluorescence and fluorescent imaging was performed as described in 2.2.3.

As shown in Figure 6.18, green fluorescence was observed when LoVo cells were incubated with the anti-CEA affimer and no fluorescence was observed when incubated with the control affimer. No affimer specific fluorescence was observed in HEK293 cells incubated with either target or control affimers.

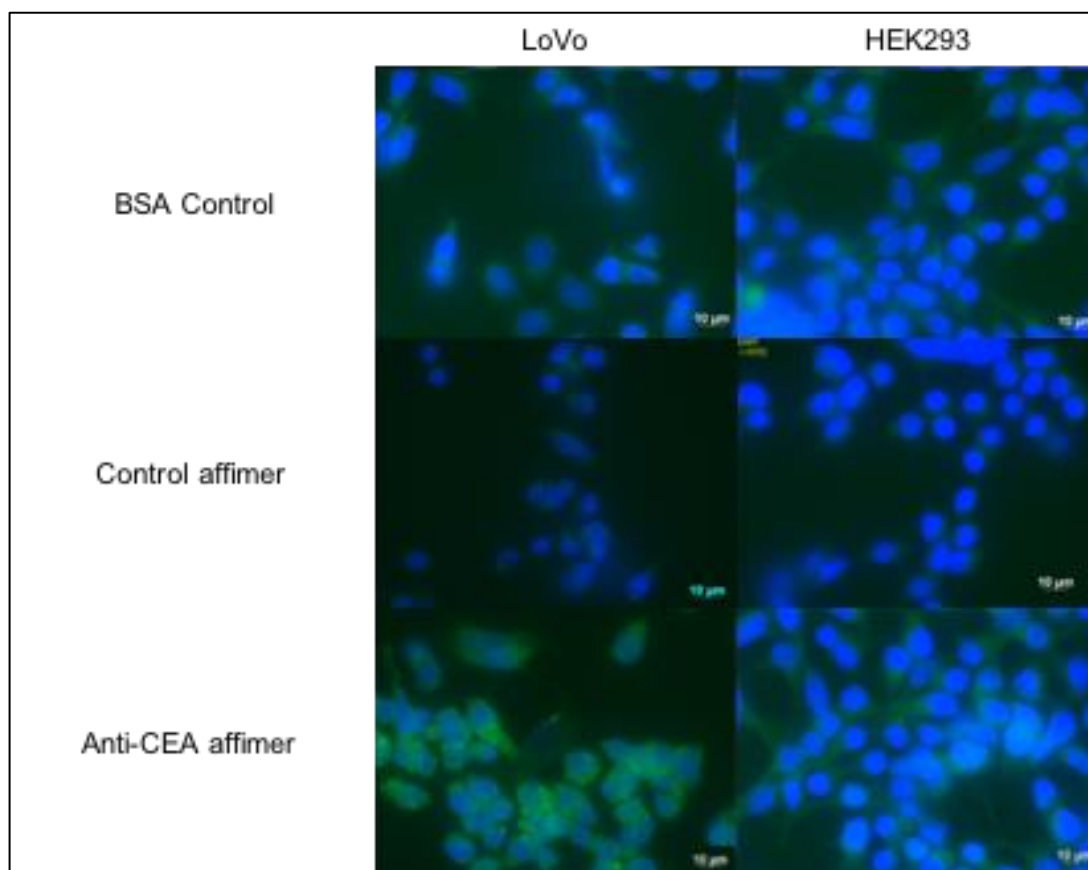


**Figure 6.18. Binding of target and control affimers on target and control cell lines using immunofluorescence.** Blue fluorescence is DAPI. Green fluorescence is Streptavidin DyLight 488 protein using FITC filter. Magnification x63. Scalebar = 10  $\mu\text{m}$ . 0.1% bovine serum albumin served as a control. Images in this figure are representative of at least 3 independent experiments. See 2.2.3 of Materials and Methods for the detailed protocol. The target anti-CEA affimer binds selectively to the LoVo cell line and the control affimer does not bind selectively to either the control or target cell line.

### 6.2.5.2 Testing variants of anti-CEA affimer maleimide functionalised nanoparticle conjugates

Control ( $\gamma$ SUMO), target (anti-CEA II) and target (anti-CEA III) affimer-conjugated NPs (AffMNP), as well as a mixture of anti-CEA II and anti-CEA III affimer-conjugated NPs were incubated with target (LoVo) and control (HEK293) cell lines. Protocol was performed as per 2.4.5.1. Fluorescence from AffMNPs was measured and quantified.

As shown in Figure 6.19, a 9% ( $p>0.9999$ ) and 32% ( $p>0.9999$ ) increase in fluorescence intensity was observed in LoVo cells incubated with anti-CEA II AffMNP and anti-CEA III AffMNP as compared to cell media only treated cells. In addition, a 32% ( $p>0.9999$ ) increase in fluorescence was also observed in anti-CEA II/III AffMNP incubated LoVo cells. No significant difference (7%) in fluorescence was observed in control AffMNP incubated LoVo cells ( $p>0.9999$ ).

In control HEK293 cells no significant fluorescence was observed when incubated with anti-CEA II AffMNP (3% increase,  $p>0.9999$ ), anti-CEA III AffMNP (4% increase,  $p>0.9999$ ) and anti-CEA II/III AffMNP (3% increase,  $p>0.9999$ ). Upon comparing anti-CEA II/III AffMNP incubated HEK293 and LoVo cells, a 29% ( $p=0.0338$ ) increase in fluorescence was found in anti-CEA II/III AffMNP incubated LoVo cells (Figure 6.19).

The anti-CEA affimers were found to be mildly specific in binding to LoVo cells when comparing control and anti-CEA AffMNP incubated LoVo cells. *Control AffMNP vs. anti-CEA II AffMNP*: 16% increase in *anti-CEA II AffMNP* ( $p>0.9999$ ). *Control AffMNP vs. anti-CEA III AffMNP*: 39% increase in *anti-CEA III AffMNP* ( $p>0.8499$ ). *Control AffMNP vs. anti-CEA II/III AffMNP*: 39% increase in *anti-CEA II/III AffMNP* ( $p>0.8422$ ) (Figure 6.19).

All subsequent experiments were conducted with anti-CEA II/III AffMNP.

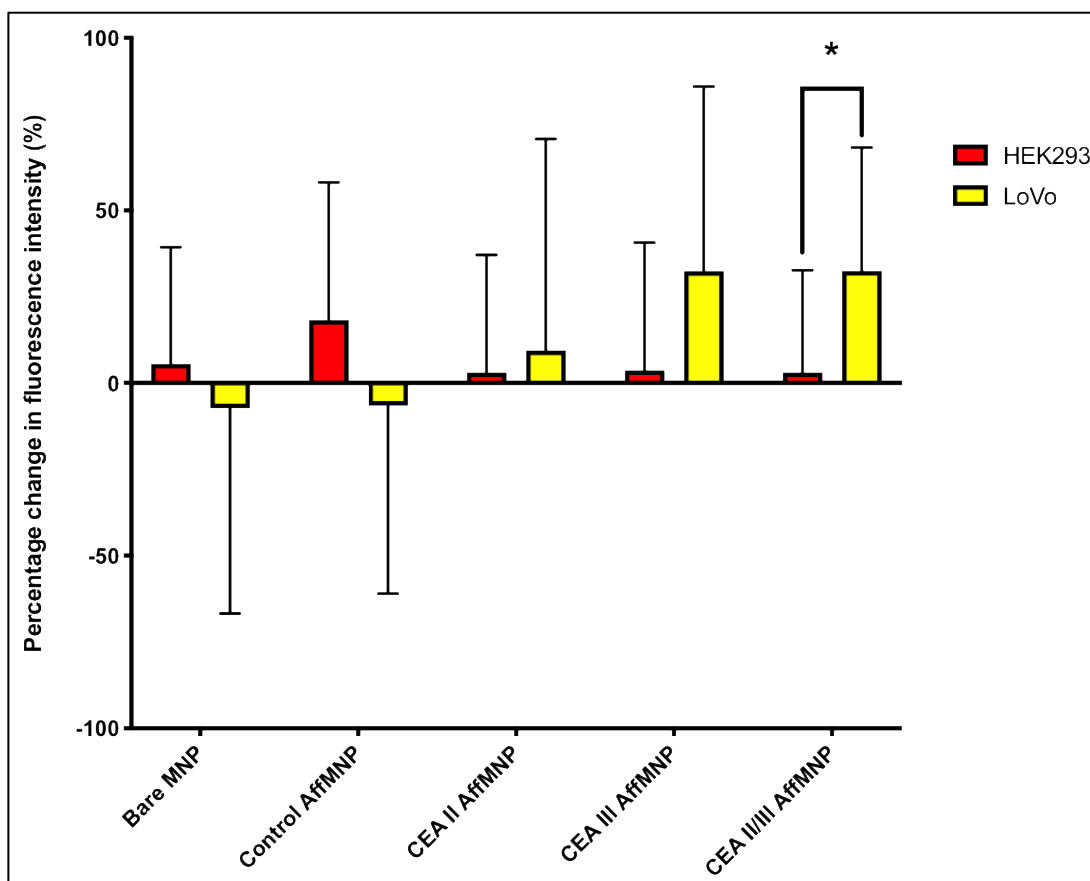


**Figure 6.19. Comparison of binding of control and various target affimer-NP conjugates (AffMNP) against target and control cell lines.** Results represent mean values of at least 3 independent experiments with SD. Experiments were performed in triplicate. Statistically significant difference of fluorescence normalised to cell media only treated cells was considered at  $p < 0.05$  (\*) and  $p < 0.0001$  (\*\*). See 2.4.5.1 of Materials and Methods for the detailed protocol. The increase in fluorescence intensity is greater when the target cell line was incubated with either anti-CEA III AffMNP or anti-CEA II/III AffMNP mixture, as compared to anti-CEA II AffMNP alone. There was also little non-specific binding of any of the target AffMNPs to the control cell line.

### 6.2.5.3 Comparing different incubation settings for affimer-conjugated nanoparticle

To determine the optimum incubation settings of anti-CEA II/III affimer-conjugated NPs on LoVo cells, a binding assay was carried out as per the protocol described in 2.4.5.2.

Figure 6.20 shows that a significant increase in fluorescence was observed when LoVo cells were incubated overnight with anti-CEA II/III AffMNP at both temperatures as

compared to cell media only treated cells. *Room temperature*: 19% ( $p < 0.0001$ ) and 4°C: 17% ( $p = 0.0003$ ). No non-significant difference (2%) was observed between the two overnight temperatures ( $p = 0.9844$ ).

No significant difference in fluorescence compared to cell media only treated cells was observed when LoVo cells were incubated with anti-CEA II/III AffMNP for 2 hours at either temperature. *Room temperature*: 5% ( $p = 0.6402$ ) and 4°C: 9% ( $p = 0.0946$ ) (Figure 6.20).

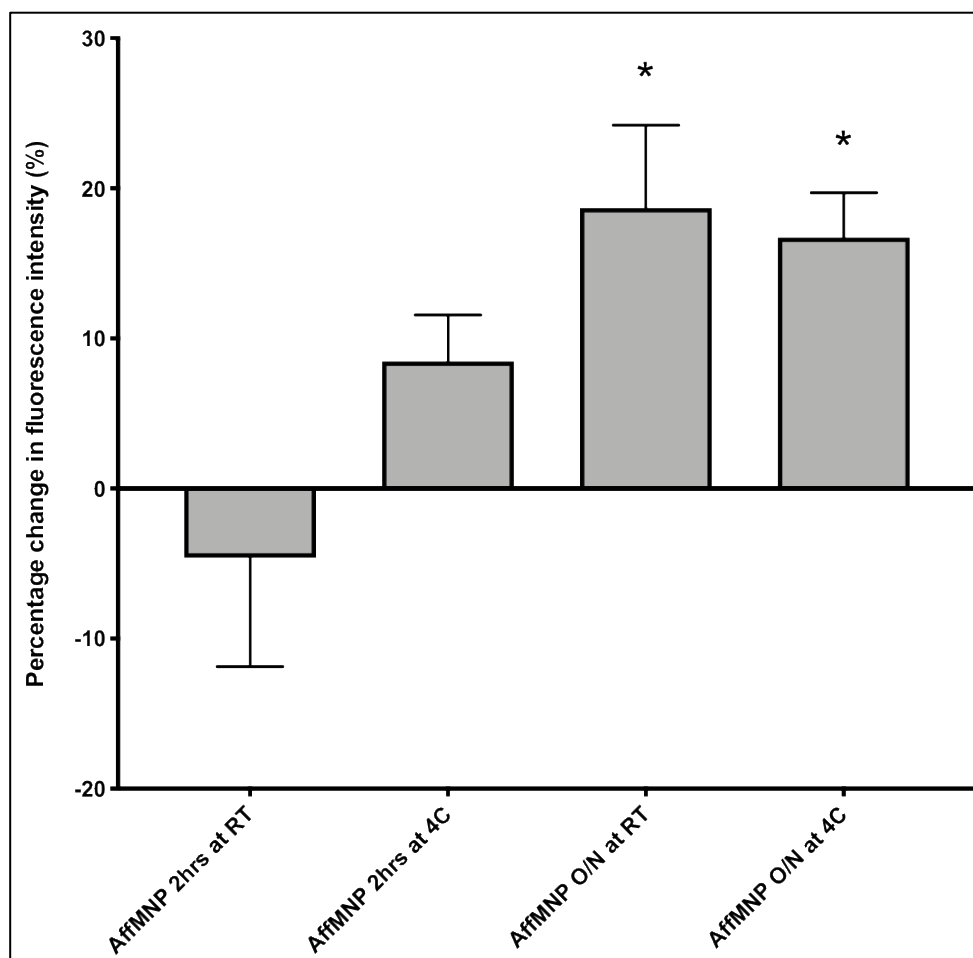


**Figure 6.20. Assessing optimum conditions for binding of affimer-conjugated NP (AffMNP) against the target (LoVo) cell line.** Results represent mean values of at least 3 independent experiments with SD. Experiments were performed in triplicate. Fluorescence was normalised to cell media only treated cells. Statistically significant difference of fluorescence normalised to cell media only treated cells was considered at  $p < 0.0001$  (\*). See 2.4.5.2 of Materials and Methods for the detailed protocol. Incubation of the AffMNP with the LoVo cells overnight at room temperature showed the greatest increase in fluorescence intensity.

#### 6.2.5.4 Testing target and control affimer–nanoparticle conjugates against target and control cell lines

Control and target anti-CEA II/III affimer-conjugated NPs were tested against control (HEK293) and target (LoVo) cell lines using the protocol described in 2.4.5.3.

Figure 6.21 shows that a 56% increase in fluorescence was observed when LoVo cells were incubated with anti-CEA II/III AffMNP as compared to cell media only treated cells.

( $p < 0.0001$ ). No significant difference (14%,  $p = 0.3348$ ) was observed when HEK293 cells were incubated with anti-CEA II/III AffMNP. A significant difference of 42%, was found between HEK293 and LoVo cells incubated with anti-CEA II/III AffMNP ( $p < 0.0001$ ).

No significant increase in fluorescence was observed when either cell lines were incubated with control AffMNP. *LoVo*: 16% ( $p = 0.2953$ ) and *HEK293*: 4% ( $p = 0.9770$ )  
Figure 6.21. *LoVo* cells were found to be 40% more fluorescent when incubated with anti-CEA II/III AffMNP as compared to control AffMNP ( $p < 0.0001$ ). Whereas, a 11% ( $p = 0.5797$ ) increase in fluorescence was observed in HEK293 cells.

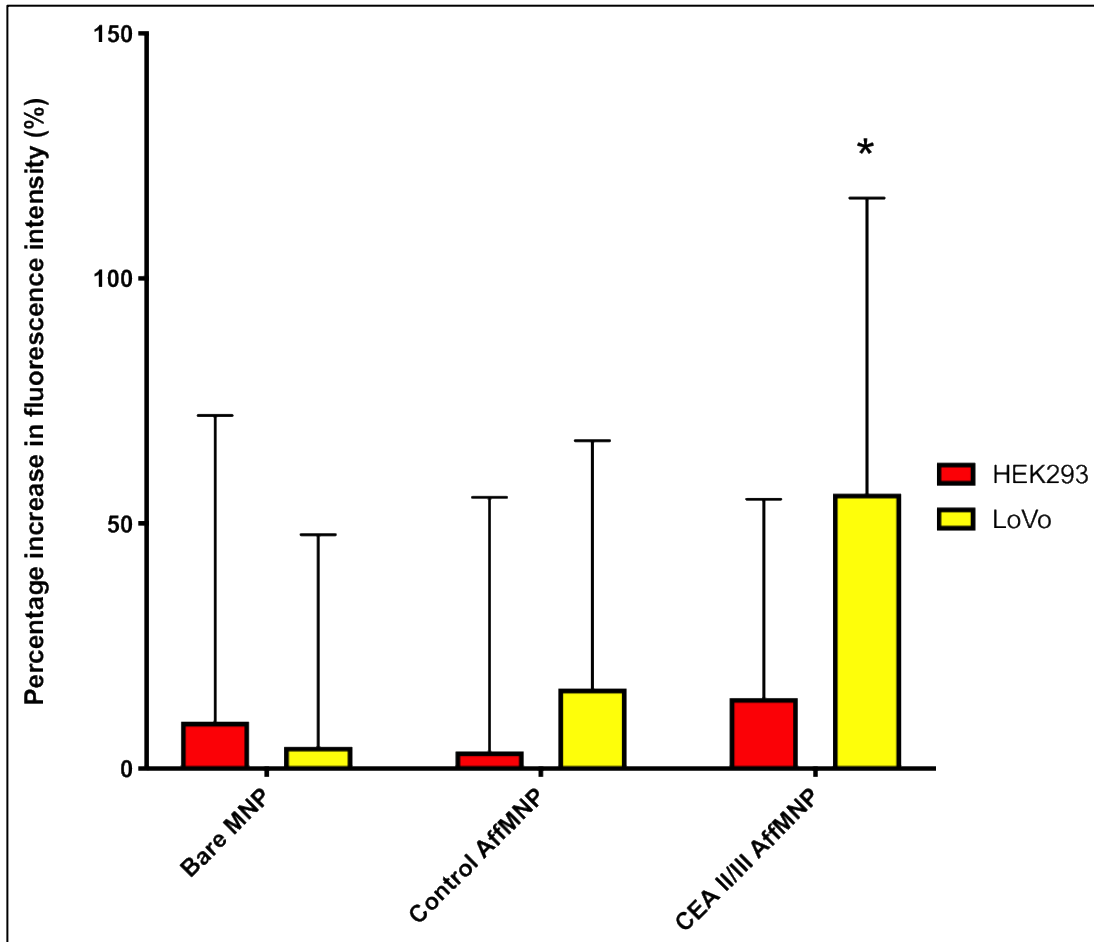


**Figure 6.21. Binding of target and control affimer-conjugated NPs (AffMNP) against target and control cell lines.** Results represent mean values of at least 3 independent experiments with SD. Experiments were performed in triplicate. Statistically significant difference of fluorescence normalised to cell media only treated cells was considered at  $p < 0.0001$  (\*\*). See 2.4.5.3 of Materials and Methods for the detailed protocol. A significant increase in fluorescence intensity is seen only when the target AffMNP is incubated with the target cell line (LoVo).

Figure 6.22 shows that red CN-PPV/PLGA-PEG NP fluorescence is seen in anti-CEA AffMNP incubated LoVo cells. No red CN-PPV/PLGA-PEG NP fluorescence was observed when the target cell line was incubated with control affimer-NP conjugates. Red fluorescence from CN-PPV/PLGA-PEG NPs was not seen when either the target or control affimer-NP conjugates were incubated with the control cell line HEK293, supporting the findings seen in Figure 6.21.

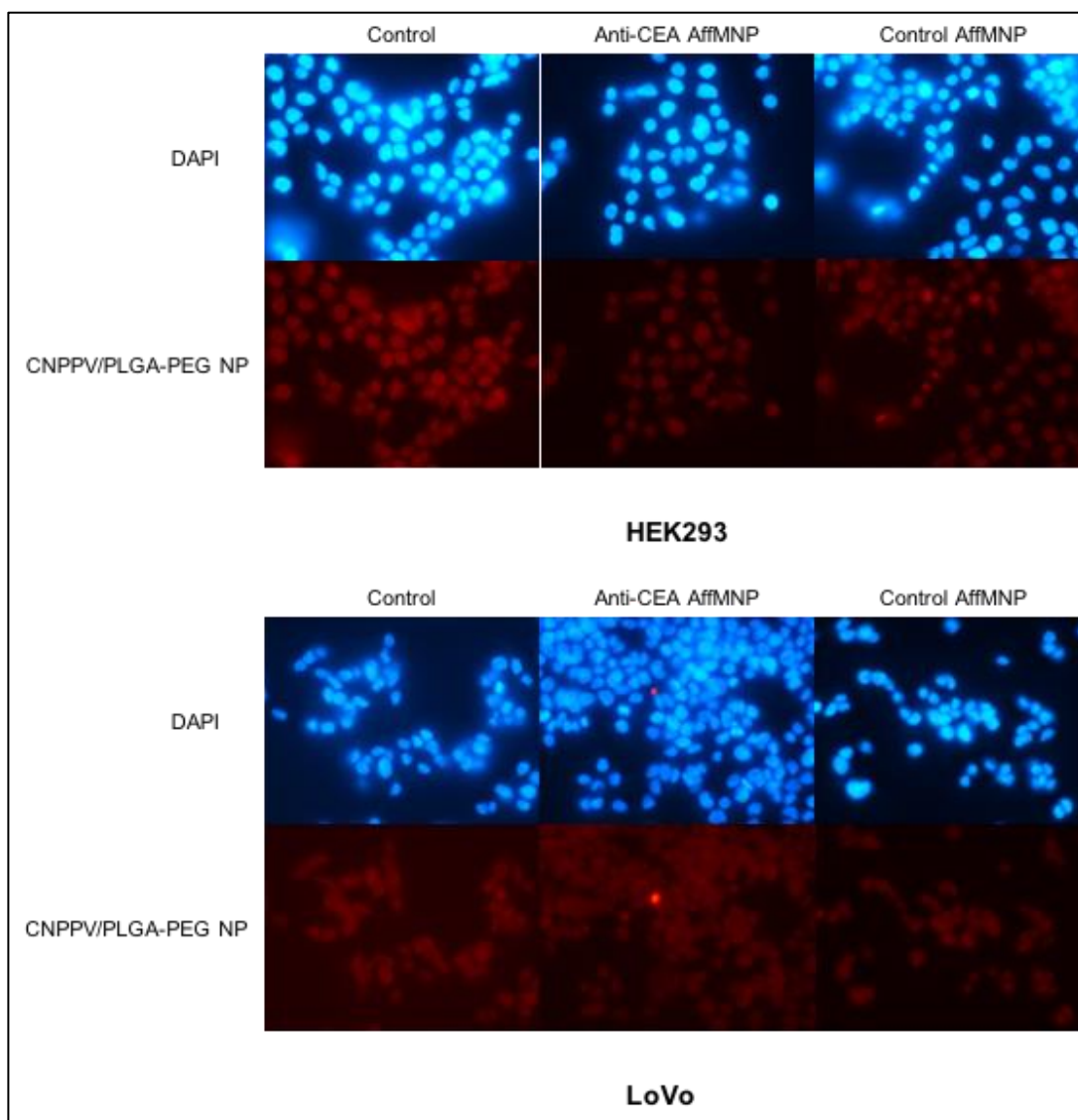


**Figure 6.22. Binding of target and control affimer-NP conjugates (AffMNP) on target and control cell lines using immunofluorescence on fixed cells.** Blue fluorescence is DAPI using DAPI filter. Red fluorescence is CN-PPV NP using 5-ALA filter. Magnification x63. Scalebar = 10  $\mu$ m. 0.5% skimmed milk blocking served as control. Images in this figure are representative of at least 3 independent experiments. See 2.4.5.3 of Materials and Methods for the detailed protocol. The presence of red fluorescence indicates target affimer-NP conjugates selectively bind to LoVo cells, not the control HEK293 cell line.

### 6.3 Discussion

The maleimide functional group contains a reactive imide functional group that can undergo an addition reaction with sulfhydryl groups to form a very stable thioether linkage(233) which cannot be broken under normal physiological conditions. Maleimide

also reacts ~1000 fold faster with sulfhydryl groups than with amine groups between pH 6.5-7.5 and is a popular choice for the conjugation of cysteine-containing compounds such as proteins(274). Chemical and structural stability with high degree of specificity and reactivity of this thioether bond are the reasons why maleimide was chosen in this research project as the terminal functional group for conjugating the targeting agents to CN-PPV/PLGA-PEG NPs. As discussed in 4.3, the reduction of antibodies to produce half-antibody fragments with free sulfhydryl groups was not a viable route for conjugation to maleimide functionalised NPs. Therefore, an alternative conjugation method through the potential use of a heterobifunctional crosslinker was assessed.

Heterobifunctional crosslinkers have different chemically reactive groups at each end of the molecular structure, that can bind to different functional groups on target proteins or macromolecules. This is especially useful for site-directed and orientated conjugation reactions(275). As previously discussed in 4.3, orientated conjugation between NPs and targeting agents is desirable to maintain the ability of targeting agents to effectively bind to their target antigens without compromised binding affinity. The heterobifunctional crosslinker, 3-(2-pyridyldithio)propionyl hydrazide (PDPH), was chosen for this project as previous studies have successfully shown that it can be used in the preparation of antibody conjugates for clinical applications(276).

One of the purposes of PDPH is to act as a thiolation reagent providing sulfhydryl functional groups for conjugation to oxidised glycoproteins(233). As shown in Figure 6.1, PDPH contains sulfhydryl-reactive pyridyldithiol and aldehyde-reactive hydrazide functional groups at either end of the molecule. Hydrazide functional groups will spontaneously react with oxidised glycoprotein side chains on antibodies forming stable hydrazone bonds. When the pyridyldithiol groups have been displaced, free sulfhydryl

groups become exposed and react with double bonds in maleimide functional groups subsequently forming thioether bonds.

The conjugation of both anti-CEA and anti-CD31 antibodies to maleimide functionalised CN-PPV/PLGA-PEG NPs through the use of the PDPH heterobifunctional crosslinker was investigated. Immunofluorescence studies were performed to confirm the binding of oxidised antibodies to PDPH. Neither the oxidised antibodies nor the heterobifunctional crosslinker are inherently fluorescent, therefore fluorescence in cells should only be observed if oxidised antibodies have successfully bound to PDPH which had been labelled with a maleimide functionalised green fluorescent dye. The presence of green fluorescence in target (LoVo) and both control (EA.hy926 and HEK293) cell lines incubated with anti-CEA antibody–dye labelled PDPH conjugates suggests that non-specific binding of conjugates to cells had occurred (Figure 6.2).

This is further confirmed in Figure 6.3, which shows non-specific binding of anti-CEA antibody–dye labelled PDPH conjugates to all cell lines despite bovine serum albumin being used to reduce the possibility of non-specific binding instead of 0.5% skimmed milk solution. The individual components of the conjugation process were then investigated in order to attempt to identify which part of the conjugate was responsible for the non-specific binding.

Figure 6.4 shows that in the presence of the DyLight™ 488 Maleimide dye, green fluorescence is seen on both the target and control cell lines. This occurs even when the DyLight™ dye's maleimide functional group is blocked by either PDPH or cysteine. Sulfhydryl groups are popular for conjugation as they are present in most proteins and are located in the side chains of the amino acid, cysteine(277–279). However, this could mean that the proteins within the cell surface membrane (i.e. tyrosine kinase receptors

such as the insulin and epidermal growth factor receptors, cell adhesion molecules and G protein coupled receptors such as the beta-2 adrenergic receptor) would be targets for any maleimide functional group. The findings depicted in Figure 6.4 could therefore represent the unintentional binding of unoccupied maleimide functional groups on the DyLight™ dye to these cell surface membrane bound proteins. The fluorescence seen with blocked DyLight™ 488 Maleimide dye and PDPH-DyLight™ 488 Maleimide dye conjugates are similar and less intense than fluorescence observed with the unblocked DyLight™ 488 Maleimide dye alone. This could indicate that molecules of DyLight™ dye had not been sufficiently saturated with either cysteine or PDPH, leaving unoccupied maleimide functional groups available to bind to the cell surface proteins. Figure 6.4 also shows that no fluorescence was seen with either the oxidised antibody alone nor the heterobifunctional crosslinker alone, confirming that neither of these are inherently fluorescent and are therefore not responsible for the aberrant fluorescence. Following this, the DyLight™ 488 Maleimide dye was no longer used for visualising the binding of antibody-PDPH to cells. The use of PDPH was continued in the antibody-NP conjugation process.

Figure 6.5 demonstrates that the optimal conjugation time for the PDPH crosslinker to bind to maleimide functionalised NPs was 30 minutes, therefore this was used in all subsequent experiments. After determining this step of the conjugation protocol, binding assays and immunofluorescence studies were carried out to confirm the conjugation of anti-CEA antibodies to 25% maleimide functionalised NPs (Figure 6.6 and Figure 6.7). Conjugation was found to be successful using this approach and therefore further assays and immunofluorescence studies were performed testing both the target (anti-CEA) and control (anti-CD31) antibody-NP conjugates against all three cell lines (LoVo, EA.hy926 and HEK293) (Figure 6.8 and Figure 6.9).

In theory, anti-CEA conjugates should only bind to CEA-positive LoVo cells and anti-CD31 conjugates should only bind to CD31-positive EA.hy926 cells. Neither antibody conjugates should bind to HEK293 cells. Figure 6.8 shows significant differences in fluorescence when the target (anti-CEA) and control (anti-CD31) antibody-NP conjugates are incubated with the target (LoVo) and control (EA.hy926 and HEK293) cell lines respectively. However, Figure 6.8 also shows significant differences in fluorescence when the target and control antibody-NP conjugates are incubated with their respective control cell lines indicating non-specific binding of both antibody-NP conjugates.

To investigate the cause of non-specific binding of antibody conjugates to their control cell lines different optimisation steps of the conjugation protocol were investigated (Figure 6.10 to Figure 6.16). Due to logistical reasons, only the target antibody-NP conjugate was used for the optimisation experiments as there was a limited supply of the target antibody and it was not financially prudent to use large quantities of the control antibody for optimisation purposes.

Firstly, different extraction methods to remove excess unbound oxidised anti-CEA antibodies were compared (Figure 6.10). Centrifugation was found to be the most effective method in removing excess oxidised anti-CEA antibody, thereby improving the binding of anti-CEA antibody-NP conjugates to LoVo cells by reducing the binding of free oxidised antibodies. This is in comparison to the use of no extraction methods where the low levels of difference in fluorescence between anti-CEA AbMNP/free unbound oxidised anti-CEA antibody mixture treated LoVo cells and cell media only LoVo cells were seen. This suggests that free oxidised anti-CEA antibodies are occupying cell surface CEA antigens and preventing the anti-CEA antibody-NP conjugates from being able to bind. Hydrazide functional groups in PDPH can react with free aldehyde groups if they are not occupied by oxidised glycoprotein side chains on antibodies. Therefore, unbonded

hydrazide functional groups could potentially and inadvertently react and bind to aldehyde groups found on glycoproteins within the extracellular domain of cell membranes, such as immunoglobulins(280). Therefore, the additional step of blocking unoccupied hydrazide functional groups with galactose was evaluated in the conjugation protocol (Figure 6.11). Non-specific binding of anti-CEA antibody-NP conjugates was seen on the two control cell lines. However, following the addition of galactose blocking to block unoccupied hydrazide functional groups a decrease in fluorescence was observed in both control cell lines. Although this did not improve specificity of anti-CEA antibody-NP conjugate binding to control cell lines, these findings indicate that unoccupied hydrazide functional groups on PDPH crosslinkers may partially be responsible for non-specific binding of anti-CEA antibody-NP conjugates to control cell lines. Furthermore, from the findings in Figure 6.11, the addition of galactose-mediated blocking reduced the ability of anti-CEA antibody-NP conjugates to bind to LoVo cells. The reasons for this phenomenon are currently unclear and did not offer a solution to improve antibody-NP conjugate binding specificity.

Next, the optimum incubation time for conjugation when oxidised anti-CEA antibodies and PDPH-MNP conjugates are mixed together was determined (Figure 6.12). No substantial improvements in reducing non-specific binding were found by altering the length of time the antibodies had to conjugate and bind to the PDPH-MNP conjugates. A minor difference was found between 1 and 2 hours, therefore for all subsequent experiments the antibodies were mixed with PDPH-MNP conjugates for 1 hour.

Following on, the next optimisation step was to assess whether increasing the amount of oxidised anti-CEA antibody in the conjugation mixture could improve the efficiency of the conjugation system. It was found that increasing the amount of anti-CEA antibody in the conjugation reaction did not improve anti-CEA antibody-NP conjugate binding to LoVo

cells and also did not decrease the non-specific binding of anti-CEA antibody-NP conjugates to control cell lines (Figure 6.13). The addition of galactose blocking agent to the increased anti-CEA antibody-NP conjugates was found to have further negatively impacted binding to LoVo cells, which is similar to the findings described above in the addition of galactose to block unoccupied hydrazide functional groups. In addition, galactose blocking of increased anti-CEA antibody-NP conjugates increased non-specific binding to control cell lines. Subsequently, increasing the amount of oxidised anti-CEA antibody in conjugation reactions was not considered.

The next optimisation step was to dilute the maleimide functionalised NPs used in conjugation reactions to assess whether this could improve the binding specificity of anti-CEA antibody-NP conjugates (Figure 6.14). The results contradict the findings in Figure 6.8. For every dilution of maleimide functionalised NPs used in this optimisation step, anti-CEA antibody-NP conjugates bound appropriately to LoVo cells with no significant binding to either of the two control cell lines. The only difference between the findings in Figure 6.8 and Figure 6.14 is the dilution of NPs. Therefore, it is not clear why specific binding was observed as the antibody-NP conjugates were only found to bind to LoVo cells. No significant difference in the intensity of fluorescence was measured between the different dilutions of the maleimide functionalised NPs. There was no clear advantage of diluting the MNPs in the conjugation process.

The next step that was investigated was the influence of post-conjugation reaction PBS wash cycles (Figure 6.15). PBS-mediated washing of cells is important to remove unbound antibody-NP conjugates and to reduce non-specific binding and fluorescence in control cell lines only. As shown in Figure 6.15, it was found that the number of wash cycles exceeding two washes reduced fluorescence intensities in LoVo and both control cell lines. It could be postulated that the reasons for this finding may be that the anti-CEA

antibody-NP conjugates were not effectively binding to CEA antigens on LoVo cells. The fluorescence observed in control cell lines could have possibly been due to the inadequate removal of conjugates from cells following PBS washes. Although in this research project I was unable to examine the influence of one wash cycle or the possible use of another washing agent such as Hank's Balanced Salt Solution. These are factors to consider for future *in vitro* antibody-NP conjugation experiments that could address the non-specific binding that has been observed.

Optimum conditions for incubation of anti-CEA antibody-NP conjugates on cell lines were also investigated (Figure 6.16). From the results, it is clear that overnight incubation at 37°C resulted in the best incubation conditions for antibody-NP conjugates on cells. However, non-specific binding was still present and observed in both control cell lines, even following the addition of galactose to block unoccupied hydrazide functional groups. As described above, the addition of galactose decreased the change in fluorescence seen when blocked anti-CEA antibody-NP conjugates were incubated with all three cell lines as compared to unblocked anti-CEA antibody-NP conjugates (Figure 6.11). The inclusion of overnight incubation at 37°C alongside galactose blocking further increased the change in fluorescence between blocked and unblocked antibody-NP conjugates.

All the antibody-NP optimisation steps described in this chapter are summarised in Table 6.1.

<b>Table 6.1. Summary of nanoparticle conjugation protocol optimisation steps</b>			
Optimisation step number	Optimisation parameter	Optimisation step outcome	Corresponding result
1	Extraction of unconjugated antibody post conjugation	Centrifugation is the optimal extraction method	Figure 6.10
2	Galactose-blockage of unoccupied hydrazide functional groups on PDPH	Decreased binding of target AbMNP to all 3 cell lines	Figure 6.11
3	Incubation time for conjugation of antibody and PDPH-MNP conjugate	No improvement on reducing non-specific binding between different times	Figure 6.12
4	Increasing the amount of antibody in conjugation reactions	No improvement on reducing non-specific binding between normal and increased amounts of antibody	Figure 6.13
5	Dilution of MNP in conjugation reactions	No effect on binding to different cell lines between the different dilutions	Figure 6.14
6	PBS wash cycles	Reduced fluorescence intensities with more than 2 wash cycles	Figure 6.15
7	Conditions for incubation of AbMNP to cell lines	Overnight at 37°C is the optimal incubation condition	Figure 6.16

The purpose of the different optimisation steps of the antibody-NP conjugation process was an attempt to elucidate factors involved in the non-specific binding and varying levels of fluorescence. Unfortunately, definitive evidence of any underlying cause has not been found during the scope of this research project.

One potential factor that could be causing non-specific binding is the PEGylation of CN-PPV/PLGA-PEG NPs. A disadvantage of NP PEGylation is that the steric hinderance and neutral surface charge, which helps PEGylated nanomedicines to evade MPS, can hinder extracellular interactions and reduce binding of the nanomedicines to target tissues and reduce intracellular uptake(281,282). A study by Woodle *et al.*(283) found that PEGylation of antibody-conjugated liposomes has an adverse effect on the antibody, preventing it from binding to its target antigen and the authors propose that alternative targeting agents such as peptides or oligosaccharides may improve binding to target tissues. Jokerst *et al.*(282) found that using functionalised PEG (such as succimide-, maleimide- or alkyne-functional groups) for conjugation to targeting agents could increase non-specific binding due to the electrical surface charges generated by the functional group on the terminal end of the PEG molecule. If the functional group causes the NP to become positively or, in particular, negatively charged, then the NP will non-specifically bind to protein structures(284). However, Schneider *et al.*(285) found that PEGylation of their antibody-NP conjugates reduced non-specific binding to cerebral extracellular matrix. Their study conjugated the monoclonal antibody, ITEM4, to PEGylated and non-PEGylated carboxylate-modified polystyrene NPs to actively target Fn14. Fn14 is a cell surface receptor that is upregulated in glioblastoma tumours. The authors tested both the non-PEGylated and PEGylated antibody-NP conjugates against rodent brain extracellular matrix components to determine whether non-specific binding was present. The non-PEGylated Fn14 antibody-NP bound irreversibly to the extracellular matrix components whereas minimal non-specific interactions between the PEGylated Fn14 antibody-NP conjugates and extracellular matrix components were observed.

Another potential cause for non-specific binding of antibody-NP conjugates is the physical shape of the NP, which may influence the specificity and affinity of the antibody's interactions with their target antigens. Barua *et al.*(286) compared the binding

of bare and Trastuzumab (anti-HER2 receptor monoclonal antibody)-coated antibody nanorods and nanospheres to HER2+ (BT-474 and SK-BR-3) and HER2- (MDA-MB-231) breast cancer cell lines. Their study showed that the Trastuzumab-coated antibody nanorods exhibited increased binding to the HER2+ cell lines and decreased binding to HER2- cell lines, as compared to the Trastuzumab-coated antibody nanospheres. This study demonstrated that nanomedicines of similar chemical properties but different physical and structural properties can substantially influence the binding of the nanomedicines to target cells and antigens.

During this research project, it was found that the average increase in fluorescence was 187% (range: 90% – 252%) when anti-CEA antibody-NP conjugates were incubated with CEA-positive LoVo cells as compared to cell media only treated cells, when accumulating the results for optimisation steps 1 to 5. However, for optimisation steps 6 and 7 the average increase in fluorescence was 37% (range: 16% - 49%).

Characterisation of the non-functionalised NP was conducted over time (refer to Figure 5.5) and there was no evidence of a decrease in the intensity of non-functionalised NP fluorescence. During this research project, non-functionalised NPs were stored in deionised distilled water and antibody-NP conjugates were stored in cell media solution. It would be interesting to observe the impact of the solutions used to store NPs on the absorption spectra of the functionalised CN-PPV/PLGA-PEG NPs over time.

The results depicted in Figure 6.8 exhibit little non-specific binding of the bare 25% maleimide functionalised NP to all three cell lines, which is in keeping with the results from previous non-specific binding experiments (refer to Figure 5.11 and Figure 5.12). Substantial increased fluorescence was observed when bare 25% maleimide functionalised NPs were incubated with the three cell lines (Figure 6.14). Similarly, significant increase in fluorescence, as compared to cell media only treated cells, was

also seen when bare 25% maleimide functionalised NPs were incubated in all cell lines for all optimisation experiments (Figure 6.11, Figure 6.12, Figure 6.13 and Figure 6.15). However, no increase in fluorescence was observed when bare streptavidin functionalised NPs were incubated with the three cell lines (Figure 6.17). Figure 6.16F also shows that there was significant increase in fluorescence when bare maleimide functionalised NPs were incubated with HEK293 cells overnight at 37°C.

As previously discussed in 5.3, other studies have observed the non-specific binding of NPs to cell lines. These studies have proposed that this could be due to negatively charged PEG(157), or the high lipid solubility of PEG enabling it to be absorbed into the cell surface membrane(269). Although it was not explored in this research project, the effect of PEG and the binding of bare 25% maleimide functionalised CN-PPV/PLGA-PEG NPs will need to be further investigated.

A possible reason for non-specific binding of the antibody-NP conjugates and bare maleimide functionalised NPs could be the maleimide functional groups. Excess or unoccupied functional groups can lead to increased non-specific binding(287). Although maleimide reactions are exclusive to sulfhydryl groups in the pH range 6.5-7.5, if the cell media environment become more basic in  $\text{pH} > 8$ , then the reactivity and likelihood of maleimide functional groups reacting with amine groups is significantly increased(233). The maleimide may then react with free amine groups on cell surface proteins. Some proteins within the cell surface membrane, such as the beta-2 adrenergic receptor and the epidermal growth factor receptor, have exposed free sulfhydryl groups(288) which may bind to unoccupied maleimide functional groups on antibody-NP conjugates leading to inappropriate and non-targeting agent mediated binding. Maleimide functional groups can also undergo hydrolysis (to an open maleamic acid form), rendering them unreactive to sulfhydryl groups(233) and preventing them from successfully conjugating NPs to

antibodies. To address this, the protein streptavidin, was bound to the CN-PPV/PLGA-PEG NPs and conjugated to biotinylated antibodies to evaluate whether this could improve this nanomedicine platform. The added benefit of using streptavidin functionalised NPs is that the heterobifunctional crosslinker, PDPH, is no longer required as streptavidin will bind to the biotinylated antibodies. The removal of PDPH will exclude unoccupied hydrazide groups on the PDPH crosslinker as a source of inappropriate and non-specific binding.

Figure 6.17 shows significant increase in fluorescence as compared to cell media only treated cells, when target (anti-CEA) and control (anti-CD31) antibody-streptavidin NP conjugates were incubated with the target and control cell lines respectively. However, Figure 6.17 also shows significant increase in fluorescence when the target and control antibody-streptavidin NP conjugates are incubated with their respective control cell lines, indicating inappropriate non-specific binding of both antibody-streptavidin functionalised NP conjugates. This is similar to the findings observed with maleimide functionalised antibody conjugates (Figure 6.8). These findings may represent unoccupied streptavidin functional groups on NPs reacting with proteins located on the cell surface membrane or potentially the same underlying disadvantages of PEGylation may be producing the inappropriate binding. The increase in fluorescence when anti-CEA antibody-streptavidin functionalised NP conjugates were incubated with LoVo cells was also low at 37%. This is in keeping with the increase in fluorescence seen in the latter optimisation steps with maleimide functionalised NP conjugates.

A different recognition molecule was then investigated to see if this could resolve some of the issues surrounding non-specific binding detailed above. The use of antibodies was substituted for affimers. Immunofluorescence of both the target (anti-CEA) and control (ySUMO) affimers was performed on the target (LoVo) and control (HEK293) cell lines

(Figure 6.18). The target affimer (anti-CEA III) was found to selectively bind to the target LoVo cell line. The control affimer was found to not bind to either the target or the control cell line. This demonstrated that the target and control affimers were suitable for further experiments. Two separate anti-CEA affimers (anti-CEA II and anti-CEA III) had been investigated with the recommendation that a mixture of the two affimers may be more specific. A previous research project (289), also undertaken at the University of Leeds, investigated the development and application of anti-CEA affimer-based biosensors. In this study, it was observed that a polyclonal antibody-based biosensor system expanded the range and affinity for CEA detection, as compared to a monoclonal antibody-based biosensor. Similarly, a heterogenous mixture of affimers incorporated into a biosensor system composed of three different anti-CEA affimer clones (anti-CEA I, anti-CEA II and anti-CEA III) had a similar detection range to the polyclonal antibody biosensor system.

Experiments were conducted to assess the ability of the target and control affimers to bind to the cell lines. Figure 6.19 shows that increase in fluorescence was greater when the target cell line was incubated with either anti-CEA III AffMNP or anti-CEAII/III AffMNP mixture, as compared to anti-CEA II AffMNP alone. There was also little non-specific binding of any of the target AffMNPs to the control cell line. The optimum incubation settings for AffMNP conjugates needed to be determined and for this the anti-CEA II/III AffMNP mixture was used. When exploring affimers for *in vivo* studies, the incubation temperatures reported in the literature are either at room temperature or 4-5°C(290). Figure 6.20 shows that the optimum incubation conditions for the anti-CEA II/III AffMNP mixture on LoVo and HEK293 cell lines was overnight at room temperature. However, only further slight increase in fluorescence was seen when the target AffMNP mixture was incubated overnight at room temperature compared to overnight at 4°C. The metabolic processes and enzyme viability of cells would be impaired at 4°C, therefore incubation at room temperature was chosen as this would help to preserve the normal

physiological function of cells. Selected target and control affimer-NP conjugates were tested against the target and control cell lines using the optimum incubation parameters. Figure 6.21 demonstrates that target affimer-NP conjugates selectively bound to LoVo cells. This could represent a more accurate and specific targeted fluorescent probe than the antibody-NP conjugates. Tiede *et al.*(290) compared antibody and affimer binding to VEGFR2 (vascular endothelial growth factor receptor-2, a key mediator in the formation of new blood vessels) in human pancreatic tissue. Immunohistochemical analysis found increased staining of VEGFR2 using affimer, as compared to antibody binding and staining of VEGFR2. The authors hypothesised that the smaller sizes of affimers enabled efficient tissue penetration, and the affimer's epitope (specific binding site of affimer on the receptor) may have been more readily accessible. Taken together, both of these factors may have allowed a larger number of affimers to bind to VEGFR2 as compared to the VEGFR2-targeting antibodies. Similar to this study, a similar comparison of anti-CEA antibody-NP and affimer-NP conjugates binding to target (LoVo) and control (HEK293 and EA.hy926) cell lines will need to be conducted to confirm which of the two recognition molecule bound NP systems is better.

In summary, this chapter details and describes the work that was done to identify and conjugate a suitable targeting agent to the fluorescent semi-conducting polymer (CN-PPV/PLGA-PEG) NPs. This was done in an effort to develop a fluorescent probe that can accurately target colorectal cancer cells. Despite both target (anti-CEA) and control (anti-CD31) antibodies being specific for the CEA and CD31 cell surface proteins, following conjugation to the MNP non-specific binding of both antibody-conjugates was observed. Despite taking optimisation steps towards eliminating non-specific binding no credible solution was found to address non-specific binding and differences in the change of fluorescence. Possible factors such as the binding of unoccupied maleimide functional groups, PEGylation of NPs, physical structure of NPs and storage conditions could have influenced the results. Streptavidin bound NPs were also investigated

however, similar non-specific binding was observed. Substituting antibodies for affimers showed more positive findings but requires further exploration.

## **Chapter Seven**

**Research summary, conclusion,  
limitations and future work**

## **7 Research summary, conclusion, limitations and future work**

### **7.1 Summary and conclusions**

One of the major and currently unmet challenges in colorectal cancer surgery is the accuracy in determining the status of sentinel lymph nodes with metastatic disease. This is vital in order to appropriately stratify the extent of surgical resection. One potential method that has been investigated to address this is the use of fluorescent probes during laparoscopic surgery, to intraoperatively visualise and detect lymph node metastases.

The aims of this research project were to 1) Evaluate the application of 5-aminolevulinic acid (5-ALA) mediated fluorescence in patients undergoing colorectal cancer surgery (GLiSten trial), 2) Evaluate CEA-targeting antibody and affimer for the development of a novel fluorescent probe, 3) Evaluate the semiconducting organic polymer CN-PPV as a fluorescent probe to detect colorectal cancer cells and 4) Test the binding of anti-CEA antibody/affimer-conjugated CN-PPV NPs in different cell types.

As detailed in Chapter 3, the GLiSten trial demonstrated that 5-ALA did not meet the sensitivity and specificity requirements to be used as an accurate fluorescent probe that could be used for fluorescent-guided colorectal cancer surgery. In addition, no significant differences in gene expression between fluorescent and non-fluorescent tumours were found, which requires further exploration. Using current technologies being applied in surgery, fluorescent-guided colorectal cancer surgery and the detection of lymph node metastases is feasible. A newer and more advanced fluorescent probe is required with high sensitivity and specificity for colorectal cancers that could improve the outcomes of colorectal cancer surgery.

In Chapter 4, both target (anti-CEA) and control (anti-CD31) antibodies showed specificity for their respective cell surface antigens. Initially, the preferred orientated and direct conjugation to maleimide functionalised NPs to enhance the antigen-binding ability of antibodies through producing half-antibody fragments, via reducing whole antibodies, was explored but found to be a non-viable option. An alternative conjugation strategy was sought after finding that the volume of half-antibody fragment generated was too low. For future work, alternative antibody reduction protocols or optimisation of the current protocol should be explored. In addition, the presence of the glycoprotein chain on the target anti-CEA antibody was confirmed. However, the location of the chain on the antibody was not determined. This will need to be undertaken to establish that the glycoprotein chain is not located within the antigen binding site. The direct binding of antibody-to-NP would eliminate the need for the heterobifunctional crosslinker.

The alternative conjugation pathway utilising heterobifunctional crosslinkers to conjugate maleimide functionalised NPs to oxidised antibodies proved to be feasible and allowed antibodies to retain antigen-specific binding. Similarly, the alternative targeting agents, anti-CEA (target) and  $\gamma$ -SUMO (control) affimers, were also found to be efficient in specifically binding to their respective antigens.

Chapter 5 details the characterisation of the CN-PPV/PLGA-PEG non-functionalised and maleimide functionalised NPs. With peak absorption and emission at 470nm and 650nm respectively (wide Stokes shift), these NPs are potential candidates for developing probes for fluorescent-guided surgery. Both non-functionalised and maleimide functionalised NPs also demonstrated physical stability over prolonged periods of time with no change in their optical properties. Maleimide functionalisation of NPs using light PEG chains also demonstrated efficient cellular uptake and stability in physical sizes and

absorbance/emission properties over time. Maleimide functionalised NPs were also found to induce very little cytotoxicity.

In Chapter 6, target and control antibodies were conjugated to maleimide functionalised CN-PPV/PLGA-PEG NPs using the heterobifunctional crosslinker, PDPH. Both antibody-NP conjugates bound to their respective target cell lines and antigens. However, non-specific binding of both target and control antibody-NP conjugates was also found. Optimisation of the antibody-NP conjugation protocol to address the non-specific binding was undertaken but a clear explanation for the underlying cause of non-specific binding was not found. An alternative conjugation strategy was investigated utilising streptavidin-functionalised NPs and biotinylated antibodies, but these antibody-streptavidin NP conjugates also demonstrated the same pattern of non-specific binding.

Finally, affimer-conjugated CN-PPV NPs were explored and found to bind to target cell lines with reduced non-specific binding to control cell lines. Affimer-conjugated CN-PPV NPs could potentially be more effective agents for the active targeting of colorectal cancer cells and aid fluorescence guided surgery.

## **7.2 Limitations of study**

During the characterisation of CN-PPV/PLGA-PEG NPs described in Chapter 5, the effects of centrifugation and repeated centrifugation following wash steps on the hydrodynamic diameter and emitted fluorescence of the MNP were investigated. It would be of interest to have conducted characterisation of these processed MNPs over time to examine changes in hydrodynamic diameters and fluorescence profiles over time.

In Chapter 6, the pattern of fluorescence observed when investigating the conjugation between the oxidised antibodies and the heterobifunctional crosslinker, PDPH, demonstrated non-specific binding to control cell lines. Other studies have suggested that the non-specific binding observed could have potentially been due to unoccupied maleimide functional groups on the DyLight™ 488 Maleimide dye that was used during experiments. Reduction of the PDPH crosslinker prior to conjugation to the DyLight™ 488 Maleimide dye will need to be investigated as well as investigating the effect of increasing the concentration of cysteine to further block any unoccupied maleimide functional groups. The 6<sup>th</sup> optimisation step assessed the impact of multiple wash cycles on the non-specific binding of antibody-NP conjugates. Less than two wash cycles (i.e. one wash or no washes) were not evaluated and therefore the full impact of the wash cycles cannot be assessed.

Another potential limitation of this research project was the PEGylation of the CN-PPV NPs. As discussed in Chapter 6, PEGylation can hinder the binding of targeted-NPs to their respective antigens. PEGylation can also create an electrical surface charge polarising the NP, leading to non-specific binding of the antibody-NP conjugate to cell surface proteins. This is supported by the similar pattern of non-specific binding seen when between maleimide and streptavidin functionalised antibody-NP conjugates. However, it is not known why this is contradicted by the lack of non-specific binding seen when the target affimer-NP conjugate was incubated with control cell lines.

### **7.3 Future work**

In this study, NP characterisation studies were carried out over time however, storage of the NPs was in an aqueous solution. It would be interesting to see whether there is any difference in the stability of the non-functionalised and maleimide functionalised NP over

time when stored in more physiologically representative solutions such as cell culturing medium and may give an explanation as to the variation seen in emitted fluorescence in Chapter 6. Further work also needs to be conducted in identifying the cause of the non-specific binding of bare maleimide-functionalised NPs seen in Chapter 6, contradicting the findings in Chapter 5. Determining whether there is any batch-to-batch variability in the PEG component of non-functionalised and maleimide functionalised NP, or if time-induced changes to PEG could be responsible for the non-specific binding and differences in emitted fluorescence seen in Chapter 6 is important.

With regards to optimising the antibody-NP conjugation process reduction of the PDPH heterobifunctional crosslinker, prior to conjugation to maleimide functionalised NPs would be an important step to investigate. In this study, blocking unoccupied hydrazide groups with galactose was conducted however, the blocking of unoccupied maleimide functional groups, using cysteine, should have also been investigated. The use of a different heterobifunctional crosslinker could also be investigated however, the direct conjugation of antibody-to-NP is ideal and would eliminate the need for a crosslinker. There is also an inherent disadvantage in using crosslinkers as this would not allow for a direct comparison between antibody-NP and affimer-NP conjugates. This was shown by Barua *et al.*(286), who demonstrated that the physical and structural properties of NPs can influence the ability of targeted NPs to bind to their antigens. It would also be of interest to investigate whether changes made to the shapes and structures of targeted CNPVV/PLGA-PEG NPs could influence their ability to specifically identify and bind to antigens. Smith *et al.*(291) demonstrated that increasing the concentration of functional groups on the surface of NPs enhanced the amount of protein binding to the NP. It would be of interest to test a range of NPs with varying concentrations of maleimide present on their surfaces to see if this had an impact on the antibody-NP conjugates ability to specifically bind to target antigens.

To summarise this research project, fluorescent guided surgery is a viable strategy in stratifying the extent of resection in colorectal cancer patients on the basis of their lymph node status if an accurate, sensitive fluorescent probe can be developed. Transitioning away from the conventional 5-ALA, the NP investigated in this study fulfils the requirements of a clinical fluorescent probe however, it requires modification with a suitable CEA-targeting agent to enable it to actively target colorectal cancers. Different conjugation strategies have been employed to create a specific antibody-NP conjugate. However, further work is required to optimise this system. Affimer-NP conjugate appears to be a more promising candidate as a fluorescent probe and additional work should be undertaken to continue developing this through pre-clinical studies (both *in vitro* and *in vivo*) and progression towards potential clinical use in the future.

## References

## 8 References

1. Cancer Research UK. Bowel cancer statistics [Internet]. Available from: <https://www.cancerresearchuk.org/health-professional/cancer-statistics/statistics-by-cancer-type/bowel-cancer>
2. Public Health England. Cancer survival in England: national estimates for patients followed up to 2017 [Internet]. Office of National statistics. 2019. Available from: <https://www.ons.gov.uk/peoplepopulationandcommunity/healthandsocialcare/conditionsanddiseases/bulletins/cancersurvivalinengland/stageatdiagnosisandchildhoodpatientsfollowedupto2018>
3. National Institute for Health and Care Excellence. Colorectal cancer: the diagnosis and management of colorectal cancer [Internet]. NICE Pathways. 2011. Available from: <https://www.nice.org.uk/guidance/cg131>
4. Knowles B. Colorectal Cancer Pathways : Interim Report [Internet]. 2016. Available from: [https://www.cancerresearchuk.org/sites/default/files/colorectal\\_pathways\\_interim\\_report\\_v2.pdf](https://www.cancerresearchuk.org/sites/default/files/colorectal_pathways_interim_report_v2.pdf)
5. National Institute for Health and Care Excellence. Colorectal Cancer Overview [Internet]. NICE Guidance. Available from: <https://www.nice.org.uk/guidance/qs20>
6. National Institute for Health and Care Excellence. Managing local colorectal tumours - NICE Pathways [Internet]. NICE Pathways. 2015. Available from: <http://pathways.nice.org.uk/pathways/colorectal-cancer/managing-local-colorectal-tumours#content=view-node:nodes-surgery-to-remove-resectable-tumours>

7. National Institute for Health and Care Excellence. Laparoscopic surgery for colorectal cancer [Internet]. NICE Pathways. 2006. Available from: <https://www.nice.org.uk/guidance/ta105>
8. National Institute for Health and Care Excellence. Managing advanced and metastatic colorectal cancer [Internet]. NICE Pathways. 2015. Available from: <https://pathways.nice.org.uk/pathways/colorectal-cancer#path=view%3A/pathways/colorectal-cancer/managing-advanced-and-metastatic-colorectal-cancer.xml&content=view-index>
9. Andrew H, Gossedge G, Croft J, Corrigan N, Brown JM, West N, et al. Next Generation intraoperative Lymph node staging for Stratified colon cancer surgery (GLiSten): a multicentre, multinational feasibility study of fluorescence in predicting lymph node-positive disease. *Effic Mech Eval*. 2016;
10. Farinella E, Viganò L, Fava MC, Mineccia M, Bertolino F, Capussotti L. In vivo lymph node mapping and pattern of metastasis spread in locally advanced mid/low rectal cancer after neoadjuvant chemoradiotherapy. *Int J Colorectal Dis*. 2013;
11. Kato S, Kawamura J, Kawada K, Hasegawa S, Sakai Y. Fluorescence diagnosis of metastatic lymph nodes using 5-aminolevulinic acid (5-ALA) in a mouse model of colon cancer. *J Surg Res*. 2012;
12. Hirche C, Mohr Z, Kneif S, Doniga S, Murawa D, Strik M, et al. Ultrastaging of colon cancer by sentinel node biopsy using fluorescence navigation with indocyanine green. *Int J Colorectal Dis*. 2012;27(3):319–24.
13. Albayrak Y, Ören D, Du CG, KURT A, OREN D, GUNDOGDU C, et al. Intraoperative sentinel lymph node mapping in patients with colon cancer: Study of 38 cases. *Turkish J Gastroenterol*. 2011;22(3):286–92.

14. Morton DL, Wen D-RR, Wong JH, Economou JS, Cagle L a, Storm FK, et al. Technical details of intraoperative lymphatic mapping for early stage melanoma. Morton et al 1992. Arch Surg [Internet]. 2005;127(4):1–8. Available from: papers2://publication/uuid/909C8E05-3488-4700-8FD3-620D497CCA82
15. Bao F, Zhao LY, Balde AI, Liu H, Yan J, Li TT, et al. Prognostic impact of lymph node skip metastasis in Stage III colorectal cancer. Color Dis. 2016;18(9):O322–9.
16. Tiernan JP, Ingram N, Marston G, Perry SL, Rushworth J V., Coletta PL, et al. CEA-targeted nanoparticles allow specific in vivo fluorescent imaging of colorectal cancer models. Nanomedicine. 2015;
17. Emmanuel A, Haji A. Complete mesocolic excision and extended (D3) lymphadenectomy for colonic cancer: is it worth that extra effort? A review of the literature. Int J Colorectal Dis. 2016;31(4):797–804.
18. Søndena K, Quirke P, Hohenberger W, Sugihara K, Kobayashi H, Kessler H, et al. The rationale behind complete mesocolic excision (CME) and a central vascular ligation for colon cancer in open and laparoscopic surgery: Proceedings of a consensus conference. Int J Colorectal Dis. 2014;29(4):419–28.
19. Hohenberger W, Weber K, Matzel K, Papadopoulos T, Merkel S. Standardized surgery for colonic cancer: Complete mesocolic excision and central ligation - Technical notes and outcome. Color Dis. 2009;11(4):354–64.
20. Kontovounisios C, Kinross J, Tan E, Brown G, Rasheed S, Tekkis P. Complete mesocolic excision in colorectal cancer: A systematic review. Color Dis. 2015;

21. West NP, Kobayashi H, Takahashi K, Perrakis A, Weber K, Hohenberger W, et al. Understanding optimal colonic cancer surgery: Comparison of Japanese D3 resection and european complete mesocolic excision with central vascular ligation. *J Clin Oncol*. 2012;30(15):1763–9.
22. Bertelsen CA, Neuenschwander AU, Jansen JE, Wilhelmsen M, Kirkegaard-Klitbo A, Tenma JR, et al. Disease-free survival after complete mesocolic excision compared with conventional colon cancer surgery: a retrospective, population-based study. *Lancet Oncol* [Internet]. 2015 Feb;16(2):161–8. Available from: <https://linkinghub.elsevier.com/retrieve/pii/S1470204514711684>
23. West NP, Hohenberger W, Weber K, Perrakis A, Finan PJ, Quirke P. Complete mesocolic excision with central vascular ligation produces an oncologically superior specimen compared with standard surgery for carcinoma of the colon. *J Clin Oncol*. 2010;28(2):272–8.
24. Bertelsen CA, Neuenschwander AU, Jansen JE, Wilhelmsen M, Kirkegaard-Klitbo A, Tenma JR, et al. Disease-free survival after complete mesocolic excision compared with conventional colon cancer surgery: a retrospective, population-based study. *Lancet Oncol* [Internet]. 2015 Feb;16(2):161–8. Available from: <http://dx.doi.org/10.1016/>
25. Chang GJ, Rodriguez-Bigas MA, Skibber JM, Moyer VA. Lymph node evaluation and survival after curative resection of colon cancer; Systematic review. *J Natl Cancer Inst*. 2007;99:433–41.
26. Saha S, Seghal R, Patel M, Doan K, Dan A, Bilchik A, et al. A multicenter trial of sentinel lymph node mapping in colorectal cancer: Prognostic implications for nodal staging and recurrence. *Am J Surg*. 2006;191(3):305–10.
27. Rosenberg J, Fischer A, Haglind E. Current controversies in colorectal

surgery: The way to resolve uncertainty and move forward. *Color Dis.* 2012;14(3):266–9.

28. Bertelsen CA, Bols B, Ingeholm P, Jansen JE, Neuenschwander AU, Vilandt J. Can the quality of colonic surgery be improved by standardization of surgical technique with complete mesocolic excision? *Color Dis.* 2011;
29. Killeen S, Mannion M, Devaney A, Winter DC. Complete mesocolic resection and extended lymphadenectomy for colon cancer: A systematic review. *Color Dis.* 2014;
30. Willaert W, Mareel M, Van De Putte D, Van Nieuwenhove Y, Pattyn P. Lymphatic spread, nodal count and the extent of lymphadenectomy in cancer of the colon. *Cancer Treat Rev.* 2014;40:405–13.
31. Llamas-Elvira JM, Rodríguez-Fernández A, Gutiérrez-Sáinz J, Gomez-Rio M, Bellon-Guardia M, Ramos-Font C, et al. Fluorine-18 fluorodeoxyglucose PET in the preoperative staging of colorectal cancer. *Eur J Nucl Med Mol Imaging.* 2007;34(6):859–67.
32. Amin MB, Edge S, Greene F, Byrd DR, Brookland RK, Washington MK, et al., editors. *AJCC Cancer Staging Manual*. 8th ed. Springer International Publishing; 2017.
33. Dighe S, Blake H, Koh M-D, Swift I, Arnaout A, Temple L, et al. Accuracy of multidetector computed tomography in identifying poor prognostic factors in colonic cancer. *Br J Surg [Internet]*. 2010;97(9):1407–15. Available from: <http://doi.wiley.com/10.1002/bjs.7096>
34. Dighe S, Purkayastha S, Swift I, Tekkis PP, Darzi A, A'Hern R, et al. Diagnostic precision of CT in local staging of colon cancers: A meta-analysis. *Clin Radiol.* 2010;65(9):708–19.
35. Burt BM, Humm JL, Kooby DA, Squire OD, Mastorides S, Larson SM. Using

Positron Emission Tomography with [ 18 F ] FDG to Predict Tumor Behavior in Experimental Colorectal Cancer 1. *Neoplasia*. 2001;3(3):189–95.

36. Dighe S, Swift I, Magill L, Handley K, Gray R, Quirke P, et al. Accuracy of radiological staging in identifying high-risk colon cancer patients suitable for neoadjuvant chemotherapy: A multicentre experience. *Color Dis*. 2012;14(4):438–44.
37. Morton DL, Wen DR, Wong JH, Economou JS, Cagle LA, Storm FK, et al. Technical Details of Intraoperative Lymphatic Mapping for Early Stage Melanoma. *Arch Surg [Internet]*. 1992 Apr 1;127(4):392–9. Available from: <http://archsurg.jamanetwork.com/article.aspx?doi=10.1001/archsurg.1992.01420040034005>
38. Miyashiro I, Hiratsuka M, Kishi K, Takachi K, Yano M, Takenaka A, et al. Intraoperative diagnosis using sentinel node biopsy with indocyanine green dye in gastric cancer surgery: An institutional trial by experienced surgeons. *Ann Surg Oncol*. 2013;20(2):542–6.
39. Matsuda T, Takeuchi H, Tsuwano S, Nakahara T, Mukai M, Kitagawa Y. Sentinel node mapping in adenocarcinoma of the esophagogastric junction. *World J Surg*. 2014;38(9):2337–44.
40. Niu C, Wang Z, Zuo G, Krupka TM, Ran H, Zhang P, et al. Poly(Lactide-Co-Glycolide) ultrasonographic microbubbles carrying sudan black for preoperative and intraoperative localization of lymph nodes. *Clin Breast Cancer*. 2012;12(3):199–206.
41. PureFireCa.com. Treating Early Stage Invasive Breast Carcinoma [Internet]. [www.medicallook.com](http://www.medicallook.com). [cited 2019 Jun 15]. Available from: [http://www.medicallook.com/tests/Sentinel\\_node\\_biopsy.html](http://www.medicallook.com/tests/Sentinel_node_biopsy.html)
42. ClinicalGate. Intra-operative picture of axillary sentinel lymph node biopsy

[Internet]. Available from: <https://clinicalgate.com/the-axilla-current-management-including-sentinel-node-and-lymphoedema/>

43. Association of Breast Surgery at. Surgical guidelines for the management of breast cancer. *Eur J Surg Oncol* [Internet]. 2009;35:S1–22. Available from: <http://linkinghub.elsevier.com/retrieve/pii/S0748798309000274>
44. Chan SH, Ng C, Looi LM. Intraoperative methylene blue sentinel lymph node mapping in colorectal cancer. *ANZ J Surg*. 2008;78(9):775–9.
45. Bembenek AE, Rosenberg R, Wagler E, Gretschel S, Sandler A, Siewert J-RR, et al. Sentinel Lymph Node Biopsy in Colon Cancer: A Prospective Multicenter Trial. *Ann Surg*. 2007;245(6):858–63.
46. Bilchik AJ, Nora DT, Sobin LH, Turner RR, Trocha S, Krasne D, et al. Effect of lymphatic mapping on the new tumor-node-metastasis classification for colorectal cancer. *J Clin Oncol*. 2003;21(4):668–72.
47. Saha S, Johnston G, Korant A, Shaik M, Kanaan M, Johnston R, et al. Aberrant drainage of sentinel lymph nodes in colon cancer and its impact on staging and extent of operation. *Am J Surg*. 2013;205(3):302–6.
48. Cozzaglio L, Bottura R, Di Rocco M, Gennari L, Doci R. Sentinel lymph node biopsy in gastric cancer: possible applications and limits. *Eur J Surg Oncol* [Internet]. 2011;37(1):55–9. Available from: <http://www.ncbi.nlm.nih.gov/pubmed/21115231>
49. Ishizaki M, Kurita A, Kubo Y, Takashima S, Nishina T, Nishimura E. Evaluation of sentinel node identification with isosulfan blue in gastric cancer. *Eur J Surg Oncol*. 2006;32(2):191–6.
50. Bianchi PP, Petz W, Casali L. Laparoscopic lymphatic roadmapping with blue dye and radioisotope in colon cancer. *Color Dis*. 2011;
51. Retter SM, Herrmann G, Schiedeck THK. Clinical value of sentinel node

mapping in carcinoma of the colon. *Color Dis* [Internet]. 2011 Aug;13(8):855–9. Available from: <http://doi.wiley.com/10.1111/j.1463-1318.2010.02293.x>

52. Park JS, Chang IT, Park SJ, Kim BG, Choi YS, Cha SJ, et al. Comparison of ex vivo and in vivo injection of blue dye in sentinel lymph node mapping for colorectal cancer. *World J Surg*. 2009;33(3):539–46.
53. Wang S, Zhang Q, Luo XF, Li J, He H, Yang F, et al. Magnetic graphene-based nanotheranostic agent for dual-modality mapping guided photothermal therapy in regional lymph nodal metastasis of pancreatic cancer. *Biomaterials*. 2014;35(35):9473–83.
54. Kim HJ, Choi G-S. Clinical Implications of Lymph Node Metastasis in Colorectal Cancer: Current Status and Future Perspectives. *Ann Coloproctol*. 2019;35(3):109–17.
55. Quadros CA, Lopes A, Araújo I. Retroperitoneal and lateral pelvic lymphadenectomy mapped by lymphoscintigraphy for rectal adenocarcinoma staging. *Jpn J Clin Oncol*. 2010;40(8):746–53.
56. Van Der Zaag ES, Bouma WH, Tanis PJ, Ubbink DT, Bemelman WA, Buskens CJ. Systematic review of sentinel lymph node mapping procedure in colorectal cancer. Vol. 19, *Annals of Surgical Oncology*. 2012. p. 3449–59.
57. Mulsow J, Winter DC, O’Keane JC, O’Connell PR. Sentinel lymph node mapping in colorectal cancer. Vol. 90, *British Journal of Surgery*. 2003. p. 659–67.
58. Cahill RA. What’s wrong with sentinel node mapping in colon cancer? *World J Gastroenterol* [Internet]. 2007 Dec 21;13(47):6291. Available from: <http://www.ncbi.nlm.nih.gov/pubmed/18081216>

59. National Institute for Health and Care Excellence. OSNA for colon cancer staging [Internet]. NICE Guidance. 2016. Available from: <https://www.nice.org.uk/advice/mib77>
60. Tamaki Y. One-step nucleic acid amplification (OSNA): where do we go with it? *Int J Clin Oncol*. 2017;22(1):3–10.
61. Güller U, Zettl A, Worni M, Langer I, Cabalzar-Wondberg D, Viehl CT, et al. Molecular investigation of lymph nodes in colon cancer patients using one-step nucleic acid amplification (OSNA): A new road to better staging? *Cancer*. 2012;118(24):6039–45.
62. Croner RS, Geppert CI, Bader FG, Nitsche U, Späth C, Rosenberg R, et al. Molecular staging of lymph node-negative colon carcinomas by one-step nucleic acid amplification (OSNA) results in upstaging of a quarter of patients in a prospective, European, multicentre study. *Br J Cancer*. 2014;110(10):2544–50.
63. Vogelaar FJ, Reimers MS, van der Linden RLA, van der Linden JC, Smit VTHBM, Lips DJ, et al. The Diagnostic Value of One-Step Nucleic acid Amplification (OSNA) for Sentinel Lymph Nodes in Colon Cancer Patients. *Ann Surg Oncol*. 2014;21(12):3924–30.
64. Yamamoto H, Tomita N, Inomata M, Furuhashi T, Miyake Y, Noura S, et al. OSNA-Assisted Molecular Staging in Colorectal Cancer: A Prospective Multicenter Trial in Japan. *Ann Surg Oncol*. 2016;23(2):391–6.
65. Rosenberg R, Friederichs J, Gertler R, Hoos A, Mueller J, Nahrig J, et al. Prognostic evaluation and review of immunohistochemically detected disseminated tumor cells in peritumoral lymph nodes of patients with pN0 colorectal cancer. *Int J Colorectal Dis [Internet]*. 2004 Sep 10;19(5):430–7. Available from: <http://link.springer.com/10.1007/s00384-003-0559-z>

66. Robertson CA, Evans DH, Abrahamse H. Photodynamic therapy (PDT): A short review on cellular mechanisms and cancer research applications for PDT. *J Photochem Photobiol B Biol.* 2009;96(1):1–8.
67. Contributors W. Fluorescence [Internet]. Wikipedia, The Free Encyclopedia. 2020. Available from: <https://en.wikipedia.org/wiki/Fluorescence>
68. Berg K. Photosensitizers in Medicine [Internet]. 2009. Available from: <http://photobiology.info/Berg.html>
69. Abrahamse H, Hamblin MR. New photosensitizers for photodynamic therapy. *Biochem J* [Internet]. 2016 Feb 15;473(4):347–64. Available from: <https://www.ncbi.nlm.nih.gov/pubmed/26862179>
70. Lakowicz JR. Introduction to Fluorescence. In: *Principles of Fluorescence Spectroscopy* [Internet]. Boston, MA: Springer US; 1999. p. 1–23. Available from: [https://doi.org/10.1007/978-1-4757-3061-6\\_1](https://doi.org/10.1007/978-1-4757-3061-6_1)
71. Mamontova A V, Grigoryev AP, Tsarkova AS, Lukyanov KA, Bogdanov AM. Struggle for photostability: Bleaching mechanisms of fluorescent proteins. *Russ J Bioorganic Chem* [Internet]. 2017 Nov;43(6):625–33. Available from: <https://doi.org/10.1134/S1068162017060085>
72. Cohen S, Pellach M, Kam Y, Grinberg I, Corem-Salkmon E, Rubinstein A, et al. Synthesis and characterization of near IR fluorescent albumin nanoparticles for optical detection of colon cancer. *Mater Sci Eng C.* 2013;33(2):923–31.
73. Stokes GG. 1853. On the Change of Refrangibility of Light and the exhibition thereby of the Chemical Rays. In: Stokes GG, editor. *Mathematical and Physical Papers* [Internet]. Cambridge: Cambridge University Press; 2009. p. 22–9. (Cambridge Library Collection - Mathematics; vol. 4). Available from:

<https://www.cambridge.org/core/books/mathematical-and-physical-papers/1853-on-the-change-of-refrangibility-of-light-and-the-exhibition-thereby-of-the-chemical-rays/925396AE7AB2CEAF702C09A4D0D29750>

74. Reisch A, Klymchenko AS. Fluorescent Polymer Nanoparticles Based on Dyes: Seeking Brighter Tools for Bioimaging. *Small*. 2016;12(15):1968–92.
75. Frank D, Tyagi C, Tomar L, Choonara YE, du Toit LC, Kumar P, et al. Overview of the role of nanotechnological innovations in the detection and treatment of solid tumors. *Int J Nanomedicine*. 2014;9(1):589–613.
76. Surre J, Saint-Ruf C, Collin V, Orenca S, Ramjeet M, Matic I. Strong increase in the autofluorescence of cells signals struggle for survival. *Sci Rep [Internet]*. 2018;8(1):12088. Available from: <https://doi.org/10.1038/s41598-018-30623-2>
77. Gao S, Chen D, Li Q, Ye J, Jiang H, Amatore C, et al. Near-infrared fluorescence imaging of cancer cells and tumors through specific biosynthesis of silver nanoclusters. *Sci Rep [Internet]*. 2014 Mar 17;4:4384. Available from: <https://doi.org/10.1038/srep04384>
78. Owens E, Henary M, El Fakhri G, Soo Choi H. Tissue-Specific Near-Infrared Fluorescence Imaging. *Acc Chem Res*. 2016;49(9):1731–40.
79. Khot MI, Downey CL, Armstrong G, Svavarsdottir HS, Jarral F, Andrew H, et al. The role of ABCG2 in modulating responses to anti-cancer photodynamic therapy. *Photodiagnosis Photodyn Ther [Internet]*. 2020 Mar;29(August):101579. Available from: <https://linkinghub.elsevier.com/retrieve/pii/S1572100019304247>
80. Krammer B, Plaetzer K. ALA and its clinical impact, from bench to bedside. *Photochem Photobiol Sci*. 2008;7(3):283–9.
81. Liu Y, Ma K, Jiao T, Xing R, Shen G, Yan X. Water-insoluble photosensitizer

nanocolloids stabilized by supramolecular interfacial assembly towards photodynamic therapy. *Sci Rep.* 2017;7(February):1–8.

82. Castano AP, Demidova TN, Hamblin MR. Mechanisms in photodynamic therapy: Part one - Photosensitizers, photochemistry and cellular localization. Vol. 1, *Photodiagnosis and Photodynamic Therapy.* 2004. p. 279–93.
83. Patel RH, Wadajkar AS, Patel NL, Kavuri VC, Nguyen KT, Liu H. Multifunctionality of indocyanine green-loaded biodegradable nanoparticles for enhanced optical imaging and hyperthermia intervention of cancer. *J Biomed Opt.* 2012;17(4):046003.
84. Liberale G, Vankerckhove S, Galdon MG, Donckier V, Larsimont D, Bourgeois P. Fluorescence imaging after intraoperative intravenous injection of indocyanine green for detection of lymph node metastases in colorectal cancer. *Eur J Surg Oncol.* 2015;41(9):1256–60.
85. Baiocchi GL, Diana M, Boni L. Indocyanine green-based fluorescence imaging in visceral and hepatobiliary and pancreatic surgery: State of the art and future directions. *World J Gastroenterol.* 2018;24(27):2921–2840.
86. Fujiwara M, Mizukami T, Suzuki A, Fukamizu H. Sentinel lymph node detection in skin cancer patients using real-time fluorescence navigation with indocyanine green: preliminary experience. *J Plast Reconstr Aesthetic Surg [Internet].* 2009 Oct 1 [cited 2018 Aug 15];62(10):e373–8. Available from: <https://www.sciencedirect.com/science/article/pii/S1748681508003434>
87. Hirche C, Dresel S, Krempien R, Hünerbein M. Sentinel node biopsy by indocyanine green retention fluorescence detection for inguinal lymph node staging of anal cancer: Preliminary experience. *Ann Surg Oncol.* 2010;17(9):2357–62.

88. Hirche C, Murawa D, Mohr Z, Kneif S, Hünerbein M. ICG fluorescence-guided sentinel node biopsy for axillary nodal staging in breast cancer. *Breast Cancer Res Treat* [Internet]. 2010 Jun;121(2):373–8. Available from: <https://doi.org/10.1007/s10549-010-0760-z>
89. Tajima Y, Murakami M, Yamazaki K, Masuda Y, Kato M, Sato A, et al. Sentinel node mapping guided by indocyanine green fluorescence imaging during laparoscopic surgery in gastric cancer. *Ann Surg Oncol*. 2010;17(7):1787–93.
90. Watanabe J, Ota M, Suwa Y, Ishibe A, Masui H, Nagahori K. Real-time indocyanine green fluorescence imaging-guided complete mesocolic excision in laparoscopic flexural colon cancer surgery. *Dis Colon Rectum*. 2016;59(7):701–5.
91. Watanabe J, Ota M, Suwa Y, Ishibe A, Masui H, Nagahori K. Evaluation of lymph flow patterns in splenic flexural colon cancers using laparoscopic real-time indocyanine green fluorescence imaging. *Int J Colorectal Dis*. 2017;32(2):201–7.
92. Currie AC, Brigid A, Thomas-Gibson S, Suzuki N, Moorghen M, Jenkins JT, et al. A pilot study to assess near infrared laparoscopy with indocyanine green (ICG) for intraoperative sentinel lymph node mapping in early colon cancer. *Eur J Surg Oncol* [Internet]. 2017;43(11):2044–51. Available from: <https://doi.org/10.1016/j.ejso.2017.05.026>
93. Emile SH, Elfeki H, Shalaby M, Sakr A, Sileri P, Laurberg S, et al. Sensitivity and specificity of indocyanine green near-infrared fluorescence imaging in detection of metastatic lymph nodes in colorectal cancer: Systematic review and meta-analysis. *J Surg Oncol* [Internet]. 2017 Nov;116(6):730–40. Available from: <http://doi.wiley.com/10.1002/jso.24701>
94. Cahill RA, Anderson M, Wang LM, Lindsey I, Cunningham C, Mortensen NJ.

- Near-infrared (NIR) laparoscopy for intraoperative lymphatic road-mapping and sentinel node identification during definitive surgical resection of early-stage colorectal neoplasia. *Surg Endosc Other Interv Tech.* 2012;
95. Yuasa Y, Seike J, Yoshida T, Takechi H, Yamai H, Yamamoto Y, et al. Sentinel lymph node biopsy using intraoperative indocyanine green fluorescence imaging navigated with preoperative CT lymphography for superficial esophageal cancer. *Ann Surg Oncol.* 2012;19(2):486–93.
  96. Rink M, Babjuk M, Catto JWF, Jichlinski P, Shariat SF, Stenzl A, et al. Hexyl aminolevulinate-guided fluorescence cystoscopy in the diagnosis and follow-up of patients with non-muscle-invasive bladder cancer: A critical review of the current literature. Vol. 64, *European Urology.* 2013. p. 624–38.
  97. Burger M, Stief CG, Zaak D, Stenzl A, Wieland WF, Jocham D, et al. Hexaminolevulinate Is Equal to 5-Aminolevulinic Acid Concerning Residual Tumor and Recurrence Rate Following Photodynamic Diagnostic Assisted Transurethral Resection of Bladder Tumors. *Urology.* 2009;74(6):1282–6.
  98. Schumacher MC, Holmäng S, Davidsson T, Friedrich B, Pedersen J, Wiklund NP. Transurethral Resection of Non-Muscle-Invasive Bladder Transitional Cell Cancers With or Without 5-Aminolevulinic Acid Under Visible and Fluorescent Light: Results of a Prospective, Randomised, Multicentre Study. *Eur Urol.* 2010;57(2):293–9.
  99. Hillemanns P, Weingandt H, Stepp H, Baumgartner R, Xiang W, Korell M. Assessment of 5-aminolevulinic acid-induced porphyrin fluorescence in patients with peritoneal endometriosis. *Am J Obstet Gynecol.* 2000;183(1):52–7.
  100. Löning M, Diddens H, Küpker W, Diedrich K, Hüttmann G. Laparoscopic Fluorescence Detection of Ovarian Carcinoma Metastases Using 5-Aminolevulinic Acid-Induced Protoporphyrin IX. *Cancer.* 2004;100(8):1650–

- 6.
101. Stummer W, Pichlmeier U, Meinel T, Wiestler OD, Zanella F, Reulen H-J. Fluorescence-guided surgery with 5-aminolevulinic acid for resection of malignant glioma: a randomised controlled multicentre phase III trial. *Lancet Oncol* [Internet]. 2006 May;7(5):392–401. Available from: <https://linkinghub.elsevier.com/retrieve/pii/S1470204506706659>
102. Stummer W, Tonn J-C, Mehdorn HM, Nestler U, Franz K, Goetz C, et al. Counterbalancing risks and gains from extended resections in malignant glioma surgery: a supplemental analysis from the randomized 5-aminolevulinic acid glioma resection study. *J Neurosurg* [Internet]. 2011;114(3):613–23. Available from: <http://thejns.org/doi/10.3171/2010.3.JNS097>
103. Barone DG, Lawrie TA, Hart MG. Image guided surgery for the resection of brain tumours. *Cochrane database Syst Rev* [Internet]. 2014 Jan 28;2014(1):CD009685. Available from: <http://doi.wiley.com/10.1002/14651858.CD009685.pub2>
104. Moesta KT, Ebert B, Handke T, Nolte D, Nowak C, Haensch WE, et al. Protoporphyrin IX Occurs Naturally in Colorectal Cancers and Their Metastases Protoporphyrin IX Occurs Naturally in Colorectal Cancers and Their Metastases 1. *Cancer Res*. 2001;61:991–9.
105. Regula J, MacRobert AJ, Gorchein A, Buonaccorsi GA, Thorpe SM, Spencer GM, et al. Photosensitisation and photodynamic therapy of oesophageal, duodenal, and colorectal tumours using 5 aminolaevulinic acid induced protoporphyrin IX--a pilot study. *Gut* [Internet]. 1995;36(1):67–75. Available from: <http://gut.bmj.com/cgi/doi/10.1136/gut.36.1.67>
106. Nakamura M, Nishikawa J, Hamabe K, Goto A, Nishimura J, Shibata H, et al. Preliminary study of photodynamic diagnosis using 5-aminolevulinic acid

- in gastric and colorectal tumors. *World J Gastroenterol*. 2015;21(21):6706–12.
107. Minamikawa T, Matsuo H, Kato Y, Harada Y, Otsuji E, Yanagisawa A, et al. Simplified and optimized multispectral imaging for 5-ALA-based fluorescence diagnosis of malignant lesions. *Sci Rep*. 2016;6:1–9.
108. Harada K, Harada Y, Beika M, Koizumi N, Inoue K, Murayama Y, et al. Detection of lymph node metastases in human colorectal cancer by using 5-aminolevulinic acid-induced protoporphyrin IX fluorescence with spectral unmixing. *Int J Mol Sci*. 2013;
109. Jain RK, Stylianopoulos T. Delivering nanomedicine to solid tumors. *Nat Rev Clin Oncol* [Internet]. 2010 Sep 14;7:653. Available from: <http://dx.doi.org/10.1038/nrclinonc.2010.139>
110. Nichols JW, Bae YH. Odyssey of a cancer nanoparticle: From injection site to site of action. *Nano Today*. 2012;7(6):606–18.
111. Jordan VC. Tamoxifen: A most unlikely pioneering medicine. *Nat Rev Drug Discov*. 2003;2(3):205–13.
112. Bryan J. From breast cancer treatment to prevention: The story of tamoxifen. *Pharm J*. 2009;282(7538):137–8.
113. Ingle JN, Ahmann DL, Green SJ, Edmonson JH, Bisel HF, Kvols LK, et al. Randomized clinical trial of diethylstilbestrol versus tamoxifen in postmenopausal women with advanced breast cancer. *Nejm*. 1981;304(1):16–21.
114. Gail MH, Brinton LA, Byar DP, Corle DK, Green SB, Schairer C, et al. Projecting individualized probabilities of developing breast cancer for white females who are being examined annually. *J Natl Cancer Inst*. 1989;81(24):1879–86.

115. Cuzick J. First results from the International Breast Cancer Intervention Study (IBIS-I): A randomised prevention trial. *Lancet*. 2002;360(9336):817–24.
116. Powles TJ, Hardy JR, Ashley SE, Farrington GM, Cosgrove D, Davey JB, et al. A pilot trial to evaluate the acute toxicity and feasibility of tamoxifen for prevention of breast cancer. *Br J Cancer*. 1989;60(1):126–31.
117. Menon JU, Jadeja P, Tambe P, Vu K, Yuan B, Nguyen KT. Nanomaterials for photo-based diagnostic and therapeutic applications. *Theranostics*. 2013;3(3):152–66.
118. Lammers T, Kiessling F, Hennink WE, Storm G. Drug targeting to tumors: Principles, pitfalls and (pre-) clinical progress. *J Control Release* [Internet]. 2012;161(2):175–87. Available from: <http://dx.doi.org/10.1016/j.jconrel.2011.09.063>
119. M. Cardoso M, N. Peca I, C. A. Roque A. Antibody-Conjugated Nanoparticles for Therapeutic Applications. *Curr Med Chem*. 2012;19(19):3103–27.
120. Merisko-Liversidge E, Liversidge GG, Cooper ER. Nanosizing: A formulation approach for poorly-water-soluble compounds. *Eur J Pharm Sci* [Internet]. 2003 Feb 1 [cited 2018 Jul 3];18(2):113–20. Available from: <https://www.sciencedirect.com/science/article/pii/S0928098702002518?via%3Dihub>
121. Gu FX, Karnik R, Wang AZ, Alexis F, Levy-Nissenbaum E, Hong S, et al. Targeted nanoparticles for cancer therapy. *Nano Today*. 2007;2(3):14–21.
122. Miller MA, Weissleder R. Imaging the pharmacology of nanomaterials by intravital microscopy: Toward understanding their biological behavior. *Adv Drug Deliv Rev*. 2017;113:61–86.

123. Yang L, Zhang X, Ye M, Jiang J, Yang R, Fu T, et al. Aptamer-conjugated nanomaterials and their applications. *Adv Drug Deliv Rev.* 2012;63:1361–70.
124. Matsumura Y, Maeda H. A new concept for macromolecular therapeutics in cancer chemotherapy: mechanism of tumoritropic accumulation of proteins and the antitumor agent smancs. *Cancer Res [Internet].* 1986 Dec 1 [cited 2018 Jul 3];46(12 Pt 1):6387–92. Available from: <http://www.ncbi.nlm.nih.gov/pubmed/2946403>
125. Nakamura Y, Mochida A, Choyke PL, Kobayashi H. Nanodrug Delivery: Is the Enhanced Permeability and Retention Effect Sufficient for Curing Cancer? *Bioconjug Chem.* 2016;27(10):2225–38.
126. Movassaghian S, Merkel OM, Torchilin VP. Applications of polymer micelles for imaging and drug delivery. *Wiley Interdiscip Rev Nanomedicine Nanobiotechnology.* 2015;7(5):691–707.
127. Matsumura Y. The drug discovery by nanomedicine and its clinical experience. *Jpn J Clin Oncol.* 2014;44(6):515–25.
128. Heldin CH, Rubin K, Pietras K, Östman A. High interstitial fluid pressure - An obstacle in cancer therapy. *Nat Rev Cancer.* 2004;4(10):806–13.
129. Narayanan E, Wakaskar R. Utilization of nanoparticulate therapy in cancer targeting. Schumacher U, editor. *Cogent Med [Internet].* 2018 Jul 26;5(1):1–9. Available from: <https://doi.org/10.1080/2331205X.2018.1504504>
130. Danhier F. To exploit the tumor microenvironment: Since the EPR effect fails in the clinic, what is the future of nanomedicine? *J Control Release [Internet].* 2016;244:108–21. Available from: <http://dx.doi.org/10.1016/j.jconrel.2016.11.015>
131. Kim JH, Kim YS, Park K, Lee S, Nam HY, Min KH, et al. Antitumor efficacy

- of cisplatin-loaded glycol chitosan nanoparticles in tumor-bearing mice. *J Control Release*. 2008;127(1):41–9.
132. Cho KJ, Moon HT, Park G, Jeon OC, Byun Y, Lee Y. Preparation of sodium deoxycholate (DOC) conjugated heparin derivatives for inhibition of angiogenesis and cancer cell growth. *Bioconjug Chem*. 2008;19(7):1346–51.
133. Chytil P, Etrych T, Koňák Č, Šírová M, Mrkvan T, Bouček J, et al. New HPMA copolymer-based drug carriers with covalently bound hydrophobic substituents for solid tumour targeting. *J Control Release*. 2008;127(2):121–30.
134. Rosenblum D, Joshi N, Tao W, Karp JM, Peer D. Progress and challenges towards targeted delivery of cancer therapeutics. *Nat Commun* [Internet]. 2018 Dec 12;9(1):1410. Available from: <http://dx.doi.org/10.1038/s41467-018-03705-y>
135. Maeda H, Tsukigawa K, Fang J. A Retrospective 30 Years After Discovery of the Enhanced Permeability and Retention Effect of Solid Tumors: Next-Generation Chemotherapeutics and Photodynamic Therapy—Problems, Solutions, and Prospects. *Microcirculation*. 2016;23(3):173–82.
136. Michiels C, Tellier C, Feron O. Cycling hypoxia: A key feature of the tumor microenvironment. *Biochim Biophys Acta - Rev Cancer* [Internet]. 2016 Aug 1 [cited 2018 Jul 3];1866(1):76–86. Available from: <https://www.sciencedirect.com/science/article/pii/S0304419X16300440?via%3Dihub>
137. Glentis A, Gurchenkov V, Vignjevic DM. Assembly, heterogeneity, and breaching of the basement membranes. *Cell Adhes Migr*. 2014;8(3):236–45.
138. Kalluri R. Basement membranes: structure, assembly and role in tumour

- angiogenesis. *Nat Rev Cancer* [Internet]. 2003 Jun 1;3:422. Available from: <http://dx.doi.org/10.1038/nrc1094>
139. Miao L, Huang L. Exploring the Tumor Microenvironment with Nanoparticles. In: Mirkin CA, Meade TJ, Petrosko SH, Stegh AH, editors. *Nanotechnology-Based Precision Tools for the Detection and Treatment of Cancer* [Internet]. Cham: Springer International Publishing; 2015. p. 193–226. Available from: [https://doi.org/10.1007/978-3-319-16555-4\\_9](https://doi.org/10.1007/978-3-319-16555-4_9)
140. Zhang B, Hu Y, Pang Z. Modulating the tumor microenvironment to enhance tumor nanomedicine delivery. *Front Pharmacol*. 2017;8(DEC):1–16.
141. Xiang D, Shigdar S, Qiao G, Wang T, Kouzani AZ, Zhou SF, et al. Nucleic acid aptamer-guided cancer therapeutics and diagnostics: The next generation of cancer medicine. *Theranostics*. 2015;5(1):23–42.
142. Wagner V, Dullaart A, Bock A-K, Zweck A. The emerging nanomedicine landscape. *Nat Biotechnol* [Internet]. 2006 Oct 1;24:1211. Available from: <http://dx.doi.org/10.1038/nbt1006-1211>
143. Tiernan JP, Perry SL, Verghese ET, West NP, Yeluri S, Jayne DG, et al. Carcinoembryonic antigen is the preferred biomarker for in vivo colorectal cancer targeting. *Br J Cancer*. 2013;108(3):662–7.
144. Friedman A, Claypool S, Liu R. The Smart Targeting of Nanoparticles. *Curr Pharm Des* [Internet]. 2013;19(35):6315–29. Available from: <http://www.eurekaselect.com/openurl/content.php?genre=article&issn=1381-6128&volume=19&issue=35&spage=6315>
145. Peng H-SS, Chiu DT. Soft fluorescent nanomaterials for biological and biomedical imaging. *Chem Soc Rev* [Internet]. 2015;44(14):4699–722. Available from: <http://xlink.rsc.org/?DOI=C4CS00294F>
146. GOLD P, FREEDMAN SO. Demonstration of Tumor-Specific Antigens in

- Human Colonic Carcinomata By Immunological Tolerance and Absorption Techniques. *J Exp Med.* 1965;121:439–62.
147. Diamandis EP, Bast RC, Gold P, Chu TM, Magnani JL. Reflection on the discovery of carcinoembryonic antigen, prostate-specific antigen, and cancer antigens CA125 and CA19-9. *Clin Chem.* 2013;59(1):22–31.
148. Scott AM, Allison JP, Wolchok J. Monoclonal antibodies in cancer therapy. *Cancer Immun.* 2012;12(May):14.
149. Gold P, Freedman SO. Specific carcinoembryonic antigens of the human digestive system. *J Exp Med.* 1965;122(3):467–81.
150. Coulson A, Levy A, Gossell-Williams M. Monoclonal antibodies in cancer therapy: Mechanisms, successes and limitations. *West Indian Med J.* 2014;63(6):650–4.
151. Liu JKH. The history of monoclonal antibody development - Progress, remaining challenges and future innovations. *Ann Med Surg.* 2014;3(4):113–6.
152. Eloy JO, Petrilli R, Trevizan LNF, Chorilli M. Immunoliposomes: A review on functionalization strategies and targets for drug delivery. *Colloids Surfaces B Biointerfaces* [Internet]. 2017;159:454–67. Available from: <https://doi.org/10.1016/j.colsurfb.2017.07.085>
153. Moorthy BS, Xie B, Moussa EM, Iyer LK, Chandrasekhar S, Panchal JP, et al. Structure of Monoclonal Antibodies. In: Rosenberg A, Demeule B, editors. *Biobetters: Protein Engineering to Approach the Curative* [Internet]. New York, NY: Springer New York; 2015. p. 81–9. Available from: [https://doi.org/10.1007/978-1-4939-2543-8\\_6](https://doi.org/10.1007/978-1-4939-2543-8_6)
154. Schematic diagram of IgG monoclonal antibody [Internet]. Available from: <http://what-when-how.com/wp->

content/uploads/2012/04/tmp4B106.jpg%0D%0A

155. Makaraviciute A, Jackson CD, Millner PA, Ramanaviciene A. Considerations in producing preferentially reduced half-antibody fragments. *J Immunol Methods*. 2016;
156. Kavousipour S, Khademi F, Zamani M, Vakili B, Mokarram P. Novel biotechnology approaches in colorectal cancer diagnosis and therapy. *Biotechnol Lett*. 2017;39(6):785–803.
157. Vigor KL, Kyrtatos PG, Minogue S, Al-Jamal KT, Kogelberg H, Tolner B, et al. Nanoparticles functionalised with recombinant single chain Fv antibody fragments (scFv) for the magnetic resonance imaging of cancer cells. *Biomaterials*. 2010;31(6):1307–15.
158. Antibody fragments [Internet]. [www.absoluteantibody.com](http://www.absoluteantibody.com). Available from: <https://absoluteantibody.com/antibody-resources/antibody-engineering/antibody-fragments/>
159. Nelson AL. Antibody fragments: hope and hype. *MAbs* [Internet]. 2010/01/27. 2010;2(1):77–83. Available from: <https://pubmed.ncbi.nlm.nih.gov/20093855>
160. Margarida M, Requite C, Cecília A, Roque ACA, Cardoso MM, Peça IN, et al. Antibody-Conjugated Nanoparticles for Therapeutic Applications SCENT: Hybrid gels for rapid microbial detection View project Enhancement of oxygen transport by functionalized magnetic nanoparticles (FMP) in non-Newtonian highly viscous microbial fermentat. *Curr Med Chem*. 2012;19:3103–27.
161. Škrlec K, Štrukelj B, Berlec A. Non-immunoglobulin scaffolds: A focus on their targets. *Trends Biotechnol*. 2015;33(7):408–18.
162. Chames P, Van Regenmortel M, Weiss E, Baty D. Therapeutic antibodies:

- Successes, limitations and hopes for the future. *Br J Pharmacol*. 2009;157(2):220–33.
163. Pastor F. Aptamers: A new technological platform in cancer immunotherapy. *Pharmaceuticals*. 2016;9(4):1–13.
164. Naidoo J, Page DB, Li BT, Connell LC, Schindler K, Lacouture ME, et al. Toxicities of the anti-PD-1 and anti-PD-L1 immune checkpoint antibodies. *Ann Oncol*. 2015;26(12):2375–91.
165. Ward S, Brett SJ, Castello-cortes A, Brunner MD, Panoskaltsis N, D P, et al. Cytokine Storm in a Phase 1 Trial of the Anti-CD28 Monoclonal Antibody TGN1412. *Response*. 2006;1018–28.
166. da Paz MC, Almeida Santos M de FM, Santos CMB, da Silva SW, de Souza LB, Lima ECD, et al. Anti-CEA loaded maghemite nanoparticles as a theragnostic device for colorectal cancer. *Int J Nanomedicine*. 2012;7:5271–82.
167. DeLong JC, Murakami T, Yazaki PJ, Hoffman RM, Bouvet M. Near-infrared-conjugated humanized anti-carcinoembryonic antigen antibody targets colon cancer in an orthotopic nude-mouse model. *J Surg Res [Internet]*. 2017;218:139–43. Available from: <https://doi.org/10.1016/j.jss.2017.05.069>
168. Cho YS, Yoon TJ, Jang ES, Soo Hong K, Young Lee S, Ran Kim O, et al. Cetuximab-conjugated magneto-fluorescent silica nanoparticles for in vivo colon cancer targeting and imaging. *Cancer Lett*. 2010;299(1):63–71.
169. Fay F, McLaughlin KM, Small DM, Fennell DA, Johnston PG, Longley DB, et al. Conatumumab (AMG 655) coated nanoparticles for targeted proapoptotic drug delivery. *Biomaterials [Internet]*. 2011;32(33):8645–53. Available from: <http://dx.doi.org/10.1016/j.biomaterials.2011.07.065>
170. Schmid D, Fay F, Small DM, Jaworski J, Riley JS, Tegazzini D, et al.

- Efficient drug delivery and induction of apoptosis in colorectal tumors using a death receptor 5-targeted nanomedicine. *Mol Ther.* 2014;22(12):2083–92.
171. Hsieh WJ, Liang CJ, Chieh JJ, Wang SH, Lai IR, Chen JH, et al. In vivo tumor targeting and imaging with anti-vascular endothelial growth factor antibody-conjugated dextran-coated iron oxide nanoparticles. *Int J Nanomedicine.* 2012;
172. Benedetto G, Vestal CG, Richardson C. Aptamer-Functionalized Nanoparticles as “Smart Bombs”: The Unrealized Potential for Personalized Medicine and Targeted Cancer Treatment. *Target Oncol.* 2015;10(4):467–85.
173. Banerjee J, Nilsen-Hamilton M. Aptamers: Multifunctional molecules for biomedical research. *J Mol Med.* 2013;91(12):1333–42.
174. McCarthy JR, Bhaumik J, Karver MR, Sibel Erdem S, Weissleder R. Targeted nanoagents for the detection of cancers. *Mol Oncol.* 2010;4(6):511–28.
175. Chen C, Zhou S, Cai Y, Tang F. Nucleic acid aptamer application in diagnosis and therapy of colorectal cancer based on cell-SELEX technology. *npj Precis Oncol* [Internet]. 2017;1(1):37. Available from: <http://www.nature.com/articles/s41698-017-0041-y>
176. Ellington AD, Szostak JW. In vitro selection of RNA molecules that bind specific ligands. *Nature* [Internet]. 1990 Aug 30;346:818. Available from: <http://dx.doi.org/10.1038/346818a0>
177. Tuerk C, Gold L. Systematic evolution of ligands by exponential enrichment: RNA ligands to bacteriophage T4 DNA polymerase. *Science* (80- ) [Internet]. 1990 Aug 3;249(4968):505 LP – 510. Available from: <http://science.sciencemag.org/content/249/4968/505.abstract>

178. Chandola C, Neerathilingam M. Aptamers for Targeted Delivery: Current Challenges and Future Opportunities. In: Role of Novel Drug Delivery Vehicles in Nanobiomedicine [Internet]. IntechOpen; 2020. p. 0–22. Available from: <https://www.intechopen.com/books/role-of-novel-drug-delivery-vehicles-in-nanobiomedicine/aptamers-for-targeted-delivery-current-challenges-and-future-opportunities>
179. Zhou G, Wilson G, Hebbard L, Duan W, Liddle C, George J, et al. Aptamers: A promising chemical antibody for cancer therapy. *Oncotarget* [Internet]. 2016;7(12):13446–63. Available from: [www.impactjournals.com/oncotarget](http://www.impactjournals.com/oncotarget)
180. Ahmadzadeh-Raji M, Ghafar-Zadeh E, Amouabediny G. An optically-transparent aptamer-based detection system for colon cancer applications using gold nanoparticles electrodeposited on indium tin oxide. *Sensors (Switzerland)*. 2016;16(7).
181. Li Y, Duo Y, Bao S, He L, Ling K, Luo J, et al. EpCAM aptamer-functionalized polydopamine-coated mesoporous silica nanoparticles loaded with DM1 for targeted therapy in colorectal cancer. *Int J Nanomedicine* [Internet]. 2017;12:6239–57. Available from: <https://www.ncbi.nlm.nih.gov/pubmed/28894364>
182. Shigdar S, Lin J, Yu Y, Pastuovic M, Wei M, Duan W. RNA aptamer against a cancer stem cell marker epithelial cell adhesion molecule. *Cancer Sci*. 2011;102(5):991–8.
183. Li L, Xiang D, Shigdar S, Yang W, Li Q, Lin J, et al. Epithelial cell adhesion molecule aptamer functionalized PLGA-lecithin-curcumin-PEG nanoparticles for targeted drug delivery to human colorectal adenocarcinoma cells. *Int J Nanomedicine* [Internet]. 2014;9:1083–96. Available from: <http://www.ncbi.nlm.nih.gov/pubmed/24591829>
184. Jalalian SH, Taghdisi SM, Hamedani NS, Kalat SAM, Lavaee P, ZandKarimi

- M, et al. Epirubicin loaded super paramagnetic iron oxide nanoparticle-aptamer bioconjugate for combined colon cancer therapy and imaging in vivo. *Eur J Pharm Sci.* 2013;50(2):191–7.
185. Ng EWM, Shima DT, Calias P, Cunningham Jr. ET, Guyer DR, Adamis AP. Pegaptanib, a targeted anti-VEGF aptamer for ocular vascular disease. *Nat Rev Drug Discov* [Internet]. 2006 Feb 1;5:123. Available from: <http://dx.doi.org/10.1038/nrd1955>
186. Ng EWM, Adamis AP. Anti-VEGF aptamer (pegaptanib) therapy for ocular vascular diseases. *Ann N Y Acad Sci.* 2006;1082:151–71.
187. Taghdisi SM, Danesh NM, Sarreshtehdar Emrani A, Tabrizian K, Zandkarimi M, Ramezani M, et al. Targeted delivery of Epirubicin to cancer cells by PEGylated A10 aptamer. *J Drug Target.* 2013;21(8):739–44.
188. Mallikaratchy P, Tang Z, Tan W. Cell specific aptamer-photosensitizer conjugates as a molecular tool in photodynamic therapy. *ChemMedChem.* 2008;3(3):425–8.
189. Soundararajan S, Chen W, Spicer EK, Courtenay-Luck N, Fernandes DJ. The nucleolin targeting aptamer AS1411 destabilizes Bcl-2 messenger RNA in human breast cancer cells. *Cancer Res.* 2008;68(7):2358–65.
190. Shieh Y-A, Yang S-J, Wei M-F, Shieh M-J. Aptamer-Based Tumor-Targeted Drug Delivery for Photodynamic Therapy. *ACS Nano* [Internet]. 2010 Mar 23;4(3):1433–42. Available from: <https://doi.org/10.1021/nn901374b>
191. Schädlich A, Caysa H, Mueller T, Tenambergen F, Rose C, Göpferich A, et al. Tumor accumulation of NIR fluorescent PEG-PLA nanoparticles: Impact of particle size and human xenograft tumor model. *ACS Nano.* 2011;5(11):8710–20.
192. A. Kudgus R, Bhattacharya R, Mukherjee P. *Cancer Nanotechnology:*

- Emerging Role of Gold Nanoconjugates. *Anticancer Agents Med Chem* [Internet]. 2011 Dec 1;11(10):965–73. Available from: <http://www.eurekaselect.com/openurl/content.php?genre=article&issn=1871-5206&volume=11&issue=10&spage=965>
193. Matsumura Y, Maeda H. A New Concept for Macromolecular Therapeutics in Cancer Chemotherapy: Mechanism of Tumor-tropic Accumulation of Proteins and the Antitumor Agent Smancs. *Cancer Res.* 1986;46(8):6387–92.
194. Pikarsky E, Porat RM, Stein I, Abramovitch R, Amit S, Kasem S, et al. NF- $\kappa$ B functions as a tumour promoter in inflammation-associated cancer. *Nature* [Internet]. 2004 Sep 25;431(7007):461–6. Available from: <http://www.nature.com/articles/nature02924>
195. Hobbs SK, Monsky WL, Yuan F, Roberts WG, Griffith L, Torchilin VP, et al. Regulation of transport pathways in tumor vessels: Role of tumor type and microenvironment. *Proc Natl Acad Sci* [Internet]. 1998 Apr 14;95(8):4607–12. Available from: <http://www.pnas.org/cgi/doi/10.1073/pnas.95.8.4607>
196. Moghimi SM, Porter CJH, Muir IS, Illum L, Davis SS. Non-phagocytic uptake of intravenously injected microspheres in rat spleen: Influence of particle size and hydrophilic coating. *Biochem Biophys Res Commun* [Internet]. 1991 Jun;177(2):861–6. Available from: <https://linkinghub.elsevier.com/retrieve/pii/0006291X9191869E>
197. Suk JS, Xu Q, Kim N, Hanes J, Ensign LM. PEGylation as a strategy for improving nanoparticle-based drug and gene delivery. *Adv Drug Deliv Rev.* 2016;99:28–51.
198. Ahmad Khanbeigi R, Abelha TF, Woods A, Rastoin O, Harvey RD, Jones MC, et al. Surface Chemistry of Photoluminescent F8BT Conjugated Polymer Nanoparticles Determines Protein Corona Formation and

- Internalization by Phagocytic Cells. *Biomacromolecules*. 2015;
199. Howes P, Green M. Colloidal and optical stability of PEG-capped and phospholipid-encapsulated semiconducting polymer nanospheres in different aqueous media. *Photochem Photobiol Sci*. 2010;9(8):1159–66.
  200. Carrstensen H, Müller RH, Müller BW. Particle size, surface hydrophobicity and interaction with serum of parenteral fat emulsions and model drug carriers as parameters related to RES uptake. *Clin Nutr*. 1992;11(5):289–97.
  201. Norman ME, Williams P, Illum L. Human serum albumin as a probe for surface conditioning (opsonization) of block copolymer-coated microspheres. *Biomaterials*. 1992;13(12):841–9.
  202. Owens DE, Peppas NA. Opsonization, biodistribution, and pharmacokinetics of polymeric nanoparticles. *International Journal of Pharmaceutics*. 2006.
  203. Choi KY, Min KH, Yoon HY, Kim K, Park JH, Kwon IC, et al. PEGylation of hyaluronic acid nanoparticles improves tumor targetability in vivo. *Biomaterials*. 2011;32(7):1880–9.
  204. Sadauskas E, Danscher G, Stoltenberg M, Vogel U, Larsen A, Wallin H. Protracted elimination of gold nanoparticles from mouse liver. *Nanomedicine Nanotechnology, Biol Med [Internet]*. 2009;5(2):162–9. Available from: <http://dx.doi.org/10.1016/j.nano.2008.11.002>
  205. Lu J, Liang M, Li Z, Zink JI, Tamanoi F. Biocompatibility, Biodistribution, and Drug-Delivery Efficiency of Mesoporous Silica Nanoparticles for Cancer therapy in Animals. *NIH Public Acces*. 2011;6(16):1794–805.
  206. Hanini A, Schmitt A, Kacem K, Chau F, Ammar S, Gavard J. Evaluation of iron oxide nanoparticle biocompatibility. *Int J Nanomedicine*. 2011;6:787–94.
  207. Nishimori H, Kondoh M, Isoda K, Tsunoda S ichi, Tsutsumi Y, Yagi K. Silica nanoparticles as hepatotoxicants. *Eur J Pharm Biopharm*. 2009;72(3):496–

- 501.
208. Pilloni M, Nicolas J, Marsaud V, Bouchemal K, Frongia F, Scano A, et al. PEGylation and preliminary biocompatibility evaluation of magnetite-silica nanocomposites obtained by high energy ball milling. *Int J Pharm*. 2010;401(1–2):103–12.
209. Hashim Z. *Semiconducting Polymer Nanospheres : Organic Alternatives to Quantum Dots ?* Kings College London; 2013.
210. Torchilin VP. Multifunctional, stimuli-sensitive nanoparticulate systems for drug delivery. *Nat Rev Drug Discov* [Internet]. 2014;13(11):813–27. Available from: <http://dx.doi.org/10.1038/nrd4333>
211. Povsic TJ, Vavalle JP, Aberle LH, Kasprzak JD, Cohen MG, Mehran R, et al. A Phase 2, randomized, partially blinded, active-controlled study assessing the efficacy and safety of variable anticoagulation reversal using the REG1 system in patients with acute coronary syndromes: Results of the RADAR trial. *Eur Heart J*. 2013;34(31):2481–9.
212. Ganson NJ, Povsic TJ, Sullenger BA, Alexander JH, Zelenkofske SL, Sailstad JM, et al. Pre-existing anti-polyethylene glycol antibody linked to first-exposure allergic reactions to pegnivacogin, a PEGylated RNA aptamer. *J Allergy Clin Immunol* [Internet]. 2016 May;137(5):1610-1613.e7. Available from: <https://linkinghub.elsevier.com/retrieve/pii/S009167491501667X>
213. Pu K, Chattopadhyay N, Rao J. Recent Advances of Semiconducting Polymer Nanoparticles in In Vivo Molecular Imaging. *J Control Release* [Internet]. 2016;240:312–22. Available from: <http://dx.doi.org/10.1016/j.jconrel.2016.01.004>
214. Lian W, Litherland SA, Badrane H, Tan W, Wu D, Baker H V., et al.

Ultrasensitive detection of biomolecules with fluorescent dye-doped nanoparticles. *Anal Biochem.* 2004;

215. Kolitz-Domb M, Corem-Salkmon E, Grinberg I, Margel S. Synthesis and characterization of bioactive conjugated near-infrared fluorescent proteinoidpoly(L-lactic acid) hollow nanoparticles for optical detection of colon cancer. *Int J Nanomedicine.* 2014;9(1):5041–53.
216. Kogan-Zviagin I, Shamay Y, Nissan A, Sella-Tavor O, Golan M, David A. Intra-colonic administration of a polymer-bound NIRF probe for improved colorectal cancer detection during colonoscopy. *J Control Release.* 2014;
217. Yan L, Zhang Y, Xu B, Tian W. Fluorescent nanoparticles based on AIE fluorogens for bioimaging. *Nanoscale [Internet].* 2016;8(5):2471–87. Available from: <http://xlink.rsc.org/?DOI=C5NR05051K>
218. Yaghini E, Turner HD, Le Marois AM, Suhling K, Naasani I, MacRobert AJ. In vivo biodistribution studies and ex vivo lymph node imaging using heavy metal-free quantum dots. *Biomaterials.* 2016;104:182–91.
219. Peet J, Kim JY, Coates NE, Ma WL, Moses D, Heeger AJ, et al. Efficiency enhancement in low-bandgap polymer solar cells by processing with alkane dithiols. *Nat Mater [Internet].* 2007 May 27;6:497. Available from: <http://dx.doi.org/10.1038/nmat1928>
220. Mei JG, Diao Y, Appleton A., Fang L, Bao Z. Integrated materials design of organic semiconductors for field-effect transistors. *J Am Chem Soc.* 2013;6724–46.
221. Rose A, Zhu Z, Madigan CF, Swager TM, Bulović V. Sensitivity gains in chemosensing by lasing action in organic polymers. *Nature [Internet].* 2005 Apr 14;434:876. Available from: <http://dx.doi.org/10.1038/nature03438>
222. Sanghvi AB, Miller KP-H, Belcher AM, Schmidt CE. *Biomaterials*

functionalization using a novel peptide that selectively binds to a conducting polymer. *Nat Mater* [Internet]. 2005 May 15;4:496. Available from: <http://dx.doi.org/10.1038/nmat1397>

223. Ding D, Liu J, Feng G, Li K, Hu Y, Liu B. Bright far-red/near-infrared conjugated polymer nanoparticles for in vivo bioimaging. *Small*. 2013;9(18):3093–102.
224. Ahmed E, Morton SW, Hammond PT, Swager TM. Fluorescent multiblock  $\pi$ -conjugated polymer nanoparticles for in vivo tumor targeting. Vol. 25, *Advanced Materials*. 2013. p. 4504–10.
225. Bao B, Ma M, Chen J, Yuwen L, Weng L, Fan Q, et al. Facile preparation of multicolor polymer nanoparticle bioconjugates with specific biorecognition. *ACS Appl Mater Interfaces*. 2014;6(14):11129–35.
226. Howes P. *Synthesis of organic and inorganic nanoparticles*. Kings College London;
227. Khanbeigi RA, Hashim Z, Abelha TF, Pitchford S, Collins H, Green M, et al. Interactions of stealth conjugated polymer nanoparticles with human whole blood. *J Mater Chem B*. 2015;3(12):2463–71.
228. Lyu Y, Pu K. Recent Advances of Activatable Molecular Probes Based on Semiconducting Polymer Nanoparticles in Sensing and Imaging. *Adv Sci*. 2017;4(6).
229. Kemal E, Abelha TF, Urbano L, Peters R, Owen DM, Howes P, et al. Bright, near infrared emitting PLGA-PEG dye-doped CN-PPV nanoparticles for imaging applications. *RSC Adv*. 2017;7(25):15255–64.
230. Morton D, Brown G, Ferry D, Gray R, Magill L, Quirke P, et al. FOxTROT - Fluoropyrimidine, Oxaliplatin and Targeted Receptor pre-Operative Therapy for high risk colon cancer FOxTROT – 2 stage trial. In.

231. Loughrey M, Quirke P, Shepherd N. Dataset for Colorectal Cancer Histopathology Reports. 3rd edn (Document number G049) [Internet]. Standards and datasets for reporting cancers. Available from: [www.rcpath.org/resourceLibrary/dataset-for-colorectal-cancer-histopathology-reports-3rd-edition-.html](http://www.rcpath.org/resourceLibrary/dataset-for-colorectal-cancer-histopathology-reports-3rd-edition-.html)
232. Dako. Monoclonal Mouse Clone JC70A Code M0823 [Internet]. Available from: [https://www.agilent.com/en/product/immunohistochemistry/antibodies-controls/primary-antibodies/cd31-endothelial-cell-\(dako-omnis\)-76224](https://www.agilent.com/en/product/immunohistochemistry/antibodies-controls/primary-antibodies/cd31-endothelial-cell-(dako-omnis)-76224)
233. Hermanson GT. Bioconjugation techniques [Internet]. Vol. 10, Academic Press. 2008. 0123705010 p. Available from: [http://scholar.google.com/scholar?hl=en&rlz=1G1GGLQ\\_ENUS242&q=bioc onjugate+techniques+hermanson&um=1&ie=UTF-8&sa=N&tab=ps#3](http://scholar.google.com/scholar?hl=en&rlz=1G1GGLQ_ENUS242&q=bioc onjugate+techniques+hermanson&um=1&ie=UTF-8&sa=N&tab=ps#3)
234. Liberale G, Bourgeois P, Larsimont D, Moreau M, Donckier V, Ishizawa T. Indocyanine green fluorescence-guided surgery after IV injection in metastatic colorectal cancer: A systematic review. *Eur J Surg Oncol*. 2017;43(9):1656–67.
235. Barone DG, Lawrie TA, Hart MG. Image guided surgery for the resection of brain tumours ( Review ). *Cochrane Libr* [Internet]. 2015;(1). Available from: <http://www.thecochranelibrary.com>
236. Chand M, Bhangu A, Wotherspoon A, Stamp GWH, Swift RI, Chau I, et al. EMVI-positive stage ii rectal cancer has similar clinical outcomes as stage iii disease following pre-operative chemoradiotherapy. *Ann Oncol* [Internet]. 2014;25(4):858–63. Available from: <http://dx.doi.org/10.1093/annonc/mdu029>
237. Van Eeghen EE, Flens MJ, Mulder MMR, Loffeld RJLF. Extramural venous invasion as prognostic factor of recurrence in stage 1 and 2 colon cancer. *Gastroenterol Res Pract*. 2017;2017.

238. Imbeaud S, Graudens E, Boulanger V, Barlet X, Zaborski P, Eveno E, et al. Towards standardization of RNA quality assessment using user-independent classifiers of microcapillary electrophoresis traces. *Nucleic Acids Res* [Internet]. 2005 Mar 30;33(6):e56–e56. Available from: <https://pubmed.ncbi.nlm.nih.gov/15800207>
239. Tendeng C, Bylesjo M. GLiSten Gene Expression Analysis. 2016.
240. National Institute for Health and Care Excellence. Colorectal cancer overview [Internet]. NICE Pathways. 2016. Available from: <http://pathways.nice.org.uk/pathways/colorectal-cancer>
241. Kondo Y, MURAYAMA Y, KONISHI H, MORIMURA R, KOMATSU S, SHIOZAKI A, et al. Fluorescent detection of peritoneal metastasis in human colorectal cancer using 5-aminolevulinic acid. *Int J Oncol*. 2014;
242. Matsuo H, Harada Y, Minamikawa T, Kato Y, Murayama Y, Otsuji E, et al. Efficient fluorescence detection of protoporphyrin IX in metastatic lymph nodes of murine colorectal cancer stained with indigo carmine. *Photodiagnosis Photodyn Ther*. 2017;19(May):175–80.
243. Nguyen QT, Tsien RY. Fluorescence-guided surgery with live molecular navigation - a new cutting edge. *Nat Rev Cancer*. 2013;13:653–62.
244. Ewelt C, Nemes A, Senner V, Wölfer J, Brokinkel B, Stummer W, et al. Fluorescence in neurosurgery: Its diagnostic and therapeutic use. Review of the literature. Vol. 148, *Journal of Photochemistry and Photobiology B: Biology*. 2015. p. 302–9.
245. Isomoto H, Nanashima A, Senoo T, Ogiwara K, Hashisako M, Ohnita K, et al. In vivo fluorescence navigation of gastric and upper gastrointestinal tumors by 5-aminolevulinic acid mediated photodynamic diagnosis with a laser-equipped video image endoscope. *Photodiagnosis Photodyn Ther*.

2015;12(2):201–8.

246. Lever J, Krzywinski M, Altman N. Principal component analysis. *Nat Methods* [Internet]. 2017;14(7):641–2. Available from: <https://doi.org/10.1038/nmeth.4346>
247. Ashraf SQ, Umana P, Mössner E, Ntouroupi T, Brünker P, Schmidt C, et al. Humanised IgG1 antibody variants targeting membrane-bound carcinoembryonic antigen by antibody-dependent cellular cytotoxicity and phagocytosis. *Br J Cancer*. 2009;101(10):1758–68.
248. Mutin M, Dignat-George F, Sampol J. Immunologic phenotype of cultured endothelial cells: Quantitative analysis of cell surface molecules. *Tissue Antigens*. 1997;50(5):449–58.
249. ATCC, Standards L. 293[HEK-293] (ATCC CRL-1573) [Internet]. Available from: [https://www.lgcstandards-atcc.org/products/all/CRL-1573.aspx?geo\\_country=gb#documentation](https://www.lgcstandards-atcc.org/products/all/CRL-1573.aspx?geo_country=gb#documentation)
250. Kausaite-Minkstimiene A, Ramanaviciene A, Kirlyte J, Ramanavicius A. Comparative Study of Random and Oriented Antibody Immobilization Techniques on the Binding Capacity of Immunosensor. *Anal Chem* [Internet]. 2010 Aug 1;82(15):6401–8. Available from: <https://doi.org/10.1021/ac100468k>
251. Hu C-MJ, Kaushal S, Cao HST, Aryal S, Sartor M, Esener S, et al. Half-Antibody Functionalized Lipid–Polymer Hybrid Nanoparticles for Targeted Drug Delivery to Carcinoembryonic Antigen Presenting Pancreatic Cancer Cells. *Mol Pharm* [Internet]. 2010 Jun 7;7(3):914–20. Available from: <https://doi.org/10.1021/mp900316a>
252. Balevicius Z, Ramanaviciene A, Baleviciute I, Makaraviciute A, Mikoliunaite L, Ramanavicius A. Evaluation of intact- and fragmented-antibody based

- immunosensors by total internal reflection ellipsometry. *Sensors Actuators B Chem* [Internet]. 2011;160(1):555–62. Available from:  
<http://www.sciencedirect.com/science/article/pii/S0925400511007520>
253. Makaraviciute A, Ramanaviciene A. Site-directed antibody immobilization techniques for immunosensors. *Biosens Bioelectron* [Internet]. 2013;50:460–71. Available from:  
<http://www.sciencedirect.com/science/article/pii/S0956566313004570>
254. Dulay SB, Gransee R, Julich S, Tomaso H, O' Sullivan CK. Automated microfluidically controlled electrochemical biosensor for the rapid and highly sensitive detection of *Francisella tularensis*. *Biosens Bioelectron* [Internet]. 2014;59:342–9. Available from:  
<http://www.sciencedirect.com/science/article/pii/S095656631400205X>
255. Crivianu-Gaita V, Romaschin A, Thompson M. High efficiency reduction capability for the formation of Fab' antibody fragments from F(ab)<sub>2</sub> units. *Biochem Biophys Reports*. 2015;2:23–8.
256. Ranadive GN, Rosenzweig HS, Epperly MW, Seskey T, Bloomer WD. A new method of technetium-99m labeling of monoclonal antibodies through sugar residues. A study with TAG-72 specific CC-49 antibody. *Nucl Med Biol*. 1993;20(6):719–26.
257. Alam F, Yadav N. Potential applications of quantum dots in mapping sentinel lymph node and detection of micrometastases in breast carcinoma. *J Breast Cancer*. 2013;16(1):1–11.
258. Contributors W. Mie Scattering [Internet]. 2021. Available from:  
[https://en.wikipedia.org/wiki/Mie\\_scattering](https://en.wikipedia.org/wiki/Mie_scattering)
259. Danaei M, Dehghankhold M, Ataei S, Hasanzadeh Davarani F, Javanmard R, Dokhani A, et al. Impact of particle size and polydispersity index on the

clinical applications of lipidic nanocarrier systems. *Pharmaceutics*. 2018;10(2):1–17.

260. Sharma A, Cornejo C, Mihalic J, Geyh A, Bordelon DE, Korangath P, et al. Physical characterization and in vivo organ distribution of coated iron oxide nanoparticles. *Sci Rep*. 2018;8(1):1–12.
261. Pozzi D, Colapicchioni V, Caracciolo G, Piovesana S, Capriotti AL, Palchetti S, et al. Effect of polyethyleneglycol (PEG) chain length on the bio-nano-interactions between PEGylated lipid nanoparticles and biological fluids: From nanostructure to uptake in cancer cells. *Nanoscale*. 2014;6(5):2782–92.
262. Miteva M, Kirkbride K, Kilchrist K, Werfel T, Li H, Nelson C, et al. Tuning PEGylation of mixed micelles to overcome intracellular and systemic siRNA delivery barriers. *Biomaterials*. 2015;38:97–107.
263. Boni L, David G, Dionigi G, Rausei S, Cassinotti E, Fingerhut A. Indocyanine green-enhanced fluorescence to assess bowel perfusion during laparoscopic colorectal resection. *Surg Endosc*. 2016;30(7):2736–42.
264. Bernini, Marco. Casella, Donato. Mariotti C. Indocyanine green-enhanced fluorescence for assessing parathyroid perfusion during thyroidectomy. *GS Gland Surg*. 2017;6(6):745–50.
265. Biswas S, Nandi A, Dhara A, Baral A, Saha H, Mukherjee N, et al. Effect of centrifugation time on the optical properties of colloidal silicon nanoparticle. *Mater Today Proc*. 2018;5(3):10028–33.
266. Chee SS, Lee JH. Synthesis of tin nanoparticles through modified polyol process and effects of centrifuging and drying on nanoparticles. *Trans Nonferrous Met Soc China (English Ed)*. 2012;22(SUPPL.3):707–11.
267. La Spina R, Spampinato V, Gilliland D, Ojea-Jimenez I, Ceccone G.

Influence of different cleaning processes on the surface chemistry of gold nanoparticles. *Biointerphases* [Internet]. 2017;12(3):031003. Available from: <http://dx.doi.org/10.1116/1.4994286>

268. Shi W, Casas J, Venkataramasubramani M, Tang L. Synthesis and Characterization of Gold Nanoparticles with Plasmon Absorbance Wavelength Tunable from Visible to Near Infrared Region. *ISRN Nanomater.* 2012;2012:1–9.
269. Zhang Y, Kohler N, Zhang M. Surface modification of superparamagnetic iron oxide nanoparticles and their intracellular uptake. *Biomaterials.* 2002;23:1553–61.
270. Khaled Y, Shamsuddin S, Tiernan JP, McPherson M, Hughes T, Millner P, et al. Theranostic CEA-affimer functionalised silica nanoparticles allow specific in vitro fluorescent imaging of colorectal cancer cells. *J Surg Oncol.* 2018;44 (Supple.
271. Obaid G, Chambrier I, Cook MJ, Russell DA. Cancer targeting with biomolecules: A comparative study of photodynamic therapy efficacy using antibody or lectin conjugated phthalocyanine-PEG gold nanoparticles. *Photochem Photobiol Sci.* 2015;14(4):737–47.
272. ThermoScientific. Chemical structure of PDPH crosslinking reagent [Internet]. Available from: <https://www.thermofisher.com/order/catalog/product/22301#/22301>
273. Sigma-Aldrich. Chemical structure of heterobifunctional crosslinker, PDPH (3-(2-pyridyldithio)propionyl hydrazide) [Internet]. Available from: <https://www.sigmaaldrich.com/catalog/product/aldrich/803480?lang=en&region=GB>
274. Ravi S, Krishnamurthy VR, Caves JM, Haller CA, Chaikof EL. Maleimide-

- thiol coupling of a bioactive peptide to an elastin-like protein polymer. *Acta Biomater* [Internet]. 2011/10/25. 2012 Feb;8(2):627–35. Available from: <https://pubmed.ncbi.nlm.nih.gov/22061108>
275. Zara JJ, Wood RD, Boon P, Kim CH, Pomato N, Bredehorst R, et al. A carbohydrate-directed heterobifunctional cross-linking reagent for the synthesis of immunoconjugates. *Anal Biochem*. 1991;194(1):156–62.
276. Yin H, Meng T, Shu L, Mao M, Zhou L, Chen H, et al. Novel reduction-sensitive micellar nanoparticles assembled from Rituximab–doxorubicin conjugates as smart and intuitive drug delivery systems for the treatment of non-Hodgkin’s lymphoma. *Chem Biol Drug Des*. 2017;90(5):892–9.
277. ThermoScientific. Sulfhydryl-reactive Crosslinker Chemistry [Internet]. Available from: <https://www.thermofisher.com/uk/en/home/life-science/protein-biology/protein-biology-learning-center/protein-biology-resource-library/pierce-protein-methods/sulfhydryl-reactive-crosslinker-chemistry.html>
278. Torres AG, Gait MJ. Exploiting cell surface thiols to enhance cellular uptake. *Trends Biotechnol* [Internet]. 2012;30(4):185–90. Available from: <http://www.sciencedirect.com/science/article/pii/S016777991100206X>
279. Rothstein A. Sulfhydryl Groups in Membrane Structure and Function. In: Bronner F, Kleinzeller ABT-CT in M and T, editors. *Current Topics in Membranes and Transport* [Internet]. Academic Press; 1971. p. 135–76. Available from: <http://www.sciencedirect.com/science/article/pii/S0070216108600325>
280. Barb AW, Falconer DJ, Subedi GP. Chapter Nine - The Preparation and Solution NMR Spectroscopy of Human Glycoproteins Is Accessible and Rewarding. In: Wand AJBT-M in E, editor. *Biological NMR Part A* [Internet]. Academic Press; 2019. p. 239–61. Available from:

<http://www.sciencedirect.com/science/article/pii/S0076687918303008>

281. Ahmed-Sebak A. Limitations of PEGylated Nanocarriers: Unfavourable Physicochemical Properties, Biodistribution Patterns and Cellular and Subcellular Fates. *Int J Appl Pharm.* 2018 Sep 1;10.
282. Jokerst J V., Lobovkina T, Zare RN, Gambhir SS. Nanoparticle PEGylation for imaging and therapy. *Nanomedicine.* 2011;6(4):715–28.
283. Woodle MC. Poly(ethylene glycol)-Grafted Liposome Therapeutics. In: Poly(ethylene glycol) [Internet]. American Chemical Society; 1997. p. 5–60. (ACS Symposium Series; vol. 680). Available from: <https://doi.org/10.1021/bk-1997-0680.ch005>
284. Li B, Lane LA. Probing the biological obstacles of nanomedicine with gold nanoparticles. *Wiley Interdiscip Rev Nanomedicine Nanobiotechnology.* 2019;11(3):1–27.
285. Schneider CS, Perez JG, Cheng E, Zhang C, Mastorakos P, Hanes J, et al. Minimizing the non-specific binding of nanoparticles to the brain enables active targeting of Fn14-positive glioblastoma cells. *Biomaterials* [Internet]. 2015;42:42–51. Available from: <http://www.sciencedirect.com/science/article/pii/S0142961214012319>
286. Barua S, Yoo J-W, Kolhar P, Wakankar A, Gokarn YR, Mitragotri S. Particle shape enhances specificity of antibody-displaying nanoparticles. *Proc Natl Acad Sci* [Internet]. 2013 Feb 26;110(9):3270 LP – 3275. Available from: <http://www.pnas.org/content/110/9/3270.abstract>
287. Liu R, Kay BK, Jiang S, Chen S. Nanoparticle delivery: Targeting and nonspecific binding. *MRS Bull.* 2009;34(6):432–40.
288. Nanda JS, Lorsch JR. Chapter Seven - Labeling of a Protein with Fluorophores Using Maleimide Derivatization. In: Lorsch JBT-M in E, editor.

Laboratory Methods in Enzymology: Protein Part A [Internet]. Academic Press; 2014. p. 79–86. Available from:

<http://www.sciencedirect.com/science/article/pii/B9780124200708000076>

289. Shamshuddin SH. Biosensors for detection of colorectal cancer [Internet]. University of Leeds; 2019. Available from:  
<http://etheses.whiterose.ac.uk/23772/>
290. Tiede C, Bedford R, Heseltine SJ, Smith G, Wijetunga I, Ross R, et al. Affimer proteins are versatile and renewable affinity reagents. *Elife* [Internet]. 2017 Jun 27;6:e24903. Available from:  
<https://pubmed.ncbi.nlm.nih.gov/28654419>
291. Smith JE, Sapsford KE, Tan W, Ligler FS. Optimization of antibody-conjugated magnetic nanoparticles for target preconcentration and immunoassays. *Anal Biochem* [Internet]. 2010/11/13. 2011 Mar 1;410(1):124–32. Available from: <https://pubmed.ncbi.nlm.nih.gov/21078282>
292. Jablonski diagram illustrating the excitation of a molecule from ground state to its excited state and the resulting fluorescence. [Internet]. Available from:  
<https://gauravtiwari.org/jablonski-diagram/>
293. Excitation and emission spectra of indocyanine green [Internet]. Available from:  
[http://www.iss.com/image/technicalNotes/PC1/LWPS\\_thumb15.png%0D%0A](http://www.iss.com/image/technicalNotes/PC1/LWPS_thumb15.png%0D%0A)